Springer ThesesRecognizing Outstanding Ph.D. Research

Shohei Saga

The Vector Mode in the Second-order Cosmological Perturbation Theory



Springer Theses

Recognizing Outstanding Ph.D. Research

Aims and Scope

The series "Springer Theses" brings together a selection of the very best Ph.D. theses from around the world and across the physical sciences. Nominated and endorsed by two recognized specialists, each published volume has been selected for its scientific excellence and the high impact of its contents for the pertinent field of research. For greater accessibility to non-specialists, the published versions include an extended introduction, as well as a foreword by the student's supervisor explaining the special relevance of the work for the field. As a whole, the series will provide a valuable resource both for newcomers to the research fields described, and for other scientists seeking detailed background information on special questions. Finally, it provides an accredited documentation of the valuable contributions made by today's younger generation of scientists.

Theses are accepted into the series by invited nomination only and must fulfill all of the following criteria

- They must be written in good English.
- The topic should fall within the confines of Chemistry, Physics, Earth Sciences, Engineering and related interdisciplinary fields such as Materials, Nanoscience, Chemical Engineering, Complex Systems and Biophysics.
- The work reported in the thesis must represent a significant scientific advance.
- If the thesis includes previously published material, permission to reproduce this must be gained from the respective copyright holder.
- They must have been examined and passed during the 12 months prior to nomination.
- Each thesis should include a foreword by the supervisor outlining the significance of its content.
- The theses should have a clearly defined structure including an introduction accessible to scientists not expert in that particular field.

More information about this series at http://www.springer.com/series/8790

Shohei Saga

The Vector Mode in the Second-order Cosmological Perturbation Theory

Doctoral Thesis accepted by the Nagoya University, Nagoya, Japan



Author
Dr. Shohei Saga
Yukawa Institute for Theoretical Physics
Kyoto University
Kyoto
Japan

Supervisor Prof. Takahiko Matsubara Department of Physics Nagoya University Nagoya Japan

ISSN 2190-5053 ISSN 2190-5061 (electronic) Springer Theses ISBN 978-981-10-8006-7 ISBN 978-981-10-8007-4 (eBook) https://doi.org/10.1007/978-981-10-8007-4

Library of Congress Control Number: 2017963283

© Springer Nature Singapore Pte Ltd. 2018

This work is subject to copyright. All rights are reserved by the Publisher, whether the whole or part of the material is concerned, specifically the rights of translation, reprinting, reuse of illustrations, recitation, broadcasting, reproduction on microfilms or in any other physical way, and transmission or information storage and retrieval, electronic adaptation, computer software, or by similar or dissimilar methodology now known or hereafter developed.

The use of general descriptive names, registered names, trademarks, service marks, etc. in this publication does not imply, even in the absence of a specific statement, that such names are exempt from the relevant protective laws and regulations and therefore free for general use.

The publisher, the authors and the editors are safe to assume that the advice and information in this book are believed to be true and accurate at the date of publication. Neither the publisher nor the authors or the editors give a warranty, express or implied, with respect to the material contained herein or for any errors or omissions that may have been made. The publisher remains neutral with regard to jurisdictional claims in published maps and institutional affiliations.

Printed on acid-free paper

This Springer imprint is published by Springer Nature
The registered company is Springer Nature Singapore Pte Ltd.
The registered company address is: 152 Beach Road, #21-01/04 Gateway East, Singapore 189721, Singapore

Supervisor's Foreword

The cosmological perturbation theory has succeeded to describe state-of-the-art cosmological observations. Cosmological perturbations can be decomposed into the scalar, vector, and tensor modes. Current observations are precisely described by the scalar mode, while the vector and tensor modes have not been observed yet. It is known that the vector mode does not arise from the linear perturbation theory in the standard cosmology. In this thesis, Dr. Shohei Saga focuses on the vector mode induced from the second-order perturbation theory.

The vector mode inevitably appears from nonlinear couplings of first-order scalar modes. The aim of this thesis is to reveal a role of the second-order vector mode in observational cosmology. In order to give precise predictions of the second-order vector mode, Dr. Saga investigated the second-order Boltzmann equation together with the tight-coupling approximation in the radiation dominated era.

By using the second-order Boltzmann code, Dr. Saga applied the second-order vector mode to the generation of cosmological magnetic fields in the early universe. Resultant magnetic fields can be a good candidate of cosmological magnetic fields when the details of the dynamo mechanism on cosmological scales are clarified. Dr. Saga also applied the second-order vector mode to observations of weak gravitational lensing. The detectability of the second-order vector mode is discussed by assuming the ongoing and forthcoming weak lensing observations.

In the course of further developments of precision cosmology, the vector mode can be one of the promising tools in studying cosmological physics. A number of results in this thesis by Dr. Saga are truly important in this respect.

Tsukuba, Japan April 2017 Prof. Takahiko Matsubara

Parts of this thesis have been published in the following journal articles:

- 1. S. Saga, K. Ichiki, K. Takahashi and N. Sugiyama, "Magnetic field spectrum at cosmological recombination revisited," Phys. Rev. D **91** (2015) no.12, 123510.
- 2. S. Saga, D. Yamauchi and K. Ichiki, "Weak lensing induced by second-order vector mode," Phys. Rev. D **92** (2015) no.6, 063533.
- 3. S. Saga, "Observable cosmological vector mode in the dark ages," Phys. Rev. D **94** (2016) no.6, 063523.

and are reprinted with permission. Copyright 2015–2016 by the American Physical Society.

Acknowledgements

First of all, I am profoundly grateful to my supervisor, Takahiko Matsubara, for his scientific and stimulative advices. His supervised seminar and textbooks promote a better understanding of the basics of cosmology and the large-scale structure.

I am also very grateful to Prof. Naoshi Sugiyama for his instructive advices about my thesis studies as a collaborator and providing the conducive environment including the computing resources and top-level academic staffs. I deeply thank my collaborators, Kiyotomo Ichiki, Keitaro Takahashi, Daisuke Yamauchi, and Maresuke Shiraishi for useful discussions and helpful comments about theoretical and numerical technique. My thesis studies are accomplished owing to innumerable discussions with them.

I thank staff members of Cosmology Group in the Nagoya University, Hiroyuki Tashiro, Atsushi Nishizawa, Yuko Urakawa, Sachiko Kuroyanagi, Kenji Hasegawa, and Daisuke Nitta for scientific discussions. I also thank all students of Cosmology Group, especially the same period students Shinsuke Asaba and Daichi Kashino, for scientific and non-scientific communications. In particular, I should express my gratitude to the secretary of Cosmology Group, Hitomi Tanaka, for supports of our office works. Owing to her great kindness, I can dedicate my Ph.D. life to my thesis studies.

I have been supported by a Grant-in-Aid for Japan Society for the Promotion of Science (JSPS) Research under Grant No. 14J00063 for three years. I also acknowledge the Kobayashi-Maskawa Institute for the Origin of Particles and the Universe, Nagoya University, for providing useful computing resources for accomplishing my thesis studies.

Finally, I would like to be grateful to my family for their continuous encouragement in my life.

Contents

1	Intr	oductio	on	1		
	1.1	Gener	al Introduction	1		
		1.1.1	Background Cosmology	1		
		1.1.2	Linear Perturbation Theory	2		
		1.1.3	Cosmological Seed	3		
		1.1.4	Scalar, Vector, and Tensor Modes	4		
		1.1.5	Gravitational Waves—Tensor Mode	4		
		1.1.6	Minor Mode—Vector Mode	5		
	1.2	Secon	d Order Perturbation Theory	6		
		1.2.1	History and Development	6		
		1.2.2	Example—Second-Order Tensor Mode	8		
	1.3	This T	Thesis	9		
		1.3.1	Aim of This Thesis—Second-Order Vector Mode	9		
		1.3.2	Structure of This Thesis	10		
	Refe	rences		10		
2	Basi	cs of C	Cosmological Perturbation Theory	15		
	2.1		, Vector, and Tensor Decomposition	16		
	2.2	Einste	in Equation	18		
		2.2.1	Einstein Tensor	18		
		2.2.2	Energy-Momentum Tensor	21		
	2.3	Boltzr	mann Equation—Basics	26		
	2.4	Boltzmann Equation—Streaming Term				
	2.5			30		
		2.5.1	Lorentz Invariant Volume	31		
		2.5.2	Scattering Amplitude	31		
		2.5.3	Delta Function	32		
		2.5.4	Distribution Function of Electrons	33		
		2.5.5	Summary of Collision Terms (q'-Integral)	34		

xii Contents

		2.5.6 Collision Term $(q$ - and p' -Integral)	35				
		2.5.7 Perturbed Boltzmann Equation	38				
	2.6	Nonrelativistic Particles	41				
		2.6.1 Zeroth Moment—Continuity Equation	42				
		2.6.2 First Moment—Euler Equation	44				
	2.7	Example—Vector Mode	45				
		2.7.1 Vector-Mode Einstein Equation	45				
		2.7.2 Vector-Mode Boltzmann Equation	46				
		2.7.3 Configuration in Fourier Space	49				
	Refe	rences	50				
3	Generation of Magnetic Fields						
	3.1	Introduction	53				
	3.2	Harrison Mechanism	56				
	3.3	Results: Cosmological Magnetic Fields	60				
	0.0	3.3.1 Evolutions of Magnetic Fields	61				
		3.3.2 Spectra of Magnetic Fields	62				
			65				
		3.3.4 Nonhelical Magnetic Fields	67				
	3.4	Conclusion	68				
		ences	70				
4	Was	k Lensing	75				
•	4.1	Introduction	75 75				
	4.2	Formulation of Weak Lensing	77				
	7.2	4.2.1 Preliminary	78				
		4.2.2 CMB Lensing	81				
		4.2.3 Cosmic Shear	86				
	4.3	Models: Parity-Odd Signals	91				
	4.5	4.3.1 Second-Order Vector Mode—Numerical Descriptions	91				
		4.3.2 Second-Order Vector Mode—Analytical Descriptions	93				
		4.3.3 Tensor Modes	93				
		4.3.4 Comparison of Each Model	99				
	4.4	Results and Discussions	99				
	4.4		99 103				
			103				
5		6	107				
	5.1		107				
	5.2	č	801				
			109				
		1 · · · · · · · · · · · · · · · · · · ·	111				
			113				
		5.2.4 Perturbed Equation	14				

Contents xiii

		5.2.5	Evolution of the Spin Temperature	117				
		5.2.6	Evolution of the Gas Temperature	119				
	5.3	Result	s and Discussions	122				
		5.3.1	21 cm Lensing Curl Mode	122				
		5.3.2	Detectability and Discussions	125				
	5.4	Conclu	asion	126				
	Refe	rences		127				
6	Summary of This Thesis							
Appendix A: Riemannian Geometry								

Chapter 1 Introduction

Abstract Recent development of various cosmological observations plays an important role in establishing the standard cosmology. Here, the standard cosmology means the theory that the universe begins with the extreme high temperature, called the hot big-bang model, and with the initial conditions seeded in the inflationary era. The universe based on the standard cosmology contains a dark energy, dark matters, and baryons. In this section, we introduce the history and development of the cosmological perturbation theory and clarify the standpoint of this thesis.

Keywords Cosmological perturbation theory · Cosmic microwave background radiation · Non-gaussianity

1.1 General Introduction

1.1.1 Background Cosmology

When we study the universe as a target of physics, we follow the cosmological principle. The cosmological principle says that the universe is homogeneous and isotropic only on sufficiently large scales. Although the cosmological principle is correct only on large scales, it can explain the universe well on sufficiently large scales. By applying the cosmological principle to the general relativity, the evolution of the universe can be expressed only by one time-dependent parameter, i.e., the scale factor. As a result, the universe is no longer static, but dynamic. A. Einstein originally introduced a cosmological constant to realize the static universe. However, the Hubble's law was found in 1929 [1]. We could confirm the expansion of the universe from the Hubble's law and subsequently, the static universe was denied. (Note that, although Lemeître has discovered the same law in 1927, the expansion law of the universe was not named the Lemeître's law. This is because Lemeître reported the discovery of the expansion in the minor journal written in French [2].)

Moreover, A. A. Penzias and R. W. Wilson accidentally discovered the cosmic microwave background (CMB) in 1965 [3]. The temperature of the CMB is the same everywhere with an almost black body spectrum. This result shows the universe

2 1 Introduction

is isotropic. The discovery of the CMB also supports the hot big-bang universe. Nowadays, the fact of the hot big-bang universe reaches the consensus. The Hubble constant, namely the current expansion speed of the universe, is determined with 5-10% statistical accuracy.

1.1.2 Linear Perturbation Theory

Although the cosmological principle is correct on large scales, we can trivially see that the universe is not locally isotropic, e.g., there exist the distribution of galaxies, the CMB fluctuations, and so on. In order to explain the observed inhomogeneous and anisotropic universe, we use the perturbation theory in the standard cosmology, that is, the cosmological perturbation theory.

In 1946, E. Lifshitz introduced the linear perturbation to the homogeneous and isotropic universe for the first time [4]. The analysis performed by E. Lifshitz contained some misunderstandings due to the lack of the knowledge about the relativistic cosmology. Afterward, E. Lifshitz and I. Khalatnikov corrected the previous study with more detailed analysis in 1963 [5]. The early studies of the cosmological perturbation theory focus on the structure formation of the universe, corresponding to the density fluctuations on super-horizon scales. This is because, we have been able to observe the cosmological perturbations only through the distribution of galaxies before discovering the CMB anisotropy. Although the relativistic cosmological perturbation theory has been gradually developed, there was a little understanding about the gauge choice. There is uncertainty of the global coordinate choice how we determine the background universe. This freedom of the coordinate choice is called the gauge degrees of freedom. According to the freedom of the coordinate choice, the solution of the cosmological perturbations on super-horizon scales includes the unphysical degrees of freedom. In Ref. [4], Lifshitz had worked in the synchronous gauge, in which a gauge mode appears as an unphysical solution due to the gauge freedom. Many studies tackled to remove the unphysical degrees of freedom. For example, in 1967, E. R. Harrison found that when we work in the Newtonian gauge, there is no residual gauge freedom [6]. Furthermore, Bardeen [7] in 1980 and Kodama and Sasaki [8] in 1984 developed a formalism which does not depend on the gauge choice, i.e., the gauge-invariant cosmological perturbation theory. These studies provide understandings about the linear-order cosmological perturbation theory. Owing to the above studies, when we perform the cosmological perturbation theory, we need to treat carefully about the gauge choice or to formulate by using the gauge-invariant variables.

During the advance of the cosmological perturbation theory to explain the density perturbation, P. J. E. Peebles and J. T. Yu applied the cosmological perturbation theory to the CMB physics in 1970 [9]. They discussed the evolution of the adiabatic perturbations in the hot big-bang model and estimated the contribution of the adiabatic perturbations on the CMB temperature fluctuations. That was the first result to give the numerical calculation of the realistic universe including photons and

1.1 General Introduction 3

baryons. Compared with the detection of the CMB fluctuations in 1992 by COBE satellite [10], this early study would be the pioneering work. As some observations show the evidence of cold dark matters, e.g., the measurements of galaxy rotation curves [11], the cosmological perturbation theory included the dark matter component in 1984 [12, 13]. Moreover, many studies have developed the theory for CMB fluctuations from qualitative and quantitative aspects as follows. R. K. Sachs and A. M. Wolfe succeeded to estimate the contribution of the gravitational potential on the CMB temperature fluctuation [14], what we call the Sachs-Wolfe effect. The Sachs-Wolfe effect is caused by the gravitational redshift. J. Silk found that the CMB fluctuation is exponentially suppressed due to the diffusion of photons during the epoch of recombination [15]. According to an analytic approach provided by W. Hu and N. Sugiyama in 1995 [16], the features of the CMB fluctuation was well understood. These pioneering works and observations bring us to the discovery of the inhomogeneous and anisotropic universe.

The discovery phase of the CMB anisotropy study is currently almost finished. By using the state-of-the-art observations, the new era of precision cosmology has begun. We can subsequently acquire rich information about the nature of the universe. At the moment, we can measure several cosmological observations with a high precision, for example, the CMB temperature anisotropy, CMB E-mode polarization, galaxy clustering, etc., [17–20]. However, even if the cosmological observation becomes high precision measurement, we know only about the information of the linear-order scalar mode. Our knowledge of the standard cosmology would be only the tip of the iceberg.

1.1.3 Cosmological Seed

In the previous subsection, the seed of fluctuations is not mentioned. In the standard cosmology, we believe that the scalar mode is generated in the inflationary epoch from the quantum fluctuations of the scalar field, called the inflaton, which drives the accelerating expansion at the early stage of the universe. The inflationary scenario can not only resolve the problems of the standard big-bang model (i.e., the Horizon problem, monopole problem, and flatness problem) but also generate the seed of fluctuations.

In the very early universe with accelerating expansion, the physical law is obeyed by the unknown model of particle physics which can explain the physics of the Planck scale. Although the Planck scale physics has not been build yet, we can study the inflation mechanism phenomenologically by introducing the scalar field. Following the cosmological principle, the universe does not have the particular direction. We therefore assign the scalar field as the source of the accelerating expansion. Note that, however, the observational evidence of the scalar field has not been existed until the discovery of the scalar particle with spin-0 by CERN in 2013 [21, 22]. Although it is known that the Higgs inflation model cannot work, the detection of the scalar particle

4 1 Introduction

is highly suggestive for the inflation driven by the scalar field. Thus, the origin of cosmological perturbations would be a key probe for the particle physics.

1.1.4 Scalar, Vector, and Tensor Modes

In the context of the cosmological perturbation theory, we can decompose the perturbations into the scalar, vector, and tensor modes with respect to the rotational symmetry. As long as we work in the linear-order perturbation theory, each mode evolves independently. In the universe, the dominant mode is the scalar one. For example, the CMB temperature fluctuations are explained by the scalar mode. As we stressed before, it has been succeeded to explain many phenomena by only the scalar mode, but the vector and tensor modes. The liner-order scalar mode brings the success of the precision cosmology. Under the current situation of cosmological observations, where should we go next? One of the directions would be focusing on the vector and tensor modes. Although the vector and tensor modes have not been detected yet, the strong support for the tensor mode appeared in 1975 and 2015. The introduction of the tensor mode is shown in the next section.

1.1.5 Gravitational Waves—Tensor Mode

In the context of the cosmological perturbation theory, the degrees of freedom of gravitational waves (GWs) correspond to the tensor mode. The detection of GWs has been the key subject to confirm accuracy of general relativity, that is, the standard model of cosmology.

As soon as the completion of general relativity by Einstein in 1916, GWs were predicted as waves propagating in the space-time with the light velocity. The first indirect detection of GWs was done by R. A. Hulse and J. H. Taylor in 1975 [23]. They found that the orbital period of the binary pulser (PSR B1913+16) is decreasing. Accounting for the decreasing rate of the orbital period due to emissions of GWs, they estimated the energy decreasing rate of the binary pulser. The decreasing rate of the orbital period determined from general relativity can completely explain the observed data. In this way, GWs were indirectly observed and used to test general relativity [24, 25]. Note that the binary pulser PSR B1913+16 is currently called the Hulse-Taylor binary.

After the indirect detection of GWs by observing the Hulse-Taylor binary in 1975, the next target of the GWs observation becomes the direct detection. While many observations attempt to detect GWs emitted from astronomical events for a long time, we had not been able to detect GWs directly. This is because the amplitude of GWs is extremely small. However, at last in 2015 (last year), it was reported that GWs are directly detected by the Laser Interferometer Gravitational-Wave Observatory (LIGO) team [26]. This detected first GWs source was named

1.1 General Introduction 5

GW150914. GW150914 confirms general relativity and is the first direct evidence of GWs. GW150914 is the signal from the binary black hole merger with masses of about 35 times and 30 times the mass of the Sun and subsequently releases the energy as GWs about 3 times the mass of Sun. Owing to this event, we can also give a strong constraint on general relativity [27, 28]. Thus, the era of gravitational wave astronomy begins. Further ground- and space-based observations of GWs are planned, such as, eLISA [29], BBO [30], and KAGRA [31]. We expect that many events related to the GW emission would be observed in the near future.

Some observations have the sensitivity to GWs originated from not astronomical events but a primordial origin, that is, primordial gravitational waves. In the inflationary era, we expect that GWs are also generated from the quantum fluctuations of the space-time metric, and it is called primordial GWs. In principle, it is possible to confirm the existence of primordial GWs by using the CMB B-mode polarization [32, 33]. However, the amplitude of primordial GWs strongly depends on the inflation models, e.g., the potential of the inflaton, the interaction of the inflaton, and so on. The simplest inflation model: the single-field slow-roll inflation, is expected to result in a small amplitude of primordial GWs. Therefore, even in the state-of-the-art observations, we have not caught any hint of primordial GWs yet [34–38]. The detection of primordial GWs will become a next breakthrough since primordial GWs can directly relate to the inflation mechanism, that is, the high energy physics.

Although the CMB fluctuations are the strong probe to study the high energy physics, we cannot see the universe beyond the CMB last scattering surface. On the other hand, primordial GWs are transparent rather than CMB photons even if the universe is in the hot plasma. Therefore, the observation of primordial GWs is the quite important subject to seek the early universe.

1.1.6 Minor Mode—Vector Mode

Contrary to the scalar and tensor modes, the vector mode is quite unusual. The vector mode is never generated in the inflationary era if we assume the inflation model driven by the scalar field. Even if the vector mode is generated in the inflationary era by introducing some new interactions between the scalar and vector sectors, after all, the vector mode must decay with the expansion of the universe. In many literatures of the cosmological perturbation theory, therefore they has not been regarded the vector mode as an important one. However, as well as the tensor mode, the vector mode leads to the characteristic signal in the cosmological observations, e.g., the CMB B-mode polarization. Furthermore, some inflation models or exotic matters generate not only the tensor mode but also the vector mode. The vector mode can become the probe of beyond the standard cosmology.

In the linear perturbation theory, the vector mode never arises. If we expand the cosmological perturbation up to the second order, the scalar, vector and tensor modes are no longer independent modes. Because of the mode coupling among scalar, vector, and tensor perturbations, the product of two first-order scalar perturbations 6 1 Introduction

can induce the vector and tensor perturbations at second-order. The worth of the second-order cosmological perturbation theory is not only in the improvement of accuracy of the theory but also in the appearance of new effects which do not arise in the first-order cosmological perturbation theory, such as, the second-order vector and tensor modes. In this thesis, we focus on the second-order vector mode from the coupling of first-order scalar modes. Before moving the introduction of the second-order vector mode, we see the history of the second-order cosmological perturbation theory in the following sections.

1.2 Second Order Perturbation Theory

1.2.1 History and Development

Here, we review the history and development of the second-order cosmological perturbation theory. The standard cosmology is based on the Einstein equation and Boltzmann equation, i.e., the Einstein-Boltzmann system. The Einstein and Boltzmann equations provide the evolutions of the space-time metric and of the fluid components, respectively, and which coevolve. The full treatment of this system is quite difficult and some earlier studies focus on estimating the part of contributions. J. P. Ostriker and E. T. Vishniac estimate the second-order effects on the CMB temperature fluctuation in 1986 [39], what is called the Ostriker-Vishniac effect. After the reionization epoch, the density perturbation of free electrons generated by the reionization and CMB photons interact with each other due to the inverse Compton scattering. According to this process, the energy of free electrons turns into the energy of CMB photons. J. P. Ostriker and E. T. Vishniac found that the second-order CMB temperature fluctuations generated by the inverse Compton scattering is larger than the primary one around $\theta \sim 1'$ scales. Although the second-order fluctuations have been believed to be smaller than the primary fluctuations, they found that the second-order fluctuations can dominate on small scales. This is because the Silk damping washes out the primary fluctuations on small scales.

The Ostriker-Vishniac effect is only a part of the effects of the second-order CMB fluctuations. Further studies have shown the other contributions on the second-order CMB fluctuations. In 1994, W. Hu et al. derived the full second-order CMB fluctuation induced from the scattering between photons and electrons without the polarization of photons [40]. Although the interaction terms between photons and electrons up to the second order are quite complicated, they gave interpretations of each contribution. Furthermore, they estimated the CMB temperature fluctuation coming from the most dominant term. Before performing this study, we cannot deny the possibility that the Ostriker-Vishniac effect cancels out with other second-order terms. However, W. Hu et al. showed that the Ostriker-Vishniac does not vanish even if we consider all second-order terms.

The above study focused on only the interaction term between photons and electrons. However, we should provide second-order gravitational effects to complete the second-order perturbation theory. In the early 2000s, the second-order Einstein-Boltzmann system has been well studied including second-order gravitational terms [41–44]. In particular, not only the Boltzmann equation for photons but also that for baryons and dark matters was formulated up to the second order. Although the effect of the gravitational lensing was also formulated with the unified treatment, it has been known that the gravitational lensing induces the CMB B-mode polarization which becomes the noise to detect primordial GWs. Therefore, the formulation of the gravitational lensing had been performed independently as the remapping approach to calculate the angular power spectrum of CMB B-mode polarizations induced by the gravitational lensing in 2000 [45].

The formulation of the second-order Einstein-Boltzmann system has been progressed by including the polarization of photons into the Compton scattering term [46–49]. These formulations allow us to compute the second-order CMB fluctuations including polarizations of photons. However, there is a difficulty of the numerical calculation. In the first-order perturbation theory, in order to calculate the angular power spectrum of CMB fluctuations, we can use the line-of-sight integration developed by U. Seljak in 1996 [50]. This formula can powerfully reduce the cost of numerical calculations. On the other hand, this formula is no longer available in the second-order perturbation theory. Related to the fact, the theoretical aspect of the second-order CMB fluctuations has been developed. For example, some formulae to reduce the numerical cost are proposed, e.g., the transport operator formalism by Fidler et al. [51] and the curve-of-sight formalism by Saito et al. [52]. These formalisms correspond to the second-order version of the line-of-sight integration in the first-order perturbation theory.

The gauge dependence of the second-order perturbation theory was quite non-trivial. For example, although the first-order tensor mode is a gauge invariant variable itself, the second-order tensor mode depends on the gauge choice. A. Naruko et al. showed the gauge-invariant Boltzmann equation up to the second order in Ref. [53]. Owing to these efforts, it is possible to estimate the CMB B-mode polarization from the second-order vector and tensor modes. The current estimation shows that the CMB B-mode polarization from the second-order vector and tensor modes is negligibly small. The amplitude of the second-order CMB B-mode polarization is recast as the tensor-to-scalar ratio as $r \approx 10^{-7} \sim 10^{-6}$ [49, 54, 55]. From this result, we can conclude that the second-order CMB B-mode polarization from the second-order vector and tensor modes would not affect in the future observations.

There is another interesting topic about the second-order perturbation theory, what is called the intrinsic bispectrum. The Gaussianity of primordial fluctuations is quite important to constrain the inflation model. The simplest inflation model, i.e., the single-field slow-roll inflation, predicts almost Gaussian fluctuations [56]. Contrary to the single-field slow-roll inflation, some exotic models result in non-Gaussian fluctuations due to the non-linearity of the interaction terms in the Lagrangian [57]. We can explore the non-Gaussianity of fluctuations by using the bispectrum as a cosmological probe. When the nature of fluctuations is non-Gaussian, the bispectrum

8 1 Introduction

has a non-zero value. If we believe the simplest inflation model, fluctuations generated in the inflationary era are almost Gaussian. The current CMB observations show that the non-Gaussian signature is consistent with zero [58]. Therefore, the single-field slow-roll inflation is well motivated from the observation of the CMB bispectrum. However, even if the primordial non-Gaussianity is absent, the second-order perturbations induce the intrinsic non-Gaussianity (or the intrinsic bispectrum) in the CMB bispectrum due to the non-linear evolution of the fluctuations. D. Nitta et al. estimated the intrinsic non-Gaussianity from the coupling of first-order scalar modes in 2009 [43]. They showed that the intrinsic bispectrum has a peak at the shape of the local-type non-Gaussianity. Furthermore, the other second-order effects were included in the calculation of the intrinsic non-Gaussianity by Pettinari [59]. The intrinsic bispectrum has been currently constructed.

Thus, the second-order perturbation theory has been applied to the CMB fluctuations in many respects. Here, we would strongly stress that the above developments of the second-order perturbation theory are just for the CMB fluctuations. Many phenomena from the second-order perturbation theory, not limited for the CMB fluctuations, should be paid attention complementarily.

1.2.2 Example—Second-Order Tensor Mode

The second-order tensor mode is a good example to see further applications of the second-order perturbation theory. Although the signal of the second-order tensor mode is imprinted on the CMB B-mode polarization, we can also observe the second-order tensor mode as second-order GWs. Even if the primordial GWs have negligible amplitude, the second-order GWs must appear from the non-linear coupling of the scalar modes. Estimation of the second-order GWs has been well studied as follows [60–64].

On the horizon scales at the matter-radiation equality, the amplitude of the second-order GWs exceeds that of primordial GWs with the tensor-to-scalar ratio $r\approx 0.1$ at the present time. On small scales, second-order GWs have larger amplitude than primordial GWs with $r\lesssim 10^{-4}$. According to this fact, second-order GWs become relevant in direct detection experiments, e.g., DECIGO [65] and the atomic gravitational wave interferometric sensors [66]. By using these future experiments, second-order GWs would be expected to be observed directly. Thus, we can test the standard cosmology complementarily not limited CMB fluctuations.

Before closing this section, we emphasize again that the second-order perturbation theory does not have free parameters since second-order perturbations are induced from the first-order scalar modes which are well determined by the current cosmological observations.

1.3 This Thesis 9

1.3 This Thesis

1.3.1 Aim of This Thesis—Second-Order Vector Mode

Under the above mentioned history, we focus on cosmological probes induced from the second-order vector mode except for the CMB fluctuations in this thesis. The second-order scalar and tensor modes have been studied well because these first-order modes have been paid much attention. On the other hand, there has been less interest in the cosmological vector mode. We explore the second-order vector mode by using the cosmological probes throughout this thesis.

We should be careful to choose the observable to explore the (second-order) vector mode. For example, the CMB temperature fluctuation and E-mode polarization are dominated by the first-order scalar mode. In order to obtain the pure effect of the second-order vector mode, we need to focus on appropriate observables like the CMB B-mode polarization which only coming from not the scalar but vector and tensor modes. Due to the above reason, we mainly tackle three observables to reveal the role of the second-order vector mode in the context of the observational cosmology [67–69].

First, we study the generation of cosmological magnetic fields. The origin of magnetic fields with large coherent length, called cosmological magnetic fields, has been an open question, although many models are proposed to generate magnetic fields. In the first-order perturbation theory, magnetic fields never arise from the standard cosmology. On the other hand, it is possible to lead cosmological magnetic fields by expanding perturbations up to the second order. We consider the generation mechanism from the second-order perturbation theory.

Second, photons emitted from the CMB last scattering surface and galaxies are deflected by foreground perturbations including the scalar, vector, and tensor modes, called CMB lensing and cosmic shear, respectively. The CMB lensing and cosmic shear induced from the scalar mode are well studied by current observations. On the other hand, the vector and tensor modes result in the characteristic signature in the deflection angle of emitted photons from each source. Analysis of the second-order vector or tensor mode in the weak lensing has not been studied yet. We give the predictions of weak lensing signal from the second-order perturbation theory and discuss the detectability of these signals by assuming ongoing and forthcoming experiments.

Third, we focus on the 21 cm photons emitted by a neutral hydrogen atom. Physical mechanism is the same as the CMB lensing but different from the luminous source. Before the reionization, there are large amount of neutral hydrogen atoms which emit photons due to the hyperfine structure, what we call the 21 cm radiation. 21 cm photons are also deflected and therefore they induce the weak lensing signals, i.e., the 21 cm lensing. In spite that we have not observed the 21 cm radiation yet, it is important to discuss the detectability and meaning of outcomes before the 21 cm observations launch. This study makes us possible to access more precision cosmology.

10 1 Introduction

1.3.2 Structure of This Thesis

This thesis is organized as follows. In Chap. 2, we review the cosmological perturbation theory up to the second order. Since the first-order perturbation theory in the standard cosmology is well established by many authors, we do not discuss the details in this thesis. We formulate the perturbed Einstein and Boltzmann equations up to the second order. The scalar, vector, and tensor decomposition is performed. In Chap. 3, we apply the second-order vector mode to the generation of cosmological magnetic fields. In order to generate cosmological magnetic fields, we rely on the Harrison mechanism in the primordial plasma. We also review the Harrison mechanism based on the Boltzmann equations for electrons, protons, and photons. Finally, we show the magnetic power spectrum at cosmological recombination. In Chap. 4, in order to formulate the weak lensing signal, we need to solve the perturbed geodesic equation and the geodesic deviation equation for the CMB lensing and cosmic shear, respectively. By using the parity symmetry, we can decompose the lensing signals into the parityeven and parity-odd signal. The parity-odd signal is coming only from the vector and tensor modes. We provide the parity-odd signal from the second-order vector and tensor modes. Furthermore, we discuss the detectability of the second-order vector and tensor modes in the weak lensing experiments. In Chap. 5, we discuss the 21 cm radiation in the dark ages. We formulate the Boltzmann equation for the 21 cm photons and derive the 21 cm angular power spectrum. We apply the 21 cm signal to the weak lensing effect and discuss the detectability of the second-order vector mode in the 21 cm lensing experiments. In Chap. 6, in order to close this thesis, we conclude the role of the second-order vector mode in the context of the observational cosmology. Moreover, we also devote the future direction and possibility of the presented studies.

References

- E. Hubble, A relation between distance and radial velocity among extra-galactic nebulae. Proc. Natl. Acad. Sci. 15, 168–173 (1929)
- 2. M. Livio, Lost in translation: mystery of the missing text solved. Nature 479, 171 (2011)
- 3. A.A. Penzias, R.W. Wilson, A measurement of excess antenna temperature at 4080 Mc/s. APJ 142, 419–421 (1965)
- E. Lifshitz, On the gravitational stability of the expanding universe. J. Phys. (USSR) 10, 116 (1946)
- E. Lifshitz, I. Khalatnikov, Investigations in relativistic cosmology. Adv. Phys. 12, 185–249 (1963)
- E.R. Harrison, Normal modes of vibrations of the universe. Rev. Mod. Phys. 39, 862–882 (1967)
- 7. J.M. Bardeen, Gauge-invariant cosmological perturbations. Phys. Rev. 22, 1882–1905 (1980)
- H. Kodama, M. Sasaki, Cosmological perturbation theory. Progress Theor. Phys. Suppl. 78, 1 (1984)
- P.J.E. Peebles, J.T. Yu, Primeval adiabatic perturbation in an expanding universe. APJ 162, 815 (1970)

G.F. Smoot, C.L. Bennett, A. Kogut, E.L. Wright, J. Aymon, N.W. Boggess, E.S. Cheng, G. de Amici, S. Gulkis, M.G. Hauser, G. Hinshaw, P.D. Jackson, M. Janssen, E. Kaita, T. Kelsall, P. Keegstra, C. Lineweaver, K. Loewenstein, P. Lubin, J. Mather, S.S. Meyer, S.H. Moseley, T. Murdock, L. Rokke, R.F. Silverberg, L. Tenorio, R. Weiss, D.T. Wilkinson, Structure in the COBE differential microwave radiometer first-year maps. APJ 396, L1–L5 (1992)

- V.C. Rubin, W.K. Ford Jr., Rotation of the andromeda nebula from a spectroscopic survey of emission regions. APJ 159, 379 (1970)
- J.R. Bond, G. Efstathiou, Cosmic background radiation anisotropies in universes dominated by nonbaryonic dark matter. APJ 285, L45–L48 (1984)
- N. Vittorio, J. Silk, Fine-scale anisotropy of the cosmic microwave background in a universe dominated by cold dark matter. APJ 285, L39–L43 (1984)
- R.K. Sachs, A.M. Wolfe, Perturbations of a cosmological model and angular variations of the microwave background. APJ 147, 73 (1967)
- 15. J. Silk, Cosmic black-body radiation and galaxy formation. APJ 151, 459 (1968)
- W. Hu, N. Sugiyama, Anisotropies in the cosmic microwave background: an analytic approach. Astrophys. J. 444, 489–506 (1995), arXiv:astro-ph/9407093
- 17. S.D.S.S. Collaboration, M. Tegmark et al., Cosmological constraints from the SDSS luminous red galaxies. Phys. Rev. D 74, 123507 (2006), arXiv:astro-ph/0608632
- W.M.A.P. Collaboration, G. Hinshaw et al., Nine-Year Wilkinson Microwave Anisotropy Probe (WMAP) observations: cosmological parameter results. Astrophys. J. Suppl. 208, 19 (2013), arXiv:1212.5226
- A.G. Sanchez et al., The clustering of galaxies in the SDSS-III Baryon Oscillation Spectroscopic Survey: cosmological implications of the full shape of the clustering wedges in the data release 10 and 11 galaxy samples. Mon. Not. Roy. Astron. Soc. 440(3), 2692–2713 (2014), arXiv:1312.4854
- P.A.R. Ade, Planck Collaboration et al., Planck 2015 results. XIII. Cosmological parameters. Astron. Astrophys. 594, A13 (2016), arXiv:1502.01589
- C.M.S. Collaboration, S. Chatrchyan et al., Observation of a new boson at a mass of 125 GeV with the CMS experiment at the LHC. Phys. Lett. B 716, 30–61 (2012), arXiv:1207.7235
- ATLAS Collaboration, G. Aad et al., Observation of a new particle in the search for the Standard Model Higgs boson with the ATLAS detector at the LHC. Phys. Lett. B 716, 1–29 (2012), arXiv:1207.7214
- 23. R.A. Hulse, J.H. Taylor, Discovery of a pulsar in a binary system. APJ 195, L51-L53 (1975)
- J.H. Taylor, J.M. Weisberg, A new test of general relativity-ravitational radiation and the binary pulsar PSR 1913+16. APJ 253, 908–920 (1982)
- 25. J.M. Weisberg, J.H. Taylor, Relativistic binary pulsar B1913+16: thirty years of observations and analysis. ASP Conference Series, vol. 328 (2005), p. 25, arXiv:astro-ph/0407149
- Virgo, LIGO Scientific Collaboration, B.P. Abbott et al., Observation of gravitational waves from a binary black hole merger. Phys. Rev. Lett. 116(6), 061102 (2016), arXiv:1602.03837
- 27. Virgo, LIGO Scientific Collaboration, B.P. Abbott et al., Tests of general relativity with GW150914. Phys. Rev. Lett. 116(22), 221101 (2016), arXiv:1602.03841
- Virgo, LIGO Scientific Collaboration, B.P. Abbott et al., Observing gravitational-wave transient GW150914 with minimal assumptions. Phys. Rev. D 93(12), 122004 (2016), arXiv:1602.03843. Addendum: Phys. Rev. D 94(6), 069903 (2016)
- P. Amaro-Seoane, S. Aoudia, S. Babak, P. Binetruy, E. Berti et al., eLISA/NGO: Astrophysics and cosmology in the gravitational-wave millihertz regime. GW Notes 6, 4–110 (2013), arXiv:1201.3621
- J. Crowder, N.J. Cornish, Beyond LISA: exploring future gravitational wave missions. Phys. Rev. D 72, 083005 (2005), arXiv:gr-qc/0506015
- KAGRA Collaboration Collaboration, K. Somiya, Detector configuration of KAGRA: the Japanese cryogenic gravitational-wave detector. Class. Quant. Grav. 29, 124007 (2012), arXiv:1111.7185
- 32. M. Kamionkowski, A. Kosowsky, A. Stebbins, Statistics of cosmic microwave background polarization. Phys. Rev. D 55, 7368–7388 (1997), arXiv:astro-ph/9611125

12 1 Introduction

33. M. Zaldarriaga, U. Seljak, An all sky analysis of polarization in the microwave background. Phys. Rev. D 55, 1830–1840 (1997), arXiv:astro-ph/9609170

- 34. B. Reichborn-Kjennerud, A.M. Aboobaker, P. Ade, F. Aubin, C. Baccigalupi et al., EBEX: a balloon-borne CMB polarization experiment, arXiv:1007.3672
- QUIET Collaboration Collaboration, D. Samtleben, Measuring the cosmic microwave background radiation (CMBR) polarization with QUIET. Nuovo Cim. B 122, 1353–1358 (2007), arXiv:0802.2657
- W.M.A.P. Collaboration, C.L. Bennett et al., Nine-Year Wilkinson Microwave Anisotropy Probe (WMAP) observations: final maps and results. Astrophys. J. Suppl. 208, 20 (2013), arXiv:1212.5225
- QUaD collaboration Collaboration, M. Brown et al., Improved measurements of the temperature and polarization of the CMB from QUaD. Astrophys. J. 705, 978–999 (2009), arXiv:0906.1003
- H. Chiang, P. Ade, D. Barkats, J. Battle, E. Bierman et al., Measurement of CMB polarization power spectra from two years of BICEP data. Astrophys. J. 711, 1123–1140 (2010), arXiv:0906.1181
- 39. J.P. Ostriker, E.T. Vishniac, Generation of microwave background fluctuations from nonlinear perturbations at the ERA of galaxy formation. APJ **306**, L51–L54 (1986)
- W. Hu, D. Scott, J. Silk, Reionization and cosmic microwave background distortions: a complete treatment of second order compton scattering. Phys. Rev. D 49, 648–670 (1994), arXiv:astro-ph/9305038
- 41. N. Bartolo, S. Matarrese, A. Riotto, The full second-order radiation transfer function for large-scale cmb anisotropies. JCAP **0605**, 010 (2006), arXiv:astro-ph/0512481
- 42. N. Bartolo, S. Matarrese, A. Riotto, CMB anisotropies at second-order. 2: analytical approach. JCAP **0701**, 019 (2007), arXiv:astro-ph/0610110
- D. Nitta, E. Komatsu, N. Bartolo, S. Matarrese, A. Riotto, CMB anisotropies at second order III: bispectrum from products of the first-order perturbations. JCAP 0905, 014 (2009), arXiv:0903.0894
- L. Senatore, S. Tassev, M. Zaldarriaga, Cosmological perturbations at second order and recombination perturbed. JCAP 0908, 031 (2009), arXiv:0812.3652
- 45. W. Hu, Weak lensing of the CMB: a harmonic approach. Phys. Rev. D 62, 043007 (2000), arXiv:astro-ph/0001303
- 46. C. Pitrou, The radiative transfer at second order: a full treatment of the boltzmann equation with polarization. Class. Quant. Grav. 26, 065006 (2009), arXiv:0809.3036
- 47. C. Pitrou, J.-P. Uzan, F. Bernardeau, The cosmic microwave background bispectrum from the non-linear evolution of the cosmological perturbations. JCAP **1007**, 003 (2010), arXiv:1003.0481
- 48. C. Pitrou, The radiative transfer for polarized radiation at second order in cosmological perturbations. Gen. Rel. Grav. 41, 2587–2595 (2009), arXiv:0809.3245
- 49. M. Beneke, C. Fidler, Boltzmann hierarchy for the cosmic microwave background at second order including photon polarization. Phys. Rev. D **82**, 063509 (2010), arXiv:1003.1834
- 50. U. Seljak, M. Zaldarriaga, A line of sight integration approach to cosmic microwave background anisotropies. Astrophys. J. **469**, 437–444 (1996), arXiv:astro-ph/9603033
- 51. C. Fidler, K. Koyama, G.W. Pettinari, A new line-of-sight approach to the non-linear Cosmic Microwave Background. JCAP1504(04), 037 (2015), arXiv:1409.2461
- R. Saito, A. Naruko, T. Hiramatsu, M. Sasaki, Geodesic curve-of-sight formulae for the Cosmic Microwave Background: a unified treatment of redshift, time delay, and lensing. JCAP 1410(10), 051 (2014), arXiv:1409.2464
- 53. A. Naruko, C. Pitrou, K. Koyama, M. Sasaki, Second-order Boltzmann equation: gauge dependence and gauge invariance. Class. Quant. Grav. 30, 165008 (2013), arXiv:1304.6929
- M. Beneke, C. Fidler, K. Klingmuller, B polarization of cosmic background radiation from second-order scattering sources. JCAP 1104, 008 (2011), arXiv:1102.1524
- C. Fidler, G.W. Pettinari, M. Beneke, R. Crittenden, K. Koyama, D. Wands, The intrinsic B-mode polarisation of the Cosmic Microwave Background. JCAP 1407, 011 (2014), arXiv:1401.3296

 J.M. Maldacena, Non-Gaussian features of primordial fluctuations in single field inflationary models. JHEP 0305, 013 (2003), arXiv:astro-ph/0210603

- E. Komatsu, D.N. Spergel, Acoustic signatures in the primary microwave background bispectrum. Phys. Rev. D 63, 063002 (2001), arXiv:astro-ph/0005036
- Planck Collaboration, P.A.R. Ade, N. Aghanim, M. Arnaud, F. Arroja, M. Ashdown, J. Aumont,
 C. Baccigalupi, M. Ballardini, A.J. Banday et al., Planck 2015 results. XVII. Constraints on
 primordial non-Gaussianity. Astron. Astrophys. 594, A17 (2016), arXiv:1502.01592
- 59. G.W. Pettinari, C. Fidler, R. Crittenden, K. Koyama, D. Wands, The intrinsic bispectrum of the Cosmic Microwave Background. JCAP 1304, 003 (2013), arXiv:1302.0832
- S. Mollerach, D. Harari, S. Matarrese, CMB polarization from secondary vector and tensor modes. Phys. Rev. D 69, 063002 (2004), arXiv:astro-ph/0310711
- 61. K.N. Ananda, C. Clarkson, D. Wands, The cosmological gravitational wave background from primordial density perturbations. Phys. Rev. D **75**, 123518 (2007), arXiv:gr-qc/0612013
- 62. H. Assadullahi, D. Wands, Constraints on primordial density perturbations from induced gravitational waves. Phys. Rev. D 81, 023527 (2010), arXiv:0907.4073
- D. Baumann, P.J. Steinhardt, K. Takahashi, K. Ichiki, Gravitational wave spectrum induced by primordial scalar perturbations. Phys. Rev. D 76, 084019 (2007), arXiv:hep-th/0703290
- S. Saga, K. Ichiki, N. Sugiyama, Impact of anisotropic stress of free-streaming particles on gravitational waves induced by cosmological density perturbations. Phys. Rev. D 91(2), 024030 (2015), arXiv:1412.1081
- N. Seto, S. Kawamura, T. Nakamura, Possibility of direct measurement of the acceleration of the universe using 0.1-Hz band laser interferometer gravitational wave antenna in space. Phys. Rev. Lett. 87, 221103 (2001), arXiv:astro-ph/0108011
- S. Dimopoulos, P.W. Graham, J.M. Hogan, M.A. Kasevich, S. Rajendran, Atomic gravitational wave interferometric sensor. Phys. Rev. D 78, 122002 (2008)
- 67. S. Saga, K. Ichiki, K. Takahashi, N. Sugiyama, Magnetic field spectrum at cosmological recombination revisited. Phys. Rev. D **91**(12), 123510 (2015), arXiv:1504.03790
- S. Saga, D. Yamauchi, K. Ichiki, Weak lensing induced by second-order vector mode. Phys. Rev. D 92(6), 063533 (2015), arXiv:1505.02774
- S. Saga, Observable cosmological vector mode in the dark ages. Phys. Rev. D 94(6), 063523 (2016), arXiv:1607.03973

Chapter 2

Basics of Cosmological Perturbation Theory

Abstract Although the cosmological principle is correct on large enough scales, observed universe is not trivially homogeneous and isotropic. According to the perturbation theory, we try to explain the inhomogeneous and anisotropic universe, that is, the cosmological perturbation theory. The cosmological perturbation theory is based on the Einstein-Boltzmann system. Therefore, we focus on the perturbed Einstein-Boltzmann system. In the background level, we introduce dark energy which causes the accelerating expansion at the present time. The relativistic and non relativistic fluids in the universe are assumed photons, massless neutrinos, baryons, and dark matters. Consequently, we obtain the second-order Einstein-Boltzmann system. In particular, as an example, we show the feature of the second-order vector perturbation.

Keywords Scalar, vector, and tensor decomposition Einstein-Boltzmann system • Cosmological vector mode

In this part, we review the cosmological perturbation theory up to the second order. Throughout this thesis, we work in the Poisson gauge (see e.g., [1]) whose metric is given by

$$ds^{2} = a^{2}(\eta) \left[-e^{2\Psi} d\eta^{2} + 2\omega_{i} d\eta dx^{i} + \left(e^{-2\Phi} \delta_{ij} + h_{ij} \right) dx^{i} dx^{j} \right], \qquad (2.1)$$

where the gauge conditions $\omega^{i}_{,i} = h^{ij}_{,j} = 0$ and the traceless condition $h^{i}_{i} = 0$ are imposed on ω_{i} and h_{ij} .

Owing to the gauge conditions and the traceless condition, ω_i and h_{ij} contain only the vector and tensor modes themselves, respectively. $a(\eta)$ is a scale factor and η is the conformal time which related to the cosmological time as $\mathrm{d}t = a\mathrm{d}\eta$. Note that a $\mathrm{dot} \ \dot{\Box}$ and a comma $\Box_{,i}$ denote the derivative with respect to the coordinate x^i and the conformal time η , respectively. Raising or lowering indices of perturbations are done by δ_{ij} .

The physical meanings of Ψ , Φ , ω_i , and h_{ij} are the perturbation of the time shift (what we call the lapse function or the Newtonian potential), that of the spacial volume, that of the displacement vector, and the anisotropy of the space, respectively. In this part, the definition of the Fourier transformation is as follows:

$$f(\mathbf{x}) = \int \frac{\mathrm{d}^3 \mathbf{k}}{(2\pi)^3} \tilde{f}(\mathbf{k}) e^{i\mathbf{k}\cdot\mathbf{x}} . \tag{2.2}$$

Note that throughout this part, we use the units in which $c = \hbar_{\rm pl} = 1$. We obey the rule that the subscripts and superscripts of the Greek characters and alphabets run from 0 to 3 and from 1 to 3, respectively.

Before performing the cosmological perturbation theory, we summarize the background universe. The spatially-flat Friedmann-Lemaître-Robertson-Walker metric in the conformal time is given by

$$ds^{2} = a^{2}(\eta) \left[-d\eta^{2} + dx^{2} \right]. \tag{2.3}$$

We assume the energy-momentum tensor in the homogeneous and isotropic universe as

$$T^{\mu}_{\ \nu} = \text{diag}(-\rho, p, p, p)$$
 (2.4)

Under the above condition and the Einstein equation with a cosmological constant, we determine the evolution of the scale factor and fluids as

$$\mathcal{H}^2 = \frac{8\pi G}{3} a^2 \sum_{i} \rho_i + \frac{a^2 \Lambda}{3} , \qquad (2.5)$$

$$\dot{\mathcal{H}} = -\frac{4\pi G}{3} a \sum_{i} (\rho_i + p_i) + \frac{a\Lambda}{3} , \qquad (2.6)$$

$$\dot{\rho}_i = -3\mathcal{H}(\rho_i + p_i) \,, \tag{2.7}$$

where $\mathcal{H} \equiv \dot{a}/a$. In the case of nonrelativistic particles, p=0 and relativistic particles, p=1/3. Here, we do not discuss the first-order perturbation theory since that is well discussed in large amount of previous studies.

2.1 Scalar, Vector, and Tensor Decomposition

In this section, we will see the scalar, vector, and tensor decomposition by using the difference of the rotational transformation. First of all, we define the polarization vector with respect to the unit wave vector \hat{k} as

$$\epsilon^{(\lambda)}(\hat{k}) = \frac{1}{\sqrt{2}} \left[\hat{e}_x(\hat{k}) + i\lambda \hat{e}_y(\hat{k}) \right], \qquad (2.8)$$

where $\lambda = \pm 1$ represents for the helicity states. Note that, for simplicity, the wave vector sets the same direction to the z-axis, namely, $k \parallel \hat{z}$. The polarization vector obeys following relations:

$$\hat{k}^a \epsilon_a^{(\lambda)}(\hat{k}) = 0 \,, \tag{2.9}$$

$$\epsilon_a^{(\lambda)*}(\hat{\boldsymbol{k}}) = \epsilon_a^{(-\lambda)}(\hat{\boldsymbol{k}}) = \epsilon_a^{(\lambda)}(-\hat{\boldsymbol{k}}),$$
 (2.10)

$$\epsilon_a^{(\lambda)}(\hat{k})\epsilon_a^{(\lambda')}(\hat{k}) = \delta_{\lambda, -\lambda'}$$
 (2.11)

Moreover, we also define the polarization tensor by using the polarization vector as

$$e_{ab}^{(\pm 2)}(\hat{k}) = -\sqrt{\frac{3}{2}} \epsilon_a^{(\pm 1)}(\hat{k}) \epsilon_b^{(\pm 1)}(\hat{k})$$
 (2.12)

According to the above definition, the polarization vector and tensor are transformed by the rotational transformation around the z-axis with the rotational angle ϕ as

$$\epsilon_a^{(\pm 1)}(\hat{\mathbf{k}}) \to \tilde{\epsilon}_a^{(\pm 1)}(\hat{\mathbf{k}}) = \epsilon_a^{(\pm 1)}(\hat{\mathbf{k}})\epsilon^{\pm i\phi}$$
, (2.13)

$$e_{ab}^{(\pm 2)}(\hat{k}) \to \tilde{e}_{ab}^{(\pm 2)}(\hat{k}) = e_{ab}^{(\pm 2)}(\hat{k})e^{\pm 2i\phi}$$
 (2.14)

The polarization vector and tensor are used to perform the scalar, vector, and tensor decomposition. We define the projection tensors for the mode decomposition by using the polarization vector and tensor as

$$O_a^{(0)}(\hat{k}) \equiv -i\hat{k}_a$$
, (2.15)

$$O_{ab}^{(0)}(\hat{k}) \equiv -\hat{k}_a \hat{k}_b + \frac{\delta_{a,b}}{3} ,$$
 (2.16)

$$O_a^{(\lambda)}(\hat{\mathbf{k}}) \equiv i \,\lambda \epsilon_a^{(\lambda)}(\hat{\mathbf{k}}) \,, \tag{2.17}$$

$$O_{ab}^{(\lambda)}(\hat{\mathbf{k}}) \equiv \frac{\lambda}{2} \left(\hat{k}_a \epsilon_b^{(\lambda)}(\hat{\mathbf{k}}) + \hat{k}_b \epsilon_a^{(\lambda)}(\hat{\mathbf{k}}) \right) , \qquad (2.18)$$

$$O_{ab}^{(\sigma)}(\hat{\mathbf{k}}) \equiv e_{ab}^{(\sigma)}(\hat{\mathbf{k}}) , \qquad (2.19)$$

where individual projection tensors of different modes are orthogonal by definition. By using the projection tensors defined in Eqs. (2.15)–(2.19), we define the scalar, vector, and tensor modes as

$$\omega_a(\mathbf{k}) = \omega_0(\mathbf{k}) O_a^{(0)}(\hat{\mathbf{k}}) + \sum_{\lambda = \pm 1} \omega_\lambda(\mathbf{k}) O_a^{(\lambda)}(\hat{\mathbf{k}}) , \qquad (2.20)$$

$$h_{ab}(\mathbf{k}) = h_{iso}(\mathbf{k})\delta_{a,b} + h_0(\mathbf{k})O_{ab}^{(0)}(\hat{\mathbf{k}}) + \sum_{\lambda = \pm 1} h_{\lambda}(\mathbf{k})O_{ab}^{(\lambda)}(\hat{\mathbf{k}}) + \sum_{\sigma = \pm 2} h_{\sigma}(\mathbf{k})O_{ab}^{(\sigma)}(\hat{\mathbf{k}}),$$
(2.21)

where ω_0 , $h_{\rm iso}$, and h_0 are corresponding to the scalar mode. ω_λ and h_λ are the vector mode. h_σ is the tensor mode. If we assume that ω_a and h_{ab} are the metric perturbations in the Poisson gauge, some variables vanish as $\omega_0 = h_{\rm iso} = h_0 = h_\lambda = 0$ due to the gauge conditions. In other word, ω_a and h_{ab} in the Poisson gauge include the vector and tensor modes only, respectively. By using the orthogonality of the projection

tensors, the inverses of the decompositions (2.20) and (2.21) can be given by

$$\omega_0(\mathbf{k}) = -O_a^{(0)}(\hat{\mathbf{k}})\omega_a(\mathbf{k}) , \qquad (2.22)$$

$$\omega_{\lambda}(\mathbf{k}) = O_a^{(-\lambda)}(\hat{\mathbf{k}})\omega_a(\mathbf{k}) , \qquad (2.23)$$

$$h_0(\mathbf{k}) = \frac{3}{2} O_{ab}^{(0)}(\hat{\mathbf{k}}) h_{ab}(\mathbf{k}) , \qquad (2.24)$$

$$h_{\lambda}(\mathbf{k}) = -2O_{ab}^{(-\lambda)}(\hat{\mathbf{k}})h_{ab}(\mathbf{k}),$$
 (2.25)

$$h_{\sigma}(\mathbf{k}) = \frac{2}{3} O_{ab}^{(-\sigma)}(\hat{\mathbf{k}}) h_{ab}(\mathbf{k}) . \tag{2.26}$$

2.2 Einstein Equation

In this subsection, we will see the perturbed Einstein equation up to the second order:

$$G^{(1,2)\mu}_{\ \nu} = 8\pi G T^{(1,2)\mu}_{\ \nu} \ .$$
 (2.27)

We need to know the first- and second-order Einstein tensor and energy-momentum tensor. Throughout this thesis, we ignore the first-order vector and tensor modes. This is because the vector mode never arise from the first-order perturbation theory in the standard cosmology. In addition, the first-order tensor mode would have a small amplitude, namely, tensor-to-scalar ratio $r \lesssim 0.12$ [2].

2.2.1 Einstein Tensor

First, we show the perturbation of the Einstein tensor which is in the left-hand side of the Einstein equation. The metric perturbations can be expanded as

$$\Phi = \Phi^{(1)} + \frac{1}{2}\Phi^{(2)} , \qquad (2.28)$$

$$\Psi = \Psi^{(1)} + \frac{1}{2}\Psi^{(2)} , \qquad (2.29)$$

$$\omega_i = \frac{1}{2}\omega_i^{(2)} \,, \tag{2.30}$$

$$h_{ij} = \frac{1}{2} h_{ij}^{(2)} \,. \tag{2.31}$$

It is convenient to move to Fourier space. Second-order terms can be written in Fourier space as

$$X(\mathbf{x})Y(\mathbf{x}) = \int_{\mathbf{k}} \tilde{X}(\mathbf{k}_1)\tilde{Y}(\mathbf{k}_2) , \qquad (2.32)$$

where we define

$$\int_{\mathbf{k}} \left[\cdots \right] \equiv \int \frac{\mathrm{d}^3 \mathbf{k}_1}{(2\pi)^3} \int \frac{\mathrm{d}^3 \mathbf{k}_2}{(2\pi)^3} \delta_{\mathrm{D}}^3 (\mathbf{k} - \mathbf{k}_1 - \mathbf{k}_2) \left[\cdots \right]. \tag{2.33}$$

Note that $\delta_D^3(\mathbf{k} - \mathbf{k}_1 - \mathbf{k}_2)$ is the Dirac delta function.

In Appendix A, we summarize the formulae of Riemannian geometry in the Poisson gauge, e.g., the Einstein tensor. By using Eqs. (2.22)–(2.26), the scalar, vector, and tensor modes of the Einstein tensor (A.27)–(A.30) can be expressed in Fourier space.

The scalar mode of the Einstein tensor:

$$\frac{1}{2}a^{2}G^{(2)0}{}_{0} = 3\mathcal{H}^{2}\Psi^{(2)}(\mathbf{k}) + 3\mathcal{H}\dot{\Phi}^{(2)}(\mathbf{k}) + k^{2}\Phi^{(2)}(\mathbf{k})
+ \int_{\mathbf{k}} \left[-3\dot{\Phi}^{(1)}(k_{1})\dot{\Phi}^{(1)}(k_{2}) - 6\mathcal{H}^{2}\Psi^{(1)}(k_{1})\Psi^{(1)}(k_{2}) + 4k_{1}^{2}\Phi^{(1)}(k_{1})\Phi^{(1)}(k_{2}) \right]
+ \int_{\mathbf{k}} \left[-12\mathcal{H}\dot{\Phi}^{(1)}(k_{1})\Psi^{(1)}(k_{2}) - k_{1}k_{2}(\hat{\mathbf{k}}_{1} \cdot \hat{\mathbf{k}}_{2})\Phi^{(1)}(k_{1})\Phi^{(1)}(k_{2}) \right], \quad (2.34)$$

$$\left(-O_i^{(0)}\right) \frac{1}{2} a^2 G^{(2)0}{}_i = k \left(\dot{\Phi}^{(2)}(\mathbf{k}) + \mathcal{H}\Psi^{(2)}(\mathbf{k})\right)$$

$$- \int_{\mathbf{k}} \left[4k_1 \left(\dot{\Phi}^{(1)} + \mathcal{H}\Psi^{(1)}\right) (k_1) \Psi^{(1)}(k_2) + 2k_1 \Psi^{(1)}(k_1) \dot{\Phi}^{(1)}(k_2) \right] \sqrt{\frac{4\pi}{3}} Y_{1,0}^*(\hat{\mathbf{k}}_1) ,$$

$$(2.35)$$

$$\left(-O_{i}^{(0)}\right) \frac{1}{2} a^{2} G^{(2)i}{}_{0} = -k \left(\dot{\Phi}^{(2)}(\mathbf{k}) + \mathcal{H}\Psi^{(2)}(\mathbf{k})\right)
- \int_{\mathbf{k}} k_{1} \left[4 \left(\dot{\Phi}^{(1)} + \mathcal{H}\Psi^{(1)}\right) (k_{1}) \Phi^{(1)}(k_{2}) - 2\Psi^{(1)}(k_{1}) \dot{\Phi}^{(1)}(k_{2})\right] \sqrt{\frac{4\pi}{3}} Y_{1,0}^{*}(\hat{\mathbf{k}}_{1}),$$
(2.36)

$$\left(\frac{3}{2}O_{ij}^{(0)}\right)\frac{1}{2}a^{2}G^{(2)i}{}_{j} = -\frac{1}{2}k^{2}\left(\Phi^{(2)}(\mathbf{k}) - \Psi^{(2)}(\mathbf{k})\right)
+ \int_{\mathbf{k}}k_{1}k\left[\Phi^{(1)}(k_{1})\Phi^{(1)}(k_{2}) - \Psi^{(1)}(k_{1})\Psi^{(1)}(k_{2}) - 2\Phi^{(1)}(k_{1})\Psi^{(1)}(k_{2})\right]\sqrt{\frac{4\pi}{3}}Y_{1,0}^{*}(\hat{\mathbf{k}}_{1})
+ \int_{\mathbf{k}}k_{1}^{2}\left[-\Phi^{(1)}(k_{1})\Phi^{(1)}(k_{2}) - \Psi^{(1)}(k_{1})\Psi^{(1)}(k_{2})\right]\sqrt{\frac{4\pi}{5}}Y_{2,0}^{*}(\hat{\mathbf{k}}_{1}),$$
(2.37)

$$\begin{split} \delta_{ij} \frac{1}{2} a^{2} G^{(2)i}{}_{j} &= 3 \Big[\dot{\Phi}^{(2)}(\mathbf{k}) + \mathcal{H} \dot{\Psi}^{(2)}(\mathbf{k}) + 2 \mathcal{H} \dot{\Phi}^{(2)}(\mathbf{k}) \Big] \\ &+ k^{2} \left(\Phi^{(2)}(\mathbf{k}) - \Psi^{(2)}(\mathbf{k}) \right) + 3 \left(2 \dot{\mathcal{H}} + \mathcal{H}^{2} \right) \Psi^{(2)}(\mathbf{k}) \\ &+ \int_{\mathbf{k}} \Big[-6 \left(2 \dot{\mathcal{H}} + \mathcal{H}^{2} \right) \Psi^{(1)}(k_{1}) \Psi^{(1)}(k_{2}) \Big] \\ &+ \int_{\mathbf{k}} \Big[-12 \Psi^{(1)}(k_{1}) \left(\ddot{\Phi}^{(1)} + \mathcal{H} \dot{\Psi}^{(1)} + 2 \mathcal{H} \dot{\Phi}^{(1)} \right) (k_{2}) \Big] \\ &+ \int_{\mathbf{k}} \Big[+4 k_{1}^{2} \left(\Phi^{(1)} - \Psi^{(1)} \right) (k_{1}) \Phi^{(1)}(k_{2}) \Big] \\ &+ \int_{\mathbf{k}} \Big[-9 \dot{\Phi}^{(1)}(k_{1}) \dot{\Phi}^{(1)}(k_{2}) - 6 \dot{\Psi}^{(1)}(k_{1}) \dot{\Phi}^{(1)}(k_{2}) - 3 k_{1} k_{2} (\hat{\mathbf{k}}_{1} \cdot \hat{\mathbf{k}}_{2}) \Psi^{(1)}(k_{1}) \Psi^{(1)}(k_{2}) \Big] \\ &+ \int_{\mathbf{k}} k_{1} k_{2} (\hat{\mathbf{k}}_{1} \cdot \hat{\mathbf{k}}_{2}) \left[-\Phi^{(1)}(k_{1}) \Phi^{(1)}(k_{2}) + \Psi^{(1)}(k_{1}) \Psi^{(1)}(k_{2}) + 2 \Phi^{(1)}(k_{1}) \Psi^{(1)}(k_{2}) \right]. \end{split}$$

The vector mode of the Einstein tensor:

$$\left(O_{i}^{(-\lambda)}\right) \frac{1}{2} a^{2} G^{(2)0}{}_{i} = -\frac{1}{4} k^{2} \omega_{\lambda}^{(2)}(\mathbf{k})
- \int_{\mathbf{k}} \left[4k_{1} \left(\dot{\Phi}^{(1)} + \mathcal{H}\Psi^{(1)}\right) (k_{1}) \Psi^{(1)}(k_{2}) + 2k_{1} \Psi^{(1)}(k_{1}) \dot{\Phi}^{(1)}(k_{2}) \right] \sqrt{\frac{4\pi}{3}} Y_{1,\lambda}^{*}(\hat{\mathbf{k}}_{1}),$$
(2.39)

$$\begin{split} \left(O_{i}^{(-\lambda)}\right)\frac{1}{2}a^{2}G^{(2)i}{}_{0} &= \left(\mathcal{H}^{2} - \dot{\mathcal{H}} + \frac{1}{4}k^{2}\right)\omega_{\lambda}^{(2)}(\mathbf{k}) \\ &- \int_{\mathbf{k}}k_{1}\left[4\dot{\Phi}^{(1)}(k_{1})\Phi^{(1)}(k_{2}) + 4\mathcal{H}\Psi^{(1)}(k_{1})\Phi^{(1)}(k_{2}) - 2\Psi^{(1)}(k_{1})\dot{\Phi}^{(1)}(k_{2})\right]\sqrt{\frac{4\pi}{3}}Y_{1,\lambda}^{*}(\hat{\mathbf{k}}_{1})\,, \end{split}$$

$$(2.40)$$

$$\begin{split} \left(-2O_{ij}^{(-\lambda)}\right) \frac{1}{2} a^2 G^{(2)i}{}_j &= \frac{k}{2} \left(\dot{\omega}_{\lambda}^{(2)}(\mathbf{k}) + 2\mathcal{H} \omega_{\lambda}^{(2)}(\mathbf{k}) \right) \\ &+ \int_{\mathbf{k}} k_1 k \left[\Phi^{(1)}(k_1) \Phi^{(1)}(k_2) - \Psi^{(1)}(k_1) \Psi^{(1)}(k_2) - 2\Phi^{(1)}(k_1) \Psi^{(1)}(k_2) \right] \sqrt{\frac{4\pi}{3}} Y_{1,\lambda}^*(\hat{\mathbf{k}}_1) \\ &+ \int_{\mathbf{k}} \sqrt{\frac{4}{3}} k_1^2 \left[\Phi^{(1)}(k_1) \Phi^{(1)}(k_2) + \Psi^{(1)}(k_1) \Psi^{(1)}(k_2) \right] \sqrt{\frac{4\pi}{5}} Y_{2,\lambda}^*(\hat{\mathbf{k}}_1) \,. \end{split} \tag{2.41}$$

The tensor mode of the Einstein tensor:

$$\left(\frac{2}{3}O_{ij}^{(-\sigma)}\right)\frac{1}{2}a^{2}G^{(2)i}{}_{j} = \frac{1}{4}\left(\ddot{h}_{\sigma}^{(2)}(\mathbf{k}) + 2\mathcal{H}\dot{h}_{\sigma}^{(2)}(\mathbf{k}) + k^{2}h_{\sigma}^{(2)}(\mathbf{k})\right)
+ \int_{\mathbf{k}} \frac{2}{3}k_{1}^{2}\left[\Phi^{(1)}(k_{1})\Phi^{(1)}(k_{2}) + \Psi^{(1)}(k_{1})\Psi^{(1)}(k_{2})\right]\sqrt{\frac{4\pi}{5}}Y_{2,\sigma}^{*}(\hat{\mathbf{k}}_{1}).$$
(2.42)

For the sake of brevity, we omit the time dependence of all variables. We set $k \parallel \hat{z}$ in the above expression. The first-order scalar mode depends on only the amplitude of the wave vector since evolution equations for the first-order scalar mode do not

depend on the direction of the wave vector. On the other hand, the second-order modes depend on not only the amplitude of the wave vector but also the direction of that one. Therefore, we denote that arguments of the second-order modes are indicated the direction of the wave vector.

2.2.2 Energy-Momentum Tensor

Second, the right-hand side in the Einstein equation, that is, the energy-momentum tensor, is perturbed up to the second order here. Although there are some definitions of the energy-momentum tensor, we start from the distribution function of each particle in this thesis. The energy-momentum tensor can be defined by using the distribution function as

$$T^{\mu}{}_{\nu} = \int \sqrt{-g} \frac{d^3 P^i}{(2\pi)^3 |P_0|} P^{\mu} P_{\nu} f , \qquad (2.43)$$

where P^{μ} is the canonical momentum in the generalized coordinate (here, corresponding to the Poisson gauge). There is a relation for the Jacobian of the generalized coordinate as

$$\sqrt{-g} \frac{d^3 P^i}{|P_0|} = \frac{d^3 P_i}{\sqrt{-g} |P^0|}.$$
 (2.44)

The integral in Eq. (2.43) must be done in the Poisson gauge since the distribution function is defined in the Poisson gauge. However, we can easily perform the integral explicitly by moving to the Local Inertial Frame Instantaneously at Rest with respect to Comoving Observer. Following Ref. [3], indices in the Poisson gauge are used as the Greek characters $\mu, \nu, \dots = 0, 1, 2, 3$ and those in the local inertial frame are used as $A, B, C \dots = 0, 1, 2, 3$. We relate the four-momentum in the Poisson gauge P^{μ} and the local inertial frame P^{A} by using the tetrad. The tetrad obeys following relation:

$$[e_A]^{\mu}[e_B]^{\nu}g_{\mu\nu} = \eta_{AB} . \qquad (2.45)$$

Consequently, four-momenta in each coordinate can relate as

$$P^{\mu} = [e_A]^{\mu} p^A . \tag{2.46}$$

The components of the tetrad in the Poisson gauge can be explicitly written down as

$$[e_0]^0 = \frac{e^{-\Psi}}{a} \,, \tag{2.47}$$

$$[e_i]^0 = \frac{1}{a} \left[e^{\Phi - 2\Psi} \delta^i{}_j - \frac{1}{2} h^i{}_j \right] \omega^j , \qquad (2.48)$$

$$[e_0]^i = 0 (2.49)$$

$$[e_j]^i = \frac{1}{a} \left[e^{\Phi} \delta^i{}_j - \frac{1}{2} h^i{}_j - \frac{3}{2} \Phi h^i{}_j - \frac{1}{2} \omega_i \omega_j + \frac{3}{8} h^i{}_k h^k{}_j \right], \qquad (2.50)$$

where the tetrad is not unique since it is possible to change the different local inertial frames by using the Lorentz transformation. The general discussion is presented in Ref. [3].

From the relation Eq. (2.46), we can write down the relation between the four-momentum in the Poisson gauge and the local inertial frame as

$$P^{0} = \frac{E}{a}e^{-\Psi} \left(1 + \frac{p}{E}\omega_{i}\hat{n}^{i} \right) , \qquad (2.51)$$

$$P^{i} = \frac{p}{a} e^{\Phi} \hat{n}^{j} \left(\delta^{i}_{j} - \frac{1}{2} h^{i}_{j} \right) , \qquad (2.52)$$

$$P_0 = g_{0\mu} P^{\mu} = -aEe^{\Psi},$$
 (2.53)

$$P_i = g_{i\mu} P^{\mu}$$

$$=ae^{-\Phi}\left(p_i+E\omega_i+\frac{1}{2}h_{ik}p^k\right)\,, (2.54)$$

where we define $p^0 = E$ and $p^i = p\hat{n}^i$. The Einstein relation is also held in Eqs. (2.51)–(2.54), namely, $P^{\mu}P_{\mu} = -E^2 + p^i p_i \equiv -m^2$. From here, we proceed the calculation of the energy-momentum tensor in Eq. (2.43). The determinant of the metric tensor metric and Jacobian are given by

$$\sqrt{-g} = a^4 e^{\Psi - 3\Phi} ,$$
 (2.55)

$$d^3 P^i = \frac{e^{3\Phi}}{a^3} d^3 p \ . \tag{2.56}$$

Finally, the energy-momentum tensor can be written in terms of the local inertial frame as

$$T^{\mu}{}_{\nu} = \int \frac{d^3p}{(2\pi)^3} \frac{P^{\mu}P_{\nu}}{E} f . \qquad (2.57)$$

In order to proceed the derivation of the energy-momentum tensor, we perturb the distribution function as

$$f(\eta, x^{i}, p, \hat{n}^{i}) = f^{(0)}(\eta, p) + f^{(1)}(\eta, x^{i}, p, \hat{n}^{i}) + \frac{1}{2}f^{(2)}(\eta, x^{i}, p, \hat{n}^{i}), \quad (2.58)$$

where only the distribution function of the zeroth order depends on the time and amplitude of the momentum since the zeroth-order distribution function of photons is a Planckian distribution.

The description of the distribution function is a microscopic picture. It is possible to relate the macroscopic components, that is, the average density ρ , density perturbation δ , velocity v_i , and anisotropic stress $\Pi^i{}_i$ as

$$\int \frac{d^3 p}{(2\pi)^3} p f^{(0)} = \rho^{(0)} , \qquad (2.59)$$

$$\frac{1}{\rho^{(0)}} \int \frac{d^3 p}{(2\pi)^3} p f^{(1,2)} = \delta^{(1,2)} , \qquad (2.60)$$

$$\int \frac{d^3p}{(2\pi)^3} p^i f^{(1)} = \frac{4}{3} \rho^{(0)} v^{(1)i} , \qquad (2.61)$$

$$\int \frac{d^3p}{(2\pi)^3} p^i \frac{1}{2} f^{(2)} = \frac{4}{3} \rho^{(0)} \frac{1}{2} v^{(2)i} + \frac{4}{3} \rho^{(0)} \delta^{(1)} v^{(1)i} , \qquad (2.62)$$

$$\int \frac{d^3 p}{(2\pi)^3} \frac{p^i p_j}{p} f = \rho^{(0)} \Pi^i{}_j + \frac{1}{3} \rho^{(0)} \delta^i{}_j \left[1 + \delta^{(1)} + \frac{1}{2} \delta^{(2)} \right], \qquad (2.63)$$

where we used the following formulae:

$$\int n_i d\Omega = 0 , \qquad (2.64)$$

$$\int n_i n_j n_k d\Omega = 0 , \qquad (2.65)$$

$$\int n_i n_j d\Omega = \frac{4\pi}{3} \delta_{ij} , \qquad (2.66)$$

$$\int n_i n_j n_k n_l d\Omega = \frac{4\pi}{15} \left(\delta_{ij} \delta_{kl} + \delta_{ik} \delta_{jl} + \delta_{il} \delta_{jk} \right) . \tag{2.67}$$

The energy-momentum tensor is corresponding to massless particles, e.g., photons and massless neutrinos.

On the other hand, in the case of massive particles, e.g., dark matters or baryons, we adopt the Maxwell-Boltzmann distribution function with a mass m and a mean velocity $v_{\rm m}$ as

$$g_{\rm m}(\boldsymbol{q}) = n_{\rm m} \left(\frac{2\pi}{mT_{\rm m}}\right)^{3/2} \exp\left[-\frac{(\boldsymbol{q} - m\boldsymbol{v}_{\rm m})^2}{2mT_{\rm m}}\right]. \tag{2.68}$$

Moreover, the moments of this distribution function are evaluated as

$$\int \frac{d^3q}{(2\pi)^3} g_{\rm m}(\mathbf{q}) = n_{\rm m} , \qquad (2.69)$$

$$\int \frac{d^3q}{(2\pi)^3} q_i g_{\rm m}(\mathbf{q}) = m n_{\rm m} v_{\rm mi} \ (= \rho_{\rm m} v_{\rm mi}) \ , \tag{2.70}$$

$$\int \frac{d^3q}{(2\pi)^3} \frac{q^i}{E} g_{\rm m}(\mathbf{q}) = n_{\rm m} v_{\rm mi} , \qquad (2.71)$$

$$\int \frac{d^3q}{(2\pi)^3} q_i q^j g_m(\mathbf{q}) = m^2 n_{\rm m} v_{\rm m} i v_{\rm m} j + m n_{\rm m} T_{\rm m} \delta^i{}_j , \qquad (2.72)$$

$$\int \frac{d^3q}{(2\pi)^3} \frac{q_i}{E} \frac{q^j}{E} g_{\rm m}(\mathbf{q}) = n_{\rm m} v_{\rm mi} v_{\rm mj} + n_{\rm m} \frac{T_{\rm m}}{m} \delta^i{}_j . \tag{2.73}$$

Thus, the energy-momentum tensor for massless particles and massive particles can be derived.

The energy-momentum tensor for massless particles:

$$T^{0}_{0} = -\rho^{(0)} \left(1 + \delta^{(1)} + \frac{1}{2} \delta^{(2)} \right) ,$$
 (2.74)

$$T^{0}{}_{i} = \frac{4}{3}\rho^{(0)}e^{-(\Phi+\Psi)}\left[\left(v^{(1)}_{i} + \frac{1}{2}v^{(2)}_{i} + \delta^{(1)}v^{(1)}_{i}\right) + \omega_{i}\right], \qquad (2.75)$$

$$T^{i}_{0} = -\frac{4}{3}\rho^{(0)}e^{\Phi+\Psi}\left(v^{(1)i} + \frac{1}{2}v^{(2)i} + \delta^{(1)}v^{(1)i}\right), \qquad (2.76)$$

$$T^{i}{}_{j} = \rho \left[\Pi^{i}{}_{j} + \frac{1}{3} \delta^{i}{}_{j} \left(1 + \delta^{(1)} + \frac{1}{2} \delta^{(2)} \right) \right]. \tag{2.77}$$

The energy-momentum tensor for massive particles:

$$T^{0}_{0} = -\rho^{(0)} \left(1 + \delta^{(1)} + \frac{1}{2} \delta^{(2)} \right),$$
 (2.78)

$$T^{0}{}_{i} = e^{-(\Phi + \Psi)} \rho^{(0)} \left[\left(v_{i}^{(1)} + \frac{1}{2} v_{i}^{(2)} + \delta^{(1)} v_{i}^{(1)} \right) + \omega_{i} \right], \tag{2.79}$$

$$T^{i}_{0} = -e^{\Phi + \Psi} \rho^{(0)} \left(v^{(1)i} + \frac{1}{2} v^{(2)i} + \delta^{(1)} v^{(1)i} \right), \qquad (2.80)$$

$$T^{i}_{j} = \rho \left(v_{i}^{(1)} v_{j}^{(1)} + \frac{T_{m}}{m} \delta^{i}_{j} \right).$$
 (2.81)

As well as the Einstein tensor, the energy-momentum tensor can be decomposed into the scalar, vector, and tensor modes. Hereafter, we indicate massless particles and massive particles as $s = \gamma$ and s = m, respectively.

The energy-momentum tensor of the scalar mode:

$$\frac{1}{2}T_{\rm s}^{(2)0}{}_{0} = -\rho_{\rm s}^{(0)} \left(\frac{1}{2}\delta_{\rm s}^{(2)}(\pmb{k})\right) , \qquad (2.82)$$

$$\left(-O_{i}^{(0)}\right) \frac{1}{2} T_{s}^{(2)0}{}_{i} = \left(\rho_{s}^{(0)} + \rho_{s}^{(0)}\right) \left(\frac{1}{2} v_{s0}^{(2)}(\mathbf{k})\right)$$

$$+ \left(\rho_{s}^{(0)} + \rho_{s}^{(0)}\right) \int_{\mathbf{k}} \left[v_{s0}^{(1)}(k_{1}) \left(\delta_{s}^{(1)} - \Phi^{(1)} - \Psi^{(1)}\right)(k_{2})\right] \sqrt{\frac{4\pi}{3}} Y_{1,0}^{*}(\hat{\mathbf{k}}_{1}),$$

$$(2.83)$$

$$\left(-O_{i}^{(0)}\right) \frac{1}{2} T_{s}^{(2)i}{}_{0} = -\left(\rho_{s}^{(0)} + p_{s}^{(0)}\right) \left(\frac{1}{2} v_{s0}^{(2)}(\mathbf{k})\right)$$

$$-\left(\rho_{s}^{(0)} + p_{s}^{(0)}\right) \int_{\mathbf{k}} \left[v_{s0}^{(1)}(k_{1}) \left(\delta_{s}^{(1)} + \Phi^{(1)} + \Psi^{(1)}\right)(k_{2})\right] \sqrt{\frac{4\pi}{3}} Y_{1,0}^{*}(\hat{\mathbf{k}}_{1}) ,$$

$$(2.84)$$

$$\left(\frac{3}{2}O_{ij}^{(0)}\right)\frac{1}{2}T_{\gamma}^{(2)i}{}_{j} = \rho_{\gamma}^{(0)}\frac{1}{10}\Delta_{2,0}^{(2)}(\mathbf{k}), \qquad (2.85)$$

$$\left(\frac{3}{2}O_{ij}^{(0)}\right)\frac{1}{2}T_{\rm m}^{(2)i}{}_{j} = \rho_{\rm m}^{(0)}\int_{\mathbf{k}}\left[\frac{3}{2}v_{\rm m0}^{(1)}(k_{1})v_{\rm m0}^{(1)}(k_{2})\right]\left[\sqrt{\frac{4\pi}{3}}Y_{1,0}^{*}(\hat{\mathbf{k}}_{1})\sqrt{\frac{4\pi}{3}}Y_{1,0}^{*}(\hat{\mathbf{k}}_{2}) - \frac{1}{3}(\hat{\mathbf{k}}_{1}\cdot\hat{\mathbf{k}}_{2})\right],$$
(2.86)

$$\delta_{ij} \frac{1}{2} T_{\gamma}^{(2)i}{}_{j} = \rho_{\gamma}^{(0)} \left(\frac{1}{2} \delta_{\gamma}^{(2)}(\mathbf{k}) \right) + \rho_{\gamma}^{(0)} \int_{\mathbf{k}} \left[\delta_{\gamma}^{(1)}(k_{1}) \delta_{\gamma}^{(1)}(k_{2}) \right], \tag{2.87}$$

$$\delta_{ij} \frac{1}{2} T_{\rm m}^{(2)i}{}_{j} = -\rho_{\rm m}^{(0)} \int_{\mathbf{k}} \left[(\hat{\mathbf{k}}_{1} \cdot \hat{\mathbf{k}}_{2}) v_{\rm m0}^{(1)}(k_{1}) v_{\rm m0}^{(1)}(k_{2}) \right]. \tag{2.88}$$

The energy-momentum tensor of the vector mode:

$$\left(O_{i}^{(-\lambda)}\right) \frac{1}{2} T_{s}^{(2)0}{}_{i} = \left(\rho_{s}^{(0)} + p_{s}^{(0)}\right) \left(\frac{1}{2} v_{s\lambda}^{(2)}(\mathbf{k}) + \frac{1}{2} \omega_{\lambda}^{(2)}(\mathbf{k})\right) \\
+ \left(\rho_{s}^{(0)} + p_{s}^{(0)}\right) \int_{\mathbf{k}} \left[v_{s0}^{(1)}(k_{1}) \left(\delta_{s}^{(1)} - \Phi^{(1)} - \Psi^{(1)}\right) (k_{2})\right] \sqrt{\frac{4\pi}{3}} Y_{1,\lambda}^{*}(\hat{\mathbf{k}}_{1}), \tag{2.89}$$

$$\left(O_{i}^{(-\lambda)}\right) \frac{1}{2} T_{s}^{(2)i}{}_{0} = -\left(\rho_{s}^{(0)} + \rho_{s}^{(0)}\right) \left(\frac{1}{2} v_{s\lambda}^{(2)}(\mathbf{k})\right) \\
-\left(\rho_{s}^{(0)} + \rho_{s}^{(0)}\right) \int_{\mathbf{k}} \left[v_{s0}^{(1)}(k_{1}) \left(\delta_{s}^{(1)} + \Phi^{(1)} + \Psi^{(1)}\right)(k_{2})\right] \sqrt{\frac{4\pi}{3}} Y_{1,\lambda}^{*}(\hat{\mathbf{k}}_{1}), \tag{2.90}$$

$$\left(-2O_{ij}^{(-\lambda)}\right)\frac{1}{2}T_{\gamma}^{(2)i}{}_{j} = \rho_{\gamma}^{(0)}\frac{1}{5\sqrt{3}}\Delta_{2,\lambda}^{(2)}(\mathbf{k}), \qquad (2.91)$$

$$\left(-2O_{ij}^{(-\lambda)}\right)\frac{1}{2}T_{\rm m}^{(2)i}{}_{j} = \rho_{\rm m}^{(0)}\int_{\mathbf{k}} \left[2v_{\rm m0}^{(1)}(k_{1})v_{\rm m0}^{(1)}(k_{2})\right]\sqrt{\frac{4\pi}{3}}Y_{1,0}(\hat{\mathbf{k}}_{1})\sqrt{\frac{4\pi}{3}}Y_{1,\lambda}^{*}(\hat{\mathbf{k}}_{2}).$$
(2.92)

The energy-momentum tensor of the tensor mode:

$$\left(\frac{2}{3}O_{ij}^{(-\sigma)}\right)\frac{1}{2}T_{\gamma}^{(2)i}{}_{j} = \rho_{\gamma}^{(0)}\frac{1}{15}\Delta_{2,\sigma}^{(2)}(\mathbf{k}), \qquad (2.93)$$

$$\left(\frac{2}{3}O_{ij}^{(-\sigma)}\right)\frac{1}{2}T_{m}^{(2)i}{}_{j} = \rho_{m}^{(0)}\int_{\mathbf{k}}\left[\sqrt{\frac{2}{3}}v_{m0}^{(1)}(k_{1})v_{m0}^{(1)}(k_{2})\right]\sqrt{\frac{4\pi}{3}}Y_{1,\lambda}^{*}(\hat{\mathbf{k}}_{1})\sqrt{\frac{4\pi}{3}}Y_{1,\lambda}^{*}(\hat{\mathbf{k}}_{2}).$$

(2.94)

Note that the quantity $\Delta_{2,m}(k)$ is the perturbed brightness function expanded by the spherical harmonics. More detailed definition is shown in Sect. 2.3.

We derived the perturbed Einstein and energy-momentum tensors up to the second order. By substituting these results into Eq. (2.27), we can determine evolutions of the metric perturbations. However, we need to formulate the Boltzmann equation which describes evolutions of fluids. In the following subsection, we formulate the perturbed Boltzmann equation up to the second order.

2.3 Boltzmann Equation—Basics

In this subsection, we formulate the second-order Boltzmann equation. It is possible to trace the evolution of fluids by using the Boltzmann equation. The Boltzmann equation draws the evolution of the distribution function in the phase space including arbitrary interactions. In the standard cosmology, fluids in the universe are photons, massless neutrinos, baryons, and dark matters. In the early universe before the recombination, photons and electrons interact with each other through the Compton scattering. On the other hand, massless neutrinos do not interact with any matters after the neutrino decoupling. Consequently, the difference between photons and massless neutrinos is the interaction term only. This discussion is same in the case of baryons and dark matters. In this subsection, we derive the Boltzmann equation for photons and baryons following Refs. [3–6]. In this thesis, we ignore the polarization of photons which would be small effects.

The Boltzmann equation for photons can be written as

$$\frac{\mathrm{d}f}{\mathrm{d}\lambda} = \tilde{C}[f] , \qquad (2.95)$$

where λ and $\tilde{C}[f]$ are the affine parameter and the generalized collision term due to the Compton scattering, respectively. The generalized collision term due to the Compton scattering can be given by

$$\tilde{C}[f] = \int d\Pi_{\mathbf{q}} d\Pi_{\mathbf{q}'} d\Pi_{\mathbf{p}'} (2\pi)^4 \delta_{\mathrm{D}}^4 (q_{\mu} + p_{\mu} - q_{\mu}' - p_{\mu}')$$

$$\times |\mathcal{M}|^2 \left[g_{\mathrm{e}}(\mathbf{q}') f(\mathbf{p}') (1 + f(\mathbf{p})) - g_{\mathrm{e}}(\mathbf{q}) f(\mathbf{p}) (1 + f(\mathbf{p}')) \right], \quad (2.96)$$

where $d\Pi_q$, $|\mathcal{M}|^2$, $g_e(q)$, and f(p) are the Lorentz-invariant momentum volume, scattering amplitude, distribution function of electrons, and distribution function of photons, respectively. The delta function in the collision term enforces the energy and momentum conservations. Throughout this thesis, we have dropped the Pauli blocking factor $(1-g_e)$. The Pauli blocking factor can be always omitted safely in the epoch of interest, because g_e is very small after electron-positron annihilations.

The Lorentz-invariant momentum volume in the local inertial frame becomes more simple form as

$$d\Pi_{q} = \frac{d^{3}q}{(2\pi)^{3}2E(q)}.$$
 (2.97)

We rewrite the left-hand side of the Boltzmann equation in Eq. (2.95) by using the conformal time as

$$P^0 \frac{\mathrm{d}f}{\mathrm{d}n} = \tilde{C}[f] \,, \tag{2.98}$$

where we use the definition of the four-momentum:

$$P^0 = \frac{\mathrm{d}\eta}{\mathrm{d}\lambda} \,. \tag{2.99}$$

By using the tetrad, we can work in the local inertial frame. The distribution function $f(\eta, x^i, p, \hat{n}^i)$ obeys the Boltzmann equation as

$$\frac{\partial f}{\partial \eta} + \frac{\mathrm{d}x^{i}}{\mathrm{d}\eta} \frac{\partial f}{\partial x^{i}} + \frac{\mathrm{d}p}{\mathrm{d}\eta} \frac{\partial f}{\partial p} + \frac{\mathrm{d}\hat{n}^{i}}{\mathrm{d}\eta} \frac{\partial f}{\partial \hat{n}^{i}} = \frac{1}{P^{0}} \tilde{C}[f] , \qquad (2.100)$$

where the collision term is the first-order itself. Therefore, by using Eq. (2.51), the right-hand side is rewritten as

$$\frac{1}{P^0}\tilde{C}[f] = \frac{ae^{\Psi}}{E}\tilde{C}[f] \equiv e^{\Psi}C[f]. \tag{2.101}$$

Consequently, the explicit form of the redefined collision term C[f] becomes

$$C[f] = \frac{a}{E(p)} \int \frac{\mathrm{d}^{3} \mathbf{p}'}{(2\pi)^{3} 2E(p')} \frac{\mathrm{d}^{3} \mathbf{q}}{(2\pi)^{3} 2E_{\mathrm{e}}(q)} \frac{\mathrm{d}^{3} \mathbf{q}'}{(2\pi)^{3} 2E_{\mathrm{e}}(q')} (2\pi)^{4} \delta_{\mathrm{D}}^{4}(q^{\mu} + p^{\mu} - q'^{\mu} - p'^{\mu}) \times |\mathcal{M}|^{2} \left[g_{\mathrm{e}}(\mathbf{q}') f(\mathbf{p}') (1 + f(\mathbf{p})) - g_{\mathrm{e}}(\mathbf{q}) f(\mathbf{p}) (1 + f(\mathbf{p}')) \right]. \tag{2.102}$$

Next, we evaluate the left-hand side in Eq. (2.100), that is, the streaming term.

2.4 Boltzmann Equation—Streaming Term

From here, we focus on the streaming term, that is, the left-hand side of the Boltzmann equation. The streaming term is consist of the three contributions, i.e., the coordinate velocity term $\frac{\mathrm{d}x^i}{\mathrm{d}\eta}$, redshift term $\frac{\mathrm{d}p}{\mathrm{d}\eta}$, and lensing term $\frac{\mathrm{d}\hat{n}^i}{\mathrm{d}\eta}$.

First, the coordinate velocity term is easily derived from the definitions of the

First, the coordinate velocity term is easily derived from the definitions of the four-momentum in Eqs. (2.51) and (2.52) as

$$\frac{\mathrm{d}x^{i}}{\mathrm{d}\eta} = \frac{P^{i}}{P^{0}}$$

$$= \frac{p}{E}\hat{n}^{j}e^{\Phi+\Psi} \left[\delta_{ij} \left(1 - \frac{p}{E}\omega_{k}\hat{n}^{k} \right) - \frac{1}{2}h_{ij} \right].$$
(2.103)

Note that this term is also used to derive the redshift and lensing terms.

Second, the redshift and lensing terms are derived from the perturbed geodesic equation. Here we consider the geodesic equation in terms of the conformal time as

$$\frac{\mathrm{d}P^{\mu}}{\mathrm{d}\eta} + \Gamma^{\mu}{}_{\alpha\beta} \frac{P^{\alpha}P^{\beta}}{P^{0}} = 0. \tag{2.104}$$

Note that, the derivative of four-momentum with respect to the conformal time is the total derivative. Hence the total derivative should be calculated as

$$\frac{\mathrm{d}\Box}{\mathrm{d}\eta} = \frac{\partial\Box}{\partial\eta} + \frac{\mathrm{d}x^k}{\mathrm{d}\eta} \frac{\partial\Box}{\partial x^k}
= \dot{\Box} + \frac{p}{E} e^{\Phi + \Psi} \hat{n}^k \Box_{,k} .$$
(2.105)

The perturbed geodesic equation for $\mu = 0$ component is given as

$$\left(1 + \frac{E}{p}\omega^{i}n_{i}\right)\frac{1}{p}\frac{\mathrm{d}p}{\mathrm{d}\eta} + \frac{E}{p}\omega^{i}\frac{\mathrm{d}\hat{n}^{i}}{\mathrm{d}\eta} = -\mathcal{H} + \dot{\Phi} - \frac{E}{p}\dot{\omega}^{i}n_{i} - \frac{E}{p}e^{\Psi + \Phi}2\Psi_{,i}\hat{n}^{i} + \left(\frac{p}{E} - 2\frac{E}{p}\right)\mathcal{H}\omega_{i}\hat{n}^{i} - \frac{1}{2}\dot{h}_{ij}\hat{n}^{i}\hat{n}^{j}. \quad (2.106)$$

In the same way, the perturbed geodesic equation for $\mu = i$ component is given as

$$\begin{split} \left(\delta^{i}{}_{j} - \frac{1}{2}h^{i}{}_{j}\right) \left[\hat{n}^{j} \frac{\mathrm{d}p}{p} + \frac{\mathrm{d}\hat{n}^{j}}{\mathrm{d}\eta} + \frac{\mathrm{d}\hat{n}^{j}}{\mathrm{d}\eta}\right] &= -(\mathcal{H} - \dot{\Phi})\hat{n}^{i} - \frac{1}{2}\left(\dot{h}^{i}{}_{j} - \mathcal{H}h^{i}{}_{j}\right)\hat{n}^{j} - (\omega^{i}{}_{,j} - \omega_{j}{}_{,i}^{i})\hat{n}^{j} \\ &- \frac{E}{p}e^{\Phi + \Psi}\Psi^{,i} - \frac{E}{p}(\dot{\omega}^{i} + \mathcal{H}\omega^{i}) + \frac{p}{E}e^{\Phi + \Psi}\left(\Phi_{,j}\hat{n}^{j}\hat{n}^{i} - \Phi^{,i}\right) \\ &+ \frac{p}{E}\left(\mathcal{H}\omega^{i} - \frac{1}{2}h^{i}{}_{j,k}\hat{n}^{j}\hat{n}^{k} + \frac{1}{2}h_{jk}{}^{,i}\hat{n}^{j}\hat{n}^{k}\right), \end{split}$$
(2.107)

where we use the fact that $\dot{E} = p\dot{p}/E$. By multiplying Eq. (2.106) by $(1 - (E/p)\omega^i\hat{n}_i)$, and Eq. (2.107) by $(\delta_{ij} + h_{ij}/2)$, we derive

$$\frac{1}{p}\frac{\mathrm{d}p}{\mathrm{d}\eta} + \frac{E}{p}\omega^{i}\frac{\mathrm{d}\hat{n}^{i}}{\mathrm{d}\eta} = -\mathcal{H} + \dot{\Phi} - \frac{E}{p}\dot{\omega}^{i}n_{i}
- \frac{E}{p}e^{\Psi + \Phi}2\Psi_{,i}\hat{n}^{i} + \left(\frac{p}{E} - 2\frac{E}{p}\right)\mathcal{H}\omega_{i}\hat{n}^{i} - \frac{1}{2}\dot{h}_{im}\hat{n}^{i}\hat{n}^{m},$$
(2.108)

$$\frac{d\hat{n}^{i}}{d\eta} + \hat{n}^{i} \frac{1}{p} \frac{dp}{d\eta} = -(\mathcal{H} - \dot{\Phi})\hat{n}^{i} - \frac{1}{2}\dot{h}^{i}{}_{k}\hat{n}^{k} - (\omega^{i}{}_{,k} - \omega_{k}{}^{,i})\hat{n}^{k}
- \frac{E}{p}e^{\Phi + \Psi}\Psi^{,i} - \frac{E}{p}(\dot{\omega}^{i} + \mathcal{H}\omega^{i}) + \frac{p}{E}e^{\Phi + \Psi}\left(\Phi_{,j}\hat{n}^{j}\hat{n}^{i} - \Phi^{,i}\right)
+ \frac{p}{E}\left(\mathcal{H}\omega^{i} - \frac{1}{2}h^{i}{}_{j,m}\hat{n}^{j}\hat{n}^{m} + \frac{1}{2}h_{jm}{}^{,i}\hat{n}^{j}\hat{n}^{m}\right).$$
(2.109)

By combining Eqs. (2.106) and (2.109), we derive the redshift term as

$$\frac{1}{p}\frac{\mathrm{d}p}{\mathrm{d}\eta} = -\mathcal{H} + \dot{\Phi} - \frac{E}{p}\dot{\omega}^{i}n_{i} - \frac{E}{p}e^{\Phi + \Psi}\Psi_{,i}\hat{n}^{i} - \frac{m^{2}}{Ep}\mathcal{H}\omega_{i}\hat{n}^{i} - \frac{1}{2}\dot{h}_{ij}\hat{n}^{i}\hat{n}^{j}, \quad (2.110)$$

where we use the relation $p/E - E/p = -m^2/(Ep)$. Finally, by substituting Eq. (2.110) into Eq. (2.109), we derive the lensing term as

$$\frac{\mathrm{d}\hat{n}^i}{\mathrm{d}\eta} = -(\delta^{ij} - \hat{n}^i \hat{n}^j) \left[\frac{p}{E} \Psi_{,j} + \frac{E}{p} \Phi_{,j} \right] . \tag{2.111}$$

Moreover, by combining Eq. (2.109), we also derive the time-derivative of the photon momentum as

$$\frac{1}{p} \frac{\mathrm{d}p^{i}}{\mathrm{d}\eta} = -(\mathcal{H} - \dot{\Phi})\hat{n}^{i} - \frac{1}{2}\dot{\chi}^{i}{}_{k}\hat{n}^{k} - (\omega^{i}{}_{,k} - \omega_{k}{}^{,i})\hat{n}^{k} - \frac{E}{p}e^{\Phi + \Psi}\Psi^{,i} - \frac{E}{p}(\dot{\omega}^{i} + \mathcal{H}\omega^{i})
+ \frac{P}{E}e^{\Phi + \Psi}\left(\Phi_{,j}\hat{n}^{j}\hat{n}^{i} - \Phi^{,i}\right) + \frac{P}{E}\left(\mathcal{H}\omega^{i} - \frac{1}{2}\chi^{i}{}_{j,m}\hat{n}^{j}\hat{n}^{m} + \frac{1}{2}\chi_{jm}{}^{,i}\hat{n}^{j}\hat{n}^{m}\right).$$
(2.112)

Note that the above expression is the case of massive particles with a mass m. If we assume the massless particles, we set m = 0. The next thing to do is the derivation of the collision term. In the following section, we derive the collision term up to the second order.

2.5 Boltzmann Equation—Collision Term

Let us now evaluate the collision term due to the Compton scattering. In the limit of completely elastic collisions between photons and electrons, this term vanishes. Typically, in the regime of interest in this thesis, very little energy is transferred between electrons and photons in Compton scatterings. Owing to this fact, it is a good approximation to expand the collision term systematically in powers of the energy transfer. Let us demonstrate this specifically. We consider the collision process

$$\gamma(p^{\mu}) + e^{-}(q^{\mu}) \to \gamma(p'^{\mu}) + e^{-}(q'^{\mu}),$$
 (2.113)

where the quantities in the parentheses denote the particle momenta. To calculate this process, we evaluate the collision term in the Boltzmann equation of photons in Eq. (2.102).

Integrating over q', we obtain

$$C[f] = \frac{a}{p} \int \frac{d^{3} p'}{(2\pi)^{3} 2p'} \frac{d^{3} q}{(2\pi)^{3} 2E_{e}(q)} \frac{2\pi}{2E_{e}(|q+p-p'|)} \times |\mathcal{M}|^{2} \delta_{D} \Big[p - p' + E_{e}(q) - E_{e}(|q+p-p'|) \Big] \times \Big[g_{e}(q+p-p') f(p') (1+f(p)) - g_{e}(q) f(p) (1+f(p')) \Big].$$
(2.114)

In the regime of our interest, energy transfer through the Compton scattering is small and can be ignored in the first order density perturbations. The expansion parameter is the energy transfer,

$$E_{\rm e}(q) - E_{\rm e}(|q + p - p'|) \simeq \frac{(p' - p) \cdot q}{m_{\rm e}} - \frac{(p - p')}{2m_{\rm e}},$$
 (2.115)

over the temperature of the universe. Employing $p \sim T$, we can estimate the order of this expansion parameter as $\mathcal{O}(\frac{pq}{m_eT}) \sim \mathcal{O}(\frac{q}{m_e})$, which is small when electrons are nonrelativistic. Note that, in the cosmological Thomson regime, electrons in the thermal bath of photons are nonrelativistic, $p \sim \frac{q^2}{2m_e}$, and the energy of photons is much smaller than the rest mass of a electron, $p \ll m_e$. Thus, it also holds that $q \sim \sqrt{2m_ep} \gg p$, and the second term in Eq. (2.115) is usually smaller than the first one.

Now let us divide the collision integral into four parts, i.e., the denominators of the Lorentz invariant volume, the scattering amplitude, the delta function, and the distribution functions, and expand them due to the expansion parameter defined above.

2.5.1 Lorentz Invariant Volume

First of all, the denominator in the Lorentz invariant volume can be expanded to

$$\frac{1}{E_{e}(q)E_{e}(|\boldsymbol{q}+\boldsymbol{p}-\boldsymbol{p'}|)} = \left(m_{e} + \frac{1}{2m_{e}}q^{2}\right)^{-1} \left(m_{e} + \frac{1}{2m_{e}}|\boldsymbol{q}+\boldsymbol{p}-\boldsymbol{p'}|\right)^{-1} \\
\approx \frac{1}{m_{e}^{2}} \left[1 - \mathcal{E}_{\left(\frac{q}{m_{e}}\right)^{2}} - \mathcal{E}_{\left(\frac{pq}{m_{e}}\right)^{2}}\right], \tag{2.116}$$

where

$$\mathcal{E}_{(\frac{q}{m_e})^2} = \frac{q^2}{m_e^2} \,, \tag{2.117}$$

$$\mathcal{E}_{(\frac{pq}{m_e^2})} = \frac{(p - p') \cdot q}{m_e^2} , \qquad (2.118)$$

$$\mathcal{E}_{(\frac{p}{m_e})^2} = \frac{(p - p')^2}{2m_e^2} \ . \tag{2.119}$$

2.5.2 Scattering Amplitude

Second, we consider the scattering amplitude. Fortunately, it has been known that the leading term (zeroth order term), obtained by multiplying together the first term in the delta function and the zeroth-order distribution functions, is zero. It means that we only have to keep up to the first order terms when we expand the scattering amplitude and the energies, in order to keep the collision term up to the second order [7]. The scattering amplitude for Compton scattering in the rest frame of the electron is given by,

$$|\mathcal{M}|^2 = 6\pi m_{\rm e}^2 \sigma_{\rm T} \left[\frac{\tilde{p}'}{\tilde{p}} + \frac{\tilde{p}}{\tilde{p}'} - \sin^2 \tilde{\beta} \right] ,$$

$$\cos \tilde{\beta} = \tilde{\hat{p}} \cdot \tilde{\hat{p}}' , \qquad (2.120)$$

where \tilde{p} and \tilde{p}' are the energies of incident and scattered photons, \tilde{p} and \tilde{p}' are the unit vectors of \tilde{p} and \tilde{p}' , respectively, denoting the directions of the photons in this frame. The Lorentz transformation with electron's velocity (q/m_e) gives the following relations,

$$\frac{p}{\tilde{p}} = \frac{\sqrt{1 - (q/m_e)^2}}{1 - p \cdot q/(pm_e)},$$
(2.121)

$$p^{\mu}p_{\mu} = \tilde{p}^{\mu}\tilde{p}_{\mu} . \tag{2.122}$$

Using these relations, we evaluate the scattering amplitude in the CMB frame as [5]

$$|\mathcal{M}|^2 = 6\pi m_e^2 \sigma_T \left[\mathcal{M}_0 + \mathcal{M}_{(\frac{q}{m_e})} \right], \qquad (2.123)$$

where

$$\mathcal{M}_0 = 1 + \cos^2 \beta \,, \tag{2.124}$$

$$\mathcal{M}_{\left(\frac{q}{m_{\rm e}}\right)} = -2\cos\beta(1-\cos\beta)\left[\frac{q}{m_{\rm e}}\cdot\left(\hat{\boldsymbol{n}}+\hat{\boldsymbol{n}}'\right)\right]. \tag{2.125}$$

Here \hat{n} and \hat{n}' are the unit vectors of p and p', respectively.

2.5.3 Delta Function

Third, we expand the delta function to

$$\begin{split} \delta_{\mathrm{D}} \left[p - p' + E_{\mathrm{e}}(q) - E_{\mathrm{e}}(q') \right] \approx & \delta_{\mathrm{D}}(p - p') + \left. \frac{\partial \delta_{\mathrm{D}} \left[p - p' + E_{\mathrm{e}}(q) - E_{\mathrm{e}}(q') \right]}{\partial p} \right|_{q = q'} \left(E_{\mathrm{e}}(q) - E_{\mathrm{e}}(q') \right) \\ &+ \left. \frac{1}{2} \frac{\partial^2 \delta_{\mathrm{D}} \left[p - p' + E_{\mathrm{e}}(q) - E_{\mathrm{e}}(q') \right]}{\partial p^2} \right|_{q = q'} \left(E_{\mathrm{e}}(q) - E_{\mathrm{e}}(q') \right)^2 \\ &= \delta_{\mathrm{D}}(p - p') + \frac{\partial \delta_{\mathrm{D}}(p - p')}{\partial p'} \mathcal{D}_{\left(\frac{q}{m_{\mathrm{e}}}\right)} \\ &+ \frac{\partial \delta_{\mathrm{D}}(p - p')}{\partial p'} \mathcal{D}_{\left(\frac{p}{m_{\mathrm{e}}}\right)} + \frac{1}{2} \mathcal{D}_{\left(\frac{q}{m_{\mathrm{e}}}\right)}^2 \frac{\partial^2 \delta_{\mathrm{D}}(p - p')}{\partial p'^2} , \end{split} \tag{2.126}$$

where

$$\mathcal{D}_{\left(\frac{q}{m_c}\right)} = \frac{(p - p') \cdot q}{m_c} , \qquad (2.127)$$

$$\mathcal{D}_{(\frac{p}{m_e})} = \frac{(p - p')^2}{2m_e} \ . \tag{2.128}$$

2.5.4 Distribution Function of Electrons

Finally, the distribution of the electron can be expanded to

$$g_{\rm e}(\boldsymbol{q}+\boldsymbol{p}-\boldsymbol{p'}) \approx g_{\rm e}(\boldsymbol{q}) + \frac{\partial g_{\rm e}}{\partial \boldsymbol{q}} \cdot (\boldsymbol{p}-\boldsymbol{p'}) + \frac{1}{2} (p^i - p'^i) \frac{\partial^2 g_{\rm e}}{\partial q^i \partial q^j} (p^j - p'^j)$$
. (2.129)

We assume that the electrons are kept in thermal equilibrium and in the Boltzmann distribution:

$$g_{\mathrm{e}}(\boldsymbol{q}) = n_{\mathrm{e}} \left(\frac{2\pi}{m_{\mathrm{e}} T_{\mathrm{e}}} \right)^{3/2} \exp \left[-\frac{(\boldsymbol{q} - m_{\mathrm{e}} \boldsymbol{v_{e}})^{2}}{2m_{\mathrm{e}} T_{\mathrm{e}}} \right], \tag{2.130}$$

where v_e is the bulk velocity of electrons. The first- and second-derivatives of the distribution function with respect to the momentum are given as

$$\frac{\partial g_{\rm e}}{\partial q^i} = -g_{\rm e} \frac{q_i - m_{\rm e} v_{\rm ei}}{m_{\rm e} T_{\rm e}} \,, \tag{2.131}$$

$$\frac{\partial^2 g_{\rm e}}{\partial q^i \partial q^j} = -\frac{\partial g_{\rm e}}{\partial q^j} \frac{q^i - m_{\rm e} v_{\rm e}^i}{m_{\rm e} T_{\rm e}} - g_{\rm e} \frac{\delta^{ij}}{m_{\rm e} T_{\rm e}} \,. \tag{2.132}$$

By substituting the above equation, Eq. (2.129) is written as

$$g_{\mathrm{e}}(\boldsymbol{q} + \boldsymbol{p} - \boldsymbol{p}') \approx g_{\mathrm{e}}(\boldsymbol{q}) \left[1 - \mathcal{F}_{(\frac{q}{m_{\mathrm{e}}})} + \frac{1}{2} \mathcal{F}_{(\frac{q}{m_{\mathrm{e}}})}^{2} - \mathcal{F}_{(\frac{p}{m_{\mathrm{e}}})} \right],$$
 (2.133)

where

$$\mathcal{F}_{\left(\frac{q}{m_{\mathrm{e}}}\right)} = \frac{q - m_{\mathrm{e}} \mathbf{v}_{\mathrm{e}}}{m_{\mathrm{e}} T_{\mathrm{e}}} \cdot (\mathbf{p} - \mathbf{p'}) , \qquad (2.134)$$

$$\mathcal{F}_{(\frac{p}{m_{\rm c}})} = \frac{1}{2} \frac{(\mathbf{p} - \mathbf{p}')^2}{m_{\rm e} T_{\rm e}} \,. \tag{2.135}$$

Therefore, we have

$$g_{e}(\boldsymbol{q} + \boldsymbol{p} - \boldsymbol{p}') f(\boldsymbol{p}') (1 + f(\boldsymbol{p})) - g_{e}(\boldsymbol{q}) f(\boldsymbol{p}) (1 + f(\boldsymbol{p}'))$$

$$= g_{e}(\boldsymbol{q}) \left[f(\boldsymbol{p}') - f(\boldsymbol{p}) \right] - f(\boldsymbol{p}') g_{e}(\boldsymbol{q}) \mathcal{F}_{\left(\frac{q}{m_{e}}\right)}$$

$$- f(\boldsymbol{p}') g_{e}(\boldsymbol{q}) \left[\mathcal{F}_{\left(\frac{p}{m_{e}}\right)} - \frac{1}{2} \mathcal{F}_{\left(\frac{q}{m_{e}}\right)}^{2} \right] + g_{e}(\boldsymbol{q}) f(\boldsymbol{p}) f(\boldsymbol{p}') \left[-\mathcal{F}_{\left(\frac{q}{m_{e}}\right)} + \frac{1}{2} \mathcal{F}_{\left(\frac{q}{m_{e}}\right)}^{2} - \mathcal{F}_{\left(\frac{p}{m_{e}}\right)} \right].$$
(2.136)

2.5.5 Summary of Collision Terms (q'-Integral)

Combining altogether, we obtain the collision term expanded with respect to the energy transfer as (note that this expansion is not with respect to the density perturbations)

$$C[f] = \frac{3}{2}\pi^2 \frac{a\sigma_{\rm T}}{p} \int \frac{\mathrm{d}^3 \mathbf{p'}}{(2\pi)^3 p'} \int \frac{\mathrm{d}^3 \mathbf{q}}{(2\pi)^3} \left[(0\text{th order}) + (1\text{st order}) + (2\text{nd order}) \right] ,$$
(2.137)

where

0th order term:

$$\mathcal{M}_0 \delta_{\mathrm{D}}(p - p') g_{\mathrm{e}}(\mathbf{q}) \left[f(\mathbf{p'}) - f(\mathbf{p}) \right], \tag{2.138}$$

1st order terms:

$$\mathcal{M}_{0}g_{e}(\boldsymbol{q})\left[-\delta_{D}(p-p')f(\boldsymbol{p'})\mathcal{F}_{(\frac{q}{m_{e}})} + \frac{\partial\delta_{D}(p-p')}{\partial p'}\left[f(\boldsymbol{p'}) - f(\boldsymbol{p})\right]\mathcal{D}_{(\frac{q}{m_{e}})}\right] + \mathcal{M}_{(\frac{q}{m_{e}})}g_{e}(\boldsymbol{q})\delta_{D}(p-p')\left[f(\boldsymbol{p'}) - f(\boldsymbol{p})\right],$$
(2.139)

2nd order terms:

$$\mathcal{M}_{0}g_{\mathbf{e}}(\boldsymbol{q})\left[-\delta_{\mathbf{D}}(p-p')f(\boldsymbol{p'})\left(\mathcal{F}_{(\frac{p}{m_{\mathbf{e}}})}-\frac{1}{2}\mathcal{F}_{(\frac{q}{m_{\mathbf{e}}})}^{2}\right)+\frac{1}{2}\frac{\partial^{2}\delta_{\mathbf{D}}(p-p')}{\partial p'^{2}}\mathcal{D}_{(\frac{q}{m_{\mathbf{e}}})}^{2}\left[f(\boldsymbol{p'})-f(\boldsymbol{p})\right]\right]$$

$$+\frac{\partial\delta_{\mathbf{D}}(p-p')}{\partial p'}\mathcal{D}_{(\frac{p}{m_{\mathbf{e}}})}\left[f(\boldsymbol{p'})-f(\boldsymbol{p})\right]-\frac{\partial\delta_{\mathbf{D}}(p-p')}{\partial p'}\mathcal{D}_{(\frac{q}{m_{\mathbf{e}}})}f(\boldsymbol{p'})\mathcal{F}_{(\frac{q}{m_{\mathbf{e}}})}\right]$$

$$+\mathcal{M}_{(\frac{q}{m_{\mathbf{e}}})}g_{\mathbf{e}}(\boldsymbol{q})\left[-\delta_{\mathbf{D}}(p-p')f(\boldsymbol{p'})\mathcal{F}_{(\frac{q}{m_{\mathbf{e}}})}+\frac{\partial\delta_{\mathbf{D}}(p-p')}{\partial p'}\mathcal{D}_{(\frac{q}{m_{\mathbf{e}}})}\left[f(\boldsymbol{p'})-f(\boldsymbol{p})\right]\right]$$

$$+\mathcal{M}_{0}g_{\mathbf{e}}(\boldsymbol{q})f(\boldsymbol{p})f(\boldsymbol{p'})\left[-\frac{\partial\delta_{\mathbf{D}}(p-p')}{\partial p'}\mathcal{F}_{(\frac{q}{m_{\mathbf{e}}})}\mathcal{D}_{(\frac{q}{m_{\mathbf{e}}})}+\left(\frac{1}{2}\mathcal{F}_{(\frac{q}{m_{\mathbf{e}}})}^{2}-\mathcal{F}_{(\frac{p}{m_{\mathbf{e}}})}\right)\delta_{\mathbf{D}}(p-p')\right]$$

$$-g_{\mathbf{e}}(\boldsymbol{q})f(\boldsymbol{p})f(\boldsymbol{p'})\mathcal{M}_{(\frac{q}{m_{\mathbf{e}}})}\mathcal{F}_{(\frac{q}{m_{\mathbf{e}}})}\delta_{\mathbf{D}}(p-p'). \tag{2.140}$$

The above result is performed by the q'-integral. To derive the perturbed Boltzmann equation, we need to integrate p' and q. Hereafter, we proceed these integrals.

2.5.6 Collision Term (q- and p'-Integral)

The q-integral is performed straightforwardly as

$$C[f] = \frac{3}{2}\pi^2 \frac{an_e\sigma_T}{p} \int \frac{d^3 \mathbf{p'}}{(2\pi)^3 p'} [(0\text{th order}) + (1\text{st order}) + (2\text{nd order})]$$

$$= \frac{3an_e\sigma_T}{4p} \int p' dp' \int \frac{d\Omega'}{4\pi} [(0\text{th order}) + (1\text{st order}) + (2\text{nd order})],$$
(2.141)

where

0th order terms:

$$(1+\cos^2\beta)\delta_{\mathrm{D}}(p-p')\left[f(\mathbf{p'})-f(\mathbf{p})\right],\tag{2.142}$$

1st order terms:

$$(1 + \cos^{2} \beta) \frac{\partial \delta_{D}(p - p')}{\partial p'} \left[f(\mathbf{p'}) - f(\mathbf{p}) \right] (\mathbf{p} - \mathbf{p'}) \cdot \mathbf{v}_{e}$$

$$- 2 \cos \beta (1 - \cos \beta) \delta_{D}(p - p') \left[f(\mathbf{p'}) - f(\mathbf{p}) \right] (\hat{\mathbf{n}} + \hat{\mathbf{n'}}) \cdot \mathbf{v}_{e} , \qquad (2.143)$$

2nd order terms:

$$(1 + \cos^{2}\beta) \frac{\partial^{2}\delta_{D}(p - p')}{\partial p'^{2}} \left[f(\mathbf{p'}) - f(\mathbf{p}) \right] \left[\frac{1}{2} \left((\mathbf{p} - \mathbf{p'}) \cdot \mathbf{v}_{e} \right)^{2} + \frac{T_{e}}{2m_{e}} (\mathbf{p} - \mathbf{p'})^{2} \right]$$

$$- (1 + \cos^{2}\beta) \frac{\partial \delta_{D}(p - p')}{\partial p'} \left[f(\mathbf{p'}) + 2f(\mathbf{p})f(\mathbf{p'}) + f(\mathbf{p}) \right] \frac{(\mathbf{p} - \mathbf{p'})^{2}}{2m_{e}}$$

$$+ 2\cos\beta(1 - \cos\beta)\delta_{D}(p - p')f(\mathbf{p'})(1 + f(\mathbf{p})) \frac{(\mathbf{p} - \mathbf{p'})}{m_{e}} \cdot (\hat{\mathbf{n}} + \hat{\mathbf{n'}})$$

$$- 2\cos\beta(1 - \cos\beta) \frac{\partial \delta_{D}(p - p')}{\partial p'} \left[f(\mathbf{p'}) - f(\mathbf{p}) \right] \left[\left((\mathbf{p} - \mathbf{p'}) \cdot \mathbf{v}_{e} \right) \left((\hat{\mathbf{n}} + \hat{\mathbf{n'}}) \cdot \mathbf{v}_{e} \right) \right]$$

$$- 2\cos\beta(1 - \cos\beta) \frac{\partial \delta_{D}(p - p')}{\partial p'} \left[f(\mathbf{p'}) - f(\mathbf{p}) \right] \left[\frac{T_{e}}{m_{e}} (\mathbf{p} - \mathbf{p'}) \cdot (\hat{\mathbf{n}} + \hat{\mathbf{n'}}) \right].$$
(2.144)

From here, we do not expand the cosmological perturbation but the smallness of the energy transfer in Eq. (2.115). To complete the derivation of the Boltzmann equation, we expand the distribution function up to the second order as

$$f(\mathbf{p}) = f^{(0)}(\mathbf{p}) + f^{(1)}(\mathbf{p}) + \frac{1}{2}f^{(2)}(\mathbf{p}),$$
 (2.145)

$$v_{\rm e} = v_{\rm e}^{(1)} + \frac{1}{2}v_{\rm e}^{(2)}$$
 (2.146)

After substituting Eqs. (2.145) and (2.146) into Eq. (2.141), we can derive the expanded collision terms as

$$\begin{split} C[f] &= \frac{3an_{\rm e}\sigma_{\rm T}}{4p} \int p' \mathrm{d}p' \int \frac{\mathrm{d}\Omega'}{4\pi} \left[c^{(1)}(\pmb{p}, \pmb{p}') \right] \\ &+ \frac{3an_{\rm e}\sigma_{\rm T}}{4p} \int p' \mathrm{d}p' \int \frac{\mathrm{d}\Omega'}{4\pi} \left[\frac{1}{2} \left(c_{\Delta}^{(2)}(\pmb{p}, \pmb{p}') + c_{v}^{(2)}(\pmb{p}, \pmb{p}') + c_{\Delta v}^{(2)}(\pmb{p}, \pmb{p}') + c_{vv}^{(2)}(\pmb{p}, \pmb{p}') + c_{K}^{(2)}(\pmb{p}, \pmb{p}') \right], \end{split}$$

$$(2.147)$$

where

$$c^{(1)}(\mathbf{p}, \mathbf{p'}) = (1 + \cos^{2} \beta)$$

$$\times \left[\delta_{D}(p - p') \left(f^{(1)}(\mathbf{p'}) - f^{(1)}(\mathbf{p}) \right) + \frac{\partial \delta_{D}(p - p')}{\partial p'} \left(f^{(0)}(p') - f^{(0)}(p) \right) (\mathbf{p} - \mathbf{p'}) \cdot \mathbf{v}_{e}^{(1)} \right],$$
(2.148)

$$\frac{1}{2}c_{\Delta}^{(2)}(\boldsymbol{p}, \boldsymbol{p'}) = \frac{1}{2}(1 + \cos^{2}\beta)\delta_{D}(p - p')\left(f^{(2)}(\boldsymbol{p'}) - f^{(2)}(\boldsymbol{p})\right), \qquad (2.149)$$

$$\frac{1}{2}c_{v}^{(2)}(\boldsymbol{p}, \boldsymbol{p'}) = \frac{1}{2}(1 + \cos^{2}\beta)\frac{\partial\delta_{D}(p - p')}{\partial p'}\left(f^{(0)}(p') - f^{(0)}(p)\right)(\boldsymbol{p} - \boldsymbol{p'}) \cdot \boldsymbol{v}_{e}^{(2)}, \qquad (2.150)$$

$$\frac{1}{2}c_{\Delta v}^{(2)}(\boldsymbol{p},\boldsymbol{p'}) = \left(f^{(1)}(\boldsymbol{p'}) - f^{(1)}(\boldsymbol{p})\right) \\
\times \left[(1 + \cos^2 \beta) \frac{\partial \delta_{\mathrm{D}}(\boldsymbol{p} - \boldsymbol{p'})}{\partial \boldsymbol{p'}} (\boldsymbol{p} - \boldsymbol{p'}) \cdot \boldsymbol{v}_{\mathrm{e}} - 2\cos \beta (1 - \cos \beta) \delta_{\mathrm{D}}(\boldsymbol{p} - \boldsymbol{p'}) (\hat{\boldsymbol{n}} + \hat{\boldsymbol{n}'}) \cdot \boldsymbol{v}_{\mathrm{e}} \right], \tag{2.151}$$

$$\frac{1}{2}c_{vv}^{(2)}(\boldsymbol{p},\boldsymbol{p'}) = \left(f^{(0)}(p') - f^{(0)}(p)\right)(\boldsymbol{p} - \boldsymbol{p'}) \cdot \boldsymbol{v}_{e} \\
\times \left[(1 + \cos^{2}\beta) \frac{(\boldsymbol{p} - \boldsymbol{p'}) \cdot \boldsymbol{v}_{e}}{2} \frac{\partial^{2}\delta_{D}(p - p')}{\partial p'^{2}} - 2\cos\beta(1 - \cos\beta)(\hat{\boldsymbol{n}} + \hat{\boldsymbol{n}}') \cdot \boldsymbol{v}_{e} \frac{\partial\delta_{D}(p - p')}{\partial p'} \right],$$
(2.152)

$$\begin{split} \frac{1}{2}c_{K}^{(2)}(\textbf{\textit{p}},\textbf{\textit{p}}') &= (1+\cos^{2}\beta)\frac{(\textbf{\textit{p}}-\textbf{\textit{p}}')^{2}}{2m_{e}} \\ &\times \left[\left(f^{(0)}(p') - f^{(0)}(p) \right) T_{e} \frac{\partial^{2}\delta_{D}(p-p')}{\partial p'^{2}} - \left(f^{(0)}(p') + 2f^{(0)}(p) f^{(0)}(p') + f^{(0)}(p) \right) \frac{\partial\delta_{D}(p-p')}{\partial p'} \right] \\ &+ \frac{2(p-p')\cos\beta(1-\cos^{2}\beta)}{m_{e}} \\ &\times \left[\delta_{D}(p-p')f^{(0)}(p')(1+f^{(0)}(p)) - T_{e} \left(f^{(0)}(p') - f^{(0)}(p) \right) \frac{\partial\delta_{D}(p-p')}{\partial p'} \right], \end{split} \tag{2.153}$$

where we use the relation $(\boldsymbol{p} - \boldsymbol{p}') \cdot (\hat{\boldsymbol{n}} + \hat{\boldsymbol{n}}') = (p - p')(1 + \cos\beta)$. The prefactor n_e appeared in Eq. (2.147) must be expanded as $n_e = n_e^{(0)} (1 + \delta_e^{(1)})$.

We expand the distribution function by using the Legendre polynomials $P_\ell(\mu)$ for the first order as

$$f^{(1)}(\mathbf{x}, p, \hat{\mathbf{n}}) = \sum_{\ell} (2\ell + 1) f_{\ell}^{(1)}(\mathbf{x}, p) P_{\ell}(\mu) , \qquad (2.154)$$

where we define $\mu = \mathbf{n} \cdot \hat{\mathbf{v}}$ and $\mu' = \mathbf{n'} \cdot \hat{\mathbf{v}}$. This is because the first-order distribution function does not depend on the azimuthal angle. The second-order distribution function is expanded by the spherical harmonics $Y_{\ell,m}(\hat{\mathbf{n}}')$ as

$$f^{(1,2)}(\boldsymbol{x}, p', \hat{\boldsymbol{n}}') = \sum_{\ell} \sum_{m=-\ell}^{\ell} f_{\ell,m}^{(1,2)}(\boldsymbol{x}, p') (-i)^{\ell} \sqrt{\frac{4\pi}{2\ell+1}} Y_{\ell,m}(\hat{\boldsymbol{n}}') . \tag{2.155}$$

We can relate the first-order distribution function expanded by the Legendre polynomials and spherical harmonics as

$$f_{\ell m}^{(1)}(\mathbf{x}, p)\delta_{m,0} = (-i)^{-\ell}(2\ell+1)\delta_{m,0}f_{\ell}^{(1)}(\mathbf{x}, p). \tag{2.156}$$

Finally, we can proceed the p'-integral as

$$C(\mathbf{p}) = an_{\rm e}\sigma_{\rm T} \left[C^{(1)}(\mathbf{p}) + \frac{1}{2} \left(C_{\Delta}^{(2)}(\mathbf{p}) + C_{v}^{(2)}(\mathbf{p}) + C_{\Delta v}^{(2)}(\mathbf{p}) + C_{vv}^{(2)}(\mathbf{p}) + C_{K}^{(2)}(\mathbf{p}) \right) \right],$$
(2.157)

where

$$C^{(1)}(\mathbf{p}) = f_0^{(1)}(p) + \frac{1}{2} f_2^{(1)}(p) P_2(\mu) - f^{(1)}(\mathbf{p}) - p \frac{\partial f^{(0)}(p)}{\partial p} \mu v , \qquad (2.158)$$

$$\frac{1}{2}C_{\Delta}^{(2)}(\boldsymbol{p}) = \frac{1}{2} \left[f_{00}^{(2)}(\boldsymbol{p}) - f^{(2)}(\boldsymbol{p}) - \frac{1}{2} \sum_{m=-2}^{2} \frac{\sqrt{4\pi}}{5^{3/2}} f_{2m}^{(2)}(\boldsymbol{p}) Y_{2,m}(\hat{\boldsymbol{n}}) \right], \quad (2.159)$$

$$\frac{1}{2}C_v^{(2)}(\mathbf{p}) = -\frac{1}{2}p\frac{\partial f^{(0)}(p)}{\partial p}\mu v^{(2)}, \qquad (2.160)$$

$$\frac{1}{2}C_{\Delta v}^{(2)}(\mathbf{p}) = \mu v \left[f^{(1)}(\mathbf{p}) - f_0^{(1)}(p) - p \frac{\partial f_0^{(1)}(p)}{\partial p} - f_2^{(1)}(p) + \frac{1}{2}P_2(\mu) \left(f_2^{(1)}(p) - p \frac{\partial f_2^{(1)}(p)}{\partial p} \right) \right]
+ v \left[2f_1^{(1)}(p) + p \frac{\partial f_1^{(1)}(p)}{\partial p} \right]
+ \frac{1}{5}P_2(\mu) \left(-f_1^{(1)}(p) + p \frac{\partial f_1^{(1)}(p)}{\partial p} + 6f_3^{(1)}(p) + \frac{3}{2}p \frac{\partial f_3^{(1)}(p)}{\partial p} \right) \right],$$
(2.161)

$$\frac{1}{2}C_{vv}^{(2)}(\mathbf{p}) = v^2 \left[\mu^2 \left(p \frac{\partial f^{(0)}(p)}{\partial p} + \frac{11}{20} p^2 \frac{\partial^2 f^{(0)}(p)}{\partial p^2} \right) + p \frac{\partial f^{(0)}(p)}{\partial p} + \frac{3}{20} p^2 \frac{\partial^2 f^{(0)}(p)}{\partial p^2} \right],$$
(2.162)

$$\frac{1}{2}C_K^{(2)}(p) = \frac{1}{p^2 m_e} \frac{\partial}{\partial p} \left[p^4 \left\{ T_e \frac{\partial f^{(0)}(p)}{\partial p} + f^{(0)}(p) \left(1 + f^{(0)}(p) \right) \right\} \right], \tag{2.163}$$

where in order to derive the above result, we used the following formulae:

$$1 + \cos^{2} \beta = 1 + (\hat{\boldsymbol{n}} \cdot \hat{\boldsymbol{n}}')^{2}$$

$$= \frac{4}{3} \left(1 + \frac{1}{2} P_{2} (\hat{\boldsymbol{n}} \cdot \hat{\boldsymbol{n}}') \right)$$

$$= \frac{4}{3} \left(1 + \frac{2\pi}{5} \sum_{m=-2}^{2} Y_{2,m} (\hat{\boldsymbol{n}}) Y_{2,m}^{*} (\hat{\boldsymbol{n}}') \right) , \qquad (2.164)$$

$$-\cos\beta(1-\cos\beta) = -(\hat{\boldsymbol{n}}\cdot\hat{\boldsymbol{n}}')(1-(\hat{\boldsymbol{n}}\cdot\hat{\boldsymbol{n}}'))$$
$$= \frac{1}{3} - P_1(\hat{\boldsymbol{n}}\cdot\hat{\boldsymbol{n}}') + \frac{2}{3}P_2(\hat{\boldsymbol{n}}\cdot\hat{\boldsymbol{n}}'), \qquad (2.165)$$

$$\int \frac{d\phi'}{2\pi} P_n(\hat{\boldsymbol{n}} \cdot \hat{\boldsymbol{n}}') = P_n(\hat{\boldsymbol{n}} \cdot \hat{\boldsymbol{v}}) P_n(\hat{\boldsymbol{n}}' \cdot \hat{\boldsymbol{v}})$$
$$= P_n(\mu) P_n(\mu') . \tag{2.166}$$

We explain the meanings of each term. $C^{(1)}$ is the ordinal collision term in the first-order perturbation theory. When we study the first-order CMB fluctuations, it is sufficient to include this term. $C^{(2)}_{\Delta}$ is the purely second-order collision term which contributes on the second-order fluctuation as well as the ordinal first-order collision term. $C^{(2)}_{\nu}$ is the purely second-order velocity contribution. This term causes the second-order quadratic doppler effect. $C^{(2)}_{\Delta\nu}$ is the coupling of photons and velocity perturbations. $C^{(2)}_{\nu\nu}$ is the quadratic term of the velocity. And $C^{(2)}_{K}$ is the Kompaneets term which induces the spectral distortion of the CMB spectrum. The Kompaneets term does not affect the anisotropy of the fluctuations and therefore which is ignored in this part.

2.5.7 Perturbed Boltzmann Equation

From here, let us combine the perturbed streaming term and collision term. It is convenient to define the *brightness function* to remove the amplitude of momentum dependence which is given by

$$\Delta^{(1,2)}(\eta, \mathbf{x}, \hat{\mathbf{n}}) = \frac{\int dp \ p^3 f^{(1,2)}(\eta, \mathbf{x}, p, \hat{\mathbf{n}})}{\int dp \ p^3 f^{(0)}(\eta, p)}, \qquad (2.167)$$

where the denominator of the right-hand side is proportional to the mean energy density of photons.

The angle dependence of the brightness function is expanded by the spherical harmonics as

$$\Delta^{(1,2)}(\eta, \mathbf{x}, \hat{\mathbf{n}}) = \sum_{\ell} \sum_{m=-\ell}^{\ell} \Delta_{\ell,m}^{(1,2)}(\eta, \mathbf{x})(-i)^{\ell} \sqrt{\frac{4\pi}{2\ell+1}} Y_{\ell,m}(\hat{\mathbf{n}}).$$
 (2.168)

The coefficients $\Delta_{\ell,m}^{(1)}$ are related to the density perturbation, velocity, and anisotropic stress for photons as $\Delta_{0,0}^{(1)}=\delta_{\gamma}^{(1)}$, $\Delta_{1,0}^{(1)}=4v_{\gamma\,0}^{(1)}$, and $\Delta_{2,0}^{(1)}=5\Pi_{\gamma\,0}^{(1)}$, respectively. The Boltzmann equation of photons in terms of $\Delta_{\ell,m}^{(1,2)}$ at first- and second-order is written as

$$\dot{\Delta}_{\ell,m}^{(1,2)} + k \left[\frac{c_{\ell+1,m}}{2\ell+3} \Delta_{\ell+1,m}^{(1,2)} - \frac{c_{\ell,m}}{2\ell-1} \Delta_{\ell-1,m}^{(1,2)} \right] = S_{\ell,m}^{(1,2)} , \qquad (2.169)$$

where $c_{\ell,m} \equiv \sqrt{\ell^2 - m^2}$.

Here, we have translated from real space to Fourier space. The source term $S_{\ell,m}^{(2)}$ can be expressed as

$$S_{\ell m}^{(2)}(\mathbf{k}, \eta) = C_{\ell m}^{(2)}(\mathbf{k}, \eta) + \mathcal{G}_{\ell m}^{(2)}(\mathbf{k}, \eta) , \qquad (2.170)$$

Here, $C_{\ell,m}^{(2)}$ is the collision term that is proportional to $\dot{\tau}_c$, where $\dot{\tau}_c$ is the differential optical depth which is defined by the number density of the electron $n_e^{(0)}$, scale factor a, and the Thomson scattering cross-section σ_T as $\dot{\tau}_c = -an_e^{(0)}\sigma_T$, and $G_{\ell,m}^{(2)}$ denotes the gravitational effects, i.e., the lensing and the redshift terms. The collision term $C_{\ell,m}^{(2)}$ is related to Eq. (2.137) as

$$C_{\ell,m}^{(2)}(\mathbf{k},\eta) = \int d\Omega_n (-i)^{-\ell} \sqrt{\frac{2\ell+1}{4\pi}} Y_{\ell,m}^*(\hat{\mathbf{n}}) \frac{\int dp \ p^3 C^{(2)}(\eta, \mathbf{k}, p, \hat{\mathbf{n}})}{\int dp \ p^3 f^{(0)}(\eta, p)} , \quad (2.171)$$

where $\mathcal{C}^{(2)}(\eta, \boldsymbol{k}, p, \hat{\boldsymbol{n}})$ is the Fourier transformation of Eq. (2.137), while the gravitational effect $\mathcal{G}^{(2)}_{\ell,m}$ is coming from the perturbed streaming terms (2.103), (2.110), and (2.111) with the same procedure as obtaining $\mathcal{C}^{(2)}(\eta, \boldsymbol{k}, p, \hat{\boldsymbol{n}})$. In this thesis, we call $\mathcal{C}_{\ell,m}$ and $\mathcal{G}_{\ell,m}$ the scattering term and the gravitational term, respectively.

The explicit form of $\mathcal{C}_{\ell,m}^{(2)}$ and $\mathcal{G}_{\ell,m}^{(2)}$ are given as

$$\begin{split} \mathcal{C}_{\ell,m}^{(2)} &= \dot{\tau}_{c} \Delta_{\ell,m}^{(2)} - \dot{\tau}_{c} \left(\Delta_{00}^{(2)} \delta_{\ell,0} \delta_{m,0} + 4 v_{b \, m}^{(2)} \delta_{\ell,1} + \frac{1}{10} \Delta_{2,m}^{(2)} \delta_{\ell,2} \right) \\ &+ \dot{\tau}_{c} \int_{\pmb{k}} \left[-2 (\delta_{\mathbf{b}} + \Psi)^{(1)} (k_{1}) \delta_{\gamma}^{(1)} (k_{2}) - 4 (\hat{\pmb{k}}_{1} \cdot \hat{\pmb{k}}_{2}) v_{\gamma \, 0}^{(1)} (k_{1}) v_{b \, 0}^{(1)} (k_{2}) \right] \delta_{\ell,0} \delta_{m,0} \\ &+ \dot{\tau}_{c} \int_{\pmb{k}} \left[-2 (\hat{\pmb{k}}_{1} \cdot \hat{\pmb{k}}_{2}) v_{b \, 0}^{(1)} (k_{1}) v_{b \, 0}^{(1)} (k_{2}) \right] \delta_{\ell,0} \delta_{m,0} \\ &+ \dot{\tau}_{c} \int_{\pmb{k}} \left[-2 v_{b \, 0}^{(1)} (k_{1}) \Pi_{\gamma \, 0}^{(1)} (k_{2}) \right] \sqrt{\frac{4\pi}{3}} Y_{1,m}^{*} (\hat{\pmb{k}}_{1}) \delta_{\ell,1} \\ &+ \dot{\tau}_{c} \int_{\pmb{k}} \left[-8 v_{b \, 0}^{(1)} (k_{1}) (\delta_{\mathbf{b}} + \Psi)^{(1)} (k_{2}) - 6 v_{b \, 0}^{(1)} (k_{1}) \delta_{\gamma}^{(1)} (k_{2}) \right] \sqrt{\frac{4\pi}{3}} Y_{1,m}^{*} (\hat{\pmb{k}}_{1}) \delta_{\ell,1} \\ &+ \dot{\tau}_{c} \int_{\pmb{k}} \left[-\Pi_{\gamma \, 0}^{(1)} (k_{1}) (\delta_{\mathbf{b}} + \Psi)^{(1)} (k_{2}) \right] \sqrt{\frac{4\pi}{5}} Y_{2,m}^{*} (\hat{\pmb{k}}_{1}) \delta_{\ell,2} \\ &+ \dot{\tau}_{c} \int_{\pmb{k}} \left[2\Delta_{\ell,0}^{(1)} (k_{1}) (\delta_{\mathbf{b}} + \Psi)^{(1)} (k_{2}) \right] \sqrt{\frac{4\pi}{2\ell+1}} Y_{\ell,m}^{*} (\hat{\pmb{k}}_{1}) \\ &+ \dot{\tau}_{c} i (-i)^{-\ell} (-1)^{m} (2\ell+1) \sum_{\ell_{1}} \sum_{m_{1},m_{2}} (-i)^{\ell_{1}} \binom{\ell_{1}}{\ell_{1}} \ell_{\ell_{1}} \binom{\ell_{1}}{\ell_{1}} \ell_{\ell_{1}} \sqrt{\frac{4\pi}{3}} Y_{1,m_{2}}^{*} (\hat{\pmb{k}}_{2}) \\ &+ \dot{\tau}_{c} (-i)^{-\ell} (-1)^{m} (2\ell+1) \sum_{m_{1},m_{2}} \binom{1}{\ell_{1}} \ell_{\ell_{1}} \binom{\ell_{1}}{\ell_{1}} \ell_{\ell_{1},m_{1}} (\hat{\pmb{k}}_{1}) \sqrt{\frac{4\pi}{3}} Y_{1,m_{2}}^{*} (\hat{\pmb{k}}_{2}) \\ &+ \dot{\tau}_{c} (-i)^{-\ell} (-1)^{m} (2\ell+1) \sum_{m_{1},m_{2}} \binom{1}{\ell_{1}} \ell_{\ell_{1}} \binom{\ell_{1}}{\ell_{1}} \ell_{\ell_{1}} \binom{\ell_{1}}{\ell_{1}} \ell_{\ell_{1}} \binom{\ell_{1}}{\ell_{1}} \ell_{\ell_{1}} \binom{\ell_{1}}{\ell_{1}} \ell_{\ell_{1}} \binom{\ell_{1}}{\ell_{1}} \ell_{\ell_{1}} \binom{\ell_{1}}{\ell_{1}} \binom{\ell_{1}}{\ell_{1}} \ell_{\ell_{1}} \ell_{\ell_{1}$$

and

$$\begin{split} \mathcal{G}_{\ell,m}^{(2)} &= 4\dot{\Phi}^{(2)}\delta_{\ell,0}\delta_{m,0} - \sum_{\lambda = \pm 1} 4\dot{\omega}_{\lambda}^{(2)}\delta_{\ell,1}\delta_{m,\lambda} + 4k\Psi^{(2)}\delta_{\ell,1}\delta_{m,0} - \sum_{\sigma = \pm 2} 2\dot{\chi}_{\sigma}^{(2)}\delta_{\ell,2}\delta_{m,\sigma} \\ &+ 4k\int_{k} \left[\Psi^{(1)}(k_{1})\Psi^{(1)}(k_{2}) \right] \delta_{\ell,1}\delta_{m,0} + \int_{k} \left[8\Delta_{\ell,0}^{(1)}(k_{1})\dot{\Phi}^{(1)}(k_{2}) \right] \sqrt{\frac{4\pi}{2\ell+1}} Y_{\ell,m}^{*}(\hat{k}_{1}) \\ &+ 2i(-i)^{-\ell}(2\ell+1) \sum_{\ell_{2}} \sum_{m_{1},m_{2}} (-1)^{m}(2\ell_{2}+1) \begin{pmatrix} 1 & \ell_{2} & \ell \\ 0 & 0 & 0 \end{pmatrix} \begin{pmatrix} 1 & \ell_{2} & \ell \\ m_{1} & m_{2} & -m \end{pmatrix} \\ &\times \int_{k} \left[k_{1} \left(\Psi + \Phi \right)^{(1)}(k_{1}) \tilde{\Delta}_{\ell}^{(1)}(k_{2}) \right] \sqrt{\frac{4\pi}{3}} Y_{1,m_{1}}^{*}(\hat{k}_{1}) \sqrt{\frac{4\pi}{2\ell_{2}+1}} Y_{\ell_{2},m_{2}}^{*}(\hat{k}_{2}) \\ &+ \int_{k} \left[8k_{1}\Psi^{(1)}(k_{1})\Phi^{(1)}(k_{2}) \right] \sqrt{\frac{4\pi}{3}} Y_{1,m}^{*}(\hat{k}_{1})\delta_{\ell,1} \\ &- i(-i)^{-\ell}(2\ell+1) \sum_{\ell_{1}} (-i)^{\ell_{1}} \begin{pmatrix} \ell_{1} & 1 & \ell \\ 0 & 0 & 0 \end{pmatrix} \begin{pmatrix} \ell_{1} & 1 & \ell \\ 0 & 0 & 0 \end{pmatrix} \end{split}$$

$$\times \int_{\mathbf{k}} \left[2k_{1} \Delta_{\ell_{1},0}^{(1)}(k_{1}) (\Psi^{(1)} + \Phi^{(1)})(k_{2}) \right] \sqrt{\frac{4\pi}{2\ell + 1}} Y_{\ell,m}^{*}(\hat{\mathbf{k}}_{1})$$

$$- i(-i)^{-\ell} (-1)^{m} (2\ell + 1) \sum_{\ell_{1}} \sum_{m_{1},m_{2}} (-i)^{\ell_{1}} \begin{pmatrix} \ell_{1} & 1 & \ell \\ 0 & 0 & 0 \end{pmatrix} \begin{pmatrix} \ell_{1} & 1 & \ell \\ m_{1} & m_{2} & -m \end{pmatrix}$$

$$\times \int_{\mathbf{k}} \left[8k_{2} \Delta_{\ell_{1},0}^{(1)}(k_{1}) \Psi^{(1)}(k_{2}) \right] \sqrt{\frac{4\pi}{2\ell_{1} + 1}} Y_{\ell_{1},m_{1}}^{*}(\hat{\mathbf{k}}_{1}) \sqrt{\frac{4\pi}{3}} Y_{1,m_{2}}^{*}(\hat{\mathbf{k}}_{2})$$

$$+ 2i(-i)^{\ell} (-1)^{m} (2\ell + 1) \sum_{L,L',L''} \sum_{M',M''} (2L + 1)(2L' + 1)(2L'' + 1)$$

$$\times \begin{pmatrix} 1 & 1 & L' \\ 0 & 0 & 0 \end{pmatrix} \begin{pmatrix} L' & \ell & L \\ 0 & 0 & 0 \end{pmatrix} \begin{pmatrix} 1 & L & L'' \\ 0 & 0 & 0 \end{pmatrix} \begin{pmatrix} 1 & L & L'' \\ M' & M'' & -m \end{pmatrix} \begin{cases} 1 & \ell & L'' \\ L & 1 & L' \end{pmatrix}$$

$$\times \int_{\mathbf{k}} \left[k_{1} (\Psi + \Phi)^{(1)} (k_{1}) \tilde{\Delta}_{L}^{(1)}(k_{2}) \right] \sqrt{\frac{4\pi}{3}} Y_{1,M'}^{*}(\hat{\mathbf{k}}_{1}) \sqrt{\frac{4\pi}{2L'' + 1}} Y_{L'',M''}^{*}(\hat{\mathbf{k}}_{2}) ,$$

$$(2.173)$$

where Fourier wavevectors k, k_1 , and k_2 satisfy the relation $k = k_1 + k_2$. In Eq. (2.173), we have defined $\tilde{\Delta}_{\ell}^{(1)}$ as

$$\tilde{\Delta}_{\ell''}^{(1)} \equiv (2\ell'' + 3)\Delta_{\ell''+1}^{(1)} + (2\ell'' + 7)\Delta_{\ell''+3}^{(1)} + \cdots, \qquad (2.174)$$

which comes from the lensing term [8]. We can see that the lensing term contains higher multipole moments. The source term of the first-order Boltzmann equation vanish when $m \neq 0$, because we consider only the scalar mode in the first order perturbations. However for the second-order perturbations, not only the scalar mode (m=0), but also the vector $(m=\lambda)$ and tensor $(m=\sigma)$ modes arise due to nonlinear coupling, where $\lambda=\pm 1$ and $\sigma=\pm 2$, respectively. Note that in the Einstein gravity, there is no source of the modes with $|m|\geq 3$.

When considering massless neutrinos, one can set $\dot{\tau}_{\rm c}=0$ in the above equation because massless neutrinos interact with the other fluids only through gravity. We do not write down the hierarchical equation of massless neutrinos here since it is trivial. The distribution function of neutrinos is also expanded by the spherical harmonics and we write the expansion coefficients as $\mathcal{N}_{\ell,m}^{(1,2)}$.

2.6 Nonrelativistic Particles

In this section, we derive the Boltzmann equation for the nonrelativistic particles such as baryons and dark matters. Although the Boltzmann equation for relativistic particles is the hierarchical equation as shown in Eq. (2.169), the nonrelativistic particles can be truncate its hierarchical equation since the nonrelativistic particles do not have a pressure and an anisotropic stress.

The Boltzmann equation for the nonrelativistic particles reduces to the two fundamental equations, namely, the continuity equation and Euler equation. We show the derivations of the continuous and Euler equations from the Boltzmann equation. Here, we assume that protons and electrons couple strongly by the Coulomb interaction, in other words, $\delta_b \equiv \delta_e = \delta_p$ and $\boldsymbol{\textit{v}}_b \equiv \boldsymbol{\textit{v}}_e = \boldsymbol{\textit{v}}_p$.

At first, we consider the Boltzmann equation for massive particles:

$$\frac{\mathrm{d}g}{\mathrm{d}\lambda} = \tilde{C}[g] . \tag{2.175}$$

By using the conformal time, we can express the Boltzmann equation as

$$\frac{\partial g}{\partial \eta} + \frac{\mathrm{d}x^i}{\mathrm{d}\eta} \frac{\partial g}{\partial x^i} + \frac{\mathrm{d}q^i}{\mathrm{d}\eta} \frac{\partial g}{\partial q^i} = \frac{ae^{\Psi}}{E} \tilde{C}[g] \equiv e^{\Psi} C[g] . \tag{2.176}$$

By using Eqs. (2.103) and (2.110), the left-hand side of the Boltzmann equation (2.176) is rewritten as

$$\frac{\mathrm{d}g}{\mathrm{d}\eta} = \frac{\partial g}{\partial \eta} + \frac{q}{E} \hat{n}^{j} e^{\Phi + \Psi} \left[\delta_{ij} \left(1 - \frac{q}{E} \omega_{k} \hat{n}^{k} \right) - \frac{1}{2} \chi_{ij} \right] \frac{\partial g}{\partial x^{i}}
+ \left[-(\mathcal{H} - \dot{\Phi}) q^{i} - \frac{1}{2} \dot{\chi}^{i}{}_{k} q^{k} - (\omega^{i}{}_{,k} - \omega_{k}{}^{,i}) q^{k} - E e^{\Phi + \Psi} \Psi^{,i} - E (\dot{\omega}^{i} + \mathcal{H}\omega^{i}) \right]
+ \frac{1}{E} e^{\Phi + \Psi} \left(\Phi_{,j} q^{j} q^{i} - q^{2} \Phi^{,i} \right) + \frac{1}{E} \left(\mathcal{H} q^{2} \omega^{i} - \frac{1}{2} \chi^{i}{}_{j,m} q^{j} q^{m} + \frac{1}{2} \chi_{jm}{}^{,i} q^{j} q^{m} \right) \frac{\partial g}{\partial q^{i}}.$$
(2.177)

Second, let us focus on the collision term in the Boltzmann equation for massive particles. The Boltzmann equations for electrons and protons are given by

$$\frac{\mathrm{d}g_{\mathrm{e}}}{\mathrm{d}\eta}(\eta, \mathbf{x}, \mathbf{q}) = \langle c_{\mathrm{ep}} \rangle_{\mathcal{Q}\mathcal{Q}'q'} + \langle c_{\mathrm{e}} \rangle_{pp'q'}, \qquad (2.178)$$

$$\frac{\mathrm{d}g_{\mathrm{p}}}{\mathrm{d}\eta}(\eta, \boldsymbol{x}, \boldsymbol{Q}) = \langle c_{\mathrm{ep}} \rangle_{qq'Q'}, \qquad (2.179)$$

where

$$\langle \dots \rangle_{pp'q'} \equiv \int \frac{d^3p}{(2\pi)^3} \int \frac{d^3p'}{(2\pi)^3} \int \frac{d^3q'}{(2\pi)^3} \dots$$
 (2.180)

The collision term between protons and photons can be neglected since the scattering amplitude is suppressed by the factor $(m_e/m_p)^2 \approx O(10^{-7})$.

2.6.1 Zeroth Moment—Continuity Equation

By taking the zeroth moment of the Boltzmann equation for electrons (2.178), the left-hand side of Eq. (2.178) becomes

$$\langle \frac{dg_{\rm e}}{d\eta} \rangle_q = \frac{\partial n_{\rm e}}{\partial \eta} + e^{\Phi + \Psi} \left(n_{\rm e} v_{\rm e}^i \right)_{,i} + 3 \left(\mathcal{H} - \dot{\Phi} \right) n_{\rm e} + e^{\Phi + \Psi} \left(\Psi_{,i} - 2\Phi_{,i} \right) n_{\rm e} v_{\rm e}^i . \tag{2.181}$$

We can easily see that the zeroth moment of the collision term in Eq. (2.178) vanishes as follows. After taking the zeroth order moment, the right-hand side is given as $\langle c_{e\gamma} \rangle_{pp'qq'} + \langle c_{ep} \rangle_{QQ'qq'}$. The collision term is the anti-symmetric form under the exchange of $\mathbf{q} \leftrightarrow \mathbf{q}'$ and $\mathbf{p} \leftrightarrow \mathbf{p}'$. Therefore, the collision terms are evaluated as

$$\langle c_{e\gamma} \rangle_{pp'qq'} + \langle c_{ep} \rangle_{QQ'qq'} = -\left(\langle c_{e\gamma} \rangle_{p'pq'q} + \langle c_{ep} \rangle_{Q'Qq'q}\right)$$

$$= -\left(\langle c_{e\gamma} \rangle_{pp'qq'} + \langle c_{ep} \rangle_{QQ'qq'}\right)$$

$$= 0. \tag{2.182}$$

where we use the exchange of the dummy variables, namely, integration variables. In conclusion, the zeroth order moment of the Boltzmann equation is not contributed from the collision terms. The continuity equation from the Boltzmann equation is written as

$$\frac{\partial n_{\rm e}}{\partial \eta} + e^{\Phi + \Psi} (n_{\rm e} v_{\rm e}^i)_{,i} + 3(\mathcal{H} - \dot{\Phi}) n_{\rm e} + e^{\Phi + \Psi} (\Psi_{,i} - 2\Phi_{,i}) n_{\rm e} v_{\rm e}^i = 0.$$
 (2.183)

We can derive the continuity equation up to the second order as

$$\dot{n}_{\rm b}^{(0)} + 3\mathcal{H}n_{\rm b}^{(0)} = 0 , \qquad (2.184)$$

$$\dot{\delta}_{\rm h}^{(1)}(k) - 3\dot{\Phi}^{(1)}(k) + k v_{\rm h,0}^{(1)}(k) = 0, \qquad (2.185)$$

$$\begin{split} \dot{\delta}_{b}^{(2)}(\mathbf{k}) - 3\dot{\Phi}^{(2)}(\mathbf{k}) + kv_{b\,0}^{(2)}(\mathbf{k}) &= 6\int_{\mathbf{k}} \left[\dot{\Phi}^{(1)}(k_{1})\delta_{b}^{(1)}(k_{2}) \right] \\ - 2\int_{\mathbf{k}} \left[k_{1}(\hat{\mathbf{k}}_{1} \cdot \hat{\mathbf{k}}_{2}) \left(\delta_{b}^{(1)} + \Psi^{(1)} - 2\Phi^{(1)} \right) (k_{1})v_{b\,0}^{(1)}(k_{2}) \right] \\ - 2\int_{\mathbf{k}} \left[k_{2}(\delta_{b}^{(1)} + \Phi^{(1)} + \Psi^{(1)})(k_{1})v_{b\,0}^{(1)}(k_{2}) \right] \,. \end{split}$$

$$(2.186)$$

Note that the vector-mode of the Boltzmann equation for photons does not need the second-order continuity equation for baryons. We only use the first-order continuity equation to solve the Boltzmann equation for photons.

2.6.2 First Moment—Euler Equation

The first moment of the Boltzmann equation is corresponding to the Euler equation. The left-hand side of the Boltzmann equation (2.178) can be written as

$$\langle \frac{q^{i}}{E} \frac{dg}{d\eta} \rangle_{q} = \frac{\partial}{\partial \eta} (nv^{i}) + e^{\Phi + \Psi} (nv^{k}v^{i})_{,k} + e^{\Phi + \Psi} \left(n \frac{T}{m} \right)^{,i} + 4(\mathcal{H} - \dot{\Phi})nv^{i} + e^{\Phi + \Psi} \Psi^{,i} n + (\dot{\omega}^{i} + \mathcal{H}\omega^{i})n . \tag{2.187}$$

Furthermore, when we combine the first moment of the Boltzmann equations for electrons and protons, the dominant contribution on the left-hand side is protons one. On the other hand, the right-hand side can be written as

$$\langle c_{ep}(q^i + Q^i) \rangle_{OO'qq'} + \langle c_{e\gamma}q^i \rangle_{pp'qq'}.$$
 (2.188)

The first term vanishes due to the momentum conservation $\delta_{\rm D}^3(q^i+Q^i-q'^i-Q'^i)$. Moreover, the second term is rewritten by using the momentum conservation as

$$\langle c_{e\gamma}q^i \rangle_{pp'qq'} = -\langle c_{e\gamma}p^i \rangle_{pp'qq'}$$

$$= -e^{\Psi} \int \frac{d^3 \mathbf{p}}{(2\pi)^3} \left[p^i C[f] \right]. \tag{2.189}$$

Thus, we can use the result of the collision term for photons in Eq. (2.157). By using Eq. (2.157), we can easily perform the above integral as

$$\langle c_{e\gamma}q^{i}\rangle_{pp'qq'} = -e^{\Psi} \int \frac{\mathrm{d}^{3}\mathbf{p}}{(2\pi)^{3}} \left[p^{i}C[f]\right]$$

$$= \dot{\tau}_{c} \left[\frac{4}{3}\rho_{\gamma}(v_{b}^{(1)i} - v_{\gamma}^{(1)i}) + \frac{4}{3}\rho_{\gamma}\left(\frac{1}{2}v_{b}^{(2)i} - \frac{1}{2}v_{\gamma}^{(2)i}\right) + \rho_{\gamma}v_{b}^{(1)j}\Pi_{\gamma}^{(1)i}{}_{j} + \frac{4}{3}\rho_{\gamma}(\delta_{\gamma}^{(1)} + \delta_{e}^{(1)} + \Psi^{(1)})(v_{b}^{(1)i} - v_{\gamma}^{(1)i})\right].$$
(2.190)

Finally, the Euler equation for baryons is given by

$$\begin{split} &\frac{\partial v_{b}^{i}}{\partial \eta} + v_{b}^{k} v_{b,k}^{i} + e^{\Phi + \Psi} \left(\frac{T_{b}}{m_{p}} \right)_{,i} + (\mathcal{H} - \dot{\Phi}) v_{b}^{i} + e^{\Phi + \Psi} \Psi^{,i} + (\dot{\omega}^{i} + \mathcal{H}\omega^{i}) \\ &= \frac{\dot{\tau}_{c}}{R} \left[(v_{b}^{(1)i} - v_{\gamma}^{(1)i}) + \left(\frac{1}{2} v_{b}^{(2)i} - \frac{1}{2} v_{\gamma}^{(2)i} \right) \right. \\ &+ \frac{3}{4} v_{b}^{(1)j} \Pi_{\gamma}^{(1)i}{}_{j} + (\delta_{\gamma}^{(1)} + \delta_{e}^{(1)} - \delta_{b}^{(1)} + \Psi^{(1)}) (v_{b}^{(1)i} - v_{\gamma}^{(1)i}) \right], \end{split}$$
(2.191)

where $R \equiv 3\rho_{\rm b}^{(0)}/(4\rho_{\gamma}^{(0)})$ and we can set $\delta_{\rm e} = \delta_{\rm b}$ due to the Coulomb scattering. Furthermore, the term including $T_{\rm b}$ is suppressed by the proton mass and hereafter, we neglect this term. Finally, we derive the Euler equation up to the second order as

$$\dot{v}_{b\ 0}^{(1)}(k) + \mathcal{H}v_{b\ 0}^{(1)}(k) - k\Psi^{(1)}(k) = -\frac{\dot{\tau}_{c}}{R}\delta v_{\gamma b\ 0}^{(1)}, \qquad (2.192)$$

$$\begin{split} \dot{v}_{b\,m}^{(2)}(\mathbf{k}) + \mathcal{H}v_{b\,m}^{(2)}(\mathbf{k}) - k\Psi^{(2)}(\mathbf{k})\delta_{m,0} &= -\frac{\dot{\tau}_{c}}{R}\delta v_{\gamma b\,m}^{(2)} - \dot{\omega}_{m}^{(2)}(\mathbf{k}) - \mathcal{H}\omega_{m}^{(2)}(\mathbf{k}) \\ &- 2\int_{\mathbf{k}} \left[k_{1}(\hat{\mathbf{k}}_{1} \cdot \hat{\mathbf{k}}_{2})v_{b\,0}^{(1)}(k_{1})v_{b\,0}^{(1)}(k_{2}) \right] \sqrt{\frac{4\pi}{3}} Y_{1,m}^{*}(\hat{\mathbf{k}}_{1}) \\ &+ 2\int_{\mathbf{k}} \left[v_{b\,0}^{(1)}(k_{1})\dot{\Phi}^{(1)}(k_{2}) \right] \sqrt{\frac{4\pi}{3}} Y_{1,m}^{*}(\hat{\mathbf{k}}_{1}) \\ &+ 2\int_{\mathbf{k}} \left[k_{1}\Psi^{(1)}(k_{1})(\Phi^{(1)} + \Psi^{(1)})(k_{2}) \right] \sqrt{\frac{4\pi}{3}} Y_{1,m}^{*}(\hat{\mathbf{k}}_{1}) \\ &- 2\int_{\mathbf{k}} \frac{\dot{\tau}_{c}}{R} \left[\delta v_{\gamma b\,0}^{(1)}(k_{1})(\delta_{\gamma}^{(1)} + \Psi^{(1)})(k_{2}) \right] \sqrt{\frac{4\pi}{3}} Y_{1,m}^{*}(\hat{\mathbf{k}}_{1}) \\ &- \frac{\dot{\tau}_{c}}{R} \frac{3}{2} \int_{\mathbf{k}} \left[(\hat{\mathbf{k}}_{1} \cdot \hat{\mathbf{k}}_{2}) \Pi_{\gamma\,0}^{(1)}(k_{1})v_{b\,0}^{(1)}(k_{2}) \right] \sqrt{\frac{4\pi}{3}} Y_{1,m}^{*}(\hat{\mathbf{k}}_{1}) \\ &+ \frac{\dot{\tau}_{c}}{R} \frac{1}{2} \int_{\mathbf{k}} \left[v_{b\,0}^{(1)}(k_{1}) \Pi_{\gamma\,0}^{(1)}(k_{2}) \right] \sqrt{\frac{4\pi}{3}} Y_{1,m}^{*}(\hat{\mathbf{k}}_{1}) , \end{split} \tag{2.193}$$

where we define the relative velocity $\delta v_{\gamma b} \equiv v_{\gamma} - v_{b}$. The evolution equation for dark matters is derived by assuming $\dot{\tau}_{c} = 0$ in the above equation.

2.7 Example—Vector Mode

In this section, we will see an example of the second-order perturbation theory. In particular, we consider the second-order vector mode since this thesis focuses on observables induced from the second-order vector mode.

2.7.1 Vector-Mode Einstein Equation

In the case of the Einstein equation, from Eqs. (2.41), (2.91), and (2.92), the evolution equation for the vector mode is given as

$$\dot{\sigma}_{\lambda}^{(2)}(\mathbf{k}) + 2\mathcal{H}\sigma_{\lambda}^{(2)}(\mathbf{k}) = \mathcal{S}_{\lambda}^{(2)}(\mathbf{k}), \qquad (2.194)$$

where $\mathcal{S}_{\lambda}^{(2)}$ denotes the second-order source terms defined as

$$\begin{split} \mathcal{S}_{\lambda}^{(2)}(\pmb{k}) &= \frac{2}{5\sqrt{3}} \frac{1}{k} \left(8\pi G a^2 \rho_{\gamma}^{(0)} \Delta_{2,\lambda}^{(2)}(\pmb{k}) + 8\pi G a^2 \rho_{\nu}^{(0)} \mathcal{N}_{2,\lambda}^{(2)}(\pmb{k}) \right) \\ &+ \int_{\pmb{k}} 4k_1 \left[\Phi^{(1)}(\pmb{k}_1) \Psi^{(1)}(\pmb{k}_2) \right] \sqrt{\frac{4\pi}{3}} Y_{1,\lambda}^*(\hat{\pmb{k}}_1) \\ &- \int_{\pmb{k}} \frac{4}{\sqrt{3}} \frac{k_1^2}{k} \left[\Phi^{(1)}(\pmb{k}_1) \Phi^{(1)}(\pmb{k}_2) + \Psi^{(1)}(\pmb{k}_1) \Psi^{(1)}(\pmb{k}_2) \right] \sqrt{\frac{4\pi}{5}} Y_{2,\lambda}^*(\hat{\pmb{k}}_1) \\ &+ \sum_{\text{m=b,dm}} 8\pi G a^2 \rho_{\text{m}}^{(0)} \int_{\pmb{k}} \left[\frac{4}{k} v_{\text{m0}}^{(1)}(\pmb{k}_1) v_{\text{m0}}^{(1)}(\pmb{k}_2) \right] \sqrt{\frac{4\pi}{3}} Y_{1,0}^*(\hat{\pmb{k}}_1) \sqrt{\frac{4\pi}{3}} Y_{1,\lambda}^*(\hat{\pmb{k}}_2) \; . \end{split}$$

$$(2.195)$$

We can find that the second-order vector mode is sourced by the anisotropic stresses of photons and massless neutrinos and the coupling of the first-order scalar modes. We find that the anisotropic stress does not strongly affect the second-order vector mode [9]. When we consider the evolution equation up to the first order in the standard cosmology with perfect fluids, the right-hand side of Eq. (2.195) becomes zero. As a result, the vector mode has only a decaying solution, which is neglected in the linear theory.

2.7.2 Vector-Mode Boltzmann Equation

Here, we discuss the tight-coupling approximation of the vector mode which is also partially discussed in the second-order theory [10–13]. In order to solve the second-order equations numerically, we should set up the initial condition of each perturbation variable. Thus we first solve the equations analytically with $k\eta \ll 1$ and using the tight coupling approximation, and find the initial condition at sufficiently early time for our numerical calculation.

Deep in the radiation dominated era, photon and baryon fluids are tightly coupled because the opacity $\dot{\tau}_c$ is large. Although the photon and baryon fluids would behave as a single fluid, there is a small difference in motion between photon and baryon fluids. For this reason, we can expand the perturbation variables using the tight-coupling parameter which is given by

$$\epsilon \equiv \left| \frac{k}{\dot{\tau}_c} \right| \sim 10^{-2} \left(\frac{k}{1 \text{Mpc}^{-1}} \right) \left(\frac{1+z}{10^4} \right)^{-2} \left(\frac{\Omega_b h^2}{0.02} \right)^{-1} ,$$
 (2.196)

where Ω_b is the baryon density normalized by the critical density, and h is the normalized Hubble constant. In what follows, we derive the tight-coupling solution up to the first order to set the initial condition of photon and baryon fluids at the second

order in cosmological perturbations and to calculate the evolution of perturbations in a numerically stable manner.

We expand the cosmological perturbation variables using the tight-coupling parameter ϵ up to the first order as

$$\Delta^{(CPT=1,2)} = \Delta^{(CPT=1,2,TCA=\emptyset)} + \Delta^{(CPT=1,2,TCA=I)} + \cdots, \qquad (2.197)$$

where the Arabic number and the Roman number represent orders in the cosmological perturbation and the tight coupling expansion, respectively.

First, the solutions at zeroth order in the tight-coupling expansion, namely, in the tight-coupling limit, are given as

$$\delta v_{\gamma b \lambda}^{(2,\emptyset)}(\mathbf{k}) = 0, \qquad (2.198)$$

$$\Delta_{2,\lambda}^{(2,\emptyset)}(\mathbf{k}) = 20 \int_{\mathbf{k}} \left[v_{\gamma 0}^{(1,\emptyset)}(k_1) v_{\gamma 0}^{(1,\emptyset)}(k_2) \right] \mathcal{Y}_{2,\lambda}^{1,1}(\hat{\mathbf{k}}_1, \hat{\mathbf{k}}_2) , \qquad (2.199)$$

$$\Delta_{\ell>3,\lambda}^{(2,\emptyset)}(\mathbf{k}) = 0 , \qquad (2.200)$$

where $k_2 = k - k_1$ in Eq. (2.199). We define the function $\mathcal{Y}_{\ell,m}^{\ell_1,\ell_2}(\hat{k}_1,\hat{k}_2)$ as

$$\mathcal{Y}_{\ell,m}^{\ell_1,\ell_2}(\hat{\boldsymbol{k}}_1,\hat{\boldsymbol{k}}_2) \equiv (-1)^m (2\ell+1) \sum_{m_1,m_2} \begin{pmatrix} \ell_1 & \ell_2 & \ell \\ 0 & 0 & 0 \end{pmatrix} \begin{pmatrix} \ell_1 & \ell_2 & \ell \\ m_1 & m_2 & -m \end{pmatrix} \times \sqrt{\frac{4\pi}{2\ell_1+1}} Y_{\ell_1,m_1}^*(\hat{\boldsymbol{k}}_1) \sqrt{\frac{4\pi}{2\ell_2+1}} Y_{\ell_2,m_2}^*(\hat{\boldsymbol{k}}_2) . \tag{2.201}$$

In the tight-coupling limit, the relative velocity between photons and baryons vanishes as well as in the first-order cosmological perturbation theory. However, the anisotropic stress of photons is present due to the quadratic of the photon velocity.

Second, the solutions at the first order in the tight-coupling expansion are given as

$$\begin{split} \frac{1+R}{R} \delta v_{\gamma b \; \lambda}^{(2,I)}(\pmb{k}) &= \frac{\sqrt{3}}{20} \left(\frac{k}{\dot{\tau}_c}\right) \Delta_{2,\lambda}^{(2)}(\pmb{k}) - \left(\frac{\mathcal{H}}{\dot{\tau}_c}\right) \left(\omega_{\lambda}^{(2)}(\pmb{k}) + v_{b \; \lambda}^{(2)}(\pmb{k})\right) \\ &+ \int_{\pmb{k}} \left[-2 \delta v_{\gamma b \; 0}^{(1)}(k_1) (\delta_b^{(1)} + \delta_{\gamma}^{(1)} + \Psi^{(1)})(k_2) \right] \sqrt{\frac{4\pi}{3}} Y_{1,\lambda}^*(\hat{\pmb{k}}_1) \\ &+ \int_{\pmb{k}} \left[\frac{1}{2} v_{b \; 0}^{(1)}(k_1) \Pi_{\gamma \; 0}^{(1)}(k_2) \right] \sqrt{\frac{4\pi}{3}} Y_{1,\lambda}^*(\hat{\pmb{k}}_1) \\ &+ \int_{\pmb{k}} \left[2 v_{\gamma \; 0}^{(1)}(k_1) \delta v_{\gamma b \; 0}^{(1)}(k_2) \right] \sqrt{\frac{4\pi}{3}} Y_{1,\lambda}^*(\hat{\pmb{k}}_1) \\ &+ \frac{1}{R} \int_{\pmb{k}} \left[-2 \delta v_{\gamma b \; 0}^{(1)}(k_1) (\delta_{\gamma}^{(1)} + \Psi^{(1)})(k_2) \right] \sqrt{\frac{4\pi}{3}} Y_{1,\lambda}^*(\hat{\pmb{k}}_1) \\ &+ \int_{\pmb{k}} \left(\frac{k_1}{\dot{\tau}_c}\right) \left[-\frac{1}{2} \delta_{\gamma}^{(1)}(k_1) (\Psi^{(1)} + \Phi^{(1)})(k_2) - 2 \Psi^{(1)}(k_1) \delta_{\gamma}^{(1)}(k_2) \right] \sqrt{\frac{4\pi}{3}} Y_{1,\lambda}^*(\hat{\pmb{k}}_1) \end{split}$$

$$\begin{split} &+ \int_{\pmb{k}} \left(\frac{k_{2}}{\dot{\tau}_{c}}\right) \left[\frac{1}{2} v_{\gamma \, 0}^{(1)}(k_{1}) \left(\delta_{\gamma}^{(1)} + 4\Psi^{(1)}\right)(k_{2})\right] \sqrt{\frac{4\pi}{3}} Y_{1,\lambda}^{*}(\hat{\pmb{k}}_{1}) \\ &+ \int_{\pmb{k}} \left(\frac{k_{1}}{\dot{\tau}_{c}}\right) \left[-\frac{8}{3} v_{\gamma \, 0}^{(1)}(k_{1}) \delta_{\gamma}^{(1)}(k_{2})\right] \sqrt{\frac{4\pi}{3}} Y_{1,\lambda}^{*}(\hat{\pmb{k}}_{1}) \\ &+ \int_{\pmb{k}} \left(\frac{k_{2}}{\dot{\tau}_{c}}\right) \left[-\frac{2}{3} v_{b \, 0}^{(1)}(k_{1}) v_{b \, 0}^{(1)}(k_{2})\right] \sqrt{\frac{4\pi}{3}} Y_{1,\lambda}^{*}(\hat{\pmb{k}}_{1}) \\ &+ \int_{\pmb{k}} \left[-\frac{15}{4} \Pi_{\gamma \, 0}^{(1)}(k_{1}) v_{b \, 0}^{(1)}(k_{2})\right] \mathcal{Y}_{1,\lambda}^{2,1}(\hat{\pmb{k}}_{1}, \hat{\pmb{k}}_{2}) \\ &+ \frac{1}{R} \int_{\pmb{k}} \left[-\frac{5}{2} \Pi_{\gamma \, 0}^{(1)}(k_{1}) v_{b \, 0}^{(1)}(k_{2})\right] \mathcal{Y}_{1,\lambda}^{2,1}(\hat{\pmb{k}}_{1}, \hat{\pmb{k}}_{2}) \\ &+ \int_{\pmb{k}} \left(\frac{k_{1}}{\dot{\tau}_{c}}\right) \left[-\frac{10}{3} v_{b \, 0}^{(1)}(k_{1}) v_{b \, 0}^{(1)}(k_{2})\right] \mathcal{Y}_{1,\lambda}^{2,1}(\hat{\pmb{k}}_{1}, \hat{\pmb{k}}_{2}), \end{split} \tag{2.202}$$

$$\frac{9}{10}\Delta_{2,\lambda}^{(2,I)}(\mathbf{k}) = -\left(\frac{k}{\dot{\tau}_c}\right)\frac{\sqrt{3}}{3}\Delta_{1,\lambda}^{(2)}(\mathbf{k})
+ \int_{\mathbf{k}} \left[-9\Pi_{\gamma \ 0}^{(1)}(k_1)(\delta_b^{(1)} + \Psi^{(1)})(k_2)\right]\sqrt{\frac{4\pi}{5}}Y_{2,\lambda}^*(\hat{\mathbf{k}}_1)
+ \int_{\mathbf{k}} \left(\frac{k_1}{\dot{\tau}_c}\right)\left[-\frac{16}{3}v_{\gamma \ 0}^{(1)}(k_1)(\Psi^{(1)} + \Phi^{(1)})(k_2)\right]\sqrt{\frac{4\pi}{5}}Y_{2,\lambda}^*(\hat{\mathbf{k}}_1)
+ \int_{\mathbf{k}} \left[18v_{\gamma \ 0}^{(1)}(k_1)v_{\gamma \ 0}^{(1)}(k_2) + 8v_{\gamma \ 0}^{(1)}(k_1)\delta v_{\gamma b \ 0}^{(1)}(k_2)\right]\mathcal{Y}_{2,\lambda}^{1,1}(\hat{\mathbf{k}}_1, \hat{\mathbf{k}}_2)
+ \int_{\mathbf{k}} \left(\frac{k_1}{\dot{\tau}_c}\right)\left[\left(10\delta_{\gamma}^{(1)}(k_1) - 8\Phi^{(1)}\right)(k_1)v_{\gamma \ 0}^{(1)}(k_2)\right]\mathcal{Y}_{2,\lambda}^{1,1}(\hat{\mathbf{k}}_1, \hat{\mathbf{k}}_2),$$
(2.203)

$$\Delta_{3,\lambda}^{(2,I)}(\mathbf{k}) = -\left(\frac{k}{\dot{\tau}_c}\right) \frac{2\sqrt{2}}{5} \Delta_{2,\lambda}^{(2)} + 15 \int_{\mathbf{k}} \left[\Pi_{\gamma \ 0}^{(1)}(k_1) v_{\gamma \ 0}^{(1)}(k_2)\right] \mathcal{Y}_{3,\lambda}^{2,1}(\hat{\mathbf{k}}_1, \hat{\mathbf{k}}_2) ,$$

$$\Delta_{\ell>A}^{(2,I)}(\mathbf{k}) = 0 .$$
(2.204)

In order to derive the above solution, the time derivative of the first-order curvature perturbation $\dot{\Phi}$ is ignored due to the conservation of the curvature perturbation on large scales. In the right-hand side of Eqs. (2.202), (2.203), and (2.204), for simplicity, we omit the superscript for the order of the tight-coupling parameter. Note that the octopole does not vanish and higher multipoles than $\ell=3$ are equal to zero at this order [14].

2.7.3 Configuration in Fourier Space

When we solve the second-order perturbation equation, we usually move to Fourier space. In Fourier space, there are two types of the wave vector. One is the physical wave vector related to the second-order perturbations denoted as k. And another is the dummy wave vector appeared in the convolution and denoted as k_1 and k_2 . These wave vectors satisfies the triangle condition $k = k_1 + k_2$. In this section, we present the configuration of these wave vector.

To calculate the second-order power spectrum, we decompose the second-order variable into the transfer function and the primordial amplitude [15] as

$$\Delta^{(2)}(\eta, \mathbf{k}) = \int_{\mathbf{k}} \Delta_{\mathrm{T}}^{(2)}(\eta, \mathbf{k}, \mathbf{k}_{1}, \mathbf{k}_{2}) \Phi(\mathbf{k}_{1}) \Phi(\mathbf{k}_{2}) , \qquad (2.206)$$

where $\Delta_{\rm T}^{(2)}$ and Φ are the second-order transfer function and the primordial amplitude, respectively. The ensemble average of the variance of the primordial amplitude can be expressed as $\langle \Phi^*(k_1)\Phi(k_2)\rangle = (2\pi)^3 P_{\Phi}(k_1)\delta(k_1-k_2)$, where $P_{\Phi}(k)$ is the primordial power spectrum determined from cosmological observations such as CMB and large scales structure. In this thesis, we use the power-law spectrum as

$$\frac{k^3}{2\pi^2} P_{\Phi}(k) = \frac{4}{9} \mathcal{A}_s \left(\frac{k}{k_0}\right)^{n_s - 1} , \qquad (2.207)$$

where the parameters, A_s and n_s , are the amplitude and the spectral index of primordial perturbations, respectively. We set $A_s = 2.4 \times 10^{-9}$ from the WMAP nine-year results [16], and for simplicity, we consider a scale-invariant spectrum, namely, $n_s = 1.0$.

In this decomposition, the second-order power spectrum can be written as

$$P_{\Delta^{(2)}}(\eta, \mathbf{k}) = 2 \int_{\mathbf{k}} \left[\Delta_{\mathrm{T}}^{(2)}(\eta, \mathbf{k}, \mathbf{k}_{1}, \mathbf{k}_{2}) \right]^{2} P_{\Phi}(k_{1}) P_{\Phi}(k_{2}) , \qquad (2.208)$$

where we can use the symmetry under the exchange of k_1 and k_2 without loss of generality to derive the above relation. Note that $\mathbf{k} = \mathbf{k}_1 + \mathbf{k}_2$ should be satisfied implicitly, namely, $\Delta_{\mathrm{T}}^{(2)}(\eta, \mathbf{k}, \mathbf{k}_1, \mathbf{k}_2) = \Delta_{\mathrm{T}}^{(2)}(\eta, \mathbf{k}, \mathbf{k}_1, \mathbf{k} - \mathbf{k}_1)$ and $P_{\Phi}(k_2) = P_{\Phi}(|\mathbf{k} - \mathbf{k}_1|)$, as is mentioned before.

We need to solve the Einstein-Boltzmann system in (k, k_1, k_2) space. Note that the transfer function is transformed under the rotation of ϕ as

$$\Delta_{\mathrm{T}}^{(2)}(\eta, \boldsymbol{k}, \boldsymbol{k}_1, \boldsymbol{k}_2) \longrightarrow \Delta_{\mathrm{T}}^{(2)}(\eta, \boldsymbol{k}, \boldsymbol{k}_1, \boldsymbol{k}_2) e^{im\phi} . \tag{2.209}$$

In practice, we take $\phi = \theta = 0$, $\phi_1 = 0$, and $\phi_2 = \pi$ for k, k_1 , and k_2 , respectively. In other words, the transfer function under the exchange of k_1 and k_2 transforms as

$$\Delta_{\mathbf{T}}^{(2)}(\eta, \mathbf{k}, \mathbf{k}_1, \mathbf{k}_2) = (-1)^m \Delta_{\mathbf{T}}^{(2)}(\eta, \mathbf{k}, \mathbf{k}_2, \mathbf{k}_1) . \tag{2.210}$$

It is very interesting that for the case of the scalar and tensor modes, the dominant contribution comes from near the $k \sim k_1 \sim k_2$. Because the transfer functions of the scalar (m=0) and tensor $(m=\pm 2)$ modes are symmetric under the exchange of k_1 and k_2 . On the other hand, the vector mode does not have dominant contribution near the $k \sim k_1 \sim k_2$ since the transfer function of the vector mode is antisymmetric under the exchange of k_1 and k_2 .

In the vector mode, we can naively consider three configurations of the triangle $\mathbf{k} = \mathbf{k}_1 + \mathbf{k}_2$ that contribute to the power spectrum on superhorizon scales, namely, the one where both k_1 and k_2 are on superhorizon scales, where k_1 (k_2) is at superhorizon scales while k_2 (k_1) is at subhorizon scales, and where both k_1 and k_2 are at subhorizon scales. When both k_1 and k_2 are at subhorizon scales, the square of the primordial power spectrum in Eq. (2.208) does not contribute on the power spectrum because of the antisymmetric nature of the vector transfer function. In the vector mode, we therefore need a careful treatment of how to sample wave numbers in (k, k_1 , k_2) space. This difficulty does not arise in the second-order scalar and tensor modes calculations because the transfer functions of the scalar and tensor modes have a symmetry under the exchange of k_1 and k_2 .

References

- N. Bartolo, S. Matarrese, A. Riotto, CMB Anisotropies at Second Order I. JCAP 0606, 024 (2006), arXiv:astro-ph/0604416
- P.A.R. Planck Collaboration, Ade et al., Planck 2013 results. XVI. Cosmological parameters. Astron. Astrophys. 571, A16 (2014), arXiv:1303.5076
- M. Beneke, C. Fidler, Boltzmann hierarchy for the cosmic microwave background at second order including photon polarization. Phys. Rev. D 82, 063509 (2010), arXiv:1003.1834
- C. Pitrou, The Radiative transfer at second order: a full treatment of the Boltzmann equation with polarization. Class. Quant. Grav. 26, 065006 (2009), arXiv:0809.3036
- W.T. Hu, Wandering in the background: a CMB explorer. Ph.D. thesis, UC, Berkeley, 1995, arXiv:astro-ph/9508126
- M. Zaldarriaga, Fluctuations in the cosmic microwave background. Ph.D. thesis, MIT, LNS, 1998, arXiv:astro-ph/9806122
- S. Dodelson, J.M. Jubas, Reionization and its imprint on the cosmic microwave background. Astrophys. J. 439, 503–516 (1995), arXiv:astro-ph/9308019
- D. Nitta, E. Komatsu, N. Bartolo, S. Matarrese, A. Riotto, CMB anisotropies at second order III: bispectrum from products of the first-order perturbations. JCAP 0905, 014 (2009), arXiv:0903.0894
- S. Saga, D. Yamauchi, K. Ichiki, Weak lensing induced by second-order vector mode. Phys. Rev. D 92(6), 063533 (2015), arXiv:1505.02774
- K. Ichiki, K. Takahashi, N. Sugiyama, Constraint on the primordial vector mode and its magnetic field generation from seven-year Wilkinson Microwave Anisotropy Probe Observations. Phys. Rev. D 85, 043009 (2012), arXiv:1112.4705
- S. Maeda, S. Kitagawa, T. Kobayashi, T. Shiromizu, Primordial magnetic fields from secondorder cosmological perturbations: tight coupling approximation. Class. Quant. Grav. 26, 135014 (2009), arXiv:0805.0169

References 51

12. K. Takahashi, K. Ichiki, N. Sugiyama, Electromagnetic properties of the early Universe. Phys. Rev. D 77, 124028 (2008), arXiv:0710.4620

- C. Pitrou, The tight-coupling approximation for baryon acoustic oscillations. Phys. Lett. B 698, 1–5 (2011), arXiv:1012.0546
- S. Saga, K. Ichiki, N. Sugiyama, Impact of anisotropic stress of free-streaming particles on gravitational waves induced by cosmological density perturbations. Phys. Rev. D 91(2), 024030 (2015), arXiv:1412.1081
- G.W. Pettinari, The intrinsic bispectrum of the Cosmic Microwave Background. Ph.D. thesis, Portsmouth U., ICG, 2013–09, arXiv:1405.2280
- W.M.A.P. Collaboration, C.L. Bennett et al., Nine-year Wilkinson Microwave Anisotropy Probe (WMAP) observations: final maps and results. Astrophys. J. Suppl. 208, 20 (2013), arXiv:1212.5225

Chapter 3 Generation of Magnetic Fields

Abstract The origin of magnetic fields with large coherent length, called cosmological magnetic fields, has been an open question, although many models are proposed. It has been believed that cosmological magnetic fields are the resultant of amplification by the dynamo mechanism. If we believe the dynamo mechanism, we need to set seed fields in the early universe, that is, before the cosmological recombination epoch. This is because the dynamo mechanism cannot create magnetic fields from the absence of seed fields. In this part, we apply the second-order vector mode in the cosmological perturbation theory to generate seed magnetic fields. The estimation of the second-order magnetic fields has not been accomplished because there is a discrepancy between previous results with the incomplete analysis. We reproduce the previous results by the original Boltzmann code and identify the cause of the discrepancy. Consequently, we provide the fully-considered results of second-order magnetic fields.

Keywords Second-order perturbation theory • Cosmological magnetic fields Harrison mechanism

3.1 Introduction

The presence of magnetic fields on large scales is established by current observations [1–5]. Such cosmological magnetic fields coevolve with the Universe, e.g., astrophysical objects, cosmic microwave background radiation (CMB), large scale structure, and inflation. Recent observations indicate that cosmological magnetic fields have the strength about micro-Gauss on Mpc scales (see, e.g., Refs. [1, 2, 5–8], and references therein). Moreover, the pair-echo method [9–13] determines the lower bound of strength in the intergalactic magnetic fields as $B \gtrsim O(10^{-22})$ Gauss. The remarkable progress of observations indicates that cosmological magnetic fields appear everywhere even in the cosmic voids. Furthermore, the future experiments of the radio telescope such as Square Kilometer Array can survey much deeper and wider regions, and give us rich information about coevolution between cosmologi-

cal magnetic fields and baryonic matters. However, very interestingly, the origin of cosmological magnetic fields is not entirely revealed.

The key process related to evolution of magnetic fields is the dynamo mechanism [7, 14–16], which is the amplification mechanism of magnetic fields in the nonlinear magnetohydrodynamics. In the stars, galaxies, and galaxy clusters, their nonlinear evolution can amplify seed magnetic fields, and the strength of seed fields is about $10^{-20} \sim 10^{-30}$ Gauss [17]. Generally, the dynamo mechanism cannot generate magnetic fields from the absence of seed fields but amplify the seed fields, which should be set before the dynamo mechanism works. Therefore, when we believe that the origin of cosmological magnetic fields is as a result of amplification of seed fields by the dynamo mechanism, seed fields must be created in the early stage of the universe, namely before cosmological recombination.

One of the candidates to create seed fields is the quantum fluctuations of the electromagnetic fields in the inflation era. During the inflation era, the scale of fluctuations is extended beyond the Hubble horizon due to the nearly exponential expansion. At first glance, it is possible to rely on this scenario to generate large-scale magnetic fields. However, this scenario does not work since the standard Maxwell theory has the symmetry under the conformal transformation. Under this symmetry, the vector fields, such as magnetic fields, undergo decaying only and become negligible. In other words, when the conformal invariance is broken, inflationary magnetogenesis possibly works. In many of the previous studies [18-22], the authors have introduced interaction between the electromagnetic fields and the dilaton-like scalar field to break conformal invariance. However, even in this case, there are other problems in the inflationary magnetogenesis, i.e., strong-coupling and backreaction problems [23, 24]. These problems make the situation worse. Therefore we can conclude that it is difficult to generate seed fields during the inflation era alone. In the more recent studies [25–27], a new interaction between electromagnetic fields and axion-like pseudoscalar field is added in the context of dilaton-like magnetogenesis. This interaction ends up with generation of helical magnetic fields on small scales. The inverse cascade can transfer helical magnetic fields from smaller scales to much larger scales owing to conservation of the magnetic helicity. We therefore expect the existence of magnetic fields on all scales in later epochs although the detailed numerical estimation is needed [28, 29].

The cosmological phase transition is another possibility to generate seed fields (e.g., Refs. [7, 8]). In general, phase transitions release the free energy and electric charges. The released free energy is converted into the electric currents. If these electric currents have rotational components, cosmological seed fields are induced at epochs of phase transitions. However, the coherent length of seed fields generated in the cosmological phase transitions cannot exceed the Hubble horizon scale at that time due to the causality. Therefore phase transitions alone are not able to explain observed large-scale magnetic fields [30].

Another category of generation mechanism is originated from astrophysical phenomena. For example, the Biermann battery is one of the candidates of generation mechanism after the recombination epoch. The gravitational force can be described as a gradient of the scalar potential and hence cannot generate vorticity. However,

3.1 Introduction 55

the Biermann battery, which is non-adiabatic phenomena such as shocks, can generate vorticity and subsequently, seed fields are induced with the amplitude about 10^{-17} Gauss in protogalaxies [31], $10^{-17} \sim 10^{-14}$ Gauss in supernova remnants [32], and $\sim 10^{-21}$ Gauss in galaxies [33]. The Weibel instability, which is microscopic instability in the plasma, can amplify tiny seed fields at the epoch of structure formation [34, 35]. When the velocity distribution of plasma particles has an anisotropy in the phase space, the isotropized process of the velocity distribution releases the energy, and subsequently, the energy is converted into magnetic fields. Accordingly, magnetic fields amplified by the Weibel instability have a quite large amplitude of about 10^{-7} Gauss [34, 35]. However, the Biermann battery and Weibel instability can only work with the existence of baryonic matters or astrophysical objects. Therefore it is difficult to explain the origin of intergalactic magnetic fields or magnetic fields in the voids.

Yet another interesting mechanism of generating magnetic fields is the Harrison mechanism [36] in which magnetic fields are generated via vorticity of the primordial plasma. In Ref. [37], the authors have formulated the Harrison mechanism based on the cosmological perturbation theory in the primordial plasma which is a multicomponent system composed of photons, electrons, protons, dark matters, and neutrinos. In this system, photons and electrons or protons interact with each other through the Compton scattering. However, photons push electrons more frequently than protons because of the difference of scattering rates. Accordingly, the charge separation takes place. If there exist rotation-type electric fields, magnetic fields are generated. However, in the linear perturbation theory, the Harrison mechanism does not work because there is no growing mode solution for the vector-mode perturbations which induce rotation-type electric fields. In other words, the models including the active vector mode supplied by external sources, i.e., free-streaming neutrinos [38–40], cosmic defects [41, 42], and modified gravity with vector fields [43], can generate magnetic fields via the Harrison mechanism.

Moreover, it turns out that even standard cosmological perturbations can generate magnetic fields if we take into account contributions from higher-order perturbations. In fact, it is known that the second-order perturbation theory has not only the scalar mode but also the vector and tensor modes through the product of the first-order scalar perturbations. Recently, the second-order cosmological perturbation theory is well established in the context of the CMB formalisms [44–55]. For example, the B-mode polarization is calculated based on the second-order perturbation theory while there is no B-mode polarization in linear scalar perturbations.

Recently, generation of magnetic fields via the second-order perturbation has been studied in detail [56–60]. In these studies, the tight-coupling approximation is employed to estimate the amplitude of magnetic fields analytically. Each study has shown that the amplitude of generated magnetic fields is about $10^{-30} \sim 10^{-27}$ Gauss at recombination on Mpc scales. However, it is difficult to know the detail of the magnetic power spectrum since the tight-coupling approximation breaks down inside the horizon scale at recombination. By solving perturbation equations up to the second order without employing the tight-coupling approximation, it is possible to analyze the power spectrum of magnetic fields. In Ref. [61], the authors have

evaluated the spectrum generated by the vorticity of charged particles, which are induced by the nonlinear coupling between the first-order density perturbations. And they have found that resultant comoving magnetic fields have the amplitude of about 10^{-29} Gauss at recombination on Mpc scales. Subsequently, in Refs. [62, 63], the authors have studied the Harrison mechanism including the anisotropic stress of photons. They have found that the amplitude of magnetic fields has 10^{-20} Gauss at recombination on Mpc scales. However, they ignore the purely second-order velocity difference between charged particles and photons in their analysis. In Ref. [64], the authors include the purely second-order effects for the first time and analyze the spectrum of magnetic fields on superhorizon scales. In these studies, however, there are some discrepancies which have to be clarified.

In the following sections, we numerically solve the vector mode of cosmological Einstein-Boltzmann equations at the second order including all the effects relevant to the generation of magnetic fields, with a newly developed numerical code. In addition we present analytic interpretations of the shapes and time evolutions of the power spectrum of magnetic fields on sub- and superhorizon scales, and make it clear what has caused the discrepancies among the previous studies.

3.2 Harrison Mechanism

In this section, we review basic equations for the generation of magnetic fields [37, 62], i.e., perturbation equations of photon, proton, and electron fluids. While protons and electrons are conventionally treated as a single fluid, however, it is necessary to deal with proton and electron fluids separately in order to discuss the generation of magnetic fields.

Let us begin with the Euler equations. Although the Euler equation for baryons are derived in Chap. 2, we need to include the electromagnetic fields in the Euler equations for charged particles. It is convenient to start from the Euler equation in terms of the four-velocity. Those are given by

$$m_{\rm p}nu_{\rm p}^{\mu}u_{{\rm p}i;\mu} - enu_{\rm p}^{\mu}F_{i\mu} = C_{i}^{\rm pe} + C_{i}^{\rm p\gamma},$$
 (3.1)

$$m_{\rm e}nu_{\rm e}^{\mu}u_{{\rm e}i;\mu} + enu_{\rm e}^{\mu}F_{i\mu} = C_{i}^{\rm ep} + C_{i}^{\rm e\gamma},$$
 (3.2)

where $m_{\rm p(e)}$ is the proton (electron) mass, $u_{\rm p(e)}$ is the bulk velocity of protons (electrons), $F_{\mu i}$ is the usual Maxwell tensor. The interaction term is defined by using the collision term in the Boltzmann equation as

$$C_i^{xy} \equiv \int \frac{\mathrm{d}^3 \boldsymbol{p}}{(2\pi^3)} p_i C^{xy} [f(\boldsymbol{p})] , \qquad (3.3)$$

where we denote x and y as species of interaction particles. The thermal pressures of proton and electron fluids are neglected. The right-hand side of Eqs. (3.1) and

3.2 Harrison Mechanism 57

(3.2) represent the collision terms. The first terms in Eqs. (3.1) and (3.2) are collision terms for the Coulomb scattering between protons and electrons, which are given by [56]

$$C_i^{\text{pe}} = -C_i^{\text{ep}} = -(u_i - u_{ei})e^2n^2\eta_r$$
, (3.4)

where

$$\eta_{\rm r} = \frac{\pi e^2 m_{\rm e}^{1/2}}{(k_{\rm B} T_{\rm e})^{3/2}} \ln \Lambda \sim 9.4 \times 10^{-16} {\rm sec} \left(\frac{1+z}{10^5}\right)^{-3/2} \left(\frac{\ln \Lambda}{10}\right) , \qquad (3.5)$$

is the resistivity of the plasma and $\ln \Lambda \sim \mathcal{O}(1)$ is the Coulomb logarithm, which is the almost constant parameter. As is well known, this term acts as the diffusion term in the evolution equation of magnetic field. The importance of the diffusion effect can be estimated by the diffusion scale,

$$\lambda_{\text{diff}} \equiv \sqrt{\eta_{\text{r}}\tau} \sim 100 \left(\frac{\tau}{H_0^{-1}}\right)^{1/2} \text{AU}, \tag{3.6}$$

above which magnetic field cannot diffuse in the time-scale τ . Here $H_0=100h~{\rm km/s/Mpc}$ is the present Hubble parameter with h being the normalized Hubble parameter. Thus, at cosmological scales considered here, this term can be safely neglected.

The other terms expressed by $C_i^{\mathrm{p(e)}\gamma}$ are the collision terms for Compton scattering of protons (electrons) with photons. Since photons scatter off electrons preferentially compared with protons by a factor of $(m_{\mathrm{e}}/m_{\mathrm{p}})^2$, we can safely drop the term $C_i^{\mathrm{p\gamma}}$ from the Euler equation of protons. This difference in collision terms between protons and electrons ensures that small difference in velocity between protons and electrons, that is, electric current, is indeed generated once the Compton scattering becomes effective. And finally, we have only to do is to derive the expression of $C_i^{\mathrm{e\gamma}}$. The collision term between photons and electrons is already given in Eq. (2.157) and calculated as

$$C_{i}^{e\gamma} = -\int \frac{d^{3}p}{(2\pi)^{3}} p_{i} C[f]$$

$$= -\frac{4an_{e}\sigma_{T}}{3} \rho_{\gamma} \left[(v_{ei} - v_{\gamma i}) + \frac{3}{4} v_{ej} \Pi_{\gamma i}^{\ j} \right], \tag{3.7}$$

where the product of the velocity of electrons and anisotropic stress of photons in Eq. (3.7) is the anisotropic part of *radiation drag* in the context of the radiation hydrodynamics. The radiation drag is originated by the electron motion in anisotropic radiation fields with absorptions and emissions. The velocity of electrons v_{ei} obeys the Euler equation, and the velocity and anisotropic stress of photons, $v_{\gamma i}$ and $\Pi_{\gamma i}{}^{j}$, obey the Boltzmann equation.

Now we obtain the Euler equations for protons and electrons as

$$m_{\rm p}nu_{\rm p}^{\mu}u_{pi;\mu} - enu_{\rm p}^{\mu}F_{i\mu} = 0$$
, (3.8)

$$m_{\rm e}nu_{\rm e}^{\mu}u_{{\rm e}i;\mu} + enu_{\rm e}^{\mu}F_{i\mu} = \frac{4\sigma_{\rm T}\rho_{\gamma}an}{3}\left[\delta v_{\gamma {\rm b}i} - \frac{3}{4}v_{{\rm e}j}\Pi_{\gamma i}{}^{j}\right],$$
 (3.9)

where $m_{\rm p}$ is the proton mass. Here, we ignore the pressures of proton and electron fluids. In addition, the Coulomb collision term is neglected as explained below Eq. (3.6). Note that the collision term was not evaluated in a manifestly covariant way. Here the left-hand side in Eqs. (3.8) and (3.9) should be evaluated in a conformal coordinate system. We also assumed the local charge neutrality: $n=n_{\rm e}\sim n_{\rm p}$. In the case without electromagnetic fields ($F_{i\mu}=0$), the sum of the Eqs. (3.8) and (3.9) gives the Euler equation for the baryons in the standard perturbation theory. On the other hand, subtracting Eq. (3.8) multiplied by $m_{\rm e}$ from Eq. (3.9) multiplied by $m_{\rm p}$, we obtain

$$-\frac{m_{\rm p}m_{\rm e}}{e} \left[nu^{\mu} \left(\frac{j_{i}}{n} \right)_{;\mu} + j^{\mu} \left(\frac{m_{\rm p} - m_{\rm e}}{m_{\rm p} + m_{\rm e}} \frac{j_{i}}{en} - u_{i} \right)_{;\mu} \right] + en(m_{\rm p} + m_{\rm e})u^{\mu} F_{i\mu} - (m_{\rm p} - m_{\rm e})j^{\mu} F_{i\mu}$$

$$= \frac{4m_{\rm p}\rho_{\gamma}an\sigma_{\rm T}}{3} \left[\delta v_{\gamma bi} - \frac{3}{4}v_{\rm e}j\Pi_{\gamma i}{}^{j} \right], \tag{3.10}$$

where u^{μ} and j^{μ} are the center-of-mass 4-velocity of the proton and electron fluids and the net electric current, respectively, defined as

$$u^{\mu} \equiv \frac{m_{\rm p} u_{\rm p}^{\mu} + m_{\rm e} u_{\rm e}^{\mu}}{m_{\rm p} + m_{\rm e}},\tag{3.11}$$

$$j^{\mu} \equiv en(u_{\rm p}^{\mu} - u_{\rm e}^{\mu}).$$
 (3.12)

Employing the Maxwell equations $F^{\mu\nu}_{;\nu} = j^{\mu}$, we see that the quantities in the square bracket in the left-hand side of Eq. (3.10) is suppressed at the recombination epoch, compared to the second term, by a factor [65]

$$\frac{c^2}{L^2 \omega_{\rm p}^2} \sim 3 \times 10^{-40} \left(\frac{10^3 \,{\rm cm}^{-3}}{n}\right) \left(\frac{1 \,{\rm Mpc}}{L}\right)^2,\tag{3.13}$$

where c is the speed of light, L is a characteristic length of the system and $\omega_p = \sqrt{4\pi ne^2/m_e}$ is the plasma frequency.

The third term in the left-hand side of Eq. (3.10), i.e., $(m_p - m_e) j^{\mu} F_{i\mu}$, is the Hall term which can also be neglected because the Coulomb coupling between protons and electrons is so tight that $|u^i| \gg |u^i_p - u^i_e|$. Then we obtain a generalized Ohm's law:

$$u^{\mu}F_{i\mu} = \frac{4\sigma_{\rm T}\rho_{\gamma}a}{3e} \left[\delta v_{\gamma bi} - \frac{3}{4}v_{\rm ej}\Pi_{\gamma i}^{\ j}\right] \equiv C_i \ . \tag{3.14}$$

3.2 Harrison Mechanism 59

Now we derive the evolution equation for the magnetic field, which can be obtained from the Bianchi identities $F_{[\mu\nu,\lambda]}=0$, as

$$0 = \frac{3}{2} \epsilon^{ijk} u^{\mu} F_{[jk,\mu]}$$

$$= u^{\mu} \mathcal{B}^{i}_{,\mu} - \epsilon^{ijk} \left(C_{j,k} + \frac{u^{0}_{,j}}{u^{0}} C_{k} \right) - (u^{i}_{,j} \mathcal{B}^{j} - u^{j}_{,j} \mathcal{B}^{i}) + \frac{u^{0}_{,j}}{u^{0}} (\mathcal{B}^{j} u^{i} - \mathcal{B}^{i} u^{j}),$$
(3.15)

where ϵ^{ijk} is the Levi-Cività tensor and $\mathcal{B}^i \equiv (a^2B^i) = \epsilon^{ijk}F_{jk}/2$ is the magnetic field in the comoving frame [66]. We will now expand the photon energy density, fluid velocities, and photon anisotropic stress with respect to the density perturbation as

$$\rho_{\gamma}(t, x_{i}) = \rho_{\gamma}^{(0)}(t) + \rho_{\gamma}^{(1)}(t, x_{i}) + \cdots,
u^{0}(t, x_{i}) = a(t)^{-1} + u^{(1)0}(t, x_{i}) + \cdots,
u^{i}(t, x_{i}) = u^{(1)i}(t, x_{i}) + \frac{1}{2}u^{(2)i}(t, x_{i}) + \cdots,
v_{i}(t, x_{i}) = v_{i}^{(1)}(t, x_{i}) + \frac{1}{2}v_{i}^{(2)}(t, x_{i}) + \cdots,
\Pi_{\gamma}^{ij}(t, x_{i}) = \Pi_{\gamma}^{(1)ij}(t, x_{i}) + \cdots,$$
(3.16)

where the superscripts (0), (1), and (2) denote the order of expansion and t is the cosmic time. Remembering that \mathcal{B}^i is a second-order quantity, we see that all terms involving \mathcal{B}^i in Eq. (3.15), other than the first term, can be neglected. Thus we obtain

$$\frac{d\mathcal{B}^{i}}{dt} \sim \epsilon^{ijk} \left(C_{j,k} + \frac{u_{,j}^{0}}{u^{0}} C_{k} \right)
= \frac{4\sigma_{T} \rho_{\gamma}^{(0)} a}{3e} \epsilon^{ijk} \left[\frac{1}{2} \delta v_{\gamma bj,k}^{(2)} - \delta_{\gamma,j}^{(1)} \delta v_{\gamma bk}^{(1)} - \frac{3}{4} \left(v_{el}^{(1)} \Pi_{\gamma j}^{(1)l} \right)_{,k} \right],$$
(3.17)

where we used the density contrast of photons, $\delta_{\gamma,k}^{(1)} \equiv \rho_{\gamma,k}^{(1)}/\rho_{\gamma,k}^{(0)}$. Further, we employed the fact that there is no vorticity in the first order: $\epsilon^{ijk}v_{j,k}^{(1)}=0$. It should be noted that the velocity of electron fluid can be approximated to the center-of-mass velocity at this order, $v_{\rm e}^{(1)i} \sim v_{\rm b}^{(1)i}$. The physical meaning of this equation is that electrons gain (or lose) their momentum through scatterings due to the relative velocity to photons, and the anisotropic stress of photons. The momentum transfer from the photons ensures the velocity difference between electrons and protons, and thus eventually generates magnetic fields. We found that the contribution from the curvature perturbation is always much smaller than that from the density contrast of photons. Furthermore the tensor perturbation, i.e., primordial gravitational waves,

is subdominant comparing with the scalar perturbation in the current observations [67–69]. Therefore, we have omitted the curvature perturbation and the tensor perturbation in Eq. (3.17) when considering the evolution of magnetic fields. Equation (3.17) shows that the magnetic field cannot be generated in the first order. The right-hand side of Eq. (3.17) contains two types of source terms, i.e., a purely second-order term and those that consist of the products of first order quantities.

The first term in Eq. (3.17) is exactly the same as that discussed in [59]. They have estimated the amplitude of magnetic fields from these terms by considering typical values at recombination. Here, we solve the equation numerically and obtain a robust prediction of the amplitude of magnetic fields in the standard Λ CDM cosmology. In the cosmological perturbation theory, we usually decompose the perturbations into the scalar, vector, and tensor modes. Following Sect. 2.1, we split the evolution equation of magnetic fields in Eq. (3.17) into the scalar and vector parts, i.e., $\mathcal{B}_i = \mathcal{B}_0 O_i^{(0)} + \sum_{\lambda=\pm 1} \mathcal{B}_\lambda O_i^{(\lambda)}$. When we pull out the scalar mode from Eq. (3.17), we find that the right hand side of Eq. (3.17) vanishes, namely,

$$\frac{d\mathcal{B}_0}{dt} = 0. (3.18)$$

This is because magnetic fields consist of rotation of the vector potential, or in other words, magnetic fields do not have the scalar component. In contrast, the vector mode for Eq. (3.17) is given by

$$\frac{d\mathcal{B}_{\lambda}(\mathbf{k})}{dt} = \frac{4\sigma_{\mathrm{T}}\rho_{\gamma}^{(0)}a}{3e}(\lambda k) \left[-\frac{1}{2}\delta v_{\gamma b \lambda}^{(2)}(\mathbf{k}) + \int_{\mathbf{k}} \delta v_{\gamma b 0}^{(1)}(k_{1})\delta_{\gamma}^{(1)}(k_{2})\sqrt{\frac{4\pi}{3}}Y_{1,\lambda}^{*}(\hat{\mathbf{k}}_{1}) - \int_{\mathbf{k}} \frac{5}{4}v_{b 0}^{(1)}(k_{1})\Pi_{\gamma 0}^{(1)}(k_{2})\mathcal{Y}_{1,\lambda}^{1,2}(\hat{\mathbf{k}}_{1},\hat{\mathbf{k}}_{2}) \right],$$
(3.19)

where $\mathcal{Y}_{\ell,m}^{\ell_1,\ell_2}(\hat{k}_1,\hat{k}_2)$ is defined in Eq. (2.201). To estimate resultant magnetic fields, we solve the second-order Boltzmann equation for photons (2.169), Einstein equation of the vector mode (2.195), and Eq. (3.17) at the same time. In the next section, we show the result of generated magnetic fields and some discussions.

3.3 Results: Cosmological Magnetic Fields

In this section, we show the evolutions and spectra of magnetic fields driven by the Harrison mechanism. In the previous studies [60, 61, 63, 64, 70], generated magnetic fields are partially estimated by numerical or analytical ways, and there is a small discrepancy between in Refs. [63, 64]. In this paper, we build on Ref. [63] and expand the work by including all contributions numerically. The source terms of the magnetic fields consist of three contributions, i.e., $\delta_{\gamma}^{(1)} \delta v_{\gamma b}^{(1)}$, $v_{b}^{(1)} \Pi_{\gamma}^{(1)}$, and $\delta v_{\gamma b}^{(2)}$, which

hereafter we call "the slip term", "the anisotropic stress term" and "the second-order slip term", respectively.

In this paper, we focus on three issues on the generation of magnetic fields at recombination. First, we consider how large is the contribution of the second-order slip term on magnetic fields compared with the contributions of the slip and the anisotropic stress terms. Second, to evaluate the total spectrum of magnetic fields we need to include the cross-correlation terms between the sources, namely, $P_B \sim \left(\left(B_{\rm 2nd~Slip} + B_{\rm Slip} + B_{\rm Anis} \right)^2 \right)$. The cross terms can be negative and it has the possibility to cancel the generated magnetic fields from each of the source terms. Third, we try to find the cause of the small discrepancy between Refs. [63, 64]. In the following subsections, we show the evolutions and spectra of magnetic fields and the answers of the above three considerable questions.

3.3.1 Evolutions of Magnetic Fields

In Fig. 3.1, we show the evolutions of magnetic fields induced by the slip, the anisotropic stress, and the second-order slip terms. First, we focus on the evolutions of magnetic fields before the horizon crossing. The time evolutions of magnetic fields can be approximated by a power law, and the powers of the slip and the anisotropic stress terms are $B_{\rm Slip} \propto \eta^{1.5}$ and $B_{\rm Anis} \propto \eta^{0.5}$, respectively. These results correspond to the previous study [63]. Furthermore, the second-order slip term is proportional to $\eta^{0.5}$ on superhorizon scales. We can explain the coincidence of the powers between the anisotropic stress and the second-order slip terms as follows. In Eq. (2.202), the dominant terms in early times can be estimated by using the superhorizon solutions at the first order. At first glance, the term $\delta_{\gamma}^{(1)} \times \Phi^{(1)}$ in Eq. (2.202) seems to give a dominant contribution to the second-order slip term. However, because both $\delta_{\gamma}^{(1)}$ and $\Phi^{(1)}$ are scale invariant in the Poisson gauge and according to the formula of spherical harmonics, $k_1 \sqrt{\frac{4\pi}{3}} Y_{1,m}^*(\hat{k}_1) + k_2 \sqrt{\frac{4\pi}{3}} Y_{1,m}^*(\hat{k}_2) = k \delta_{m,0}$, this scale invariant term vanishes in the vector mode. As a result, we find that the most dominant term in Eq. (2.202) is that proportional to $v_b^{(1)}\Pi_{\gamma}^{(1)}$, which is the same form as the anisotropic stress term. Therefore, the powers of the time evolutions of the anisotropic stress and second-order slip terms coincide.

Next, we discuss the evolutions of magnetic fields after the horizon crossing. We can see that the magnetic fields from the slip and the anisotropic stress terms start to decay adiabatically as $\propto a^{-2}$, after the horizon crossing since their sources also diminish after the horizon crossing. On the other hand, magnetic fields induced by the second-order slip term do not decay adiabatically even after the horizon crossing. This arises from the fact that the second-order slip term $\delta v_{\gamma b}^{(2)}$ continues to grow even after the source terms from the first-order perturbations become negligible, until the corresponding scale reaches the Silk damping scale. Therefore, the purely second-order perturbations can contribute to the magnetic field generation even if

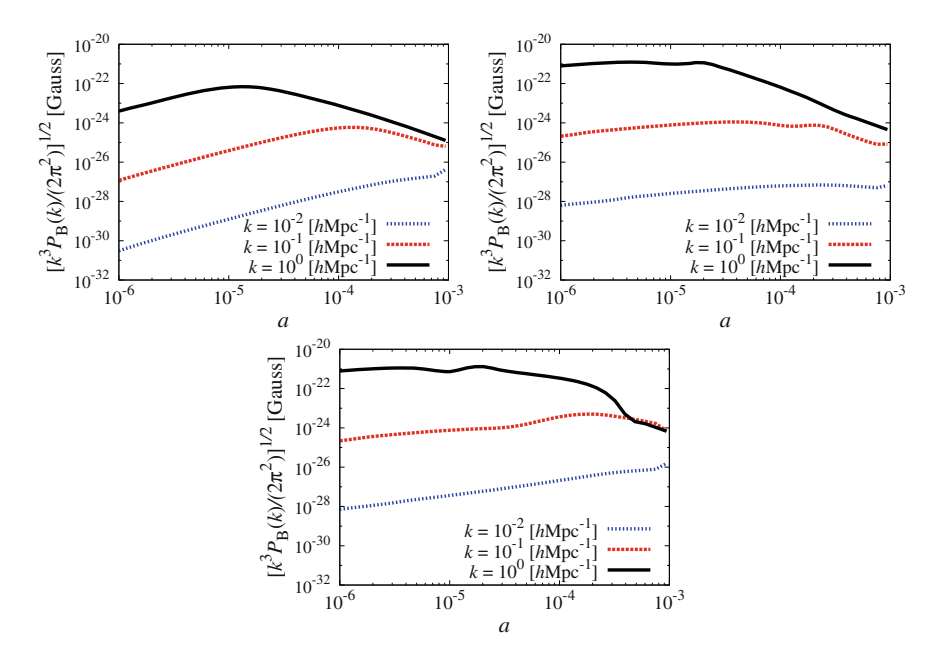


Fig. 3.1 Evolutions of generated magnetic fields sourced by the slip term ($top\ left$), the anisotropic stress term ($top\ right$), and the second-order slip term (bottom). We show evolutions of generated magnetic fields for wavenumbers $k=10^{-2}\ h\text{Mpc}^{-1}$, $10^{-1}\ h\text{Mpc}^{-1}$, and $10^{0}\ h\text{Mpc}^{-1}$ as indicated in the above panel. We can see that magnetic fields at smaller scales generated earlier and their amplitudes are larger

the product of the first-order perturbations is absent. When we neglect the product of the first-order perturbations, the evolution equations for magnetic fields are corresponding to the case of the first-order magnetic fields generation [39]. The relative velocity between photons and baryons, $\delta v_{\gamma b \ \lambda}^{(2)}$ contributes to the generation of magnetic fields after the horizon crossing. This additional enhancement can be seen in the bottom of Fig. 3.1 at $k=10^0\ h{\rm Mpc}^{-1}$. However, magnetic fields induced by the additional enhancement undergo nontrivial cancellation after the Silk damping epoch and magnetic fields decay faster than the adiabatic decay that it is proportional to a^{-2} [39]. The final amplitude of magnetic fields is consequently determined by the initial amplitude around horizon crossing.

3.3.2 Spectra of Magnetic Fields

Next, we show the spectra of magnetic fields induced by the slip, the anisotropic stress, and the second-order slip terms in Fig. 3.2. From Fig. 3.2, resultant magnetic fields are dominated by the anisotropic stress and second-order slip terms on smaller

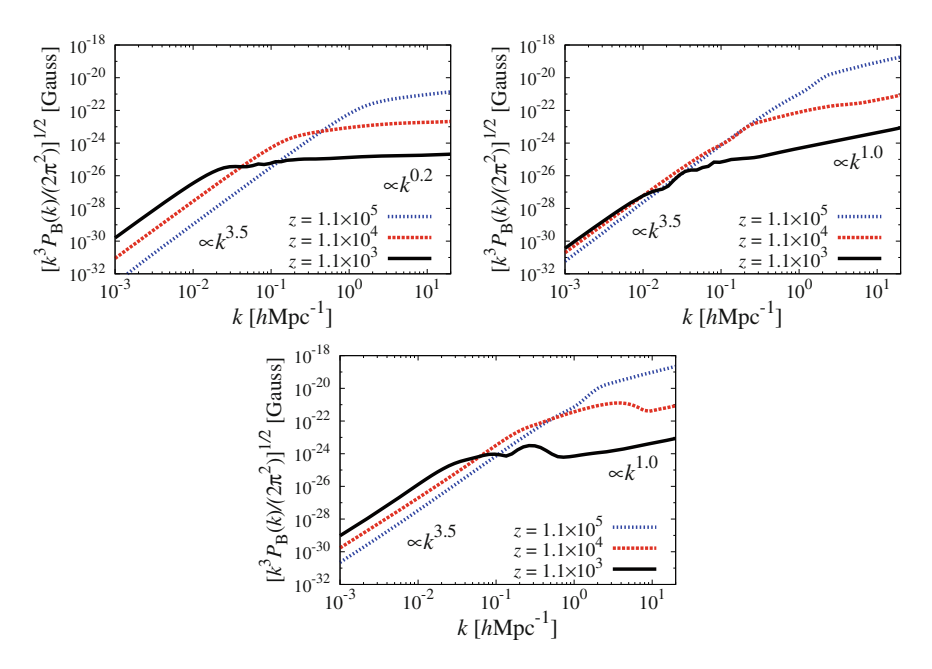


Fig. 3.2 Spectra of generated magnetic fields sourced by the slip term (top left), the anisotropic stress term (top right), and the second-order slip term (bottom). We show spectra of generated magnetic fields for redshifts $z = 1.1 \times 10^5$, 1.1×10^4 , and 1.1×10^3 as indicated in the above panel

scales, i.e., $k \gtrsim 1.0 \ h \rm{Mpc^{-1}}$, at 1+z=1100. Conversely, on these scales, the slip term is a subdominant source for magnetic fields.

On superhorizon scales, we can see that the spectra of magnetic fields are proportional to $k^{3.5}$, which also corresponds to the results about the slip and the anisotropic stress terms in Ref. [63]. This power is also consistent with the power spectrum for causal magnetic fields [71]. From Ref. [63], the magnetic power on superhorizon scales can be estimated as below. For example, we focus on magnetic fields induced by the slip term. We can integrate the evolution equation for the second-order magnetic fields (3.19) and take the ensemble average as

$$\frac{k^3}{2\pi^2} P_B(k) \bigg|_{\text{Slip}} \propto k^5 \int_{\mathbf{k}} \left(1 - \mu_1^2 \right) P_{\Phi}(k_1) P_{\Phi}(k_2) \left[S^2(k_2, k_1) - \frac{k_1}{k_2} S(k_1, k_2) S(k_2, k_1) \right], \tag{3.20}$$

where $\mu_1 = \cos \theta_1$ and $S(k_1, k_2)$ is defined as

$$S(k_1, k_2) = \int d\eta a^2(\eta) \rho_{\gamma}^{(0)}(\eta) \delta_{\gamma}^{(1)}(k_1, \eta) \delta v_{\gamma b \ 0}^{(1)}(k_2, \eta) , \qquad (3.21)$$

where for simplicity, we omit the time dependence of $S(k_1, k_2)$. To proceed the estimation of the magnetic power, we take the limit $k/k_1 \to 0$. This approximation can include the contributions from subhorizon scales. In this limit,

$$k_2 = k_1 \left[1 - \frac{k}{k_1} \mu_1 + O\left((k/k_1)^2\right) \right].$$
 (3.22)

Furthermore, we can approximate the integrated source term as $S(k_1, k_2) \approx S(k_2, k_1)$ $\approx T(k_1)$ since $S(k_1, k_2)$ can be treated as k independent in the above limit. Then by using the fact that $P_{\Phi}(k) \propto k^{n_s-4}$, Eq. (3.20) can be rewritten as

$$\frac{k^3}{2\pi^2} P_B(k) \bigg|_{\text{Slip}} \propto k^5 \int k_1^2 dk_1 \int d\mu_1 \left(1 - \mu_1^2\right) k_1^{n_s - 4} k_2^{n_s - 4} \left(1 - \frac{k_1}{k_2}\right) T^2(k_1) ,$$

$$\propto k^7 . \tag{3.24}$$

This nonlinear power law can be seen in Fig. 3.2. Note that if we use the superhorizon solution only namely $\delta^{(1)} \propto (kn)^0$ and $\delta v^{(1)} \propto k^3 n^5$ the magnetic power is returned

solution only, namely, $\delta_{\gamma}^{(1)} \propto (k\eta)^0$ and $\delta v_{\gamma b\ 0}^{(1)} \propto k^3 \eta^5$, the magnetic power is returned as $\propto k^8$. This superhorizon power does not match for our numerical results.

By using our numerical code, we trace a possible cause of the discrepancies between the results in previous studies. As we noted in Sect. 2.7.3, the transfer function of the vector mode is antisymmetric under the exchange of k_1 and k_2 , and therefore, the isosceles configuration such that $k_1 = k_2$ in Fourier space does not contribute in the calculation of the power spectrum. However, to achieve the result correctly, contributions from the configurations of $k_1 \lesssim k_2$ and $k_2 \lesssim k_1$ should be included. When these contributions are not included in the numerical calculation, the power spectrum of magnetic fields on superhorizon scales shows $\propto k^4$, which corresponds to the result obtained in Ref. [64].

On subhorizon scales, we can find that the spectra of magnetic fields induced by the slip, the anisotropic stress, and the second-order slip terms are proportional to $k^{0.2}$, $k^{1.0}$, and $k^{1.0}$, respectively. The spectra induced by the slip and the anisotropic stress terms are consistent with Ref. [63]. A noticeable feature in the spectrum induced by the second-order slip term is the additional amplification at $k \approx 5.0 \times 10^{-1} \ h\text{Mpc}^{-1}$ at z=1100. As discussed in Sect. 3.3.1, this additional amplification is due to the second-order relative velocity between photons and baryons after the horizon crossing. However, this amplification is a temporary effect and the amplified magnetic fields by this effect had been erased by the epoch of Silk damping [39]. Therefore, the amplification cannot be seen for scales $k \gtrsim 1.0 \ h\text{Mpc}^{-1}$.

The above discussion and result in this subsection are valid only for the autopower spectra of the magnetic fields from the slip, the anisotropic stress, and the second-order slip terms. In the following subsection, we focus on the total power spectrum induced by all the contributions including the cross spectra.

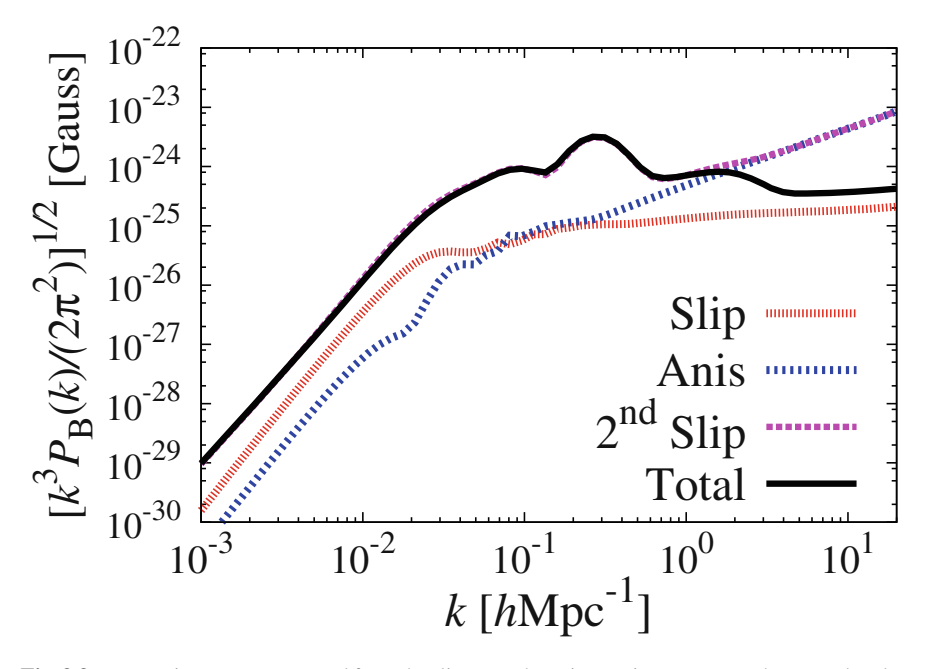


Fig. 3.3 Magnetic spectra generated from the slip term, the anisotropic stress term, the second-order slip term, and all terms included the cross terms at recombination $(1+z\simeq 1100)$

3.3.3 The Second-Order Magnetic Fields

We depict the total power spectrum at recombination in Fig. 3.3. It is clear that the second-order slip term gives a dominant contribution to the total magnetic fields. The amplitude of magnetic fields from the second-order slip term is 10 times larger than without the second-order slip term. However, we find that the magnetic fields from the second-order slip term are canceled out by the magnetic fields from the anisotropic stress term on small scales.

By using the tight coupling solution given by Eq. (2.202), this cancellation is easily understood analytically. As we mentioned in Sect. 3.3.1, the dominant term in Eq. (2.202) is the anisotropic stress term given by

$$\delta v_{\gamma b \lambda}^{(2)} \simeq \frac{1}{1+R} \int_{\mathbf{k}} \left[-\frac{5}{2} \Pi_{\gamma 0}^{(1)}(k_1) v_{b 0}^{(1)}(k_2) \right] \mathcal{Y}_{1,\lambda}^{2,1}(\hat{\mathbf{k}}_1, \hat{\mathbf{k}}_2) , \qquad (3.25)$$

while any other terms related to the anisotropic stress are subdominant with the baryon-photon ratio $R \propto 3\rho_{\rm b}^{(0)}/(4\rho_{\gamma}^{(0)})$ as a suppression factor. By substituting this expression into Eq. (3.19), the evolution of magnetic fields from the second-order slip and the anisotropic stress terms is given as

$$\frac{d\mathcal{B}_{\lambda}}{dt} \propto \left[\frac{5}{4} \frac{1}{1+R} - \frac{5}{4} \right] v_{\text{b 0}}^{(1)}(k_1) \Pi_{\gamma 0}^{(1)}(k_2) \mathcal{Y}_{1,\lambda}^{1,2}(\hat{\boldsymbol{k}}_1, \hat{\boldsymbol{k}}_2) , \qquad (3.26)$$

where the first and the last terms in the parentheses are coming from the second-order slip term and the anisotropic stress term, respectively. We can see that the two terms in the parentheses in Eq. (3.26) are canceled in the radiation dominated era, where R is negligibly small. However, in the matter dominated era, the baryon-photon ratio has large value and this cancellation does not occur.

The dominant contribution from the second-order slip term is canceled out by the contribution from the anisotropic stress term in the radiation dominated era. Conversely, there still remain some contributions from the second-order slip term as shown in Fig. 3.3 and discussed below using the tight-coupling solution. The sub-leading contribution from the second-order slip term can be written as

$$\delta v_{\gamma b \lambda}^{(2)} \simeq \frac{1}{1+R} \int_{\mathbf{k}} \left[-2\delta v_{\gamma b 0}^{(1)}(k_1) \delta_{\gamma}^{(1)}(k_2) \right] \sqrt{\frac{4\pi}{3}} Y_{1,\lambda}^*(\hat{\mathbf{k}}_1) . \tag{3.27}$$

Then, the evolution equation of magnetic fields induced by the slip and the secondorder slip terms can be rewritten as

$$\frac{d\mathcal{B}_{\lambda}}{dt} \propto \left[\frac{1}{1+R} + 1 \right] \delta v_{\gamma b \ 0}^{(1)}(k_1) \delta_{\gamma}^{(1)}(k_2) \sqrt{\frac{4\pi}{3}} Y_{1,\lambda}^*(\hat{k}_1) , \qquad (3.28)$$

where the first and the last terms in the parentheses are coming from the secondorder slip term and the slip term, respectively. From Eq. (3.28), we find that the total amplitude of the spectrum of magnetic fields is twice as large as the case only with the slip term. This tendency can be seen in Fig. 3.3.

Next, let us discuss the evolution of magnetic fields through the epoch of recombination. As the process of recombination proceeds, electrons form neutral hydrogen atoms with protons and the number of free electrons rapidly decreases. Accordingly the effect of the Compton scattering on generation of magnetic fields becomes negligible and magnetic fields are no longer generated through the Harrison mechanism. We show the power spectrum of second-order magnetic fields after the recombination epoch at $z \simeq 500$ in Fig. 3.4. In Fig. 3.4, one can find new features in the spectrum different from one at recombination on intermediate scales such as $10^{-2} h {\rm Mpc}^{-1} \lesssim k \lesssim 1.0 \ h {\rm Mpc}^{-1}$. These features are nearly consistent with Ref. [64]. For instance, magnetic fields induced by the slip term decrease on intermediate scales. On the other hand, magnetic fields induced by the second-order slip term are enhanced at cosmological recombination since the relative velocity is also enhanced at that era. We furthermore extend the magnetic spectrum to much smaller scales. On scales where 1.0 $h \mathrm{Mpc}^{-1} \gtrsim k$, magnetic fields induced by the slip, the anisotropic stress, and the second-order slip terms have the same structures as the magnetic spectrum at recombination shown in Fig. 3.3. As a result, the spectrum of second-order magnetic fields has a slightly blue tilt on small scales.

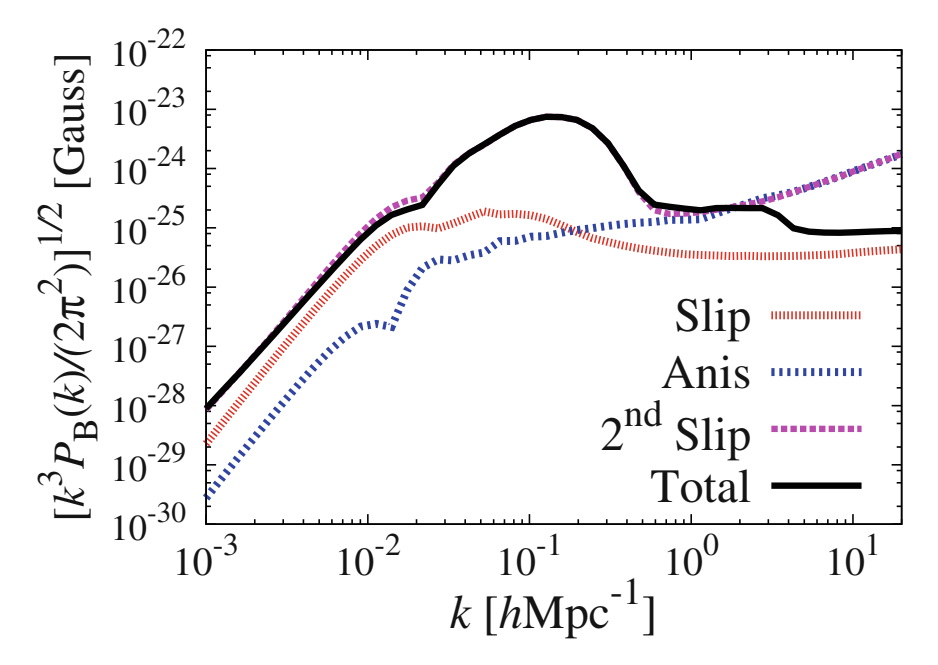


Fig. 3.4 Same as Fig. 3.3 but for after the recombination epoch as $(1 + z \approx 500)$

3.3.4 Nonhelical Magnetic Fields

Before closing this section, we investigate the possibility whether helical magnetic fields are generated in the Harrison mechanism or not since the helicity may play important roles in the cosmological observations [72–76]. In fact, in Ref. [77], the authors found the evidence of existence of helical magnetic fields on a few Mpc scales. It is believed that helical magnetic fields can only be generated through the process of parity violation. Because helicity is conserved in the standard magnetohydrodynamics, it is a good indicator to probe the generation mechanism of magnetic fields. We will show below that the Harrison mechanism does not induce helical magnetic fields since this mechanism relies on the standard Compton scattering which does not break the parity symmetry.

At first, under the existence of helical magnetic fields, the correlation of magnetic fields can be written as

$$\langle B_i(\mathbf{k})B_j(\mathbf{k}')\rangle = (2\pi)^3 \delta(\mathbf{k} - \mathbf{k}') \left[(\delta_{ij} - \hat{k}_i \hat{k}_j) \frac{P_B(k)}{2} + i \epsilon_{ijk} \hat{k}^k \frac{P_H(k)}{2} \right], \quad (3.29)$$

where $P_B(k)$ and $P_H(k)$ are the spectra of nonhelical and helical magnetic fields, respectively. The power spectrum of helical magnetic fields can be pulled by the subtraction as $\langle B_i(\mathbf{k})B_j(\mathbf{k}')\rangle - \langle B_j(\mathbf{k})B_i(\mathbf{k}')\rangle$. In the Harrison mechanism that is given by Eq. (3.17), generated magnetic fields can be symbolically expressed as

$$B_i(\mathbf{k}) \propto \epsilon_{iab} k^a \int_{\mathbf{k}} \hat{k}_1^b f(\mathbf{k}_1, \mathbf{k}_2) X^{(1)}(\mathbf{k}_1) Y^{(1)}(\mathbf{k}_2) ,$$
 (3.30)

where $f(k_1, k_2)$ is an arbitrary real function of k_1 and k_2 , and $X^{(1)}(k_1)$ and $Y^{(1)}(k_2)$ are the time integrals of first-order scalar perturbations. The scalar perturbations can be decomposed into the primordial perturbation $\Phi^{(1)}(k)$ and the transfer function $X_T(k_1)$ or $Y_T(k_2)$ as $X^{(1)}(k_1)Y^{(1)}(k_2) = \Phi^{(1)}(k_1)\Phi^{(1)}(k_2)X_T(k_1)Y_T(k_2)$. Note that we use the fact that the purely second-order variables, e.g., $\delta v_{\gamma bi}$, are composed the product of the first-order scalar perturbations.

Finally, we evaluate the helical part of the power spectrum as

$$\langle B_{i}(\mathbf{k})B_{j}(\mathbf{k}')\rangle - \langle B_{j}(\mathbf{k})B_{i}(\mathbf{k}')\rangle \propto (2\pi)^{3}\delta(\mathbf{k} - \mathbf{k}') \left(\epsilon_{iab}\epsilon_{ja'b'} - \epsilon_{jab}\epsilon_{ia'b'}\right) k^{a}k^{a'}$$

$$\times \int_{\mathbf{k}} f(\mathbf{k}_{1}, \mathbf{k}_{2})X_{T}(k_{1})Y_{T}(k_{2})P_{\Phi}(k_{1})P_{\Phi}(k_{2})$$

$$\times \left[\hat{k}_{1}^{b}\hat{k}_{1}^{b'}f(\mathbf{k}_{1}, \mathbf{k}_{2})X_{T}(k_{1})Y_{T}(k_{2}) + \frac{1}{2}\left(\hat{k}_{1}^{b}\hat{k}_{2}^{b'} + \hat{k}_{2}^{b}\hat{k}_{1}^{b'}\right)f(\mathbf{k}_{2}, \mathbf{k}_{1})X_{T}(k_{2})Y_{T}(k_{1})\right]$$

$$= 0, \qquad (3.31)$$

where we symmetrize about $b \leftrightarrow b'$ in the square bracket by using the nature of the symmetry under the exchange of k_1 and k_2 . In conclusion, the Harrison mechanism cannot induce helical magnetic fields. This result is coming from the fact that general relativity and the standard Maxwell theory do not violate the parity symmetry. Therefore, the observed helical magnetic fields call for other mechanisms to explain.

3.4 Conclusion

In this section, we reinvestigate the spectrum of magnetic fields induced by cosmological perturbations through the Harrison mechanism. If we consider the cosmological perturbation theory up to the first order, the Harrison mechanism does not work since the vector mode, which is needed for this mechanism, has only a decaying solution. However, when we expand the cosmological perturbation up to the second order, the regular solution of the vector mode is excited by the first-order scalar mode. The Harrison mechanism works in the higher-order cosmological perturbation theory.

In previous studies, the spectrum of magnetic fields induced by this mechanism has been estimated. In Ref. [63], the authors show the spectrum of second-order

3.4 Conclusion 69

magnetic fields induced by the product of the first-order perturbations, namely, the slip and anisotropic stress terms. Subsequently, in Ref. [64], the purely second-order slip term is included. By comparing these works, however, it is found that there are some discrepancies in the product of first-order perturbations. For example, the power law tails of the spectrum induced by the slip and anisotropic stress terms on large scales have different k-dependences in Refs. [63, 64]. Furthermore, the scale-dependences of the spectrum are slightly different from each other. We find that the discrepancy can be explained by the lack of sampling in the Fourier modes at $k_1 \approx k_2$ of the first-order scaler perturbations in Ref. [64], and our results agree with the ones of Ref. [63].

Let us summarize features of the magnetic fields induced by the second-order magnetic fields at cosmological recombination as follows.

- The scale dependence of magnetic fields on large scales is $\propto k^{3.5}$, which is consistent with the result in Ref. [63]. Note that magnetic fields generated by causal processes have the same power [71].
- On small scales, the spectra of magnetic fields induced by the slip, the anisotropic stress, and the second-order slip terms have the power of $k^{0.2}$, $k^{1.0}$, and $k^{1.0}$, respectively. In particular, the spectra of magnetic fields induced by the slip and anisotropic stress terms are consistent with the result in Ref. [63].
- The cancellation occurs between the anisotropic stress term and the second-order slip term on small scales in the tight coupling regime in the radiation dominated era, and the power of magnetic field spectrum becomes $\propto k^{0.2}$. This result indicates that the spectrum of magnetic fields cannot have the large amplitude as argued in Ref. [63].
- The spectrum of magnetic fields at cosmological recombination has a bump at $k \approx 5.0 \times 10^{-1} \ h\text{Mpc}^{-1}$ owing to extra amplification after the horizon crossing, where the amplitude of magnetic fields is $B_{\text{rec}} \approx 5.0 \times 10^{-24}$ Gauss. However, after all, this amplification vanishes by nontrivial flipping of the relative velocity between photons and baryons discussed in Ref. [39]. This cancellation creates characteristic diffusion scales in the magnetic fields spectrum around $k \approx 10^0 \ h\text{Mpc}^{-1}$.
- The Harrison mechanism does not work efficiency below the scale of Silk damping at the electron-positron pair creation epoch as $k_{\rm cut} \approx 10^9~h{\rm Mpc}^{-1}$, as discussed in Ref. [63]. Even if we extrapolate our numerical result toward smaller scales by using the power of $\propto k^{0.2}$ up to the cutoff scale, the amplitude of the magnetic fields at that scale cannot be larger than 10^{-23} Gauss, assuming that the linear density perturbations are scale invariant.

Finally, we discuss implications of the cosmological seed fields. The derived amplitude of magnetic fields at recombination has a peak about 5.0×10^{-24} Gauss, which is sufficient for a candidate of the seed of galactic magnetic fields [17]. However, this amplitude seems to be somewhat small to explain the intergalactic magnetic fields [10, 11]. Note that, the above amplitude is derived assuming that the primordial perturbations are scale-invariant, while primordial perturbations with a blue tilt lead a larger amplitude of the magnetic fields on smaller scales.

The magnetic fields induced by the second-order perturbation must be inevitably generated in the standard cosmology, and it is possibly that the magnetic fields act as seed fields for the turbulent dynamo during the structure formation of the universe.

References

- L.M. Widrow, Origin of galactic and extragalactic magnetic fields. Rev. Mod. Phys. 74, 775– 823 (2002), arXiv:astro-ph/0207240
- M. Giovannini, The magnetized universe. Int. J. Mod. Phys. D 13, 391–502 (2004), arXiv:astro-ph/0312614
- 3. K. Subramanian, Magnetizing the universe. PoS MRU, 071 (2007), arXiv:0802.2804
- 4. D. Ryu, D.R. Schleicher, R.A. Treumann, C.G. Tsagas, L.M. Widrow, Magnetic fields in the large-scale structure of the universe. Space Sci. Rev. 166, 1–35 (2012), arXiv:1109.4055
- A. Kandus, K.E. Kunze, C.G. Tsagas, Primordial magnetogenesis. Phys. Rept. 505, 1–58 (2011), arXiv:1007.3891
- K. Subramanian, J.D. Barrow, Microwave background signals from tangled magnetic fields. Phys. Rev. Lett. 81, 3575–3578 (1998), arXiv:astro-ph/9803261
- 7. L.M. Widrow, D. Ryu, D.R.G. Schleicher, K. Subramanian, C.G. Tsagas, R.A. Treumann, The first magnetic fields. Space Sci. Rev. **166**, 37–70 (2012), arXiv:1109.4052
- 8. R. Durrer, A. Neronov, Cosmological magnetic fields: their generation, evolution and observation. Astron. Astrophys. Rev. 21, 62 (2013), arXiv:1303.7121
- 9. A. Neronov, I. Vovk, Evidence for strong extragalactic magnetic fields from Fermi observations of TeV blazars. Science **328**, 73–75 (2010), arXiv:1006.3504
- K. Takahashi, M. Mori, K. Ichiki, S. Inoue, Lower bounds on intergalactic magnetic fields from simultaneously observed GeV-TeV light curves of the blazar Mrk 501. Astrophys. J. 744, L7 (2012), arXiv:1103.3835
- K. Takahashi, M. Mori, K. Ichiki, S. Inoue, H. Takami, Lower bounds on magnetic fields in intergalactic voids from long-term GeV-TeV light curves of the blazar Mrk 421. Astrophys. J. 771, L42 (2013), arXiv:1303.3069
- 12. W. Chen, J.H. Buckley, F. Ferrer, Search for GeV y-ray pair halos around low redshift blazars. Phys. Rev. Lett. 115, 211103 (2015), arXiv:1410.7717
- 13. C.Caprini, S. Gabici, Gamma-ray observations of blazars and the intergalactic magnetic field spectrum, Phys. Rev. D **91**(12), 123514 (2015), arXiv:1504.00383
- R.M. Kulsrud, S.W. Anderson, The spectrum of random magnetic fields in the mean field dynamo theory of the Galactic magnetic field. ApJ 396, 606–630 (1992)
- 15. J.L. Han, R.N. Manchester, E.M. Berkhuijsen, R. Beck, Antisymmetric rotation measures in our Galaxy: evidence for an A0 dynamo. A & A 322, 98–102 (1997)
- A. Brandenburg, K. Subramanian, Astrophysical magnetic fields and nonlinear dynamo theory. Phys. Rept. 417, 1–209 (2005), arXiv:astro-ph/0405052
- A.-C. Davis, M. Lilley, O. Tornkvist, Relaxing the bounds on primordial magnetic seed fields. Phys. Rev. D 60, 021301 (1999), arXiv:astro-ph/9904022
- 18. B. Ratra, Cosmological 'seed' magnetic field from inflation. ApJ **391**, L1–L4 (1992)
- K. Bamba, J. Yokoyama, Large scale magnetic fields from inflation in dilaton electromagnetism. Phys. Rev. D 69, 043507 (2004), arXiv:astro-ph/0310824
- J. Martin, J. Yokoyama, Generation of large-scale magnetic fields in single-field inflation. JCAP 0801, 025 (2008), arXiv:0711.4307
- V. Demozzi, V. Mukhanov, H. Rubinstein, Magnetic fields from inflation? JCAP 0908, 025 (2009), arXiv:0907.1030
- S. Kanno, J. Soda, M.-A. Watanabe, Cosmological magnetic fields from inflation and backreaction. JCAP 0912, 009 (2009), arXiv:0908.3509

References 71

23. T. Fujita, S. Mukohyama, Universal upper limit on inflation energy scale from cosmic magnetic field. JCAP **1210**, 034 (2012), arXiv:1205.5031

- T. Fujita, S. Yokoyama, Critical constraint on inflationary magnetogenesis. JCAP 1403, 013 (2014), arXiv:1402.0596
- C. Caprini, L. Sorbo, Adding helicity to inflationary magnetogenesis, JCAP 1410(10), 056 (2014), arXiv:1407.2809
- K.-W. Ng, S.-L. Cheng, W. Lee, Inflationary dilaton-axion magnetogenesis. Chin. J. Phys. 53, 110105 (2015), arXiv:1409.2656
- T. Fujita, R. Namba, Y. Tada, N. Takeda, H. Tashiro, Consistent generation of magnetic fields in axion inflation models. JCAP 1505(05) 054 (2015), arXiv:1503.05802
- 28. M. Christensson, M. Hindmarsh, A. Brandenburg, Inverse cascade in decaying 3-D magneto-hydrodynamic turbulence. Phys. Rev. E **64**, 056405 (2001), arXiv:astro-ph/0011321
- 29. R. Banerjee, K. Jedamzik, The evolution of cosmic magnetic fields: from the very early universe, to recombination, to the present. Phys. Rev. D **70**, 123003 (2004), arXiv:astro-ph/0410032
- 30. M. Joyce, M.E. Shaposhnikov, Primordial magnetic fields, right-handed electrons, and the Abelian anomaly. Phys. Rev. Lett. **79**, 1193–1196 (1997), arXiv:astro-ph/9703005
- G. Davies, L.M. Widrow, A possible mechanism for generating galactic magnetic fields. ApJ 540, 755–764 (2000)
- H. Hanayama, K. Takahashi, K. Kotake, M. Oguri, K. Ichiki et al., Biermann mechanism in primordial supernova remnant and seed magnetic fields. Astrophys. J. 633, 941 (2005), arXiv:astro-ph/0501538
- 33. R.M. Kulsrud, R. Cen, J.P. Ostriker, D. Ryu, The protogalactic origin for cosmic magnetic fields. Astrophys. J. **480**, 481 (1997), arXiv:astro-ph/9607141
- Y. Fujita, T.N. Kato, A possible origin of magnetic fields in galaxies and clusters: strong magnetic fields at z 10? Mon. Not. Roy. Astron. Soc. 364, 247–252 (2005), arXiv:astro-ph/0508589
- M.V. Medvedev, L.O. Silva, M. Kamionkowski, Cluster magnetic fields from large-scalestructure and galaxy-cluster shocks. Astrophys. J. 642, L1–L4 (2006), arXiv:astro-ph/0512079
- 36. E.R. Harrison, Generation of magnetic fields in the radiation ERA. MNRAS 147, 279 (1970)
- 37. K. Takahashi, K. Ichiki, H. Ohno, H. Hanayama, Magnetic field generation from cosmological perturbations. Phys. Rev. Lett. **95**, 121301 (2005), arXiv:astro-ph/0502283
- 38. A. Lewis, Observable primordial vector modes. Phys. Rev. D 70, 043518 (2004), arXiv:astro-ph/0403583
- K. Ichiki, K. Takahashi, N. Sugiyama, Constraint on the primordial vector mode and its magnetic field generation from seven-year Wilkinson Microwave Anisotropy Probe Observations. Phys. Rev. D 85, 043009 (2012), arXiv:1112.4705
- S. Saga, M. Shiraishi, K. Ichiki, Constraining primordial vector mode from B-mode polarization. JCAP 1410, 004 (2014), arXiv:1405.4810
- 41. L. Hollenstein, C. Caprini, R. Crittenden, R. Maartens, Challenges for creating magnetic fields by cosmic defects. Phys. Rev. D 77, 063517 (2008), arXiv:0712.1667
- K. Horiguchi, K. Ichiki, T. Sekiguchi, N. Sugiyama, Primordial magnetic fields from selfordering scalar fields. JCAP 1504(04), 007 (2015), arXiv:1501.06304
- S. Saga, M. Shiraishi, K. Ichiki, N. Sugiyama, Generation of magnetic fields in Einstein-Aether gravity. Phys. Rev. D 87(10), 104025 (2013), arXiv:1302.4189
- W. Hu, D. Scott, J. Silk, Reionization and cosmic microwave background distortions: a complete treatment of second order Compton scattering. Phys. Rev. D 49, 648–670 (1994), arXiv:astro-ph/9305038
- L. Senatore, S. Tassev, M. Zaldarriaga, Cosmological perturbations at second order and recombination perturbed. JCAP 0908, 031 (2009), arXiv:0812.3652
- N. Bartolo, S. Matarrese, A. Riotto, The full second-order radiation transfer function for largescale cmb anisotropies. JCAP 0605, 010 (2006), arXiv:astro-ph/0512481
- N. Bartolo, S. Matarrese, A. Riotto, CMB anisotropies at second order I. JCAP 0606, 024 (2006), arXiv:astro-ph/0604416
- 48. N. Bartolo, S. Matarrese, A. Riotto, CMB anisotropies at second-order. 2. analytical approach. JCAP **0701**, 019 (2007), arXiv:astro-ph/0610110

- C. Pitrou, J.-P. Uzan, F. Bernardeau, The cosmic microwave background bispectrum from the non-linear evolution of the cosmological perturbations. JCAP 1007, 003 (2010), arXiv:1003.0481
- 50. C. Pitrou, The radiative transfer at second order: a full treatment of the boltzmann equation with polarization. Class. Quant. Grav. 26, 065006 (2009), arXiv:0809.3036
- 51. M. Beneke, C. Fidler, K. Klingmuller, B polarization of cosmic background radiation from second-order scattering sources. JCAP 1104, 008 (2011), arXiv:1102.1524
- 52. M. Beneke, C. Fidler, Boltzmann hierarchy for the cosmic microwave background at second order including photon polarization. Phys. Rev. D 82, 063509 (2010), arXiv:1003.1834
- A. Naruko, C. Pitrou, K. Koyama, M. Sasaki, Second-order Boltzmann equation: gauge dependence and gauge invariance. Class. Quant. Grav. 30, 165008 (2013), arXiv:1304.6929
- R. Saito, A. Naruko, T. Hiramatsu, M. Sasaki, Geodesic curve-of-sight formulae for the cosmic microwave background: a unified treatment of redshift, time delay, and lensing. JCAP 1410(10), 051 (2014), arXiv:1409.2464
- C. Fidler, K. Koyama, G.W. Pettinari, A new line-of-sight approach to the non-linear Cosmic Microwave Background. JCAP 1504(04), 037 (2015), arXiv:1409.2461
- T. Kobayashi, R. Maartens, T. Shiromizu, K. Takahashi, Cosmological magnetic fields from nonlinear effects. Phys. Rev. D 75, 103501 (2007), arXiv:astro-ph/0701596
- K. Takahashi, K. Ichiki, N. Sugiyama, Electromagnetic properties of the early universe. Phys. Rev. D 77, 124028 (2008), arXiv:0710.4620
- S. Maeda, S. Kitagawa, T. Kobayashi, T. Shiromizu, Primordial magnetic fields from secondorder cosmological perturbations: tight coupling approximation. Class. Quant. Grav. 26, 135014 (2009), arXiv:0805.0169
- R. Gopal, S. Sethi, Generation of magnetic field in the pre-recombination era. Mon. Not. Roy. Astron. Soc. 363, 521–528 (2005), arXiv:astro-ph/0411170
- E. Nalson, A.J. Christopherson, K.A. Malik, Effects of non-linearities on magnetic field generation. JCAP 1409, 023 (2014), arXiv:1312.6504
- S. Matarrese, S. Mollerach, A. Notari, A. Riotto, Large-scale magnetic fields from density perturbations. Phys. Rev. D 71, 043502 (2005), arXiv:astro-ph/0410687
- K. Ichiki, K. Takahashi, H. Ohno, H. Hanayama, N. Sugiyama, Cosmological Magnetic Field: a fossil of density perturbations in the early universe. Science 311, 827–829 (2006), arXiv:astro-ph/0603631
- 63. K. Ichiki, K. Takahashi, N. Sugiyama, H. Hanayama, H. Ohno, Magnetic field spectrum at cosmological recombination, arXiv:astro-ph/0701329
- 64. E. Fenu, C. Pitrou, R. Maartens, The seed magnetic field generated during recombination. Mon. Not. Roy. Astron. Soc. 414, 2354–2366 (2011), arXiv:1012.2958
- K. Subramanian, D. Narasimha, S.M. Chitre, Thermal generation of cosmological seed magnetic fields in ionization fronts. MNRAS 271, L15 (1994)
- K. Jedamzik, V. Katalinic, A.V. Olinto, Damping of cosmic magnetic fields. Phys. Rev. D 57, 3264–3284 (1998), arXiv:astro-ph/9606080
- 67. P.A.R. Planck, Collaboration, Ade et al., Planck 2013 results. XVI. Cosmological parameters. Astron. Astrophys. **571**, A16 (2014), arXiv:1303.5076
- 68. BICEP2 Collaboration Collaboration, P. Ade et al., Detection of B-Mode polarization at degree angular scales by BICEP2. Phys. Rev. Lett. 112, 241101 (2014), arXiv:1403.3985
- W.M.A.P. Collaboration, G. Hinshaw et al., Nine-Year Wilkinson Microwave Anisotropy Probe (WMAP) Observations: cosmological parameter results. Astrophys. J. Suppl. 208, 19 (2013), arXiv:1212.5226
- E.R. Siegel, J.N. Fry, Cosmological structure formation creates large-scale magnetic fields. Astrophys. J. 651, 627–635 (2006), arXiv:astro-ph/0604526
- R. Durrer, C. Caprini, Primordial magnetic fields and causality. JCAP 0311, 010 (2003), arXiv:astro-ph/0305059
- L. Pogosian, T. Vachaspati, S. Winitzki, Signatures of kinetic and magnetic helicity in the CMBR. Phys. Rev. D 65, 083502 (2002), arXiv:astro-ph/0112536

References 73

73. C. Caprini, R. Durrer, T. Kahniashvili, The Cosmic microwave background and helical magnetic fields: The Tensor mode. Phys. Rev. D 69, 063006 (2004), arXiv:astro-ph/0304556

- 74. T. Kahniashvili, B. Ratra, Effects of cosmological magnetic helicity on the cosmic microwave background. Phys. Rev. D 71, 103006 (2005), arXiv:astro-ph/0503709
- 75. M. Shiraishi, A. Ricciardone, S. Saga, Parity violation in the CMB bispectrum by a rolling pseudoscalar. JCAP **1311**, 051 (2013), arXiv:1308.6769
- M. Shiraishi, Parity violation of primordial magnetic fields in the CMB bispectrum. JCAP 1206, 015 (2012), arXiv:1202.2847
- 77. H. Tashiro, W. Chen, F. Ferrer, T. Vachaspati, Search for CP violating signature of intergalactic magnetic helicity in the gamma ray sky, arXiv:1310.4826

Chapter 4 Weak Lensing

Abstract The vector mode imprints on the characteristic signal in the large-scale structure, i.e., the weak lensing measurements. Photons emitted from the CMB last scattering surface or galaxies are deflected by the foreground perturbations, called CMB lensing and cosmic shear, respectively. We can split the weak lensing signals into the parity-even and parity-odd signals. The parity-odd signal is induced from not the scalar mode but the vector and tensor modes. Although the parity-odd signal has not been detected yet, the parity-odd signal in the weak lensing observations will be a good probe for the second-order vector mode. In this section, we apply the second-order vector mode in the cosmological perturbation theory to the weak lensing observations. We use the full-sky formula for the weak lensing effect to predict the second-order parity-odd signal. In this part, we discuss the detectability of the second-order vector mode. Moreover, we compare the signals from primordial gravitational waves if we consider the weak lensing measurements.

Keywords Second-order perturbation theory · CMB lensing · Cosmic shear

4.1 Introduction

The recent remarkable developments of cosmological observations such as the cosmic microwave background (CMB) or large-scale structure help us to build the standard Λ CDM cosmology. The new era of high precision cosmology makes it possible to acquire rich information about the expansion history of the Universe or the features of density perturbations [1–4]. It is very important to combine several types of observations to reduce degeneracies between cosmological parameters. The weak lensing effect is a key observable for revealing the late-time evolution of density perturbations. For this purpose, in this section, we focus on the weak lensing effect.

The weak lensing effect can be roughly classified into two observables (for reviews, see e.g., [5, 6]). One is called CMB lensing, which is the gravitational deflec-

tion by the foreground large-scale structure. In CMB experiments, we can measure the deflection angle of CMB photons from observed CMB maps through the reconstruction technique [7–10]. The CMB lensing signals have been precisely detected by the Planck satellite [11] and are available to constrain cosmological parameters. Next-generation CMB observations are planned [12, 13], and CMB lensing will become a more important observable in the near future [14]. The other observable is called the cosmic shear, which can be measured by observing deformed galaxy images. The photons emitted from galaxies are deflected by forward density perturbations, deforming the intrinsic shape of galaxies. Ongoing and upcoming imaging surveys such as the Dark Energy Survey (DES) [15], Subaru Hyper Suprime-Cam (HSC) [16], Square Kilometre Array (SKA) [17], and Large Synoptic Survey Telescope (LSST) [18], can provide us with high-precision cosmic shear data. Thus, the weak lensing survey is becoming a more interesting and active area of measurement.

The first-order cosmological perturbation theory includes three independent modes: scalar, vector, and tensor. Among them, the scalar mode is the dominant component in the Universe and has been well determined by cosmological observations. Conversely, the vector and tensor modes are subdominant and have not been observed by current observations. In particular, the vector mode is often treated as the negligible component since it rapidly decays in the standard first-order cosmological perturbation theory with perfect fluids. Nearly all inflation models predict primordial gravitational waves (PGW). With a non-vanishing amplitude, namely a nonzero tensor-to-scalar ratio r, primordial gravitational waves correspond to the tensor mode. On the basis of current observations, primordial gravitational waves have the small tensor-to-scalar ratio of $r \lesssim 0.1$ [1, 19]. In the context of scalar, vector, and tensor decompositions, the weak lensing effect also can be associated with each mode. The deflection angle for CMB lensing can be written in the gradient of the scalar lensing potential (gradient-mode) and the rotation of the pseudoscalar lensing potential (curl-mode). The deformation of the shape of galaxies is described by the Jacobi map, which can be decomposed into even and odd-parity modes (E- and B-modes, respectively). The vector and tensor modes, rather than the scalar mode, induce the curl- and B-modes. Therefore, the weak lensing curl- and B-modes are key observables for exploring subdominant modes.

Some possible sources for the vector and tensor modes in extensions of the standard Λ CDM cosmology are available. The weak lensing induced by the primordial gravitational waves has been well studied [20, 21]. The primordial gravitational waves with r=O(0.1) do not have detectable amplitudes for the curl- and B-modes, even under the assumption of ideal experiments. Cosmic defects are also possible sources of the vector and tensor modes. The weak lensing effect induced by cosmic strings has been studied, and weak lensing measurements can constrain parameters related to cosmic defects [22, 23]. However, in the first-order cosmological perturbation theory, the vector and tensor modes must have model parameters, e.g., the tensor-to-scalar ratio or the strength of the cosmic string tension. The amplitudes of the weak lensing signal induced by the above model depend on the model parameters and the generated weak lensing signal has uncertainties.

4.1 Introduction 77

In the second-order cosmological perturbation theory, the second-order vector and tensor modes are naturally induced by the product of the first-order scalar modes. These modes do not have free parameters, since the first-order scalar mode is well determined by current observations. The second-order CMB polarization anisotropy induced by these modes has been discussed in the literature [24–28]. The application of these modes to the weak lensing is also possible and quite interesting. The contributions of the second-order vector and tensor modes to the gradient- and E-modes are investigated in [29–32]. As the first-order scalar mode can induce the gradientand E-modes, the contribution from the second-order vector and tensor modes to the gradient- and E-modes must be smaller than that from the first-order scalar mode. In Ref. [33], the authors estimated the curl- and B-mode signals induced by the secondorder tensor mode for the first time. The effect of the second-order tensor mode on the B-mode signal is comparable with that of the primordial gravitational waves with r = 0.4 and dominates on small scales, $10 \lesssim \ell$. However, the second-order tensor mode tends to have a smaller contribution than the second-order vector mode [24, 29–32]. Therefore, the weak lensing signal from the second-order vector mode is expected to exceed that from the second-order tensor mode.

In this section, we focus on the weak lensing curl- and B-modes induced by the second-order vector mode. The weak lensing curl- and B-modes are generated not by the scalar mode but by the vector and tensor modes. Therefore, the curl- and B-modes are good tracers of the subdominant mode in the current Universe. As the second-order vector mode must have a larger amplitude than the second-order tensor mode, it is important to estimate the weak lensing signal induced by the vector mode.

4.2 Formulation of Weak Lensing

In this section, we present a short review of the full-sky formalism for the weak lensing induced by the vector and tensor modes following Refs. [10, 22, 23]. The weak lensing can roughly be classified into two observed objects.

First, the CMB photons emitted from the last scattering surface are deflected by the gravitational potentials related to the large-scale structure, which is called CMB lensing. The CMB lensing is mainly caused by the scalar gravitational potential. However, vector and tensor perturbations can also affect the deflection angle of photons, and the vector and tensor modes imprint characteristic deflection patterns on the CMB lensing. The deflection angle of the CMB photons can be written as the gradient of the scalar potential (gradient-mode) and the rotation of the pseudo-scalar potential (curl-mode). By using the nature of the parity these lensing potentials can be reconstructed independently, even when the gradient mode dominates the CMB lensing signals [10].

Second, photons emitted from galaxies are lensed by the large-scale structure, causing the shapes of galaxies to be deformed. This is known as cosmic shear. By

studying the deformation pattern statistically, we can distinguish traces of the scalar, vector, and tensor perturbations. The deformation pattern of the shapes of galaxies can be decomposed into parity-even (E-mode) and parity-odd (B-mode) components.

In the followings, we present the full-sky formalism for the deflection angle and the deformation pattern, which are related to the geodesic equation and the Jacobi map, respectively. Note that it is sufficient to work without the Hubble expansion, namely, $a(\eta) \equiv 1$. This is because the geodesic equation is invariant under the conformal transformation.

4.2.1 Preliminary

Here, we present the mathematical tools to formulate the weak lensing. In this section, we adopt the line element in a spherical coordinate system as

$$g_{\mu\nu} dx^{\mu} dx^{\nu} = -d\eta^2 + d\chi^2 + \chi^2 \omega_{ab} d\theta^a d\theta^b , \qquad (4.1)$$

where χ is the comoving distance, and $\omega_{ab}\mathrm{d}\theta^a\mathrm{d}\theta^b=\mathrm{d}\theta^2+\sin^2\theta\mathrm{d}\varphi^2$ is the metric on the unit sphere. Only this section, $a,b\cdots$ denote the components of the spherical coordinate, e.g., $a,b=\theta$ or ϕ .

We consider a null geodesic $x^{\mu}(v)$, where v is the affine parameter. As null geodesic is invariant under the conformal transformation, $dv = a^2 d\lambda$, we can consider null geodesic without expansion of universe.

Here, we define the tangent vector $k^{\mu}(\lambda)$ along the geodesic $x^{\mu}(\lambda)$, namely,

$$k^{\mu}(v) = a^2 \frac{\mathrm{d}x^{\mu}}{\mathrm{d}v} = \frac{\mathrm{d}x^{\mu}}{\mathrm{d}\lambda} \ . \tag{4.2}$$

This tangent vector satisfies following equations as

$$g_{\mu\nu}k^{\mu}k^{\nu} = 0, \qquad (4.3)$$

$$k^{\mu}{}_{;\nu}k^{\nu} = \frac{\mathrm{d}^2 x^{\mu}}{\mathrm{d}\lambda^2} + \Gamma^{\mu}{}_{\alpha\beta} \frac{\mathrm{d}x^{\alpha}}{\mathrm{d}\lambda} \frac{\mathrm{d}x^{\beta}}{\mathrm{d}\lambda} = 0 , \qquad (4.4)$$

where the covariant derivative $k^{\mu}_{;\nu}$ and the Christoffel symbols are associated with the unperturbed metric $g_{\mu\nu}$. Note that, Eqs. (4.3) and (4.4) are the null condition for photons and the geodesic equation, respectively.

We solve the geodesic equation in the unperturbed geometry with the condition where observer is set at origin of the coordinate, namely, $(k^{\theta} = k^{\varphi} = 0)$. We can easily find the *incoming* radial solution as

$$(\eta, \chi, \theta, \phi) = (E\lambda, E(\lambda_O - \lambda), 0, 0) , \qquad (4.5)$$

where λ_O and E are the affine parameter at origin and the photon energy, respectively. Moreover, we obtain more general expression of Eq. (4.5) by rotating the spherical coordinate as

$$x^{\mu}(\lambda) = E\left(\lambda, (\lambda_O - \lambda)e_{\chi}^i\right), \tag{4.6}$$

where the unit vector e_{χ}^{i} is the direction of the photon propagation measured from the observer at the origin.

Hereafter, we use $\chi \equiv E(\lambda_O - \lambda)$ as the affine parameter. In terms of this affine parameter, the wave vector, $k^{\mu}(\chi) = dx^{\mu}/d\chi$ is rewritten as

$$\frac{\mathrm{d}x^{\mu}}{\mathrm{d}\chi} = (-1, e_{\chi}^{i}) \ . \tag{4.7}$$

We introduce the orthogonal space like basis along the light ray, e_a^{μ} , as

$$\begin{split} \hat{n}^i &= e^i_\chi(\hat{\boldsymbol{n}}) = (\sin\theta\cos\varphi, \sin\theta\sin\varphi, \cos\theta) \;, \\ e^i_\theta(\hat{\boldsymbol{n}}) &= (\cos\theta\cos\varphi, \cos\theta\sin\varphi, -\sin\theta) \;, \\ e^i_\varphi(\hat{\boldsymbol{n}}) &= (-\sin\theta\sin\varphi, \sin\theta\cos\varphi, 0) \;, \end{split} \tag{4.8}$$

where the above basis is corresponding to the basis on the background space-time in the Cartesian coordinate. The basis e^{μ}_a satisfies $g_{\mu\nu}e^{\mu}_ae^{\nu}_b=\omega_{ab}$ and $g_{\mu\nu}k^{\mu}e^{\nu}_a=g_{\mu\nu}u^{\mu}e^{\nu}_a=0$. In other words, the basis e^{μ}_a can be read as the tetrad. Furthermore, these tetrads obey as

$$e_{\chi}^{i}\partial_{i} = \partial_{\chi} , \quad e_{\theta}^{i}\partial_{i} = \frac{1}{\chi}\partial_{\theta} , \quad e_{\varphi}^{i}\partial_{i} = \frac{1}{\chi}\partial_{\varphi} .$$
 (4.9)

The above relation leads to the following relation:

$$\chi^2 e_{(a}^j e_{b)}^k \partial_j \partial_k e_{\chi}^i = -\omega_{ab} e_{\chi}^i . \tag{4.10}$$

When we derive the above relation, we use the derivative of the basis:

$$\partial_{\gamma} e_{\theta}^{i} = \partial_{\gamma} e_{\varphi}^{i} = 0 , \qquad (4.11)$$

$$\partial_a e_\chi^i = e_a^i \,, \tag{4.12}$$

$$\partial_{\theta} e_{\theta}^{i} = -e_{\gamma}^{i} \,, \tag{4.13}$$

$$\partial_{\varphi} e_{\theta}^{i} = \partial_{\theta} e_{\varphi}^{i} = \cot \theta e_{\varphi}^{i} , \qquad (4.14)$$

$$\partial_{\varphi} e_{\varphi}^{i} = -\sin\theta \left[\sin\theta e_{\chi}^{i} + \cos\theta e_{\theta}^{i} \right]. \tag{4.15}$$

Furthermore, we define the covariant derivative of a two-vector on the unit sphere, $X_a = X_i e_a^i$, in terms of the polarization basis as

$$X_{a:b} \equiv \partial_b X_a - {}^{(2)}\Gamma^c{}_{ab}X_c , \qquad (4.16)$$

where we define the connection coefficient on the two sphere as

$$^{(2)}\Gamma^{c}{}_{ab} \equiv e^{c}_{i}\partial_{b}e^{i}_{a} = \frac{1}{2}\omega^{cc'}\left(\omega_{ac',b} + \omega_{bc',a} - \omega_{ab,c'}\right). \tag{4.17}$$

Next, we define the polarization basis which is used with the spin operators, $e^a_{s_\lambda}$ with $s_\lambda = \pm 1$, as

$$e_{s_{\lambda}}^{a}(\hat{\boldsymbol{n}}) \equiv e_{s_{\lambda}}^{i} e_{i}^{a} = \left[e_{\theta}^{i}(\hat{\boldsymbol{n}}) + \frac{is_{\lambda}}{\sin \theta} e_{\varphi}^{i} \right] e_{i}^{a}, \quad \text{Spin-1 variable}$$
 (4.18)

where this polarization vectors are projected on the two-sphere by multiplying e_a^i . The components of this polarization vector are

$$e_{s_{\lambda}}^{i}(\hat{\mathbf{k}}) = (1, is_{\lambda}, 0),$$
 (4.19)

$$e_{s_{\lambda}}^{i}(\hat{\mathbf{n}}) = (\cos\theta\cos\varphi - is_{\lambda}\sin\varphi, \cos\theta\sin\varphi + is_{\lambda}\cos\varphi, -\sin\theta),$$
 (4.20)

$$e_{s_{\lambda}}^{\theta}(\hat{\boldsymbol{n}}) = 1 \;, \quad e_{s_{\lambda}}^{\varphi}(\hat{\boldsymbol{n}}) = \frac{i s_{\lambda}}{\sin \theta} \;, \tag{4.21}$$

where, throughout this note, we set the coordinate system $\hat{k} = \hat{z}$, which is corresponding to my notation and [22, 23]. Furthermore, by using these polarization vectors, the two-dimensional metric ω^{ab} and the two-dimensional Levi-Civita tensor ϵ^{ab} can be expressed as

$$\omega^{ab} = e_{+}^{(a} e_{-}^{b)}, \quad \epsilon^{ab} = i e_{+}^{[a} e_{-}^{b]}.$$
 (4.22)

By using the e_+^a , the spin-s function can be expanded by this basis as

$$_{s}X = X_{a_{1}a_{2}\cdots a_{s}}e_{+}^{a_{1}}e_{+}^{a_{2}}\cdots e_{+}^{a_{s}} \ (s \ge 0),$$
 (4.23)

$$_{s}X = X_{a_{1}a_{2}\cdots a_{|s|}}e_{-}^{a_{1}}e_{-}^{a_{2}}\cdots e_{-}^{a_{|s|}} (s < 0).$$
 (4.24)

Furthermore, the spin basis have the following relations,

$$\chi e_{\pm}^{j} \partial_{j} e_{+}^{i} = \cot \theta e_{+}^{i} , \quad \chi e_{\pm}^{j} \partial_{j} e_{\pm}^{i} = -2e_{\nu}^{i} - \cot \theta e_{\pm}^{i} , \qquad (4.25)$$

where in order to derive the above relation, we use Eqs. (4.13), (4.14), and (4.15). We take contraction of Eq. (4.25) by using e_i^a , we can get

$$e_{s,b}^a e_{s'}^b = ss' \cot \theta e_s^a . \tag{4.26}$$

And by using the above relation (4.26), we can derive the following relations.

$$(_{0}X)_{\cdot a}e_{+}^{a} = -\partial (_{0}X) , \quad (_{0}X)_{\cdot a}e_{-}^{a} = -\bar{\partial} (_{0}X) ,$$
 (4.27)

$$X_{a:b}e_s^a e_+^b = -\partial (_s X) , \quad X_{a:b}e_s^a e_-^b = -\bar{\partial} (_s X) ,$$
 (4.28)

$${}_{(0}X)_{:ab} e_{+}^{a} e_{+}^{b} = \partial^{2}({}_{0}X) , \quad {}_{(0}X)_{:ab} e_{-}^{a} e_{-}^{b} = \bar{\partial}^{2}({}_{0}X) ,$$
 (4.29)

$$(_{0}X)_{:ab} e_{+}^{a} e_{-}^{b} = \partial \bar{\partial} (_{0}X) = \bar{\partial} \partial (_{0}X) ,$$
 (4.30)

where $\bar{\partial}$ and ∂ are the spin lowering and raising operators defined as

$$\bar{\partial}_s f(\theta, \phi) \equiv -\sin^s \theta \left[\partial_\theta + i \csc \theta \partial_\phi \right] \sin^{-s} \theta_s f(\theta, \phi) , \qquad (4.31)$$

$$\partial_s f(\theta, \phi) \equiv -\sin^{-s} \theta \left[\partial_{\theta} - i \csc \theta \partial_{\phi} \right] \sin^s \theta_s f(\theta, \phi) . \tag{4.32}$$

4.2.2 CMB Lensing

CMB lensing effect is described by the perturbed geodesic equation since we can study the deflection angle of the CMB photons. The deflection angel from the last-scattering surface is

We consider two null geodesics $x^{\mu}(\chi)$ and $\tilde{x}^{\mu}(\chi) = x^{\mu}(\chi) + \xi^{\mu}(\chi)$, where $\xi^{\mu}(\chi)$ is the deviation vector field,

$$\frac{\mathrm{d}^2 \tilde{x}^{\mu}}{\mathrm{d}\chi^2} + \tilde{\Gamma}^{\mu}_{\alpha\beta} \frac{\mathrm{d}\tilde{x}^{\alpha}}{\mathrm{d}\chi} \frac{\mathrm{d}\tilde{x}^{\beta}}{\mathrm{d}\chi} = 0 , \qquad (4.33)$$

$$\frac{\mathrm{d}^2 x^{\mu}}{\mathrm{d} \chi^2} + \Gamma^{\mu}_{\alpha\beta} \frac{\mathrm{d} x^{\alpha}}{\mathrm{d} \chi} \frac{\mathrm{d} x^{\beta}}{\mathrm{d} \chi} = 0. \tag{4.34}$$

The geodesic equation of the deviation vector up to the first order can be written as

$$\frac{\mathrm{d}^2 \xi^{\mu}}{\mathrm{d} \chi^2} + \delta \Gamma^{\mu}_{\alpha\beta} \frac{\mathrm{d} x^{\alpha}}{\mathrm{d} \chi} \frac{\mathrm{d} x^{\beta}}{\mathrm{d} \chi} + 2 \Gamma^{\mu}_{\alpha\beta} \frac{\mathrm{d} x^{\alpha}}{\mathrm{d} \chi} \frac{\mathrm{d} \xi^{\beta}}{\mathrm{d} \chi} = 0 \ . \tag{4.35}$$

The equation for $\mu = 0$ component is

$$\frac{\mathrm{d}}{\mathrm{d}\chi} \left[\frac{\mathrm{d}\xi^0}{\mathrm{d}\chi} - 2\Psi - \sigma_i e_\chi^i \right] = -\Upsilon , \qquad (4.36)$$

where

$$\Upsilon \equiv -(\Psi + \Phi) - \sigma_i e_{\chi}^i + \frac{1}{2} h_{ij} e_{\chi}^i e_{\chi}^j , \qquad (4.37)$$

and the equation for $\mu = i$ components are

$$\frac{\mathrm{d}}{\mathrm{d}\chi} \left[\frac{\mathrm{d}\xi^{i}}{\mathrm{d}\chi} - 2\Phi e_{\chi}^{i} - \sigma^{i} + h^{i}{}_{j}e_{\chi}^{j} \right] = -(\Psi + \Phi)^{|i} - \sigma_{j}^{|i}e_{\chi}^{j} + \frac{1}{2}h_{jk}^{|i}e_{\chi}^{j}e_{\chi}^{k} . \quad (4.38)$$

By multiplying the basis e_a^i with $a=\theta,\phi$ to Eq. (4.38), and using Eqs. (4.9) and (4.12)

$$\frac{\mathrm{d}^2 \xi^a}{\mathrm{d}\chi^2} = \frac{1}{\chi} \omega^{ab} \left[\Upsilon_{:b} - \frac{\mathrm{d}}{\mathrm{d}\chi} \left(\chi \Omega_b \right) \right] , \tag{4.39}$$

where we define

$$\Omega_a \equiv \left(-\sigma_i + h_{ij} e_\chi^j \right) e_a^i \ . \tag{4.40}$$

Equation (4.39) can be integrated by parts with initial conditions, $\xi^a(0) = 0$ and $d\xi^a/d\chi(0) = \delta\theta_0^a$, as

$$\frac{\xi^{a}(\chi_{S})}{\chi_{S}} = \delta\theta_{0}^{a} + \omega^{ab} \int_{0}^{\chi_{S}} d\chi_{2} \int_{0}^{\chi_{2}} d\chi_{1} \frac{1}{\chi_{S}\chi_{1}} \left[\Upsilon_{:b} - \frac{d}{d\chi} \left(\chi \Omega_{b} \right) \right] (\tilde{x}^{\mu})$$

$$= \delta\theta_{0}^{a} + \omega^{ab} \int_{0}^{\chi_{S}} d\chi_{1} \int_{\chi_{1}}^{\chi_{S}} d\chi_{2} \frac{1}{\chi_{S}\chi_{1}} \left[\Upsilon_{:b} - \frac{d}{d\chi} \left(\chi \Omega_{b} \right) \right] (\tilde{x}^{\mu})$$

$$= \delta\theta_{0}^{a} + \omega^{ab} \int_{0}^{\chi_{S}} d\chi_{1} \frac{\chi_{S} - \chi_{1}}{\chi_{S}\chi_{1}} \left[\Upsilon_{:b} - \frac{d}{d\chi} \left(\chi \Omega_{b} \right) \right] (\tilde{x}^{\mu})$$

$$\approx \delta\theta_{0}^{a} + \omega^{ab} \int_{0}^{\chi_{S}} d\chi \frac{\chi_{S} - \chi}{\chi_{S}\chi} \left[\Upsilon_{:b} - \frac{d}{d\chi} \left(\chi \Omega_{b} \right) \right] (x^{\mu}) , \tag{4.41}$$

where χ_S is the conformal distance at the source (e.g., for the cosmic shear: the conformal distance at the light emitted, the CMB lensing: χ_S corresponding to the last-scattering surface) and we use the Born approximation from the third line to the fourth line in the above equation. Finally, we can define the deflection angle on the two-sphere as

$$\Delta^a(\hat{\boldsymbol{n}}) \equiv \frac{\xi^a}{\chi_S} - \delta\theta_0^a \ . \tag{4.42}$$

This deflection angle can be decomposed into a gradient of scalar lensing potential ϕ (gradient-mode) and a rotation of pseudo-scalar lensing potential ϖ (curl-mode) as

$$\Delta_a(\hat{\mathbf{n}}) = \phi_{:a}(\hat{\mathbf{n}}) + \varpi_{:b}(\hat{\mathbf{n}})\epsilon^b_{\ a} , \qquad (4.43)$$

where $\epsilon^b{}_a$ is the covariant two-dimensional Levi-Civita tensor. These potentials can be pulled as

$$\phi^{:a}_{:a}(\hat{\boldsymbol{n}}) = \Delta^{a}_{:a}(\hat{\boldsymbol{n}}) = \int_{0}^{\chi_{S}} d\chi \frac{\chi_{S} - \chi}{\chi_{S} \chi} \left[\Upsilon^{:a}_{:a} - \frac{d}{d\chi} \left(\chi \Omega^{a}_{:a} \right) \right], \qquad (4.44)$$

$$\varpi^{:a}{}_{:a}(\hat{\boldsymbol{n}}) = \Delta^{a}{}_{:b}(\hat{\boldsymbol{n}})\epsilon^{b}{}_{a} = -\int_{0}^{\chi_{s}} d\chi \frac{\chi_{s} - \chi}{\chi_{s}\chi} \left[\frac{d}{d\chi} \left(\chi \Omega^{a}{}_{:b}\epsilon^{b}{}_{a} \right) \right]. \tag{4.45}$$

According to the above relation, we can see that the vector and tensor perturbations induce not only the gradient-mode but also curl-mode. On the other hand, the scalar perturbation does not contribute the curl-mode.

The spin-0 component on the two-sphere such as the scalar ϕ and pseudo-scalar ϖ potentials can be expanded by the spherical harmonics as

$$x(\hat{\boldsymbol{n}}) = \sum_{\ell m} x_{\ell m} Y_{\ell m}(\hat{\boldsymbol{n}}) , \qquad (4.46)$$

where $x = \phi$, ϖ . The angular power spectrum of these potentials is defined as

$$C_{\ell}^{x_1 x_2} = \frac{1}{2\ell + 1} \sum_{m = -\ell}^{\ell} \left\langle x_{1,\ell m}^* x_{2,\ell m} \right\rangle. \tag{4.47}$$

Next, we rewrite Eqs. (4.44) and (4.45) in terms of the polarization basis and spin-raising/lowering operators defined in Eqs. (4.31) and (4.32) as

$$\partial \bar{\partial} \phi = \int_0^{\chi_S} d\chi \frac{\chi_S - \chi}{\chi_S \chi} \left[\partial \bar{\partial} \Upsilon + \frac{1}{2} \frac{d}{d\chi} \left\{ \chi \left(\bar{\partial}_{+1} \Omega + \partial_{-1} \Omega \right) \right\} \right], \tag{4.48}$$

$$\partial \bar{\partial} \varpi = -\frac{i}{2} \int_0^{\chi_S} d\chi \frac{\chi_S - \chi}{\chi_S \chi} \frac{d}{d\chi} \left[\chi \left(\bar{\partial}_{+1} \Omega - \partial_{-1} \Omega \right) \right] , \qquad (4.49)$$

where $_s\Omega = \Omega_a e_s^a$. In order to derive the above equation, we used Eqs. (4.28) and (4.30).

We decompose the Υ and Ω_a into the scalar, vector, and tensor modes in Fourier space as

$$\Upsilon(\eta_0 - \chi, \chi \hat{\mathbf{n}}) = \int \frac{\mathrm{d}^3 \mathbf{k}}{(2\pi)^3} \sum_{m=-2}^{+2} \Upsilon^{(m)}(\eta_0 - \chi, \mathbf{k})_0 G_{|m|,m}(\hat{\mathbf{n}}) e^{-i\mathbf{k}\cdot\mathbf{x}} , \qquad (4.50)$$

$${}_{s}\Omega(\eta_{0}-\chi,\chi\hat{\boldsymbol{n}}) = \int \frac{\mathrm{d}^{3}\boldsymbol{k}}{(2\pi)^{3}} \sum_{m=-2}^{+2} {}_{s}\Omega^{(m)}(\eta_{0}-\chi,\boldsymbol{k})_{s}G_{|m|,m}(\hat{\boldsymbol{n}})e^{-i\boldsymbol{k}\cdot\boldsymbol{x}}, \quad (4.51)$$

where we define ${}_{s}G_{\ell,m}(\hat{\boldsymbol{n}})$ as

$$_{s}G_{\ell,m}(\hat{\boldsymbol{n}}) \equiv (-i)^{\ell} \sqrt{\frac{4\pi}{2\ell+1}} {}_{s}Y_{\ell,m}(\hat{\boldsymbol{n}}) .$$
 (4.52)

Moreover, we also define

$$\Upsilon^{(0)} = -(\Psi + \Phi) , \quad \Upsilon^{(\lambda)} = -\sigma_{\lambda} , \quad \Upsilon^{(\sigma)} = \frac{1}{2} h_{\sigma} ,$$
(4.53)

and

$$_{s}\Omega^{(0)} = 0 , \quad _{s}\Omega^{(\lambda)} = \sqrt{2}s\sigma_{\lambda} , \quad _{s}\Omega^{(\sigma)} = -\sqrt{\frac{3}{2}}sh_{\sigma} .$$
 (4.54)

To proceed the calculation, we expand the left-hand side of Eqs. (4.44) and (4.45) by the basis functions as

$$x = \int \frac{\mathrm{d}^3 \mathbf{k}}{(2\pi)^3} \sum_{\ell=0}^{\infty} \sum_{m=-2}^{+2} \hat{x}_{\ell}^{(m)} {}_{0} G_{\ell,m} e^{-i\mathbf{k}\cdot\mathbf{x}} \bigg|_{\mathbf{r}=\mathbf{0}} . \tag{4.55}$$

Note that $m \ge 3$ have zero only due to the orthogonality of the basis function. Moreover, substituting Eqs. (4.50), (4.51), and (4.55) into Eqs. (4.48) and (4.49), we can derive

$$\frac{\hat{\phi}_{\ell}^{(m)}}{2\ell+1} = \int_{0}^{\chi_{S}} d\chi \frac{\chi_{S} - \chi}{\chi_{S} \chi} \left[\Upsilon^{(m)}(\eta_{0} - \chi, \boldsymbol{k})_{0} \epsilon_{\ell}^{(|m|,m)}(k\chi) + \frac{1}{\sqrt{\ell(\ell+1)}} \frac{d}{d\chi} \left\{ \chi \left({}_{+1} \Omega^{(m)}(\eta_{0} - \chi, \boldsymbol{k})_{1} \epsilon_{\ell}^{(|m|,m)}(k\chi) \right) \right\} \right], \qquad (4.56)$$

$$\frac{\hat{\varpi}_{\ell}^{(m)}}{2\ell+1} = \frac{1}{\sqrt{\ell(\ell+1)}} \int_{0}^{\chi_{S}} d\chi \frac{\chi_{S} - \chi}{\chi_{S} \chi} \frac{d}{d\chi} \left[\chi \left\{ {}_{+1} \Omega^{(m)}(\eta_{0} - \chi, \boldsymbol{k})_{1} \beta_{\ell}^{(|m|,m)}(k\chi) \right\} \right], \qquad (4.57)$$

where we use the relation $_{+1}\Omega^{(m)}=(-1)_{-1}\Omega^{(m)}$. The radial functions $_s\epsilon_L^{(\ell,m)}(x)$ and $_s\beta_L^{(\ell,m)}(x)$ are defined by using the spherical Bessel function $j_\ell(x)$ as

$$\left[{}_{s}\epsilon_{L}^{(\ell,m)}(x) + i \operatorname{sgn}(s)_{s} \beta_{L}^{(\ell,m)}(x) \right] \\
= \sum_{j} (-i)^{\ell-L+j} (2j+1) (-1)^{s+m} \begin{pmatrix} \ell & j & L \\ m & 0 & -m \end{pmatrix} \begin{pmatrix} \ell & j & L \\ -s & 0 & s \end{pmatrix} j_{j}(x) .$$
(4.58)

Note that the radial functions are the real functions and do not depend on the signature of *s*.

Finally, we rewrite Eqs. (4.56) and (4.57) as

$$\frac{\hat{x}_{\ell}^{(m)}}{2\ell+1} = \int_{0}^{\chi_{S}} k d\chi \left[\xi^{(m)} (\eta_{0} - \chi, \mathbf{k}) \mathcal{T}_{x,\ell}^{(m)}(k, \chi) \right], \tag{4.59}$$

where we define $\xi^{(m)}$ and $\mathcal{T}_{r \ell}^{(m)}$ as

$$\xi^{(0)} = -\frac{1}{2} (\Psi + \Phi) , \quad \xi^{(\lambda)} = -\sigma_{\lambda} , \quad \xi^{(\sigma)} = \sqrt{3} h_{\sigma} ,$$
 (4.60)

and

$$\mathcal{T}_{\phi,\ell}^{(0)} = 2\frac{\chi_S - \chi}{\chi_S} \frac{1}{k\chi} {}_0 \epsilon_{\ell}^{(0,0)}(k\chi) , \qquad (4.61)$$

$$\mathcal{T}_{\phi,\ell}^{(\lambda)} = \frac{1}{k\chi} \left[\frac{\chi_S - \chi}{\chi_S} {}_0 \epsilon_\ell^{(1,\lambda)}(k\chi) - \sqrt{2 \frac{(\ell-1)!}{(\ell+1)!}} {}_1 \epsilon_\ell^{(1,\lambda)}(k\chi) \right], \tag{4.62}$$

$$\mathcal{T}_{\phi,\ell}^{(\sigma)} = \frac{1}{2k\chi} \left[\frac{1}{\sqrt{3}} \frac{\chi_S - \chi}{\chi_S} {}_0 \epsilon_\ell^{(2,\sigma)}(k\chi) - \sqrt{2 \frac{(\ell-1)!}{(\ell+1)!}} {}_1 \epsilon_\ell^{(2,\sigma)}(k\chi) \right]$$

$$+\frac{1}{10\sqrt{3}}\delta_{\ell,2}\delta_{\mathcal{D}}(k\chi), \qquad (4.63)$$

$$\mathcal{T}_{\varpi,\ell}^{(0)} = 0 \;, \tag{4.64}$$

$$\mathcal{T}_{\varpi,\ell}^{(\lambda)} = -\sqrt{2\frac{(\ell-1)!}{(\ell+1)!}} \frac{1}{k\chi} {}_{1}\beta_{\ell}^{(1,\lambda)}(k\chi) , \qquad (4.65)$$

$$\mathcal{T}_{\varpi,\ell}^{(\sigma)} = -\sqrt{\frac{1}{2} \frac{(\ell-1)!}{(\ell+1)!}} \frac{1}{k\chi} {}_{1}\beta_{\ell}^{(2,\sigma)}(k\chi) , \qquad (4.66)$$

where we used the asymptotic behavior of the spherical Bessel function, namely,

$$j_{\ell}(x) \to \frac{x^{\ell}}{(2\ell+1)!!} \quad (x \to 0) \ .$$
 (4.67)

The unequal-time correlator is needed to proceed the formulation of the angular power spectrum, and which is defined as

$$\left\langle \xi^{*(m)}(\eta_0 - \chi, \mathbf{k}) \xi^{(m)}(\eta_0 - \chi', \mathbf{k'}) \right\rangle = (2\pi)^3 \delta_{m,m'} \delta_{\mathrm{D}}^3(\mathbf{k} - \mathbf{k'}) P_{|m|}(\mathbf{k}; \eta_0 - \chi, \eta_0 - \chi') ,$$
(4.68)

furthermore the angular power spectrum can be calculated as

$$\left\langle \hat{x}_{\ell}^{*(m)}(\mathbf{k})\hat{x}_{\ell}^{\prime(m')}(\mathbf{k'})\right\rangle = (2\pi)^{3}\delta_{m,m'}\delta_{D}^{3}(\mathbf{k} - \mathbf{k'})(2\ell + 1)^{2}\mathcal{M}_{\ell}^{xx'(m)}(k), \qquad (4.69)$$

where

$$\mathcal{M}_{\ell}^{xx'(m)}(k) = \int_{0}^{\chi_{S}} k d\chi \int_{0}^{\chi_{S}} k d\chi' \mathcal{T}_{x,\ell}^{(m)}(k,\chi) \mathcal{T}_{x,\ell}^{(m)}(k,\chi') P_{|m|}(k;\eta_{0}-\chi,\eta_{0}-\chi') .$$
(4.70)

As a result, we finally relate the $C_\ell^{xx'}$ and $\mathcal{M}_\ell^{xx'(m)}$ as

$$C_{\ell}^{xx'} = \frac{2}{\pi} \int_0^{\infty} dk k^2 \sum_{m=-2}^2 \mathcal{M}_{\ell}^{xx'(m)}(k)$$
 (4.71)

4.2.3 Cosmic Shear

Contrary to the formulation of the CMB lensing, to derive the full-sky formulae for the cosmic shear, we need to trace the light bundle. This is because the cosmic shear measurements observes the shape of each galaxy. The light bundle obeys the geodesic deviation equation which describes the evolution of the Jacobi map. Before moving the derivation of the Jacobi map, we comment about the difference between the derivation of deflection angle and the Jacobi map. The deflection angle is, at first, assumed that the metric perturbation and we solve the geodesic equation in the perturbed universe (4.35). Then we can derive the light path in the perturbed universe (4.41). On the other hand, the derivation of Jacobi map is needed to two null geodesics without any assumptions about the metric perturbations. We only need to the deviation vector (or connection vector) equation in the general universe.

First, we derive the geodesic derivation equation on the two-sphere. This equation is quite different from Eq. (4.35) as we mentioned before. Without any assumptions for the space-time, the two null geodesics x^{μ} and $x^{\mu} + \xi^{\mu}$ can be written as

$$\frac{\mathrm{d}^2 x^{\mu}}{\mathrm{d}\chi^2} + \Gamma^{\mu}{}_{\alpha\beta}(x) \frac{\mathrm{d}x^{\alpha}}{\mathrm{d}\chi} \frac{\mathrm{d}x^{\beta}}{\mathrm{d}\chi} = 0 , \qquad (4.72)$$

$$\frac{\mathrm{d}^2 \left(x^{\mu} + \xi^{\mu}\right)}{\mathrm{d}\chi^2} + \Gamma^{\mu}{}_{\alpha\beta}(x + \xi) \frac{\mathrm{d}\left(x^{\alpha} + \xi^{\alpha}\right)}{\mathrm{d}\chi} \frac{\mathrm{d}\left(x^{\beta} + \xi^{\beta}\right)}{\mathrm{d}\chi} = 0, \tag{4.73}$$

where we do not assume any space-time in the above equation. We can derive the geodesic derivation equation by subtracting the above equation as

$$\frac{D^2 \xi^{\mu}}{D \chi^2} = \tilde{\mathcal{T}}^{\mu}{}_{\nu} \xi^{\nu} , \qquad (4.74)$$

where we define the absolute derivative and the symmetric optical tidal matrix as

$$\frac{D\xi^{\mu}}{D\chi} \equiv \frac{\mathrm{d}x^{\alpha}}{\mathrm{d}\chi} \xi^{\mu}_{;\beta} = \frac{\mathrm{d}\xi^{\mu}}{\mathrm{d}\chi} + \Gamma^{\mu}_{\alpha\beta} \xi^{\alpha} \frac{\mathrm{d}x^{\beta}}{\mathrm{d}\chi} , \qquad (4.75)$$

$$\tilde{T}^{\mu}{}_{\nu} \equiv -\tilde{R}^{\mu}{}_{\alpha\nu\beta} \frac{\mathrm{d}x^{\alpha}}{\mathrm{d}\chi} \frac{\mathrm{d}x^{\beta}}{\mathrm{d}\chi} \ . \tag{4.76}$$

Note that the basis vectors defined in Eq. (4.8) behaves as a constant respect to the derivative $D/D\chi$, namely,

$$\frac{D}{D\chi}e_a^\mu = 0. (4.77)$$

We can project the geodesic deviation equation onto the two-sphere by using the basis e_a^{μ} as

$$\frac{\mathrm{d}^2 \xi^a}{\mathrm{d}\chi^2} = \tilde{\mathcal{T}}^a{}_b \xi^a \,, \tag{4.78}$$

where we define $\tilde{T}^a{}_b$ as

$$\tilde{\mathcal{T}}^{a}{}_{b} = -\tilde{R}_{\mu\alpha\nu\beta} \frac{\mathrm{d}x^{\mu}}{\mathrm{d}\chi} \frac{\mathrm{d}x^{\nu}}{\mathrm{d}\chi} e^{\alpha a} e^{\beta}_{b} , \qquad (4.79)$$

where we use $\Gamma^{i}_{jk}(x) = 0$ by choosing x^{μ} as the unperturbed space-time, namely, $D/D\chi = d/d\chi$.

Next we introduce the initial conditions at the observer, $\xi^a|_0 = 0$ and $d\xi^a/d\chi|_0 = \delta\theta^a_0$, and introduce the Jacobi map as

$$\xi^a = \tilde{\mathcal{D}}^a{}_b \delta \theta_0^b \,, \tag{4.80}$$

and the Jacobi map is satisfied the following equation:

$$\frac{\mathrm{d}^2 \tilde{\mathcal{D}}^a{}_b}{\mathrm{d}\chi^2} = \tilde{T}^a{}_c \tilde{\mathcal{D}}^c{}_b , \qquad (4.81)$$

with the initial condition for the Jacobi map as $\tilde{\mathcal{D}}^a{}_b\Big|_0 = 0$ and $\mathrm{d}\tilde{\mathcal{D}}^a{}_b/\mathrm{d}\chi\Big|_0 = \delta^a{}_b$. When we expand the $\tilde{\mathcal{D}}^a{}_b = \mathcal{D}^a{}_b + \delta\mathcal{D}^a{}_b$ and $\tilde{\mathcal{T}}^a{}_b = \delta\mathcal{T}^a{}_b$, the solution can be written as

$$\frac{\tilde{\mathcal{D}}^a{}_b}{\chi_S} = \delta^a{}_b + \int_0^{\chi_S} d\chi \frac{(\chi_S - \chi)\chi}{\chi_S} \delta T^a{}_b (\eta_0 - \chi, \chi \hat{\boldsymbol{n}}) , \qquad (4.82)$$

where we used the Born approximation. The explicit form of the symmetric optical tidal matrix $\delta \mathcal{T}^a{}_b$ is written as

$$\chi^{2}\delta\mathcal{T}_{ab} = \Upsilon_{:ab} - \frac{\mathrm{d}}{\mathrm{d}\chi}\left(\chi\Omega_{(a:b)}\right) + \frac{1}{2}\chi\frac{\mathrm{d}^{2}}{\mathrm{d}\chi^{2}}\left(\chi h_{ab}\right) + \chi\omega_{ab}\left[\partial_{\chi}\Upsilon - \frac{\mathrm{d}}{\mathrm{d}\chi}\left(\Omega_{i}e_{\chi}^{i}\right) - \chi\frac{\mathrm{d}^{2}}{\mathrm{d}\chi^{2}}\Phi\right],$$

$$(4.83)$$

where $h_{ab} \equiv h_{ij} e_a^i e_b^j$ and $\Omega_a = \Omega_i e_a^i$.

From here, we decompose the Jacobi matrix into the spin-0 and spin-2 variables as

$${}_{0}\tilde{\mathcal{D}} = \tilde{\mathcal{D}}_{ab}e^{a}_{+}e^{b}_{-}, \quad {}_{\pm 2}\tilde{\mathcal{D}} = \tilde{\mathcal{D}}_{ab}e^{a}_{+}e^{b}_{+}, \tag{4.84}$$

furthermore, we define the reduced shear by the Jacobi map as

$$g = -\frac{+2\tilde{\mathcal{D}}}{0\tilde{\mathcal{D}}}, \quad g^* = -\frac{-2\tilde{\mathcal{D}}}{0\tilde{\mathcal{D}}}.$$
 (4.85)

Finally, at the lowest order, the reduced shear can be written as

$$g = -\frac{1}{2} \int_0^{\chi_s} d\chi \frac{\chi_s - \chi}{\chi_s \chi} \left[\Upsilon_{:ab} - \frac{d}{d\chi} \left(\chi \Omega_{a:b} \right) \right] e_+^a e_+^b - \frac{1}{4} \left[h_{ab} e_+^a e_+^b \right]_0^{\chi_s} , \quad (4.86)$$

$$g^* = -\frac{1}{2} \int_0^{\chi_s} d\chi \frac{\chi_s - \chi}{\chi_s \chi} \left[\Upsilon_{:ab} - \frac{d}{d\chi} \left(\chi \Omega_{a:b} \right) \right] e_-^a e_-^b - \frac{1}{4} \left[h_{ab} e_-^a e_-^b \right]_0^{\chi_s} . \quad (4.87)$$

Hereafter, we introduce the E and B modes for the cosmic shear and give the full sky formalism. At first, we expand the reduced shears, which are the spin-2 variables and we expand by the spin-2 spherical harmonics as

$$g(\hat{\mathbf{n}}) = \sum_{\ell,m} (E_{\ell m} + i B_{\ell m})_{+2} Y_{\ell m}(\hat{\mathbf{n}}), \qquad (4.88)$$

$$g^*(\hat{\mathbf{n}}) = \sum_{\ell,m} (E_{\ell m} - i B_{\ell m})_{-2} Y_{\ell m}(\hat{\mathbf{n}}) , \qquad (4.89)$$

where $E_{\ell m}$ and $B_{\ell m}$ have the different parity, namely $(-1)^{\ell}$ and $(-1)^{\ell+1}$, respectively. The angular power spectrum of these modes are defined as

$$C_{\ell}^{X_1 X_2} = \frac{1}{2\ell + 1} \sum_{m = -\ell}^{\ell} \langle X_{1,\ell m}^* X_{2,\ell m} \rangle.$$
 (4.90)

Next, we rewrite Eqs. (4.86) and (4.87) in terms of the polarization basis and spin-raising and lowering operators as

$$g = -\frac{1}{2} \int_0^{\chi s} d\chi \frac{\chi_s - \chi}{\chi_s \chi} \left[\partial^2 \Upsilon + \frac{d}{d\chi} \left\{ \chi \left(\partial_{+1} \Omega \right) \right\} \right] - \frac{1}{4} \left[h_{ab} e_+^a e_+^b \right]_0^{\chi_s} , \quad (4.91)$$

$$g^* = -\frac{1}{2} \int_0^{\chi_S} \mathrm{d}\chi \frac{\chi_S - \chi}{\chi_S \chi} \left[\bar{\vartheta}^2 \Upsilon + \frac{\mathrm{d}}{\mathrm{d}\chi} \left\{ \chi \left(\bar{\vartheta}_{-1} \Omega \right) \right\} \right] - \frac{1}{4} \left[h_{ab} e_-^a e_-^b \right]_0^{\chi_S} , \quad (4.92)$$

where we used Eqs. (4.28) and (4.29). To proceed the calculation, we expand the left-hand side of Eqs. (4.91) and (4.92) by the basis functions as

$$g = -\int \frac{\mathrm{d}^3 \mathbf{k}}{(2\pi)^3} \sum_{\ell=2}^{\infty} \sum_{m=-2}^{+2} \left(\hat{E}_{\ell}^{(m)} + i \, \hat{B}_{\ell}^{(m)} \right)_{+2} G_{\ell,m} e^{-i\mathbf{k}\cdot\mathbf{x}} \bigg|_{\mathbf{x}=\mathbf{0}} , \qquad (4.93)$$

$$g^* = -\int \frac{\mathrm{d}^3 \mathbf{k}}{(2\pi)^3} \sum_{\ell=2}^{\infty} \sum_{m=-2}^{+2} \left(\hat{E}_{\ell}^{(m)} - i \, \hat{B}_{\ell}^{(m)} \right)_{-2} G_{\ell,m} e^{-i\mathbf{k}\cdot\mathbf{x}} \bigg|_{\mathbf{r}=\mathbf{0}} . \tag{4.94}$$

Furthermore, the last term appeared in Eqs. (4.91) and (4.92) is given by

$$e_{\pm}^{a}e_{\pm}^{b}h_{ab}(\eta_{0}-\chi,\chi\hat{\boldsymbol{n}}) = \int \frac{\mathrm{d}^{3}\boldsymbol{k}}{(2\pi)^{3}} \sum_{m=\sigma} \sqrt{6}h^{(m)}(\eta_{0}-\chi,\boldsymbol{k})_{\pm 2}G_{2,m}(\hat{\boldsymbol{n}})e^{-i\boldsymbol{k}\cdot\boldsymbol{x}} . \tag{4.95}$$

And substituting Eqs. (4.50), (4.51), (4.93), (4.94) and (4.95) into Eqs. (4.91) and (4.92), we can derive

$$\frac{\hat{E}_{\ell}^{(m)}}{2\ell+1} = \frac{1}{2} \sqrt{\frac{(\ell+2)!}{(\ell-2)!}} \int_{0}^{\chi_{S}} d\chi \frac{\chi_{S} - \chi}{\chi_{S}\chi} \left[\Upsilon^{(m)}(\eta_{0} - \chi, \mathbf{k})_{0} \epsilon_{\ell}^{(|m|,m)}(k\chi) \right. \\
+ \sqrt{\frac{1}{\ell(\ell+1)}} \frac{d}{d\chi} \left\{ \chi \left({}_{+1} \Omega^{(m)}(\eta_{0} - \chi, \mathbf{k}) \right)_{1} \epsilon_{\ell}^{(|m|,m)}(k\chi) \right\} \right] \\
+ \frac{\sqrt{6}}{4} \delta_{m,\pm 2} \left[h^{(m)}(\eta_{0} - \chi, \mathbf{k})_{2} \epsilon_{\ell}^{(2,m)} \right]_{0}^{\chi_{S}} , \qquad (4.96) \\
\frac{\hat{B}_{\ell}^{(m)}}{2\ell+1} = \frac{1}{2} \sqrt{\frac{(\ell+2)!(\ell-1)!}{(\ell-2)!(\ell+1)!}} \int_{0}^{\chi_{S}} d\chi \frac{\chi_{S} - \chi}{\chi_{S}\chi} \frac{d}{d\chi} \left[\chi \left({}_{+1} \Omega^{(m)}(\eta_{0} - \chi, \mathbf{k})_{1} \beta_{\ell}^{(|m|,m)}(k\chi) \right) \right] \\
+ \frac{\sqrt{6}}{4} \delta_{m,\pm 2} \left[h^{(m)}(\eta_{0} - \chi, \mathbf{k})_{2} \beta_{\ell}^{(2,m)} \right]_{0}^{\chi_{S}} . \qquad (4.97)$$

Finally, we summarize Eqs. (4.96) and (4.97) as

$$\frac{\hat{X}_{\ell}^{(m)}}{2\ell+1} = \int_{0}^{\chi_{s}} k d\chi \left[\xi^{(m)} (\eta_{0} - \chi, \mathbf{k}) \mathcal{S}_{X,\ell}^{(m)}(k, \chi) \right]. \tag{4.98}$$

Here, we take into account for the galaxy observations, namely, the imaging survey, which cannot divide the redshift accurately. Therefore, we usually assume the distribution of galaxies. The number distribution of galaxies $N(\chi)/N_{\rm g}$, where $N_{\rm g}$ is defined as

$$N_{\rm g} \equiv \int_0^\infty \mathrm{d}\chi N(\chi) \ . \tag{4.99}$$

Furthermore, we sum, in other words integrate, χ_S for each source of lensing. From this procedure, we redefine the E- and B-modes as

$$\hat{X}_{\ell}^{(m)} \to \hat{X}_{\ell}^{(m)} = \int_0^\infty d\chi_S \hat{X}_{\ell}^{(m)} \frac{N(\chi_S)}{N_g} , \qquad (4.100)$$

and from Eq. (4.98), we exchange the order of the integral calculations as

$$\int_0^\infty d\chi_S \int_0^{\chi_S} d\chi = \int_0^\infty d\chi \int_{\chi}^\infty d\chi_S.$$
 (4.101)

Practically, the source term is converted as

$$S_{X,\ell}^{(m)} \to S_{X,\ell}^{(m)} = \int_{Y}^{\infty} d\chi_S S_{X,\ell}^{(m)} \frac{N(\chi_S)}{N_{\sigma}} .$$
 (4.102)

We assume a distribution of galaxies $N(\chi)$, which can usually be taken to be (see, e.g., Ref. [34])

coverage f_{SKY} , the mean redshift z_m , and the number of the galaxies per square are infinite ivg			
	$f_{ m sky}$	$z_{\rm m}$	$N_{\rm g}$ [arcmin ⁻²]
DES	0.125	0.5	12
HSC	0.05	1.0	35
SKA	0.75	1.6	10
LSST	0.5	1.5	100

Table 4.1 The experimental specifications of DES, HSC, SKA, and LSST. It is shown that the sky coverage f_{sky} , the mean redshift z_m , and the number of the galaxies per square arc minute N_0

$$N(\chi_{\rm S}) d\chi_{\rm S} = N_{\rm g} \frac{3}{2} \frac{z_{\rm S}^2}{(0.64z_{\rm m})^3} \exp \left[-\left(\frac{z_{\rm S}}{0.64z_{\rm m}}\right)^{3/2} \right] dz_{\rm S} ,$$
 (4.103)

where $z_{\rm m}$ is the mean redshift, and the number of galaxies per square arc-minute $N_{\rm g}$. In this section, we focus on four survey designs: DES [15], HSC [16], SKA [17], and LSST [18]. The experimental specifications of each survey design are summarized in Table 4.1.

Then the taking into account for the observation, Eq. (4.98) can be rewritten as

$$\frac{\hat{X}_{\ell}^{(m)}}{2\ell+1} = \int_{0}^{\infty} k d\chi \left[\xi^{(m)} (\eta_0 - \chi, \mathbf{k}) \mathcal{S}_{X,\ell}^{(m)}(k, \chi) \right], \qquad (4.104)$$

where $\xi^{(m)}$ are defined in Eq. (4.60) and

$$S_{E,\ell}^{(0)} = \sqrt{\frac{(\ell-2)!}{(\ell+2)!}} \frac{1}{k\chi} \int_{\chi}^{\infty} d\chi_S \frac{\chi_S - \chi}{\chi_S} \frac{N(\chi_S)}{N_g} {}_0 \epsilon_{\ell}^{(0,0)}(k\chi) , \qquad (4.105)$$

$$S_{E,\ell}^{(\lambda)} = \frac{1}{2} \sqrt{\frac{(\ell-2)!}{(\ell+2)!}} \frac{1}{k\chi} \int_{\chi}^{\infty} d\chi_S \frac{N(\chi_S)}{N_g} \left[\frac{\chi_S - \chi}{\chi_S} {}_{0} \epsilon_{\ell}^{(1,\lambda)}(k\chi) - \sqrt{2 \frac{(\ell-1)!}{(\ell+1)!}} {}_{1} \epsilon_{\ell}^{(1,\lambda)}(k\chi) \right], \tag{4.106}$$

$$S_{E,\ell}^{(\sigma)} = \frac{1}{4} \sqrt{\frac{(\ell-2)!}{(\ell+2)!}} \frac{1}{k\chi} \int_{\chi}^{\infty} d\chi_{S} \frac{N(\chi_{S})}{N_{g}} \left[\frac{1}{\sqrt{3}} \frac{\chi_{S} - \chi}{\chi_{S}} o \epsilon_{\ell}^{(2,\sigma)}(k\chi) - \sqrt{2 \frac{(\ell-1)!}{(\ell+1)!}} i \epsilon_{\ell}^{(2,\sigma)}(k\chi) \right] + \frac{1}{10\sqrt{2}} \delta_{\ell,2} \delta_{D}(k\chi) + \frac{1}{2\sqrt{2}} \frac{N(\chi)}{kN_{g}} 2 \epsilon_{\ell}^{(2,\sigma)}(k\chi) , \qquad (4.107)$$

$$S_{R\ell}^{(0)} = 0, (4.108)$$

$$S_{B,\ell}^{(\lambda)} = -\sqrt{\frac{1}{2} \frac{(\ell+2)!(\ell-1)!}{(\ell-2)!(\ell+1)!}} \frac{1}{k\chi} \int_{\chi}^{\infty} d\chi_S \frac{N(\chi_S)}{N_g} {}_1 \beta_{\ell}^{(1,\lambda)}(k\chi) , \qquad (4.109)$$

$$S_{B,\ell}^{(\sigma)} = -\frac{1}{2} \sqrt{\frac{1}{2} \frac{(\ell+2)!(\ell-1)!}{(\ell-2)!(\ell+1)!}} \frac{1}{k\chi} \int_{\chi}^{\infty} d\chi_S \frac{N(\chi_S)}{N_g} {}_{1} \beta_{\ell}^{(2,\sigma)}(k\chi) + \frac{1}{2\sqrt{2}} \frac{N(\chi)}{N_g} {}_{2} \beta_{\ell}^{(2,\sigma)}(k\chi) .$$

$$(4.110)$$

Finally, the angular power spectrum of E- and B-modes can be derived as

$$C_{\ell}^{XX'} = \frac{2}{\pi} \int_0^{\infty} \mathrm{d}k k^2 \sum_{m=-2}^2 \mathcal{M}_{\ell}^{XX'(m)}(k) ,$$
 (4.111)

where

$$\mathcal{M}_{\ell}^{XX'(m)}(k) = \int_{0}^{\infty} k d\chi \int_{0}^{\infty} k d\chi' \mathcal{S}_{X,\ell}^{(m)}(k,\chi) \mathcal{S}_{X,\ell}^{(m)}(k,\chi') P_{|m|}(k;\eta_{0}-\chi,\eta_{0}-\chi') .$$
(4.112)

In the next section, we discuss the possible source of the curl and B modes including not only the vector mode but also the tensor mode.

4.3 Models: Parity-Odd Signals

In this subsection, we study possible source to generate the curl and B modes. The vector and tensor modes induce these modes. We focus on three models: the second-order vector mode, second-order tensor mode, and primordial gravitational waves with the tensor-to-scalar ratio r = 0.1.

4.3.1 Second-Order Vector Mode—Numerical Descriptions

Before evaluating the effect on the weak gravitational lensing, in this subsection we show the resultant second-order vector mode by performing a fully numerical calculation and we then discuss the feature of the power spectrum under some approximations. To do this, let us define the unequal-time power spectrum for the vector mode as

$$\langle \sigma_{\lambda}^{*}(\eta, \mathbf{k}) \sigma_{\lambda'}(\eta', \mathbf{k}') \rangle = (2\pi)^{3} \delta_{\lambda \lambda'} \delta_{D}^{3} (\mathbf{k} - \mathbf{k}') P_{\sigma}(\eta, \eta', \mathbf{k}) , \qquad (4.113)$$

where $\langle \cdots \rangle$ is the ensemble average. We derive an expression for the power spectrum by solving the evolution equation. Equations (2.194) and (2.195) is easily integrated as

$$\sigma_{\lambda}^{(2)}(\eta, \mathbf{k}) = \frac{1}{a^2(\eta)} \int_0^{\eta} d\eta' \left[a^2(\eta') \mathcal{S}_{\lambda}^{(2)}(\eta', \mathbf{k}) \right]. \tag{4.114}$$

Hence we have

$$\left\langle \sigma_{\lambda}^{(2)}(\eta, \mathbf{k}) \sigma_{\lambda'}^{(2)*}(\eta', \mathbf{k}') \right\rangle = \frac{1}{a^2(\eta) a^2(\eta')} \int_0^{\eta} d\eta_1 \int_0^{\eta'} d\eta_2 a^2(\eta_1) a^2(\eta_2) \left\langle \mathcal{S}_{\lambda}^{(2)}(\eta_1, \mathbf{k}) \mathcal{S}_{\lambda'}^{(2)*}(\eta_2, \mathbf{k}') \right\rangle. \tag{4.115}$$

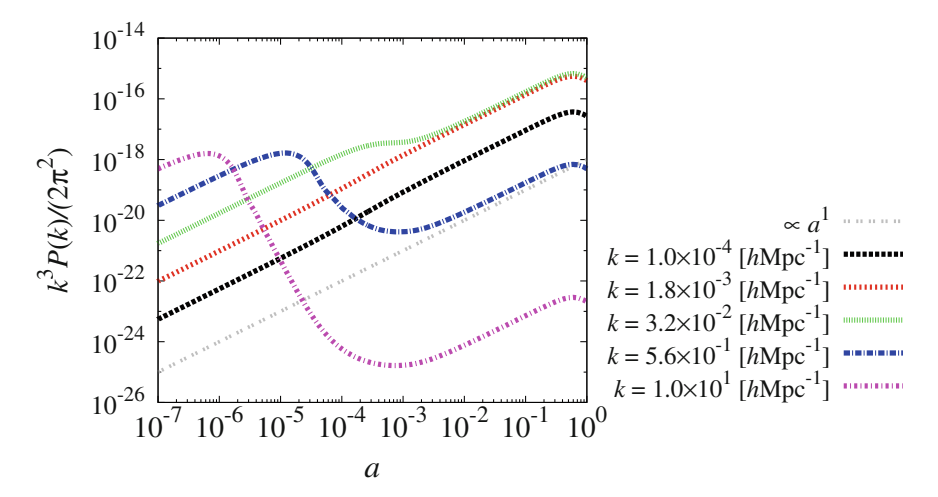


Fig. 4.1 The evolution of the second-order vector metric perturbation for scales from $k = 10^{-4} h \text{Mpc}^{-1}$ to $10^1 h \text{Mpc}^{-1}$ as indicated in the figures

Once we obtain the brightness functions for photons and neutrinos by solving the Boltzmann equation (2.169) and substitute the first-order results for the scalar metric potentials into Eqs. (2.194) and (2.195), we can obtain the power spectrum for the second-order vector mode though Eq. (4.115). We now solve the evolution equations for the vector mode by performing a fully numerical calculation. Figure 4.1 shows the equal-time power spectrum for the vector mode induced by the second-order source terms.

For illustrative purposes to show the dependence on the wavenumber, we adopt the wavenumbers as from $k=10^{-4}\ h{\rm Mpc^{-1}}$ to $10^1\ h{\rm Mpc^{-1}}$. The resultant power spectrum for the second-order vector mode during the radiation-dominated era seems to grow as $\propto a$ on super-horizon scales, while it decays on small scales after it enters the horizon scale. This is because the source of the second-order vector mode, namely the scalar potential, decays during the radiation-dominated era on sub-horizon scales. In contrast, during the matter-dominated era it always evolves as $\propto a(\eta)$ for those wavenumbers. Therefore the second-order vector modes that enter the horizon after the matter-radiation equality time do not undergo the above suppression. In Fig. 4.2, we plot the dimensionless power spectrum with various values of the redshift. We find that it scales as k^1 on large scales and k^{-4} on small scales and its peak would be determined by the time of the matter-radiation equality.

We study the analytical description of the power spectrum of second-order vector modes in the next subsection.

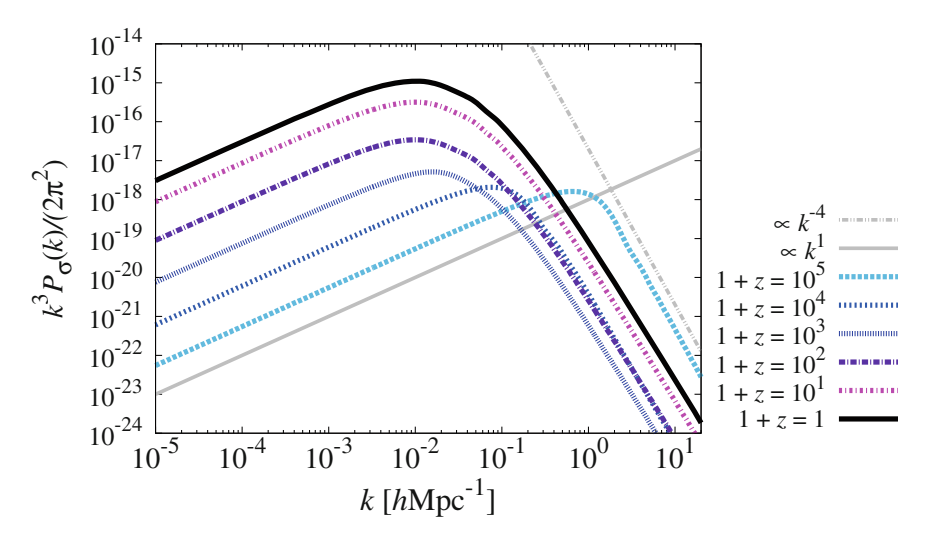


Fig. 4.2 The spectra of the second-order vector metric perturbation for redshifts from $1+z=10^5$ to 1, as indicated in the figure. Before matter-radiation equality, the feature of the second-order vector metric perturbation was determined by the horizon scale at each time. On the other hand, after matter-radiation equality, it was determined by the matter-radiation equality scale, namely, $k_{\rm eq} \approx 10^{-2} \ h{\rm Mpc}^{-1}$. We can see that the evolutions are same for all scales after matter-radiation equality $1+z_{\rm eq} \lesssim 3.3 \times 10^3$

4.3.2 Second-Order Vector Mode—Analytical Descriptions

In this subsection, we investigate the feature of the power spectrum for the second-order vector mode analytically. It is difficult to estimate the second-order vector mode analytically including the purely second-order quadrupole moments for photons and neutrinos. However, if we assume that the purely second-order quadrupole moments for photons and neutrinos, $\Delta_{2,\lambda}^{(2)}$ and $\mathcal{N}_{2,\lambda}^{(2)}$, give negligible contributions, the second-order vector metric perturbations are sourced only from the convolution of the first-order scalar metric potentials. Indeed, numerical computations reveal that the corrections of the purely second-order quadrupole moments to the vector mode amount to only about $\lesssim O(10^{-3})\%$ during the matter-dominated era, whereas, the quadrupole moments contribute several tens percent to the vector mode during the radiation-dominated era. Even in the radiation-dominated era, the scalar potentials are still dominant in Eq. (2.195). In this section, we focus on the weak lensing signals, which are mainly determined by the contributions after the matter-radiation equality, in which regime the quadrupole moments contribute at most $O(10^{-3})\%$. Therefore, it is sufficient to consider only the scalar metric potentials and we ignore the second-order quadrupole moments, if we give a rough estimation.

To simplify the analysis, we adopt the condition such that the two first-order scalar metric potentials are equal, i.e., $\Phi^{(1)} = \Psi^{(1)}$. While this is valid only if the first-order quadrupole moments are negligibly small, we keep it just for a qualitative

understanding about the behavior of the power spectrum for the vector mode. During the radiation-dominated era, the scalar potentials are constant on super-horizon scales while they decay on sub-horizon scales. On the other hand, they freeze on all scales during the matter-dominated era (e.g., see [35]). We note that under this condition the second term of the right-hand side in Eq. (2.195) should vanish. This is understood as follows: The condition we impose here implies that k_1 and k_2 are interchangeable. Moreover, the spherical harmonics has the following property:

$$k_1 Y_{1,\lambda}^*(\hat{\mathbf{k}}_1) + k_2 Y_{1,\lambda}^*(\hat{\mathbf{k}}_2) = \sqrt{\frac{3}{4\pi}} k \delta_{m,0} ,$$
 (4.116)

where we have imposed $k = k_1 + k_2$. As a result, the second line in Eq. (2.195) gives negligible contributions to the vector mode in the absence of the quadrupole moments.

Let us evaluate the vector mode during the radiation-dominated era. Since the fourth term in Eq. (2.195) is estimated through in the first-order perturbation theory as

$$v_{\text{m0}i}^{(1)} = -\frac{1}{4\pi G a^2 \rho^{(0)}} \partial_i \left(\dot{\Phi}^{(1)} + \mathcal{H} \Psi^{(1)} \right) . \tag{4.117}$$

Therefore, since we find that $8\pi Ga^2\rho_{\rm m}^{(0)}v_{\rm m0}^2\sim(\rho_{\rm m}^{(0)}/\rho^{(0)})\Phi^2$, it is suppressed by the factor $\rho_{\rm m}^{(0)}/\rho^{(0)}\ll 1$ compared with the third term. Therefore we found that the third term gives a dominant contribution to the second-order vector mode. Using the explicit expression for the spherical harmonics, the power spectrum for the vector mode induced by the third term in Eq. (2.195) can be written as

$$\frac{k^3}{2\pi^2} P_\sigma \propto k \int \mathrm{d}^3 k_1 P_\phi(k_1) P_\phi(k_2) T^2(\eta, k_1, k_2) \left[k_1^4 \sin^2 \theta_1 \cos^2 \theta_1 - k_1^2 k_2^2 \sin \theta_1 \sin \theta_2 \cos \theta_1 \cos \theta_2 \right], \tag{4.118}$$

where $\mathbf{k}_2 = \mathbf{k} - \mathbf{k}_1$, $\hat{\mathbf{k}} \cdot \hat{\mathbf{k}}_i = \cos \theta_i$, and the integrated transfer function $T(\eta, k_1, k_2)$ is defined in terms of the transfer functions for the scalar potential Φ_T as

$$T(\eta, k_1, k_2) = \frac{1}{a^2(\eta)} \int_0^{\eta} d\eta' a^2(\eta') \Phi_{T}(k_1 \eta') \Phi_{T}(k_2 \eta') . \qquad (4.119)$$

With a help of the definition of k_2 and introducing the direction cosine $\mu_1 \equiv \cos \theta_1$, Eq. (4.118) can be reduced to

$$\frac{k^3}{2\pi^2} P_{\sigma} \propto k \int_0^{\infty} dk_1 \int_{-1}^1 d\mu_1 \, k_1^5 P_{\phi}(k_1) P_{\phi}(k_2) T^2(\eta, k_1, k_2) \left(2k_1 \mu_1 - k\right) \mu_1 \left(1 - \mu_1^2\right) \,. \tag{4.120}$$

To perform this integration analytically, we assume that the transfer function of the scalar potential during the radiation-dominated era is approximated as [35]

$$\Phi_{\rm T}(k\eta) = \frac{1}{1 + (k\eta)^2} \quad (\eta < \eta_{\rm eq}) .$$
(4.121)

Substituting the above transfer function into Eq. (4.119), we have

$$T(\eta, k_1, k_2) = \frac{1}{\eta^2 k_1 k_2 \left(k_1^2 - k_2^2\right)} \left[k_1 \arctan\left(k_2 \eta\right) - k_2 \arctan\left(k_1 \eta\right) \right] \quad \left(\eta < \eta_{\text{eq}}\right). \tag{4.122}$$

In order to evaluate the behavior of the power spectrum, we split the integral of k_1 in Eq.(4.120) into two parts: the contributions from $k_1 > k$ and $k_1 < k$ for given k. In the former case, the dummy variables k_1 and k_2 are related through $k_2 = k_1 \left[1 - (k/k_1)\mu + O((k/k_1)^2) \right]$ and the integrated transfer function can be reduced to the following form:

$$T(\eta, k_1, k_2) \approx \frac{1}{2k_1^3 \eta^2} \left[\arctan(k_1 \eta) - \frac{k_1 \eta}{1 + (k_1 \eta)^2} \right] \equiv \eta \, \tau_1(k_1 \eta) \quad (\eta < \eta_{\text{eq}}) .$$
 (4.123)

Hence the contributions from the products of the first-order scalar potentials with their wavelengths shorter than k are

$$\frac{k^3}{2\pi^2} P_{\sigma} \propto k \int_{k}^{\infty} dk_1 \int_{-1}^{1} d\mu_1 k_1^6 P_{\phi}^2(k_1) \eta^2 (\tau_1(x_1))^2 \mu_1^2 (1 - \mu_1^2)
\propto k \eta \int_{k\eta}^{\infty} dx_1 (\tau_1(x_1))^2 \equiv k \eta \beta_1(k\eta) ,$$
(4.124)

where we have used the scale-invariance of the primordial power spectrum Eq. (2.207) and we have changed the variable k_1 to $x_1 \equiv k_1 \eta$. Since $\tau_1(x)$ behaves as x^0 for $x \ll 1$ and x^{-3} for $x \gg 1$, the integral of β_1 in Eq. (4.124) can be evaluated as a function of $k\eta$: $\beta_1 \propto (k\eta)^0$ for $k\eta \ll 1$, and $\beta_1 \propto (k\eta)^{-5}$ for $k\eta \gg 1$. Substituting this into Eq. (4.124), we calculate the contributions from modes with $k_1 > k$ in Eq. (4.120):

$$\frac{k^3}{2\pi^2} P_{\sigma}(k < k_1, \eta < \eta_{\text{eq}}) \propto \begin{cases} (k\eta)^1 & k\eta \ll 1\\ (k\eta)^{-4} & k\eta \gg 1 \end{cases} . \tag{4.125}$$

We can reproduce the behavior of the power spectrum, namely $\propto k^1$ for superhorizon scales and $\propto k^{-4}$ for sub-horizon scales, which can be seen in the numerical calculations.

Following the same manner, we can analyze the opposite case, namely $k_1 < k$. Expanding Eq. (4.120) in terms of the small quantity $k_1/k \ll 1$, we find that the leading order term vanishes due to the angular integration. Furthermore, we also find that the-next leading order term is suppressed by the power k_1^3 . Hence the contributions from modes with their wavelengths longer than k are suppressed by the factor k_1/k and can be treated as subdominant components. Note that although the above estimation does not work around $k \approx k_1$, the results in Eq. (4.125) is expected

to be still correct as long as we estimate the behavior roughly for the following reasons. The integrand in Eq. (4.120) does not diverge at $k = k_1$. The estimations on $k < k_1$ and $k > k_1$ are smoothly connected. Therefore, the contribution from $k \approx k_1$ is at most same order as that from $k < k_1$. Combining these results, we conclude that the power spectrum for the second-order vector mode during the radiation-dominated era is determined by the convolution of the scalar potentials with shorter wavelengths.

We discuss the peak shift of the second-order vector mode shown in Fig. 4.2 from $1+z=10^5$ to 10^4 . During the radiation-dominated era, the first-order scalar potential remains constant on super-horizon scales while it decays on sub-horizon scales. Therefore, the second-order vector mode can grow due to the constant scalar potential on super-horizon scales. On sub-horizon scales, the second-order vector mode conversely decays due to the decaying scalar potential. As a result, the peak of the second-order vector mode is determined by the horizon scale at the corresponding era and the peak keeps shifting until the matter-radiation equality.

We next consider the vector mode after the radiation-dominated era. The evolution during this era can be easily understood through Eq.(4.114). Generally, when the second-order source term remains constant (i.e., $\mathcal{S}_{\lambda}^{(2)} = \text{const.}$), the vector mode evolves as $\sigma_{\lambda}^{(2)} \propto \eta^1$. This condition is actually satisfied since the scalar potentials during the matter-dominated era freeze on all scales, as mentioned above. Hence the evolution of the second-order vector mode is given by

$$\frac{k^3}{2\pi^2} P_{\sigma} \propto \left(\sigma_{\lambda}^{(2)}\right)^2 \propto \eta^2 \propto a^1 \quad \text{(for all scales)} \,. \tag{4.126}$$

During the matter-dominated era, the shape of the spectrum for the vector mode does not dramatically change since the growing features are the same over all scales. Therefore, the information about the power spectrum during the radiation-dominated era propagates to one during the matter-dominated era, i.e., the dimensionless power spectrum during the matter dominated era is still in proportion to k^1 for super-horizon scales and k^{-4} for sub-horizon scales, respectively. Although the global feature can be understood as above, in more detail small shifts of the scalar potential such as $\Phi \to 9/10\Phi$ during the matter-radiation equality induce an additional small suppression of the second-order vector mode, as seen in Fig. 4.1. After the universe is dominated by the dark energy, the scalar potentials begin to decay for all scales, implying that the second-order vector mode generated by these potentials also decays.

Before closing this subsection, we introduce the analytic model of the power spectrum, which is originally derived in [24] (hereafter referred to as MHM). The explicit form of the approximate solution can be written as

$$\frac{k^3}{2\pi^2} P_{\sigma}^{(\text{MHM})}(k, \eta, \eta') = \frac{18}{25^2} C_{\text{V}} \Delta_{\mathcal{R}}^4(k_0) k^2 \left(\frac{k}{k_*}\right)^{-1} W_{\text{V}}(k/k_*) F(z) F(z') , \quad (4.127)$$

where $C_{\rm V} \approx 0.026$, $W_{\rm V}(x) = (1+5x+3x^2)^{-5/2}$, and $k_* = \Omega_{\rm m0}h^2\,{\rm Mpc}^{-1}$ with $\Omega_{\rm m0}$ and h being the present cosmological parameter of the nonrelativistic matter and the

Hubble constant H_0 in unit of 100 [km s⁻¹ Mpc⁻¹], respectively. The function of a redshift F(z) is given by

$$F(z) = \frac{2g^2(z)E(z)f(\Omega_{\rm m}(z))}{\Omega_{\rm m0}H_0(1+z)^2},$$
(4.128)

where $E(z) = \Omega_{\rm m0}(1+z)^3 + (1-\Omega_{\rm m0})$, $\Omega_{\rm m}(z) = \Omega_{\rm m0}(1+z)^3/E^2(z)$. We adopt $\Omega_{\rm m0} = 0.27$ as the fiducial value. We denote $f(\Omega_m(z))$ and g(z) as the dimensionless linear growth rate and the growth suppression factor, respectively. One can find that f and g are well approximated as $f \approx \Omega_{\rm m}^{7/4}(z)$ and

$$g(z) \propto \Omega_{\rm m}(z) \left[\Omega_{\rm m}^{4/7}(z) - \Omega_{\Lambda}(z) + (1 + \Omega_{\rm m}(z)/2) (1 + \Omega_{\Lambda}(z)/70) \right]^{-1}, (4.129)$$

where $\Omega_{\Lambda}(z) = (1 - \Omega_{\rm m0})/E^2(z)$ and we will normalize g so that g(0) = 1 [24, 36, 37]. We find that the transfer functions derived in MHM and those determined by the numerical calculation match after the matter-radiation equality. However, we should emphasize that for the MHM approximate power spectrum the effect from the evolution of the vector mode over all wave numbers during the radiation-dominated era is assumed to be neglected. As we will see in the subsequent analysis, this approximation leads to the non-negligible difference between the full-numerical and analytic power spectrum.

4.3.3 Tensor Modes

As we mentioned, the curl mode of the CMB lensing and the B-mode shear can be generated by not the scalar metric perturbations but the vector and/or tensor metric perturbations. In this subsection, to compare with the second-order vector mode, tensor modes are considered as alternative sources of the observables we focus on. In particular, we consider primordial gravitational waves and second-order tensor mode as intriguing examples for tensor metric perturbations. To describe the spectrum for the tensor mode, we define the spin- ± 2 operator $O_{ij}^{(\pm 2)}$ in terms of the polarization vectors defined in Eq. (2.19) as

$$O_{ij}^{(\pm 2)}(\hat{\mathbf{k}}) = -\sqrt{\frac{3}{8}} e_i^{(\pm)}(\hat{\mathbf{k}}) e_j^{(\pm)}(\hat{\mathbf{k}}). \tag{4.130}$$

Since this operator obviously satisfies the transverse-traceless condition, the secondorder tensor metric perturbations can be expanded as

$$h_{ij}(\eta, \mathbf{x}) = \int \frac{\mathrm{d}^3 \mathbf{k}}{(2\pi)^3} \sum_{\sigma = +2} h_{\sigma}(\eta, \mathbf{k}) O_{ij}^{(\sigma)}(\hat{\mathbf{k}}) e^{-i\mathbf{k}\cdot\mathbf{x}}.$$
(4.131)

With these convention, we define the unequal-time power spectrum as

$$\left\langle h_{\sigma}^{*}(\eta, \mathbf{k}) h_{\sigma'}(\eta', \mathbf{k}') \right\rangle = (2\pi)^{3} \delta_{\sigma\sigma'} \delta_{D}^{3} \left(\mathbf{k} - \mathbf{k}' \right) \frac{1}{3} P_{h}(\eta, \eta', k) . \tag{4.132}$$

Primordial gravitational waves are generated in the very early Universe and the representative sources for tensor mode. Its effect on the CMB lensing and the shear measurement has been discussed in the literature [20, 21]. For the evolution of primordial gravitational waves, we introduce the PGW transfer function $\mathcal{T}_h^{(\text{PGW})}(k\eta)$, which basically describes its sub-horizon evolution. In terms of this, we can write the power spectrum as

$$\frac{k^3}{2\pi^2} P_h^{(PGW)}(\eta, \eta', k) = r \Delta_{\mathcal{R}}^2(k_0) \left(\frac{k}{k_0}\right)^{n_t} \mathcal{T}_h^{(PGW)}(k\eta) \mathcal{T}_h^{(PGW)}(k\eta') . \tag{4.133}$$

In our analysis we adopt r = 0.1, $n_{\rm t} = 0$ as the fiducial values, and use $\mathcal{T}_h^{\rm (PGW)} = 3j_1(k\eta)/k\eta$ for simplicity. The corrections due to the effects during the radiation-dominated era would be small and we neglect this small correction throughout this section.

Similar to the case of the vector mode discussed in the previous section, the secondorder source terms induce the tensor metric perturbations, which are expected to be one of the possible sources of the curl mode and B-mode shear signals [33]. The analytic model of the power spectrum for the second-order tensor mode induced by the product of the first order scalar metric potentials has been discussed in [24, 35]. The approximate form of the power spectrum derived in [24] is given by

$$\frac{k^3}{2\pi^2} P_h^{(\text{MHM})}(\eta, \eta', k) = \frac{6}{25} C_{\text{T}} \Delta_{\mathcal{R}}^4(k_0) \left(\frac{k}{k_*}\right)^{-1} W_{\text{T}}(k/k_*) \mathcal{T}_h^{(\text{MHM})}(k\eta) \mathcal{T}_h^{(\text{MHM})}(k\eta') ,$$
(4.134)

with $C_{\rm T} \approx 0.062$ and $W_{\rm T}(x) = \left(1 + 7x + 5x^2\right)^{-3}$. The transfer function for the second-order tensor mode is

$$\mathcal{T}_h^{(\mathrm{MHM})}(k\eta) = \left(1 - \frac{3j_1(k\eta)}{k\eta}\right)g_\infty^2. \tag{4.135}$$

The correction factor g_{∞} attributed to the effect of dark energy is defined as $g_{\infty} \equiv \lim_{z \to \infty} g(z) \approx 1.3136$. We note that this formula is valid only after matter-radiation equality time. While the correction during the radiation-dominated era for the second-order tensor mode has been considered in [35], for the purposes of comparing the second-order vector and tensor modes, we will neglect such correction since it must be small [33].

4.3.4 Comparison of Each Model

For comparison, the power spectra for these models at the present time are shown in Fig. 4.3. The power spectrum for the second-order vector mode is larger than that for the second-order tensor mode. Therefore, it is expected that the secondorder vector mode induces a larger lensing signal than the second-order tensor mode on small scales. Furthermore, on small scales, the second-order vector mode has a larger amplitude than the primordial gravitational waves with r = 0.1. In other words, the second-order vector mode has the possibility of being detected by cosmological observations on small scales, unlike the primordial gravitational waves. We explain the reason why the discrepancy between the exact vector model and the analytical vector model appears. From Fig. 4.3, we can see that the amplitude of the exact model is smaller than that of the analytical vector model for $k \gtrsim k_{\rm eq}$, where $k_{\rm eq} \approx 10^{-2} \ h{\rm Mpc}^{-1}$ is the horizon scale at the time of matter-radiation equality. For $k \gtrsim k_{\rm eq}$, the analytical vector model does not consider the effect of the small suppression around the matter-radiation equality time. The small suppression on small scales arises because the first order scalar potentials, i.e., the source of the second order vector metric perturbations, decay so rapidly in the radiation dominated era that the source on those scales can sustain the vector perturbations and make them grow proportional to the scale factor only after some time has passed since the matter-radiation equality time (see the blue and magenta lines in Fig. 1). This small suppression is not included in the analytical model. The exact model is about ten times smaller than the analytical vector model for $k \gtrsim k_{eq}$.

According to the above discussion, we can understand when the suppression is determined. The analytical vector model does not change its peak since this model is calculated in the flat Λ CDM model with matters and the cosmological constant. Therefore, the difference between the analytical vector model and exact one is appeared until the matter-radiation equality. In conclusion, the factor about 10 suppression is determined at the matter-radiation equality time.

The tendency for the second-order vector mode is quite similar to that for the second-order tensor mode in Ref. [33]. In the next section, we will show the numerical results of the weak lensing induced by the second-order vector perturbation.

4.4 Results and Discussions

We show our main results and discuss the size of the effect of second-order vector modes. We now calculate the weak lensing signals from the second-order vector mode by performing the numerical calculation (hereafter referred to as the exact vector). For comparison, the results for the signals from the primordial gravitational waves with r=0.1, the second-order tensor mode (analytic tensor), the second-order vector mode (analytic vector) are also shown.

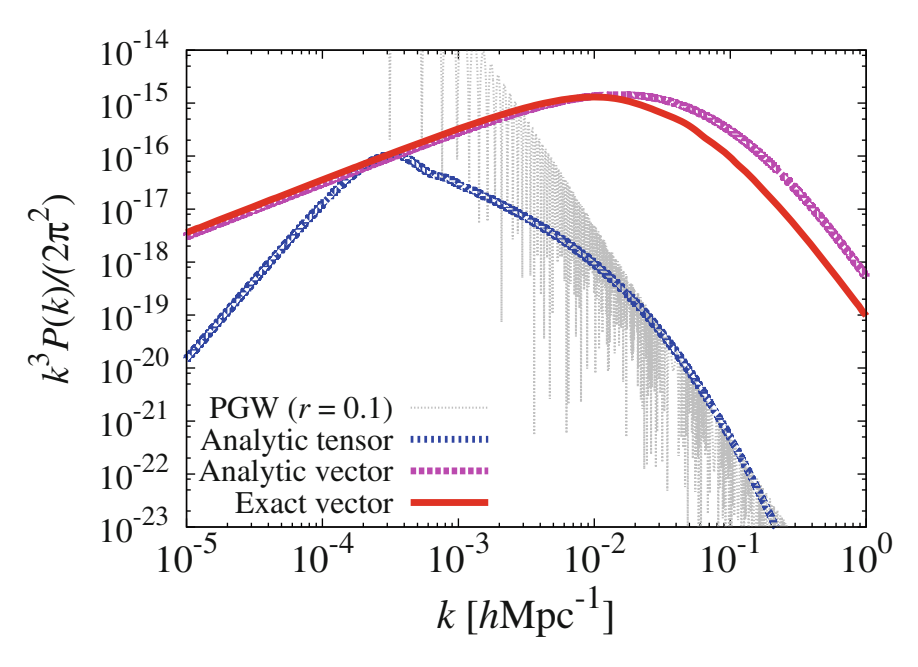


Fig. 4.3 The power spectrum of primordial gravitational waves with r=0.1 (PGW), the second-order tensor mode (Analytic tensor), the analytical approximate solution of the second-order vector mode (Analytic vector), and the numerical solution of the second-order vector mode (Exact vector) at the present time (1+z=1). The second-order vector mode dominates on small scales rather than the second-order tensor mode. The second-order vector mode derived by numerical calculation is slightly smaller than that derived by analytic approximation on smaller scales

First, we show the angular power spectrum of the curl-mode in Fig. 4.4 for the CMB lensing measurement. The CMB lensing reconstruction technique can decompose the lensing potential into the gradient and curl modes. Although the gradient mode dominates the lensing signals, owing to this technique, the information about the gradient and curl modes can be extracted independently. Even when we neglect the instrumental noise, we need to take into account for the reconstruction noise only. The noise estimated by the ideal CMB weak lensing measurement is determined by a cosmic-variance limited reconstruction of the curl-mode [8, 10]. We found that the curl-mode induced by the primordial gravitational waves dominates on large scales, $\ell \lesssim 200$, while that by the second-order vector mode dominates on small scales, $\ell \gtrsim 200$. As seen in Fig. 4.3, the power spectrum for the vector mode has a peak at the scale corresponding to matter-radiation equality. On the other hand, those for the primordial and second-order tensor modes have their peaks at the horizon scales. Therefore, the second-order vector mode can affect smaller scales than the primordial or the second-order tensor mode does. As expected, the second-order tensor mode gives a subdominant contribution to the weak lensing curl-mode. This feature is sim-

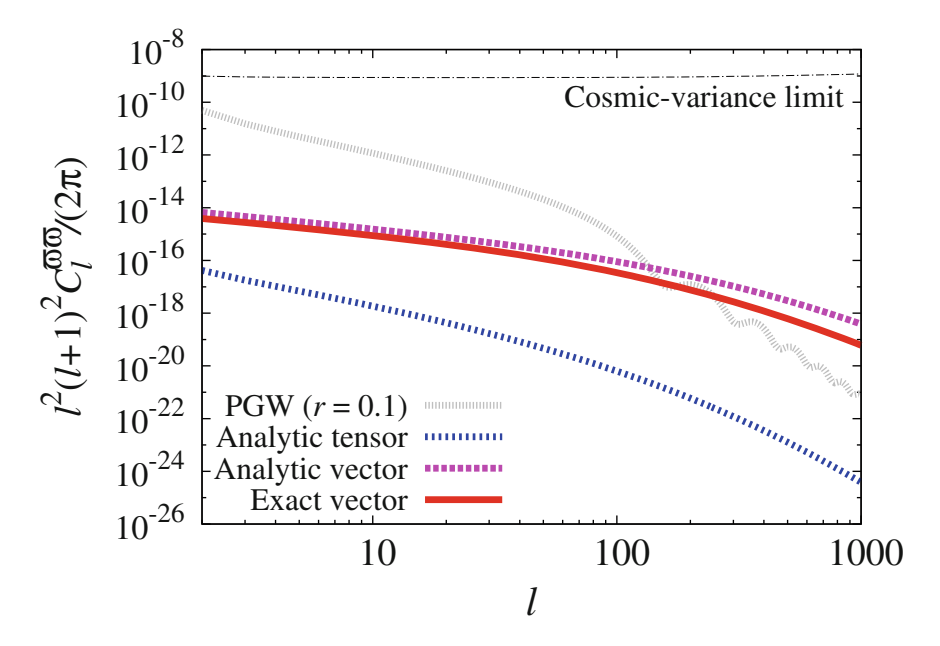


Fig. 4.4 The angular power spectrum of the weak lensing curl-mode. As we expected, the second-order vector mode dominates on small scales. Furthermore, the second-order tensor mode becomes a sub-dominant contribution to the weak lensing curl-mode. The expected noise from the cosmic variance limit is also shown

ilar to the CMB polarization anisotropy [24] and the weak lensing gradient-mode [32].

However, unfortunately, even if we consider ideal experiments, i.e., only the cosmic-variance limited error, the weak lensing curl-mode signals do not exceed the expected noise. Although the curl-mode induced by the second-order vector mode dominates the signal of the curl-mode on small scales, it will be difficult to detect the second-order vector and tensor weak lensing signals in future experiments. We conclude that the curl-mode induced by the second-order modes cannot be detected by any CMB observations in the future because of the cosmic variance limit. On the other hand, recently, a new possibility has emerged of detecting the weak lensing signals in 21 cm observations [38, 39]. The angular power spectrum of 21 cm fluctuations can be expanded up to $\ell \sim 10^7$ since they do not have diffusion scales unlike CMB fluctuations. Furthermore, the 21 cm fluctuations enable us to observe the fluctuation at different frequencies which corresponding to the different distances. Therefore, the signal-to-noise ratio can be substantially improved. For example, in Ref. [39], the observable scalar-to-tensor ratio reaches $r \approx 10^{-9}$. If this sensitivity is reached in the future observations, the 21 cm curl-mode induced by the second-order vector mode should be detected. The 21 cm fluctuations would be a good probe of the weak lensing curl-mode.

102 4 Weak Lensing

Second, we show the angular power spectrum of the B-mode shear with the four representative imaging surveys, DES, HSC, SKA, and LSST, in Fig. 4.5. Unlike the CMB lensing, the statistical error in the cosmic shear measurements is determined by the intrinsic ellipticity of each galaxy. In this section, we assume that the error mainly originates from the intrinsic ellipticity of each galaxy as

$$N_{\ell}^{\text{BB}} = \sqrt{\frac{2}{(2\ell+1)f_{\text{sky}}}} \frac{\langle \gamma_{\text{int}}^2 \rangle}{3600N_{\text{g}}(180/\pi)^2} , \qquad (4.136)$$

where $\langle \gamma_{\rm int}^2 \rangle^{1/2}$ is the root-mean-square ellipticity of galaxies. In this section, we set $\langle \gamma_{\rm int}^2 \rangle^{1/2} = 0.3$ derived in Ref. [40]. The error in the cosmic shear measurements is mainly controlled by the sky coverage $f_{\rm sky}$ and the number of the galaxies per square arc minute $N_{\rm g}$ and we show the error expected by four survey designs in Table 4.1. From Fig. 4.5, we can see that the B-mode induced by the second-order vector mode dominates on all scales except for the largest scale. However, as is the case with the CMB lensing curl-mode, the cosmic shear B-mode induced by the second-order vector mode does not exceed the expected noise for each survey design. From Eq. (4.136) and Fig. 4.5, the combined survey design parameter appeared in

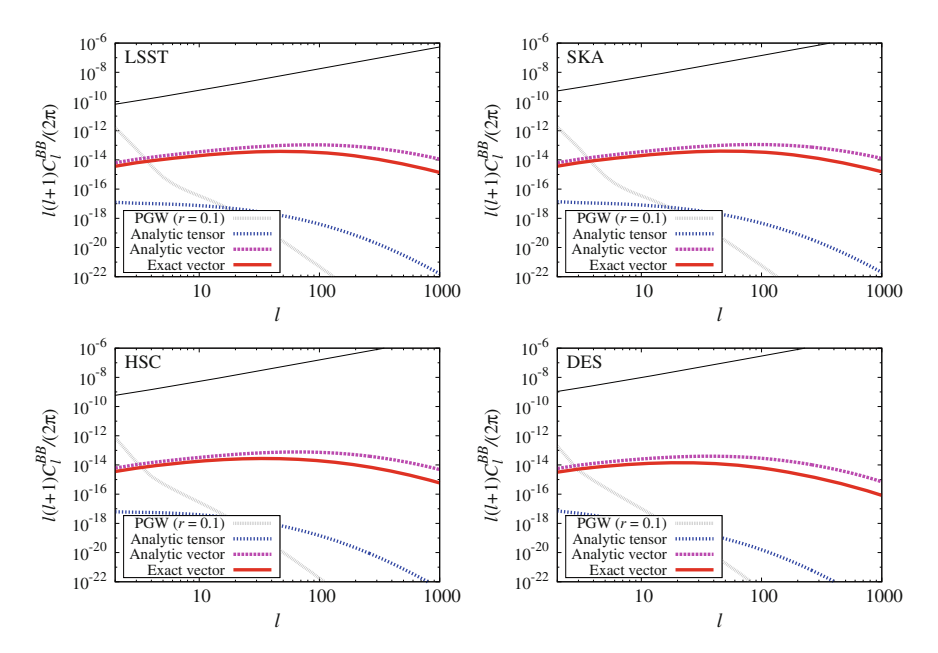


Fig. 4.5 A angular power spectra of the weak lensing B-mode assumed four survey designs: LSST (top left), SKA (top right), HSC (bottom left), and DES (bottom right). The second-order vector mode dominates the expected signals on small scales. The black solid line shows the expected statistical error for each survey

Eq. (4.136), i.e., $\sqrt{f_{\rm sky}} \times N_{\rm g}$, should be improved about 10^4 compared with LSST to detect the B-mode signal. Such an ultimate survey is quite unrealistic even in the distant future in contrast with the 21 cm lensing observations.

We note that in this section, we focus on the standard cosmological model which can characterize the primordial power spectrum by the primordial amplitude $\Delta_{\mathcal{R}}^2$ and the spectral index n_s in Eq. (2.207). However, the non-standard model may enhance the primordial power spectrum on smaller scales (e.g., [41, 42]). The second-order signals are sensitive to the enhancement on smaller scales since the mode mixing is introduced by the convolution of the small- and large-scale fluctuations. The second-order signals would be useful to probe the small-scale physics related to the inflation model.

Let us consider the difference between the weak lensing induced by the second-order vector and tensor modes. The equation of motion for the tensor metric perturbation has the form of a wave equation. Therefore, the second-order tensor mode induced by the products of the first-order scalar modes cannot be amplified when the source remains constant in the matter-dominated era on sub-horizon scales [43]. On the other hand, the evolution of the vector metric perturbation is equivalent to that of the vorticity. We can see that the vorticity with the source is well amplified in Eq. (4.114) even in such an era. Therefore, the amplitude of the second-order vector mode is larger than that of the second-order tensor mode.

To conclude this section, we remark on other second-order contributions to the weak lensing curl- and B- modes. During photon propagation, there are some corrections to the weak lensing formula induced by the geodesic effect [44, 45]. The geodesic effect would have the possibility to enhance the curl- and B-mode signals. However, this geodesic effect is induced not by the vector and tensor modes but by the product of the first-order scalar perturbations such as the Weyl potential, which we leave for future work.

4.5 Conclusion

In this section, we explored the weak lensing signals induced by the second-order vector perturbation. The weak lensing effects are classified into two observables: CMB lensing and cosmic shear. Both the signals of the CMB lensing and cosmic shear can be decomposed into two modes by using parity, namely, the gradient-and curl-modes for the CMB lensing and the E- and B-modes for the cosmic shear. The curl- and B-modes are only induced by the vector and tensor modes. In the standard cosmology, the vector mode is neglected and the source of the curl- and B-modes is limited to the case of primordial gravitational waves, which have not been observed yet. However, when we expand the cosmological perturbation theory up to the second order, the vector and tensor modes are naturally induced by the product of the first-order scalar perturbations. As the first-order scalar perturbation theory is well established by a number of observations, the second-order vector and tensor modes do not include free parameters and are well determined.

104 4 Weak Lensing

We presented the effect of the second-order vector mode on the weak lensing for the first time. The weak lensing induced by the second-order vector mode dominates on smaller scales rather than the primordial gravitational waves with r = 0.1and the second-order tensor mode. In particular, the cosmic shear induced by the second-order vector mode dominates on almost all scales. This is because the secondorder vector mode can be enhanced when the source exists in the matter-dominated epoch while the second-order tensor mode remains constant even if the source exists. This difference also affects cosmological signatures such as the CMB polarization anisotropy. However, the weak lensing signals induced by the second-order vector mode cannot exceed the expected noise estimated by the cosmic-variance limit and the shot-noise for the CMB lensing and cosmic shear, respectively. Therefore, unfortunately, it seems difficult to detect the curl- and B-modes induced by not only the second-order tensor mode but also the vector mode in the ongoing and forthcoming weak lensing observations. However, the 21 cm observations can decrease the expected noise and it may be possible that the 21 cm lensing observations can be detect the 21 cm lensing curl-mode.

Throughout this section, we assume the standard cosmological model. In other words, the primordial power spectrum is characterized by the amplitude and the spectral index. However, non-standard cosmological models can enhance the primordial power on much smaller scales. The weak lensing curl- and B-modes would become the good probe to search for the small-scale power spectrum and we leave this to future work.

References

- WMAP Collaboration, G. Hinshaw et al., Nine-year Wilkinson Microwave Anisotropy Probe (WMAP) observations: cosmological parameter results. Astrophys. J. Suppl. 208, 19 (2013), arXiv:1212.5226
- 2. Planck Collaboration Collaboration, P. Ade et al., Planck 2013 results. XV. CMB power spectra and likelihood. Astron. Astrophys. **571**, A15 (2014), arXiv:1303.5075
- SDSS Collaboration, M. Tegmark et al., Cosmological constraints from the SDSS luminous red galaxies. Phys. Rev. D 74, 123507 (2006), arXiv:astro-ph/0608632
- Supernova Search Team Collaboration, A.G. Riess et al., Observational evidence from supernovae for an accelerating universe and a cosmological constant. Astron. J. 116, 1009–1038 (1998), arXiv:astro-ph/9805201
- A. Lewis, A. Challinor, Weak gravitational lensing of the cmb. Phys. Rept. 429, 1–65 (2006), arXiv:astro-ph/0601594
- M. Bartelmann, P. Schneider, Weak gravitational lensing. Phys. Rept. 340, 291–472 (2001), arXiv:astro-ph/9912508
- T. Okamoto, W. Hu, CMB lensing reconstruction on the full sky. Phys. Rev. D 67, 083002 (2003), arXiv:astro-ph/0301031
- 8. A. Cooray, M. Kamionkowski, R.R. Caldwell, Cosmic shear of the microwave background: the Curl diagnostic. Phys. Rev. D 71, 123527 (2005), arXiv:astro-ph/0503002
- 9. C.M. Hirata, U. Seljak, Reconstruction of lensing from the cosmic microwave background polarization. Phys. Rev. D **68**, 083002 (2003), arXiv:astro-ph/0306354
- T. Namikawa, D. Yamauchi, A. Taruya, Full-sky lensing reconstruction of gradient and curl modes from CMB maps. JCAP 1201, 007 (2012), arXiv:1110.1718

References 105

11. Planck Collaboration Collaboration, P. Ade et al., Planck 2013 results. XVII. Gravitational lensing by large-scale structure. Astron. Astrophys. **571**, A17 (2014), arXiv:1303.5077

- 12. K.M. Smith, A. Cooray, S. Das, O. Dore, D. Hanson et al., CMBPol mission concept study: gravitational lensing. AIP Conf. Proc. 1141, 121 (2009), arXiv:0811.3916
- COrE Collaboration, F.R. Bouchet et al., COrE (Cosmic Origins Explorer) A White Paper, arXiv:1102.2181
- T. Namikawa, D. Yamauchi, A. Taruya, Future detectability of gravitational-wave induced lensing from high-sensitivity CMB experiments. Phys. Rev. D91(4), 043531 (2015), arXiv:1411.7427
- Dark Energy Survey Collaboration, T. Abbott et al., The dark energy survey, arXiv:astro-ph/0510346
- 16. HSC collaboration, Hyper suprime-cam design review
- M.L. Brown et al., Weak gravitational lensing with the Square Kilometre Array. PoS AASKA14, 023 (2015), arXiv:1501.03828
- LSST Science, LSST Project Collaboration, P.A. Abell et al., LSST Science Book, Version 2.0, arXiv:0912.0201
- PAR Planck Collaboration, Ade et al., Planck 2013 results. XVI. Cosmological parameters. Astron. Astrophys. 571, A16 (2014), arXiv:1303.5076
- S. Dodelson, E. Rozo, A. Stebbins, Primordial gravity waves and weak lensing. Phys. Rev. Lett. 91, 021301 (2003), arXiv:astro-ph/0301177
- 21. C. Li, A. Cooray, Weak lensing of the cosmic microwave background by foreground gravitational waves. Phys. Rev. D **74**, 023521 (2006), arXiv:astro-ph/0604179
- D. Yamauchi, T. Namikawa, A. Taruya, Weak lensing generated by vector perturbations and detectability of cosmic strings. JCAP 1210, 030 (2012), arXiv:1205.2139
- 23. D. Yamauchi, T. Namikawa, A. Taruya, Full-sky formulae for weak lensing power spectra from total angular momentum method. JCAP **1308**. 051 (2013), arXiv:1305.3348
- S. Mollerach, D. Harari, S. Matarrese, CMB polarization from secondary vector and tensor modes. Phys. Rev. D 69, 063002 (2004), arXiv:astro-ph/0310711
- C. Pitrou, J.-P. Uzan, F. Bernardeau, The cosmic microwave background bispectrum from the non-linear evolution of the cosmological perturbations. JCAP 1007, 003 (2010), arXiv:1003.0481
- M. Beneke, C. Fidler, K. Klingmuller, B polarization of cosmic background radiation from second-order scattering sources. JCAP 1104, 008 (2011), arXiv:1102.1524
- C. Fidler, G.W. Pettinari, M. Beneke, R. Crittenden, K. Koyama, D. Wands, The intrinsic B-mode polarisation of the Cosmic Microwave Background. JCAP 1407, 011 (2014), arXiv:1401.3296
- G.W. Pettinari, C. Fidler, R. Crittenden, K. Koyama, A. Lewis et al., Impact of polarization on the intrinsic cosmic microwave background bispectrum. Phys. Rev. D 90(10), 103010 (2014), arXiv:1406.2981
- T.H.-C. Lu, K. Ananda, C. Clarkson, R. Maartens, The cosmological background of vector modes. JCAP 0902, 023 (2009), arXiv:0812.1349
- T.H.-C. Lu, K. Ananda, C. Clarkson, Vector modes generated by primordial density fluctuations. Phys. Rev. D 77, 043523 (2008), arXiv:0709.1619
- K.N. Ananda, C. Clarkson, D. Wands, The Cosmological gravitational wave background from primordial density perturbations. Phys. Rev. D 75, 123518 (2007), arXiv:gr-qc/0612013
- S. Andrianomena, C. Clarkson, P. Patel, O. Umeh, J.-P. Uzan, Non-linear relativistic contributions to the cosmological weak-lensing convergence. JCAP 1406, 023 (2014), arXiv:1402.4350
- D. Sarkar, P. Serra, A. Cooray, K. Ichiki, D. Baumann, Cosmic shear from scalar-induced gravitational waves. Phys. Rev. D 77, 103515 (2008), arXiv:0803.1490
- 34. K. Yamamoto, D. Parkinson, T. Hamana, R.C. Nichol, Y. Suto, Optimizing future imaging survey of galaxies to confront dark energy and modified gravity models. Phys. Rev. D 76, 023504 (2007), arXiv:0704.2949
- 35. D. Baumann, P.J. Steinhardt, K. Takahashi, K. Ichiki, Gravitational wave spectrum induced by primordial scalar perturbations. Phys. Rev. D 76, 084019 (2007), arXiv:hep-th/0703290

106 4 Weak Lensing

 O. Lahav, P.B. Lilje, J.R. Primack, M.J. Rees, Dynamical effects of the cosmological constant, MNRAS251, 128–136 (1991)

- S.M. Carroll, W.H. Press, E.L. Turner, The cosmological constant. ARA&A 30, 499–542 (1992)
- 38. K.W. Masui, U.-L. Pen, Primordial gravity wave fossils and their use in testing inflation. Phys. Rev. Lett. **105**, 161302 (2010), arXiv:1006.4181
- L. Book, M. Kamionkowski, F. Schmidt, Lensing of 21-cm fluctuations by primordial gravitational waves. Phys. Rev. Lett. 108, 211301 (2012), arXiv:1112.0567
- 40. G. Bernstein, M. Jarvis, Shapes and shears, stars and smears: optimal measurements for weak lensing. Astron. J. 123, 583–618 (2002), arXiv:astro-ph/0107431
- 41. M. Kawasaki, T. Takayama, M. Yamaguchi, J. Yokoyama, Power spectrum of the density perturbations from smooth hybrid new inflation model. Phys. Rev. D **74**, 043525 (2006), arXiv:hep-ph/0605271
- J. Chluba, A.L. Erickcek, I. Ben-Dayan, Probing the inflaton: Small-scale power spectrum constraints from measurements of the CMB energy spectrum. Astrophys. J. 758, 76 (2012), arXiv:1203.2681
- S. Saga, K. Ichiki, N. Sugiyama, Impact of anisotropic stress of free-streaming particles on gravitational waves induced by cosmological density perturbations. Phys. Rev. D 91(2), 024030, (2015), arXiv:1412.1081
- F. Bernardeau, C. Bonvin, F. Vernizzi, Full-sky lensing shear at second order. Phys. Rev. D 81, 083002 (2010), arXiv:0911.2244
- F. Bernardeau, C. Bonvin, N. Van de Rijt, F. Vernizzi, Cosmic shear bispectrum from secondorder perturbations in General Relativity. Phys. Rev. D 86, 023001 (2012), arXiv:1112.4430

Chapter 5 21 cm Lensing in the Dark Ages

Abstract After the recombination epoch ($z \sim 1100$), free electrons couple to protons, and subsequently, neutral hydrogen atoms are formed. Before reionization $(z \sim 30)$, there has been no astronomical objects, what we called the *dark ages*. During the dark ages, there are large amount of neutral hydrogen atoms. The neutral hydrogen atom emits photons corresponding to the wavelength $\lambda_{\rm HI} \approx 21 {\rm cm}$ at the rest frame due to the hyperfine structure. Therefore, we call this emission the "21 cm radiation" or "21 cm (hydrogen) line". It is possible to observe 21 cm radiation by using the forthcoming radio telescope. The advantages of the 21 cm radiation as follows. There is no damping mechanism such as the Silk damping in the CMB fluctuations. In principle, we can pull information on very small scales from the 21 cm fluctuations. Moreover, we observe the 21 cm fluctuations tomographically since we observe the redshifted 21 cm radiation. The 21 cm radiation would become a new probe to explore much smaller scales and bring a low signal-to-noise ratio. In this part, we apply the second-order vector mode in the cosmological perturbation theory to 21 cm lensing during the dark ages. In the previous study by Book (Phys Rev Lett 108:211301 (2012), [1]), we can, in principle, detect the quite small tensor-toscalar ratio $r \approx 10^{-9}$ by using the 21 cm radiation in the dark ages. However, when we focus on the high-sensitivity experiments, the second-order vector mode cannot neglect. We discuss the effect of the second-order vector mode on the 21 cm lensing measurements. We also present the detectability of the second-order vector mode in the future observations. Moreover, we mention the observable tensor-to-scalar ratio in the 21 cm lensing measurements.

Keywords Second-order perturbation theory · 21 cm radiation · Weak lensing

5.1 Introduction

In our previous study [2], we discussed the detectability of the second-order curl mode in the CMB lensing and cosmic shear. Unfortunately, because the signal from the second-order curl mode is small, we concluded that we could not detect the second-order curl mode even with an ideal experiment for the full sky without the instrumental noise if we utilize the quadratic estimator method. However, we found that the curl mode from the second-order vector mode is comparable to that from PGWs with tensor-to-scalar ratio r < 0.1, especially so in lower redshifts because the second-order vector mode is continuously generated, while PGWs always decay in time. In other words, when there is an observation that enables us to detect PGWs with r < 0.1 through lensing, we can also detect the second-order vector mode.

In previous studies [1, 3, 4], it was shown that the 21 cm lensing has a possibility, in principle, to detect PGWs with a quite small tensor-to-scalar ratio. Long before reionization begins, no astronomical objects exist, and this era is called the dark ages. Neutral hydrogen atoms emit 21cm line radiation that originates from the hyperfine structure; see, e.g., Ref. [5]. In principle, we can observe the 21 cm radiation from the redshift $z \approx 200$ to 30 in future experiments. 21 cm photons are deflected by foreground scalar, vector, and tensor modes. Moreover, we can decompose the deflection angle of the 21 cm photons into the gradient and curl modes depending on the parity. Compared with CMB fluctuations, 21 cm radiation does not suffer from a diffusion mechanism such as Silk dumping and the 21 cm fluctuations on small scales remain until today. Consequently, the available information from 21 cm fluctuations is dramatically improved compared with that from CMB fluctuations. Furthermore, 21 cm radiation is emitted from each redshift and many maps are available. For the above reason, 21 cm lensing reconstruction noise would become quite small compared with CMB lensing reconstruction noise. Therefore, although second-order vector and tensor signals tend to be small, there is a possibility to detect these secondorder signals in 21 cm lensing.

In this section, we focus on the 21 cm lensing curl mode induced from the secondorder vector mode. Our aim is to estimate the signal-to-noise ratio of the 21 cm curl mode from the second-order vector mode in ideal experiments. In standard cosmology, the first-order vector mode always decays and is neglected in linear theory. The detection of the cosmological vector mode is quite important because it would become a proof of the cosmological perturbation theory itself and the validity of the scalar, vector, and tensor decomposition.

5.2 21 cm Radiation in the Dark Ages

Throughout this section, we focus on the redshift $z\gtrsim 30$ since we are interested in the weak lensing signals from the dark ages. During the dark ages, we can ignore the effect of Ly α photons emitted from astronomical objects. Neutral hydrogen atoms form after the recombination epoch ($z\approx 1100$), and the effect of Ly α photons from stars dominates on the evolution of neutral hydrogen atoms after $z\approx 30$. However, during $200\lesssim z\lesssim 1100$, thermal coupling between residual electrons and CMB photons brings the spin temperature of hydrogen atoms to the CMB temperature, and therefore no 21 cm signal comes from this period. Consequently, we can observe 21 cm radiation during $30\lesssim z\lesssim 200$. In this subsection, we review the 21 cm physics following in Ref. [6].

The Boltzmann equation for 21 cm photons $f_{21}(\eta, \mathbf{x}, \epsilon, \hat{\mathbf{n}})$ can be written as

$$\frac{\mathrm{d}f_{21}}{\mathrm{d}\lambda} = C_{\mathrm{H}}[f_{21}]\,,\tag{5.1}$$

where λ , ϵ , and \hat{n} are the affine parameter, the energy of 21 cm photons, and the direction of 21 cm photons, respectively. $C_{\rm H}[f_{21}]$ is the collision term due to the 21 cm interaction. The aim of this subsection, we derive the Boltzmann equation for the 21 cm photons.

5.2.1 21 cm Interaction

Here, we derive the collision term of the Boltzmann equation for 21 cm photons due to the 21 cm interaction. At first, we work in the neutral hydrogen gas rest frame. The number of 21 cm photons emitted per unit volume in a time interval $\mathrm{d}t_{\mathrm{g}}$ within solid angle $\mathrm{d}\Omega$ within energy $\mathrm{d}E$ can be written as

$$dn_{21} = \frac{1}{4\pi} \left[n_1 \left(A_{10} + B_{10} I_{\nu} \right) - n_0 \left(B_{01} I_{\nu} \right) \right] \phi_{\text{line}} (E_g - E_{21}) dt_g dE d\Omega$$

$$= \frac{1}{4\pi} \left[\left(n_1 - 3n_0 \right) \mathcal{N}_{\nu} + n_1 \right] A_{10} \phi_{\text{line}} (E_g - E_{21}) dt_g dE d\Omega , \qquad (5.2)$$

where $n_1(\eta, \boldsymbol{x})$, $n_0(\eta, \boldsymbol{x})$, A_{10} , B_{10} , and B_{01} are the number density of the neutral hydrogen gas with the excited (triplet) state, that with the ground (singlet) state, and the Einstein coefficients, respectively. And $I_{\nu}(\eta, \boldsymbol{x}, p, \hat{\boldsymbol{n}})$ is the energy intensity of the radiative fields and $\mathcal{N}_{\nu}(\eta, \boldsymbol{x}, p, \hat{\boldsymbol{n}}) \equiv c^2/(2h_{\text{pl}}\nu^3)I_{\nu}(\eta, \boldsymbol{x}, p, \hat{\boldsymbol{n}})$ is the incident photon number of the radiative fields. The $\phi_{\text{line}}(E-E_{21})$ is the line profile and we assume that the line profile is the Dirac delta function, $\phi_{\text{line}}[E-E_{21}] = \delta_{\text{D}}[E-E_{21}]$, in other words, we neglect the velocity states, or we focus on larger scales than the line width. Note that we do not need to consider the Einstein C-coefficient in the collision term of the Boltzmann equation since the C-coefficient is related to the excitation or de-excitation rates by the collision which is irrelevant to the emission or absorption processes of 21 cm photons.

The incident photons distribution \mathcal{N}_{ν} can be decomposed into the CMB photons and 21 cm photons as

$$\mathcal{N}_{\nu}(\eta, \boldsymbol{x}, p, \hat{\boldsymbol{n}}) = \mathcal{N}_{\text{CMB}}(\eta, \boldsymbol{x}, p, \hat{\boldsymbol{n}}) + \mathcal{N}_{21}(\eta, \boldsymbol{x}, p, \hat{\boldsymbol{n}})$$

$$= \left[\exp \left[\frac{h_{\text{pl}} \nu}{k_{\text{B}} T_{\text{CMB}}(\eta, \boldsymbol{x}, \hat{\boldsymbol{n}})} \right] - 1 \right]^{-1} + \mathcal{N}_{21}(\eta, \boldsymbol{x}, p, \hat{\boldsymbol{n}}), \quad (5.3)$$

where $h_{\rm pl}$ is the Planck constant. When we derive the above equation, we assume that the CMB is perfectly black body spectrum. Furthermore, in the radio astronomy, except for the very low temperature region ($\sim O(10)$ K) or the higher frequency

region than the millimeter waves (O(100) GHz), we can use the Rayleigh-Jeans Law as

$$\mathcal{N}_{\nu}(\eta, \mathbf{x}, p, \hat{\mathbf{n}}) \approx \frac{k_{\rm B} T_{\rm CMB}(\eta, \mathbf{x}, \hat{\mathbf{n}})}{h_{\rm pl} \nu} \bigg|_{\nu = \nu_{21}} + \mathcal{N}_{21}(\eta, \mathbf{x}, p, \hat{\mathbf{n}})
= \frac{T_{\rm CMB}(\eta, \mathbf{x}, \hat{\mathbf{n}})}{T_{21}} + \mathcal{N}_{21}(\eta, \mathbf{x}, p, \hat{\mathbf{n}}) \quad \text{(unit in } k_{\rm B} = h_{\rm pl} = 1) ,$$
(5.4)

where the condition $\nu = \nu_{21}$ is coming from the Delta function of the line profile. Note that $T_{21} = 0.068~{\rm K} \ll T_{\rm CMB}^{(0)} = 2.7(1+z)~{\rm K}$. The CMB temperature has fluctuation itself and we can write this accounting for working in the gas rest frame as

$$T_{\text{CMB}}(\eta, \mathbf{x}, \hat{\mathbf{n}}) = T_{\text{CMB}}^{(0)} \left[1 + \Theta_{\text{CMB}}^{(1)}(\eta, \mathbf{x}, \hat{\mathbf{n}}) - \hat{\mathbf{n}} \cdot \mathbf{v}_{g}^{(1)}(\eta, \mathbf{x}) \right].$$
 (5.5)

Next, we derive the changes of the distribution function by the 21 cm interaction during the dark ages. The changes of the number density dn_{21} can be related the changes of the distribution function as

$$dn_{21} = \frac{df}{c^3} d\Omega E^2 dE = \frac{2d\mathcal{N}_{21}}{c^3} d\Omega \nu^2 d\nu , \qquad (5.6)$$

where the factor 2 in the third equality is coming from the state of photons, namely, the photon has two polarized states. Note that the relation between the number density and the distribution function is written as

$$n = \frac{1}{ch_{\rm pl}\nu}I(t, \mathbf{x}, \nu, \hat{\mathbf{n}}) = \frac{h_{\rm pl}^3\nu^2}{c^3}f(t, \mathbf{x}, \mathbf{p}).$$
 (5.7)

We change from the gas rest frame time to the affine parameter as

$$dt_{g} = u_{g}^{\mu} dx_{\mu}$$

$$= k_{\mu} u_{g}^{\mu} d\lambda$$

$$= E_{o} d\lambda . \qquad (5.8)$$

Before moving to write down the changes of the distribution function due to the 21 cm source, we write n_0 and n_1 as a function of the spin temperature $T_s(\eta, \boldsymbol{x}, \hat{\boldsymbol{n}})$. The spin temperature is defined by the ratio of the number density in the upper states to the lower ones as

$$\frac{n_1}{n_0} = \frac{g_1}{g_0} \exp\left(-\frac{\Delta E_{10}}{k_{\rm B} T_{\rm s}}\right),$$
 (5.9)

where $n_{1,0}$, $g_{1,0}$, and ΔE_{10} are the number density for each state, the number of degenerate states for each state, and the energy difference between the upper and

lower states, respectively. In the case of the hyperfine structure of neutral hydrogen atoms, $g_1 = 3$, $g_0 = 1$, and $\Delta E_{21} = h_{\rm pl}\nu_{\rm 21cm}$, where $\nu_{\rm 21cm} \approx 1420\,{\rm MHz}$. The spin temperature is determined by the evolution of the n_1 and n_0 . In other words, the spin temperature depends on which physical process plays the excitation and deexcitation. By using Eq. (5.9), we can write

$$n_1(\eta, \mathbf{x}) - 3n_0(\eta, \mathbf{x}) = 3n_{\text{HI}}(\eta, \mathbf{x}) \frac{1 - e^{T_{21}/T_s(\eta, \mathbf{x})}}{3 + e^{T_{21}/T_s(\eta, \mathbf{x})}},$$
 (5.10)

where we use the number density of the neutral hydrogen $n_{\rm HI}$ is written by the sum of the n_0 and n_1 , namely, $n_{\rm HI} = n_0 + n_1$. By using Eqs. (5.2), (5.4), (5.6), (5.8), and (5.10), we can write

$$C_{H}[f_{21}] = \frac{c^{3}E_{21}}{4\pi E_{21}^{2}} \frac{3A_{10}n_{HI}(\eta, \mathbf{x})}{3 + e^{T_{21}/T_{s}(\eta, \mathbf{x})}} \times \left[\left(1 - e^{T_{21}/T_{s}(\eta, \mathbf{x})} \right) \left(\frac{T_{CMB}(\eta, \mathbf{x}, \hat{\mathbf{n}})}{T_{21}} + \frac{h_{pl}^{3}}{2} f_{21}(\eta, \mathbf{x}, p, \hat{\mathbf{n}}) \right) + 1 \right] \delta_{D}[E_{g} - E_{21}].$$
(5.11)

Finally, we derive the collision term due to the 21 cm interaction. The left-hand side of Eq. (5.1) is already derived in Sect. 2.4. In the next, we expand the Boltzmann equation for 21 cm photons up to the first order.

5.2.2 Perturbed Boltzmann Equation for 21 cm Photons

Hereafter, we expand each variable:

$$n_{\rm HI}(\eta, \mathbf{x}) = n_{\rm HI}^{(0)}(\eta) \left[1 + \Delta_{n_{\rm HI}}^{(1)}(\eta, \mathbf{x}) \right],$$
 (5.12)

$$T_{s}(\eta, \mathbf{x}) = T_{s}^{(0)}(\eta) \left[1 + \Delta_{T_{s}}^{(1)}(\eta, \mathbf{x}) \right], \tag{5.13}$$

$$T_{\text{CMB}}(\eta, \mathbf{x}, \hat{\mathbf{n}}) = T_{\text{CMB}}^{(0)}(\eta) \left[1 + \Theta_{\text{CMB}}^{(1)}(\eta, \mathbf{x}, \hat{\mathbf{n}}) - \hat{\mathbf{n}} \cdot \mathbf{v}_{g}^{(1)}(\eta, \mathbf{x}) \right],$$
 (5.14)

$$f_{21}(\eta, \mathbf{x}, p, \hat{\mathbf{n}}) = f_{21}^{(0)}(\eta, p) \left[1 + \Delta_{f_{21}}^{(1)}(\eta, \mathbf{x}, p, \hat{\mathbf{n}}) \right]$$
$$= f_{21}^{(0)}(\eta, p) + \delta f_{21}^{(1)}(\eta, \mathbf{x}, p, \hat{\mathbf{n}}). \tag{5.15}$$

In addition, we assume that the spin temperature is higher than the 21 cm temperature, that is, $T_{21} \ll T_{\rm s}^{(0)}$. In other words, we leave the factor $T_{21}/T_{\rm s}$ up to the first order in our calculation. This assumption is valid during the dark ages.

Performing the first-order perturbation, we derive

$$\begin{split} C_{\rm H}[f_{21}] &= \frac{3c^3 A_{10} n_{HI}^{(0)}}{16\pi E_{21}} \frac{T_{\rm s}^{(0)} - T_{\rm CMB}^{(0)}}{T_{\rm s}^{(0)}} \left[1 + \Delta_{n_{\rm HI}}^{(1)}(\eta, \mathbf{x}) \right. \\ &- \frac{T_{\rm CMB}^{(0)}}{T_{\rm s}^{(0)} - T_{\rm CMB}^{(0)}} \left(\Theta_{\rm CMB}^{(1)}(\eta, \mathbf{x}, \hat{\mathbf{n}}) - \hat{\mathbf{n}} \cdot \mathbf{v}_{\rm g}^{(1)}(\eta, \mathbf{x}) - \Delta_{T_{\rm s}}^{(1)}(\eta, \mathbf{x}) \right) \\ &- \frac{h_{\rm pl}^3}{2} \frac{T_{21}}{T_{\rm s}^{(0)} - T_{\rm CMB}^{(0)}} f_{21}^{(0)}(\eta, p) \left(1 + \Delta_{f_{21}}^{(1)}(\eta, \mathbf{x}, p, \hat{\mathbf{n}}) - \Delta_{T_{\rm s}}^{(1)}(\eta, \mathbf{x}) + \Delta_{n_{\rm HI}}^{(1)}(\eta, \mathbf{x}) \right) \right] \delta_{\rm D}[E_{\rm g} - E_{21}] \,. \end{split}$$

$$(5.16)$$

Note that the $E \propto a^{-1}$ is the photon energy measured in the expanding universe. The comoving photon energy ϵ can be expressed as $p = E = \epsilon/a$. When we treat the distribution function for 21 cm photons as the function of ϵ , namely, $f_{21} = f_{21}(\eta, \mathbf{x}, \epsilon, \hat{\mathbf{n}})$, the left-hand side of Eq. (5.1) becomes

$$\frac{\partial f_{21}}{\partial \eta} + \frac{\mathrm{d}x^{i}}{\mathrm{d}\eta} \frac{\partial f_{21}}{\partial x^{i}} + \frac{\mathrm{d}\epsilon}{\mathrm{d}\eta} \frac{\partial f_{21}}{\partial \epsilon} + \frac{\mathrm{d}\hat{n}^{i}}{\mathrm{d}\eta} \frac{\partial f_{21}}{\partial \hat{n}^{i}} = \frac{1}{P^{0}} C_{\mathrm{H}}[f_{21}]. \tag{5.17}$$

Here, we focus only the expansion of the collision term, since the left-hand side is well discussed in Sect. 2.4. By using Eqs. (2.51) and (5.17), finally, we can give the right-hand side of Eq. (5.1) as

$$\frac{1}{P^{0}}C_{H}[f_{21}] = a \frac{3c^{3}A_{10}n_{HI}^{(0)}}{16\pi E_{21}^{2}} \frac{T_{s}^{(0)} - T_{CMB}^{(0)}}{T_{s}^{(0)}} \left[1 + \Psi^{(1)} - \hat{\boldsymbol{n}} \cdot \boldsymbol{v}_{g}^{(1)}(\eta, \boldsymbol{x}) + \Delta_{n_{HI}}^{(1)}(\eta, \boldsymbol{x}) \right. \\
\left. - \frac{T_{CMB}^{(0)}}{T_{s}^{(0)} - T_{CMB}^{(0)}} \left(\Theta_{CMB}^{(1)}(\eta, \boldsymbol{x}, \hat{\boldsymbol{n}}) - \hat{\boldsymbol{n}} \cdot \boldsymbol{v}_{g}^{(1)}(\eta, \boldsymbol{x}) - \Delta_{T_{s}}^{(1)}(\eta, \boldsymbol{x}) \right) \right. \\
\left. - \frac{h_{pl}^{3}}{2} \frac{T_{21}}{T_{s}^{(0)} - T_{CMB}^{(0)}} f_{21}^{(0)}(\eta, \boldsymbol{p}) \left(1 + \Psi^{(1)} - \hat{\boldsymbol{n}} \cdot \boldsymbol{v}_{g}^{(1)}(\eta, \boldsymbol{x}) \right. \\
\left. + \Delta_{f_{21}}^{(1)}(\eta, \boldsymbol{x}, \boldsymbol{p}, \hat{\boldsymbol{n}}) - \Delta_{T_{s}}^{(1)}(\eta, \boldsymbol{x}) + \Delta_{n_{HI}}^{(1)}(\eta, \boldsymbol{x}) \right) \right] \delta_{D} \left[\frac{\epsilon}{a} \left(1 - \hat{\boldsymbol{n}} \cdot \boldsymbol{v}_{g}^{(1)}(\eta, \boldsymbol{x}) \right) - E_{21} \right], \tag{5.18}$$

where the delta function can be expanded as

$$\delta_{\mathrm{D}}\left[\frac{\epsilon}{a}\left(1-\hat{\boldsymbol{n}}\cdot\boldsymbol{v}_{\mathrm{g}}^{(1)}(\eta,\boldsymbol{x})\right)-E_{21}\right]=\delta_{\mathrm{D}}\left[\frac{\epsilon}{a}-E_{21}\right]+\epsilon\partial_{\epsilon}\delta_{\mathrm{D}}\left[\frac{\epsilon}{a}-E_{21}\right]\left(-\hat{\boldsymbol{n}}\cdot\boldsymbol{v}_{\mathrm{g}}^{(1)}(\eta,\boldsymbol{x})\right). \tag{5.19}$$

In the following section, we shoe the background equation and the first-order perturbation equation.

5.2.3 Background Equation

From here, we focus on the background evolution by using Eqs. (5.17) and (5.18). The background evolution equation for the photon distribution function can be written as

$$\frac{\partial f_{21}^{(0)}}{\partial \eta} = a \frac{3c^3 A_{10} n_{HI}^{(0)}}{16\pi E_{21}^2} \frac{T_s^{(0)} - T_{\text{CMB}}^{(0)}}{T_s^{(0)}} \left[1 - \frac{h_{\text{pl}}^3}{2} \frac{T_{21}}{T_s^{(0)} - T_{\text{CMB}}^{(0)}} f_{21}^{(0)}(\eta, \epsilon) \right] \delta_{\text{D}} \left[\frac{\epsilon}{a} - E_{21} \right], \tag{5.20}$$

furthermore, the above equation can be rewritten as

$$\frac{\partial f_{21}^{(0)}}{\partial \eta} = a \rho_{\rm s}^{(0)} \delta_{\rm D} \left[\frac{\epsilon}{a(\eta)} - E_{21} \right] - \dot{\tau}^{(0)} f_{21}^{(0)}(\eta, \epsilon) , \qquad (5.21)$$

where we define

$$\rho_{\rm s}^{(0)}(\eta) \equiv \frac{3c^3 A_{10} n_{\rm HI}^{(0)}}{16\pi E_{21}^2} \frac{T_{\rm s}^{(0)} - T_{\rm CMB}^{(0)}}{T_{\rm s}^{(0)}} , \qquad (5.22)$$

$$\dot{\tau}^{(0)}(\eta, \epsilon) \equiv a \frac{3c^3 A_{10} h_{\rm pl}^3 T_{21} n_{\rm HI}^{(0)}}{32\pi E_{21}^2 T_{\rm s}^{(0)}} \delta_{\rm D} \left[\frac{\epsilon}{a(\eta)} - E_{21} \right]
\equiv a \tau_{\rm s}^{(0)} \delta_{\rm D} \left[\frac{\epsilon}{a(\eta)} - E_{21} \right] ,$$
(5.23)

$$\tau_{\rm s}^{(0)}(\eta) \equiv \frac{3c^3 A_{10} h_{\rm pl}^3 T_{21} n_{\rm HI}^{(0)}}{32\pi E_{21}^2 T_{\rm s}^{(0)}} \ . \tag{5.24}$$

Note that the relation between τ_s and $\rho_s^{(0)}$ is

$$\tau_{\rm s}^{(0)}(\eta) = \frac{h_{\rm pl}^3}{2} \frac{T_{21}}{T_{\rm s}^{(0)} - T_{\rm CMB}^{(0)}} \rho_{\rm s}^{(0)}(\eta) . \tag{5.25}$$

This differential optical depth $\dot{\tau}^{(0)}$ defined in Eq. (5.24) can be formally integrated by using the Heaviside step function $\Theta_{\rm H}(x)$ as

$$\tau^{(0)}(\eta, \epsilon) = \left[\frac{3c^{3}A_{10}h_{\text{pl}}^{3}}{32\pi k_{\text{B}}E_{21}^{2}} \frac{n_{HI}^{(0)}(\eta_{\epsilon})}{T_{\text{s}}^{(0)}(\eta_{\epsilon})H(\eta_{\epsilon})} \right]_{\epsilon=a(\eta_{\epsilon})E_{21}} \Theta_{\text{H}}(\eta - \eta_{\epsilon})$$

$$\equiv \tau_{\epsilon}^{(0)}\Theta_{\text{H}}(\eta - \eta_{\epsilon}) , \qquad (5.26)$$

where we define

$$\tau_{\epsilon}^{(0)} \equiv \left[\frac{3c^3 A_{10} h_{\rm pl}^3}{32\pi k_{\rm B} E_{21}^2} \frac{n_{HI}^{(0)}(\eta_{\epsilon})}{T_{\rm s}^{(0)}(\eta_{\epsilon}) H(\eta_{\epsilon})} \right]_{\epsilon = a(\eta_{\epsilon}) E_{21}}.$$
 (5.27)

When we derive the above solution, we use the property of the Dirac delta function:

$$\delta_{\rm D}[f(x)] = \sum_{i} \frac{1}{|f'(a_i)|} \delta_{\rm D}[x - a_i] \quad (f(a_i) = 0) . \tag{5.28}$$

By using these definitions, we can solve Eq. (5.20):

$$f_{21}^{(0)}(\eta, E) = \frac{1 - e^{-\tau^{(0)}}}{\tau_{\epsilon}^{(0)}} \left[\frac{\rho_{\rm s}^{(0)}}{E_{21}H} \right]_{\epsilon} . \tag{5.29}$$

The relation between the brightness temperature and the distribution function is given by

$$\delta T_{\rm b} = \frac{h_{\rm pl}^3}{2k_{\rm B}} E_{\rm obs} f_{21} , \qquad (5.30)$$

where, in our notation, the distribution function of 21 cm photons f_{21} are already subtracted from the distribution function of the CMB photons. Consequently, by using the above relation, we can get the net brightness temperature as a background source of the CMB photons as

$$\delta T_{\rm h} \equiv T_{\rm h} - T_{\rm CMB} \ . \tag{5.31}$$

Finally, we can get the back ground net brightness temperature as

$$\delta T_{\rm b}^{(0)} = \left(1 - e^{-\tau^{(0)}}\right) \left[\frac{T_{\rm s}^{(0)} - T_{\rm CMB}^{(0)}}{1 + z} \right], \tag{5.32}$$

where we use the observed photon energy corresponds to the comoving energy, namely, $E_{\rm obs} = \epsilon$. This solution does not close itself. We need to know the evolution of the spin temperature. The evolution of the spin temperature can be derived by using the detailed valance of the coupling. The discussion of the detailed valance is shown in the next subsection.

5.2.4 Perturbed Equation

Next, we consider the first order perturbation. We can find that the definitions of the physical variables, the angular dependence of the direction of photons is included in $\Theta_{\text{CMB}}^{(1)}(\eta, \boldsymbol{x}, \hat{\boldsymbol{n}})$. Other terms does not depend on the photon direction, namely, the

monopole terms. Therefore we expand the CMB anisotropy for the scalar mode by multipole expansion as

$$\Theta_{\text{CMB}}^{(1)}(\eta, \mathbf{x}, \hat{\mathbf{n}}) \Big|_{\text{scalar}} = \Theta_{0,0}^{(1)}(\eta, \mathbf{x}) + \hat{\mathbf{n}} \cdot \mathbf{v}_{\gamma}^{(1)}(\eta, \mathbf{x}) + \Theta_{+}^{(1)}(\eta, \mathbf{x}, \hat{\mathbf{n}}) , \qquad (5.33)$$

where we use the fact that $\Theta_{1,0}^{(1)}(\eta, \mathbf{x}) = 4v_{\gamma 0}^{(1)}(\eta, \mathbf{x})$ and we define higher multipoles as

$$\Theta_{+}^{(1)}(\eta, \mathbf{x}, \hat{\mathbf{n}}) \equiv \sum_{\ell=2}^{\infty} (-i)^{\ell} \sqrt{\frac{4\pi}{2\ell+1}} \Theta_{\ell,0}^{(1)}(\eta, \mathbf{x}) Y_{\ell,0}(\hat{\mathbf{n}}) . \tag{5.34}$$

Therefore, we define the first-order monopole source by using the above notation as

$$\Delta_{\rm s}^{(1)} \equiv \Delta_{n_{\rm HI}}^{(1)} + \frac{T_{\rm CMB}^{(0)}}{T_{\rm s}^{(0)} - T_{\rm CMB}^{(0)}} \left(\Delta_{T_{\rm s}}^{(1)} - \Theta_{0,0}^{(1)} \right) . \tag{5.35}$$

From Eqs. (5.17), (5.18), and (5.33), the first-order Boltzmann equation can be rewritten as

$$\begin{split} &\frac{\partial \delta f_{21}^{(1)}}{\partial \eta} + \hat{n}^{i} \frac{\partial \delta f_{21}^{(1)}}{\partial x^{i}} + \dot{\tau}^{(0)} \delta f_{21}^{(1)}(\eta, \boldsymbol{x}, \epsilon, \hat{\boldsymbol{n}}) \\ &= a \rho_{s}^{(0)} \bigg[\Delta_{s}^{(1)}(\eta, \boldsymbol{x}) + \Psi^{(1)} - \hat{\boldsymbol{n}} \cdot \boldsymbol{v}_{g}^{(1)}(\eta, \boldsymbol{x}) \\ &- \frac{T_{\text{CMB}}^{(0)}}{T_{s}^{(0)} - T_{\text{CMB}}^{(0)}} \left\{ \hat{\boldsymbol{n}} \cdot \left(\boldsymbol{v}_{\gamma}^{(1)}(\eta, \boldsymbol{x}) - \boldsymbol{v}_{g}^{(1)}(\eta, \boldsymbol{x}) \right) + \Theta_{+}^{(1)}(\eta, \boldsymbol{x}, \hat{\boldsymbol{n}}) \right\} \bigg] \delta_{D} \left[\frac{\epsilon}{a} - E_{21} \right] \\ &- \dot{\tau}^{(0)} f_{21}^{(0)}(\eta, \epsilon) \left(\Delta_{n_{\text{HI}}}^{(1)}(\eta, \boldsymbol{x}) - \Delta_{T_{s}}^{(1)}(\eta, \boldsymbol{x}) + \Psi^{(1)} - \hat{\boldsymbol{n}} \cdot \boldsymbol{v}_{g}^{(1)}(\eta, \boldsymbol{x}) \right) \\ &+ \epsilon \left[\partial_{\epsilon} \dot{f}_{21}^{(0)} + \dot{\tau}^{(0)} \partial_{\epsilon} f_{21}^{(0)} \right] (-\hat{\boldsymbol{n}} \cdot \boldsymbol{v}_{g}^{(1)}(\eta, \boldsymbol{x})) - \epsilon \partial_{\epsilon} f_{21}^{(0)} \left(\dot{\Psi}^{(1)} + \dot{\Phi}^{(1)} - \frac{d\Psi^{(1)}}{d\eta} \right), \end{split}$$

$$(5.36)$$

where to remove the derivative of the delta function, we use Eq. (5.21) as

$$a\left(\rho_{s}^{(0)} - \tau_{s}^{(0)}f_{21}^{(0)}\right)\partial_{\epsilon}\delta_{D}\left[\frac{\epsilon}{a} - E_{21}\right] = \partial_{\epsilon}\dot{f}_{21}^{(0)} + \dot{\tau}^{(0)}\partial_{\epsilon}f_{21}^{(0)}. \tag{5.37}$$

If there is the residual photons or reionization photons, we need to consider the effects from the Thomson scattering as

$$\frac{1}{P^0}C_{\rm T} = \dot{\tau}_{\rm c}^{(0)} \left[f_{21}^{(1)}(\eta, \mathbf{x}, \epsilon, \hat{\mathbf{n}}) + \epsilon \partial_{\epsilon} f_{21}^{(0)}(\eta, \epsilon) (\hat{\mathbf{n}} \cdot \mathbf{v}_{\rm g}^{(1)}(\eta, \mathbf{x})) - f_{21 \rm mono}^{(1)}(\eta, \mathbf{x}, \epsilon) - \frac{1}{2} f_{21 \rm quad}^{(1)}(\eta, \mathbf{x}, \epsilon, \hat{\mathbf{n}}) \right], \tag{5.38}$$

where $\dot{\tau}_{\rm c}^{(0)} \equiv -a n_{\rm e}^{(0)} \sigma_{\rm T}$. Moreover, we define the monopole and quadruple parts of $f_{21}^{(1)}$ as $f_{21{\rm mono}}^{(1)}$ and $f_{21{\rm quad}}^{(1)}$, respectively. These can be rewritten as

$$f_{21\text{mono}}^{(1)} = f_{21\ 0}^{(1)} P_0(\hat{\boldsymbol{n}} \cdot \hat{\boldsymbol{z}})$$

= $f_{21\ 0\ 0}^{(1)} \sqrt{4\pi} Y_{0\ 0}(\hat{\boldsymbol{n}})$, (5.39)

$$f_{21\text{quad}}^{(1)} = 5f_{212}^{(1)}P_{2}(\hat{\boldsymbol{n}} \cdot \hat{\boldsymbol{z}})$$

$$= (-i)^{2} \sqrt{\frac{4\pi}{5}} f_{212,0}^{(1)} Y_{2,0}(\hat{\boldsymbol{n}}) . \tag{5.40}$$

Considering this effect, we can rewrite Eq. (5.36) (and hereafter for simplicity, we remove the argument) as

$$\begin{split} &\frac{\partial \delta f_{21}^{(1)}}{\partial \eta} + \hat{n}^{i} \frac{\partial \delta f_{21}^{(1)}}{\partial x^{i}} + \left(\dot{\tau}^{(0)} - \dot{\tau}_{c}^{(0)}\right) \delta f_{21}^{(1)} \\ &= a \rho_{s}^{(0)} \left[\Delta_{s}^{(1)} + \Psi^{(1)} - \hat{\boldsymbol{n}} \cdot \boldsymbol{v}_{g}^{(1)} - \frac{T_{\text{CMB}}^{(0)}}{T_{s}^{(0)} - T_{\text{CMB}}^{(0)}} \left\{ \hat{\boldsymbol{n}} \cdot \left(\boldsymbol{v}_{\gamma}^{(1)} - \boldsymbol{v}_{g}^{(1)} \right) + \Theta_{+}^{(1)} \right\} \right] \delta_{D} \left[\frac{\epsilon}{a} - E_{21} \right] \\ &- \dot{\tau}^{(0)} f_{21}^{(0)} \left(\Delta_{n_{\text{HI}}}^{(1)} - \Delta_{T_{s}}^{(1)} + \Psi^{(1)} - \hat{\boldsymbol{n}} \cdot \boldsymbol{v}_{g}^{(1)} \right) + \epsilon \left[\partial_{\epsilon} \dot{f}_{21}^{(0)} + \dot{\tau}^{(0)} \partial_{\epsilon} f_{21}^{(0)} \right] (-\hat{\boldsymbol{n}} \cdot \boldsymbol{v}_{g}^{(1)}) \\ &- \epsilon \partial_{\epsilon} f_{21}^{(0)} \left(\dot{\Psi}^{(1)} + \dot{\Phi}^{(1)} - \frac{d\Psi^{(1)}}{d\eta} \right) + \dot{\tau}_{c}^{(0)} \left[\epsilon \partial_{\epsilon} f_{21}^{(0)} (\hat{\boldsymbol{n}} \cdot \boldsymbol{v}_{g}^{(1)}) - \delta f_{21 \text{mono}}^{(1)} - \frac{1}{2} \delta f_{21 \text{quad}}^{(1)} \right]. \end{split} \tag{5.41}$$

As well as the formulation of the CMB fluctuations, we can use the line-of-sight integration. By performing the line-of-sight integration, after a long but straightforward calculation, we derive the line-of-sight integrated solution:

$$\begin{split} \delta f_{21}^{(1)}(\eta_{\mathrm{O}}, \mathbf{x}_{\mathrm{O}}, \epsilon, \hat{\mathbf{n}}_{\mathrm{O}}) &= e^{-\tau_{\mathrm{c}}^{(0)}} \bar{f}_{21}^{(0)} \bigg[\Delta_{\mathrm{s}}^{(1)}(\eta, \mathbf{x}) + \Psi^{(1)}(\eta, \mathbf{x}) + \hat{\mathbf{n}}_{\mathrm{O}} \cdot \mathbf{v}_{\mathrm{g}}^{(1)}(\eta, \mathbf{x}) \\ &+ \frac{T_{\mathrm{CMB}}^{(0)}}{T_{\mathrm{s}}^{(0)} - T_{\mathrm{CMB}}^{(0)}} \bigg\{ \hat{\mathbf{n}}_{\mathrm{O}} \cdot \bigg(\mathbf{v}_{\gamma}^{(1)}(\eta, \mathbf{x}) - \mathbf{v}_{\mathrm{g}}^{(1)}(\eta, \mathbf{x}) \bigg) - \Theta_{+}^{(1)}(\eta, \mathbf{x}, \hat{\mathbf{n}}_{\mathrm{O}}) \bigg\} \\ &+ \frac{\tau_{\gamma}^{(0)}}{T_{\mathrm{c}}} \bigg\{ -\frac{\mathrm{d}\Psi^{(1)}(\eta, \mathbf{x})}{\mathrm{d}\eta} + \dot{\Psi}^{(1)}(\eta, \mathbf{x}) - \dot{\Phi}^{(1)}(\eta, \mathbf{x}) + \hat{\mathbf{n}}_{\mathrm{O}} \cdot \frac{\mathrm{d}\mathbf{v}_{\mathrm{g}}^{(1)}(\eta, \mathbf{x})}{\mathrm{d}\eta} \bigg\} \bigg]_{\epsilon} \\ &+ e^{-\tau_{\mathrm{c}}^{(0)}} \bar{f}_{21,\ln\epsilon}^{(0)} \bigg[e^{\tau_{\mathrm{c}}^{(0)}} \Psi^{(1)}(\eta_{\mathrm{O}}, \mathbf{x}_{\mathrm{O}}) - \Psi^{(1)}(\eta_{\epsilon}, \mathbf{x}_{\epsilon}) + \hat{\mathbf{n}}_{\mathrm{O}} \cdot \mathbf{v}_{\mathrm{g}}^{(1)}(\eta_{\epsilon}, \mathbf{x}_{\epsilon}) \bigg] \\ &- \bar{f}_{21,\ln\epsilon}^{(0)} \int_{\eta_{\epsilon}}^{\eta_{\mathrm{O}}} \mathrm{d}\eta \ e^{-\tau_{\mathrm{c}}^{(0)}} \bigg(\Psi^{(1)}(\eta, \mathbf{x}) + \Phi^{(1)}(\eta, \mathbf{x}) \bigg) \\ &+ e^{-\tau_{\mathrm{c}}^{(0)}} \bar{f}_{21}^{(0)} \bigg(r_{\gamma}^{(0)} - 1 \bigg) \bigg[\Delta_{\mathrm{nH}}^{(1)}(\eta, \mathbf{x}) - \Delta_{T_{\mathrm{s}}}^{(1)}(\eta, \mathbf{x}) + \Psi^{(1)}(\eta, \mathbf{x}) + \hat{\mathbf{n}}_{\mathrm{O}} \cdot \mathbf{v}_{\mathrm{g}}^{(1)}(\eta, \mathbf{x}) \bigg]_{\epsilon} \\ &- \int_{\eta_{\epsilon}}^{\eta_{\mathrm{O}}} \mathrm{d}\eta \ \dot{\tau}_{\mathrm{c}}^{(0)} e^{-\tau_{\mathrm{c}}^{(0)}} \bigg[\delta f_{21\,\mathrm{mono}}^{(1)}(\eta, \mathbf{x}, \epsilon) \\ &+ f_{21,\ln\epsilon}^{(0)} \left(\hat{\mathbf{n}}_{\mathrm{O}} \cdot \mathbf{v}_{\mathrm{g}}^{(1)}(\eta, \mathbf{x}) - \Psi^{(1)}(\eta, \mathbf{x}) \right) + \frac{1}{2} \delta f_{21\,\mathrm{quad}}^{(1)}(\eta, \mathbf{x}, \epsilon, \hat{\mathbf{n}}_{\mathrm{O}}) \bigg], \end{split}$$

where we define the direction of the line-of-sight at the observer as $\hat{\pmb{n}} = -\hat{\pmb{n}}_{\rm O}$ and

$$r_{\tau}^{(0)} \equiv \frac{\tau_{\epsilon}^{(0)} e^{-\tau_{\epsilon}^{(0)}}}{1 - e^{-\tau_{\epsilon}^{(0)}}}.$$
 (5.43)

The perturbed distribution function of 21 cm photons is expanded by spherical harmonics as

$$a_{\ell,m}^{21\text{cm}}(z_{\epsilon}) = \int d\Omega Y_{\ell,m}^{*}(\hat{\boldsymbol{n}}) \delta f_{21}^{(1)}(\eta_{O}, \boldsymbol{x}_{O}, \epsilon, \hat{\boldsymbol{n}}) , \qquad (5.44)$$

where $Y_{\ell,m}(\hat{\boldsymbol{n}})$ is the spin-0 spherical harmonics and z_{ϵ} is the redshift at which the 21cm photon was emitted. Finally, we define the angular power spectrum $C_{\ell_1}^{21\text{cm}}(z_{\epsilon_1}, z_{\epsilon_2})$ as

$$\langle a_{\ell_1, m_1}^{21\text{cm}}(z_{\epsilon_1}) a_{\ell_2, m_2}^{21\text{cm}}(z_{\epsilon_2}) \rangle \equiv C_{\ell_1}^{21\text{cm}}(z_{\epsilon_1}, z_{\epsilon_2}) (-1)^{m_1} \delta_{\ell_1, \ell_2} \delta_{m_1, -m_2} . \tag{5.45}$$

In order to give the theoretical predictions, we need to formulate the evolution of the spin temperature T_s and the number density of the hydrogens $n_{\rm HI}$.

5.2.5 Evolution of the Spin Temperature

At first, we consider the evolution of the neutral hydrogen of lower (singlet) state. We write down the evolution of n_0 as

$$\frac{\partial n_0}{\partial \tau_{\rm g}} = -n_0 \left(C_{01} + 3A_{10} \mathcal{N}_{\nu 0} \right) + n_1 \left(C_{10} + A_{10} (1 + \mathcal{N}_{\nu 0}) \right) - \frac{1}{4} \frac{\partial x_{\rm e}}{\partial \tau_{\rm g}} \left(n_{\rm HI} + n_{\rm e} \right) ,$$
(5.46)

where we denote $C_{10} = C_{10}^{\rm HH} + C_{10}^{\rm eH} + C_{10}^{\rm pH}$ and $\mathcal{N}_{\nu 0}$ is the monopole part of the photon phase space density integrated over the line profile. In more detail, the monopole part is given in Ref. [6] as

$$\mathcal{N}_{\nu 0} = T_{\text{CMB}}^{(0)} \left(1 + \Theta_{0,0}^{(1)} \right) + \frac{\tau_{\eta}^{(0)}}{2} \left(T_{\text{s}}^{(0)} - T_{\text{CMB}}^{(0)} \right) \left[1 + \Delta_{\text{s}}^{(1)} + \Psi^{(1)} + \frac{1}{\mathcal{H}} \left(\dot{\Phi}^{(1)} - \frac{1}{3} \nabla \cdot \boldsymbol{v}_{\text{g}}^{(1)} \right) \right],$$

$$= T_{\text{CMB}}^{(0)} \left(1 + \Theta_{0,0}^{(1)} \right) + \frac{\tau_{\eta}}{2} \left(T_{\text{s}} - T_{\text{CMB}} \right). \tag{5.47}$$

Here, we focus on the case of reaching equilibrium, namely, the time derivative in Eq. (5.46) becomes zero. In this case, the spin temperature is determined as

$$T_{\rm s} \approx T_{\rm CMB} \frac{A_{10} + C_{10} T_{21} / T_{\rm CMB}}{A_{10} + C_{10} T_{21} / T_{\rm g}} + \frac{1}{2} T_{\rm s} \tau_{\eta} A_{10} \left(\frac{1}{C_{10} T_{21} / T_{\rm g} + A_{10}} - \frac{1}{C_{10} T_{21} / T_{\rm CMB} + A_{10}} \right), \tag{5.48}$$

where we expand with respect to τ_{η} and use the 0th order solution of $T_{\rm s}$. The zeroth order solution of $T_{\rm s}$ with respective to τ_{η} can be rewritten as familiar form without the Ly- α interaction as

$$T_{\rm s}^{-1} = \frac{T_{\rm CMB}^{-1} + x_{\rm c} T_{\rm g}^{-1}}{1 + x_{\rm c}} \,, \tag{5.49}$$

where we defined

$$x_{\rm c} \equiv \frac{C_{10}T_{21}}{A_{10}T_{\rm CMB}} \ . \tag{5.50}$$

All variables in the above equation is perturbable variables. In other words, we can expand, for example, $T_s = T_s^{(0)}(1 + \Delta_{T_s}^{(1)})$.

From Eq. (5.48), we can derive the difference between $\Delta_{T_s}^{(1)}$ and $\Delta_{T_{CMB}}^{(1)}$ as

$$\begin{split} \Delta_{T_{\rm s}}^{(1)} - \Delta_{T_{\rm CMB}}^{(1)} &= \left(R_{\rm CMB}^{(0)} - R_{\rm g}^{(0)} \right) \delta C_{10}^{(1)} + C_{10}^{(0)} \left(R_{\rm g}^{(0)} \Delta_{T_{\rm g}}^{(1)} - R_{\rm CMB}^{(0)} \Theta_{0,0}^{(1)} \right) \\ &+ \frac{1}{2} \tau_{\eta}^{(0)} A_{10} C_{10}^{(0)} \left[\Delta_{n_{\rm HI}}^{(1)} + \Psi^{(1)} + \frac{1}{\mathcal{H}} \left(\dot{\Phi}^{(1)} - \frac{1}{3} \nabla \cdot \boldsymbol{v}_{\rm g}^{(1)} \right) + \Delta_{C_{10}}^{(1)} \right. \\ &+ 2 \left(C_{10}^{(0)} R_{\rm CMB}^{(0)} - 1 \right) \Theta_{0,0}^{(1)} - 2 R_{\rm CMB}^{(0)} \delta C_{10}^{(1)} + \frac{T_{\rm CMB}^{(0)}}{T_{\rm g}^{(0)} - T_{\rm CMB}^{(0)}} \left(\Delta_{T_{\rm g}}^{(1)} - \Theta_{0,0}^{(1)} \right) \right], \end{split}$$

$$(5.51)$$

where we define

$$R_i^{-1} \equiv C_{10} + A_{10} \frac{T_i}{T_{21}} \,, \tag{5.52}$$

and its Taylor expansion with the definition $C_{10} = C_{10}^{(0)} + \delta C_{10}^{(1)} = C_{10}^{(0)} \left(1 + \Delta_{C_{10}}^{(1)}\right)$ as

$$R_i = R_i^{(0)} \left(1 + \frac{\delta R_i^{(1)}}{R_i^{(0)}} \right) , \qquad (5.53)$$

$$R_i^{(0)} = \left[C_{10}^{(0)} + A_{10} \frac{T_i^{(0)}}{T_{21}} \right]^{-1} , \qquad (5.54)$$

$$\frac{\delta R_i^{(1)}}{R_i^{(0)}} = R_i^{(0)} \left(C_{10}^{(0)} \Delta_{T_i}^{(1)} - \delta C_{10}^{(1)} \right) - \Delta_{T_i}^{(1)} , \qquad (5.55)$$

or

$$\frac{\left[T_{i}R_{i}\right]^{(1)}}{\left[T_{i}R_{i}\right]^{(0)}} = R_{i}^{(0)} \left(C_{10}^{(0)}\Delta_{T_{i}}^{(1)} - \delta C_{10}^{(1)}\right). \tag{5.56}$$

And note that by using R_i , we ca rewrite Eq. (5.48) as

$$R_{\text{CMB}} (T_{\text{s}} - T_{\text{CMB}}) = \left(T_{\text{g}} R_{\text{g}} - T_{\text{CMB}} R_{\text{CMB}} \right) + \frac{1}{2} \tau_{\eta} A_{10} \frac{T_{\text{g}} R_{\text{g}}}{T_{21}} \left(T_{\text{g}} R_{\text{g}} - T_{\text{CMB}} R_{\text{CMB}} \right) ,$$
(5.57)

this is useful form to derive Eq. (5.51). We can determine the evolution of the spin temperature by using Eq. (5.51).

5.2.6 Evolution of the Gas Temperature

In this section, we derive the gas kinetic temperature. There is no interaction between the gas and any other components, the gas decays adiabatically, namely, $T_{\rm g} \propto a^{-2}$. The derivation is following Sect. 3.2 of Ref. [7].

At first, we start from the definition of the energy-momentum tensor defined in Eq. (2.43) as

$$T_{\rm g}^{\mu\nu} = 2 \int \sqrt{-g} \frac{\mathrm{d}^3 P^i}{(2\pi)^3 |P_0|} P^{\mu} P^{\nu} g_g(P^{\mu}) .$$
 (5.58)

The divergence of the energy-momentum tensor is given by

$$T_{\rm g}^{\mu\nu}{}_{;\nu} = -2\int \frac{{\rm d}^3 \boldsymbol{p}}{(2\pi)^3 E} P^{\mu} \tilde{C}_{\gamma \rm e}[f] ,$$
 (5.59)

where we use the Boltzmann equation for g_g and $C_{\gamma e}$ is the Compton scattering term for photons used in Eqs. (2.95) and (2.96). Here, in order to derive the above relation, we use the fact that the Compton scattering term for gases and photons is only different from its sign, namely, the action-reaction law.

The energy momentum tensor for gases can be written as

$$T_{g}^{\mu\nu} = (\rho_{g} + P_{g}) u_{g}^{\mu} u_{g}^{\nu} + P_{g} g^{\mu\nu} , \qquad (5.60)$$

$$\rho_{g} = mn_{g} + \frac{1}{2}n_{g}m\bar{v}^{2}
= mn_{g} + \frac{3}{2}n_{g}k_{B}T_{g}
= mn_{g} + \frac{3}{2}P_{g},$$
(5.61)

$$P_{\rm g} = n_{\rm g} k_{\rm B} T_{\rm g} , \qquad (5.62)$$

where the four velocity can be written as

$$u_{\rm g}^{\mu} = \left(\frac{1}{a}(1 - \Psi), \frac{1}{a}v_{\rm g}\right).$$
 (5.63)

By using Eq. (2.51), the right-hand side in Eq. (5.59) can be written as

(r.h.s. in Eq. (5.59)) =
$$-2\frac{1-\Psi^{(1)}}{a}\int \frac{d^3\mathbf{p}}{(2\pi)^3} \tilde{C}_{e\gamma}[f]$$
, (5.64)

from the above form, we can find that the non-vanishing term is only the monopole part of the collision term. In other words, schematically, we can write the collision term as $C_{\rm e\gamma}[f] = C_{\rm mono}(p) + C_{\hat{n}}(p,\hat{n})$. Due to the integration of the \hat{n} , the latter term of this notation vanishes. Furthermore, the gas kinetic temperature is the second order compared to the velocity perturbation. Therefore, we need to expand the collision term up to the second order derived in Sect. 2.5. The non-vanishing part of the collision term is perfectly corresponding to the Kompaneets term.

The Kompaneets term can be written in Eq. (2.163) as

$$\tilde{C}_{e\gamma}\Big|_{K} = n_{e}\sigma_{T} \frac{1}{pm_{e}} \frac{\partial}{\partial p} \left[p^{4} \left\{ T_{g} \frac{\partial f^{(0)}(p)}{\partial p} + f^{(0)}(p) \left(1 + f^{(0)}(p) \right) \right\} \right], \quad (5.65)$$

where the zeroth order distribution function for photons is the Planckian as

$$f^{(0)}(p) = \frac{1}{\exp\left[p/(k_{\rm B}T_{\rm CMB}^{(0)})\right] - 1}.$$
 (5.66)

By performing the p-integral in Eq. (5.64) as

(r.h.s. in Eq. (5.59)) =
$$-\frac{1 - \Psi^{(1)}}{a} \frac{4\sigma_{\rm T} n_{\rm e} \rho_{\rm CMB}}{m_{\rm e}} k_{\rm B} \left(T_{\rm CMB} - T_{\rm g}\right)$$
, (5.67)

where we use $\rho_{\text{CMB}} = a_{\text{B}} T_{\text{CMB}}^4$, where $a_{\text{B}} \equiv \pi^2 k_{\text{B}}^4 / 15$, and we use the integral as

$$F(x) \equiv \frac{1}{e^x - 1} \,, \tag{5.68}$$

$$\int_0^\infty \mathrm{d}x x \frac{\partial}{\partial x} \left[x^4 T_{\mathrm{g}} \frac{\partial F(x)}{\partial x} + (k_{\mathrm{B}} T) F(x) (1 + F(x)) \right] = \frac{4}{15} \pi^4 \left(T_{\mathrm{CMB}} - T_{\mathrm{g}} \right) . \tag{5.69}$$

Finally, we can rewrite the right-hand side of Eq. (5.59) as

$$T_{\rm g}^{\mu\nu}{}_{;\nu} = -\frac{1 - \Psi^{(1)}}{a} \frac{4\sigma_{\rm T} n_{\rm e} \rho_{\rm CMB}}{m_{\rm e}} k_{\rm B} \left(T_{\rm CMB} - T_{\rm g} \right) ,$$
 (5.70)

$$\equiv -\frac{1 - \Psi^{(1)}}{a^2} \frac{\epsilon_{\rm C}}{k_{\rm B}} \,, \tag{5.71}$$

where we define

$$\epsilon_{\rm C} \equiv \frac{4a\sigma_{\rm T}\rho_{\rm CMB}n_{\rm e}}{m_{\rm e}}k_{\rm B}^2 \left(T_{\rm CMB} - T_{\rm g}\right) . \tag{5.72}$$

From here, we calculate the left-hand side of Eq. (5.71). By using the geodesic equation $u^{\mu}u^{\nu}_{;\mu} = 0$, the left-hand side of Eq. (5.71) can be written as

(l.h.s. in Eq. (5.71))⁰ =
$$(\rho_{g} + P_{g})_{,\nu} u_{g}^{0} u_{g}^{\nu} + P_{g,\nu} g^{0\nu} + (\rho_{g} + P_{g}) \theta_{g} u_{g}^{0}$$

= $\left[\frac{1}{a^{2}} \left(1 - 2\Psi^{(1)}\right)\right] \left[\dot{\rho}_{g} + (\rho_{g} + P_{g}) a\theta_{g} \left(1 + \Psi^{(1)}\right)\right],$
(5.73)

where we define the volume expansion rate of gas:

$$a\theta_{\rm g} \equiv u_{\rm g;\alpha}^{\alpha} = 3 \left[\mathcal{H} - \mathcal{H}\Psi^{(1)} - \dot{\Phi}^{(1)} + \frac{1}{3} v_{\rm g}^{(1)i}{}_{,i} \right].$$
 (5.74)

By combining Eqs. (5.71) and (5.73),

$$\dot{\rho}_{g} + \left(\rho_{g} + P_{g}\right) 3 \left(\mathcal{H} - \dot{\Phi}^{(1)} + \frac{1}{3} v_{g}^{(1)i}{}_{i}\right) = -\left(1 + \Psi^{(1)}\right) \frac{\epsilon_{C}}{k_{B}}.$$
 (5.75)

The evolution of the number density for gas can be derived from the Boltzmann equation of zeroth-moment in Sect. 2.6.1 as

$$\dot{n}_{g} + n_{g} v_{g}^{(1)i}{}_{,i} + 3 \left(\mathcal{H} - \dot{\Phi}^{(1)} \right) n_{g} = 0 ,$$
 (5.76)

and from this equation, the time derivative of the energy density for gas can be derived as

$$\dot{\rho}_{g} = \frac{3}{2}\dot{P}_{g} - 3\rho_{g}\left(\mathcal{H} - \dot{\Phi}^{(1)} + \frac{1}{3}v_{g}^{(1)i}{}_{i}\right), \qquad (5.77)$$

and finally by using these equation, the evolution equation for the pressure for gas can be derived from Eq. (5.75) as

$$\dot{P}_{g} + 2P_{g} \left(\mathcal{H} - \dot{\Phi}^{(1)} + \frac{1}{3} v_{g}^{(1)i}{}_{i} \right) = -\left(1 + \Psi^{(1)} \right) \frac{2\epsilon_{C}}{3k_{B}} . \tag{5.78}$$

By using Eqs. (5.62), (5.76), and (5.78), we finally derive the evolution equation for the gas temperature:

$$\dot{T}_{g} + 2T_{g} \left(\mathcal{H} - \dot{\Phi}^{(1)} + \frac{1}{3} v_{g}^{(1)i}{}_{i} \right) = -\left(1 + \Psi^{(1)} \right) \frac{2\epsilon_{C}}{3n_{g} k_{B}^{2}} . \tag{5.79}$$

The adiabatic decaying factor $\propto a^{-2}$ is coming from two facts that 1. the matter density is decaying with $\propto a^{-3}$, and 2. the matter density and pressure (corresponding to the gas temperature) are related to $\rho_{\rm g} \sim m_{\rm g} n_{\rm g} + 3/2 n_{\rm g} k_{\rm B} T_{\rm g}$ due to the rest

mass plus the internal energy term coming from the equipartition theorem with ideal monoatomic molecule.

Hereafter, we perform the perturbation. The zeroth order evolution equation can be written as

$$\dot{T}_{g}^{(0)} + 2\mathcal{H}T_{g}^{(0)} = -\frac{8a\sigma_{T}\rho_{CMB}^{(0)}x_{e}^{(0)}}{3m_{e}\left(1 + f_{He}^{(0)} + x_{e}^{(0)}\right)}\left(T_{CMB}^{(0)} - T_{g}^{(0)}\right), \tag{5.80}$$

where we denote the number density for gas as

$$n_{\rm e} = x_{\rm e} n_{\rm b} , \qquad (5.81)$$

$$n_{\rm g} = (1 + f_{\rm He} + x_{\rm e}) n_{\rm b} \,.$$
 (5.82)

And the first-order equation becomes

$$\dot{\Delta}_{T_{g}}^{(1)} = -\frac{2}{3}v_{g}^{(1)i}_{,i} + 2\dot{\Phi}^{(1)} + \frac{8a\sigma_{T}\rho_{CMB}^{(0)}x_{e}^{(0)}}{3m_{e}\left(1 + f_{He} + x_{e}^{(0)}\right)} \times \left[\left(1 - \frac{T_{CMB}^{(0)}}{T_{g}^{(0)}}\right)\left(\Psi^{(1)} + 4\Theta_{0,0}^{(1)} + \frac{1 + f_{He}}{1 + f_{He} + x_{e}^{(0)}}\Delta_{x_{e}}^{(1)}\right) + \frac{T_{CMB}^{(0)}}{T_{g}^{(0)}}\left(\Delta_{T_{g}}^{(1)} - \Theta_{0,0}^{(1)}\right)\right],$$
(5.83)

where we neglect the perturbation of the helium fraction.

By using Eq. (5.83), we can trace the temporal evolution of the spin temperature. In order to calculate the angular power spectrum of brightness temperature fluctuations, we use the public code subroutine: the CAMB sources [6]. The feature of the 21 cm power spectrum $C_\ell^{21 \text{cm}}(z_1, z_2)$ is well discussed in [6], and it was found that there is no dumping in the 21 cm power spectrum like the Silk dumping in the CMB power spectrum. For this reason, the available maximum multipole in the 21 cm power spectrum can reach $\ell_{\text{max}} \approx 10^6 \sim 10^7$, which corresponds to the Jeans scales. Compared with the CMB temperature power spectrum, the available mode increases by $10^3 \sim 10^4$. In addition to this fact, by varying the observing frequency, we can take a number of redshift slices. These advantages in using the 21 cm power spectrum help us to decrease 21 cm lensing reconstruction noise.

5.3 Results and Discussions

5.3.1 21 cm Lensing Curl Mode

In this section, we present main results of the 21 cm lensing. In Fig. 5.1, we show the angular power spectra of the curl mode induced from PGWs with r=0.1 and the second-order vector mode. We can see that the lensing signal from PGWs is

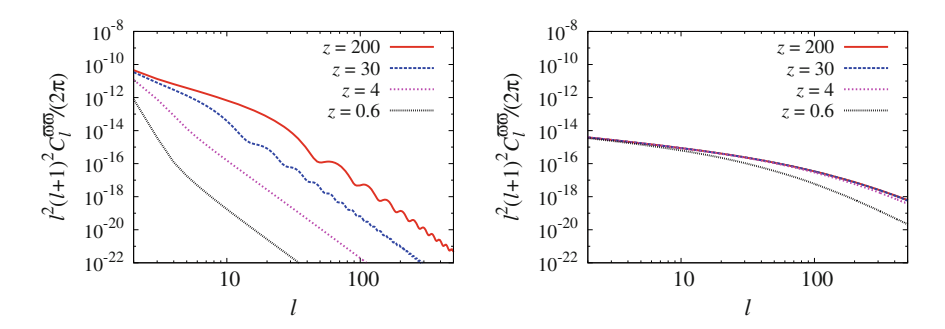


Fig. 5.1 The angular power spectra of the curl mode induced by PGWs with r=0.1 (left) and the second-order vector mode (right) for redshifts from z=200 to 0.6 as indicated in the figures. The curl mode from PGWs is substantially suppressed on small scales compared with that from the second-order vector mode

suppressed as the redshift decreases. On the other hand, the curl mode from the second-order vector mode remains almost constant. We find that the redshift dependence of the second-order vector mode is similar to that of the gradient mode from the first-order scalar potential [8]. This is because the second-order vector mode is also sourced from the first-order scalar potential. Therefore the amplitude of the second-order vector mode can have a greater amplitude than the curl mode from PGWs. The amplitude of the curl mode from the second-order vector mode is greater than that from PGWs with r=0.1 on smaller scales, such as $\ell \gtrsim 20$. Furthermore, when the tensor-to-scalar ratio is quite small, e.g., $r \lesssim 10^{-5}$, the curl mode from the second-order vector mode dominates over almost all scales. From this fact, we can conclude that even if we consider ideal observations, it would be difficult to hunt the tensor-to-scalar ratio $r \lesssim 10^{-5}$ by using 21 cm lensing.

In the next section, we show the signal-to-noise ratio of the 21 cm curl mode. Before moving the next section, we review the 21 cm lensing reconstruction for the curl mode following Ref. [1]. Because of the difference in parity between the scalar and pseudoscalar potentials (see Eq. (4.43)), we can reconstruct the gradient and curl modes separately from the maps. Throughout this section, we assume that the detectability of the curl mode is based on the quadratic estimator as was used by the Planck collaboration. The accuracy of the quadratic estimator is limited by the cosmic variance of the lensed CMB maps. In our study, by the term the *ideal experiment*, we mean that the reconstruction noise is due to the quadratic estimator without the instrumental noise.

First, as well as the CMB lensing reconstruction technique, we can reconstruct the curl mode from a single redshift slice. In this case, the reconstruction noise is given as [1, 9]

$$N_{\ell}^{\varpi\varpi} \equiv \left\langle \left| n_{\ell,m}^{\varpi} \right|^{2} \right\rangle$$

$$= \left[\frac{1}{2\ell + 1} \sum_{L_{1}, L_{2} = 2}^{\ell_{\max}} f_{\ell, L_{1}, L_{2}}^{\varpi} g_{\ell, L_{1}, L_{2}}^{\varpi} \right]^{-1} , \qquad (5.84)$$

where $f_{\ell,L_1,L_2}^{\varpi}$ and $g_{\ell,L_1,L_2}^{\varpi}$ can be expressed as follows:

$$f_{\ell,L_1,L_2}^{\varpi} = {}_{0}S_{L_1,\ell,L_2}^{\varpi}C_{L_2} - {}_{0}S_{L_2,\ell,L_1}^{\varpi}C_{L_1}, \qquad (5.85)$$

$${}_{0}S_{L,\ell,\ell'}^{\varpi} = (-i)\sqrt{\frac{(2L+1)(2\ell+1)(2\ell'+1)}{16\pi}}\sqrt{\ell(\ell+1)}\sqrt{\ell'(\ell'+1)} \times \left[\begin{pmatrix} L & \ell & \ell' \\ 0 & -1 & 1 \end{pmatrix} - \begin{pmatrix} L & \ell & \ell' \\ 0 & 1 & -1 \end{pmatrix} \right], \tag{5.86}$$

$$g_{\ell,L_1,L_2}^{\varpi} = \frac{\left(f_{\ell,L_1,L_2}^{\varpi}\right)^*}{2\tilde{C}_L\tilde{C}_{L_2}},$$
(5.87)

where C_ℓ and \tilde{C}_ℓ are the unlensed and lensed 21 cm angular power spectra, respectively. Note that due to the property of the Wigner-3j symbol, ${}_0S_{L,\ell,\ell'}^\varpi=0$, when $L+\ell+\ell'=$ even. To discuss the detectability of the 21 cm lensing curl mode, we introduce the signal-to-noise ratio as

$$\left(\frac{S}{N}\right)_{<\ell}^{\varpi\varpi} = \left[\sum_{\ell'=2}^{\ell} \left(\frac{C_{\ell'}^{\varpi\varpi}}{\Delta C_{\ell'}^{\varpi\varpi}}\right)^{2}\right]^{1/2},$$
(5.88)

where we define the error as

$$\Delta C_{\ell}^{\varpi\varpi} \equiv \sqrt{\frac{2}{2\ell+1}} \left(C_{\ell}^{\varpi\varpi} + N_{\ell}^{\varpi\varpi} \right) . \tag{5.89}$$

Note that we assume an ideal experiment where the sky coverage fraction $f_{\rm sky}$ is unity. The 21 cm angular power spectrum can extend up to the multipole moments $\ell \approx 10^6 \sim 10^7$ since there is no diffusion mechanism after the recombination epoch. Therefore, even if we use a single redshift slice to reconstruct the 21 cm curl mode, the noise spectrum from the 21 cm angular power spectrum becomes smaller than that from the CMB angular power spectrum.

Moreover, we can further reduce the noise by coadding many redshift slices. Following Ref. [1], the number of the statistically independent redshift shells can be estimated as below. The comoving distance between the neighboring statistically independent maps δR is roughly related to the highest multipole moment $\ell_{\rm max}$ used

in the lensing reconstruction as $\delta R \approx R \ell_{\rm max}^{-1}$, where R is the comoving distance corresponding to the source redshift. Therefore, the total number of available maps can be estimated as $\Delta R/\delta R \approx 0.15 \ell_{\rm max}$, where ΔR is the comoving distance between $z_{\rm min}$ and $z_{\rm max}$. If the lensing signal is mostly contributed from $z \lesssim 30$, the noise spectrum is drastically reduced by the factor of $0.15 \ell_{\rm max}$. In this section, we call this reduced noise power spectrum the coadded noise spectrum. In the following section, we present our main results and discussions.

5.3.2 Detectability and Discussions

Here, we discuss the detectability of the second-order vector mode and estimate the signal-to-noise ration based on the coadded noise spectrum. In Fig. 5.2, we depict the signal-to-noise ratio for two different values of $\ell_{\rm max}=10^5$ and 10^6 , which is our main result. For reference, we also show the signal-to-noise ratio for the case of PGWs with $r=10^{-5}$. PGWs with $r=10^{-5}$ have almost the same amplitude of the curl mode from the second-order vector mode at $\ell=2$. In the case of $\ell_{\rm max}=10^5$, the signal-to-noise ratio reaches S/N ≈ 0.11 for the PGWs and S/N ≈ 0.46 for the second-order vector mode and it would be difficult to detect the second-order vector mode and PGWs with $r=10^{-5}$. On the other hand, in the case of $\ell_{\rm max}=10^6$, we obtain S/N ≈ 4.5 for the PGWs and S/N ≈ 73 for the second-order vector mode.

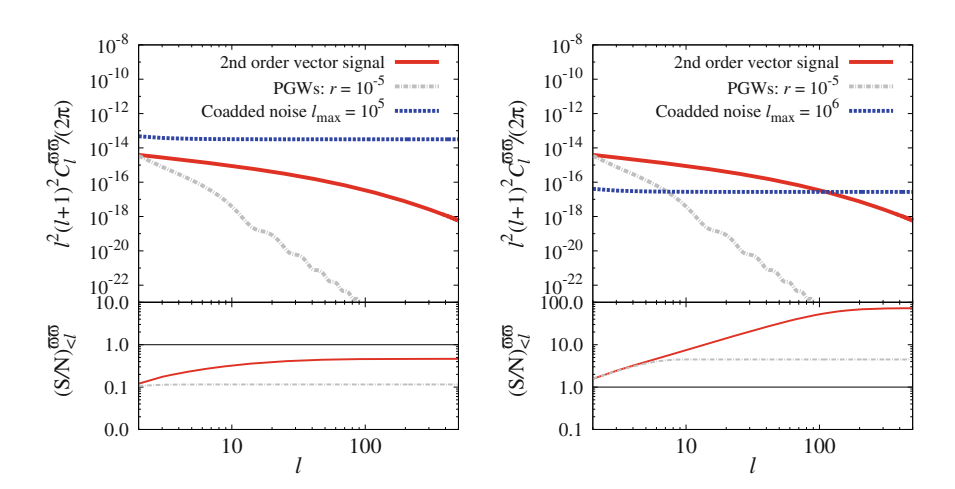


Fig. 5.2 The angular power spectrum of curl modes from the second-order vector mode and the coadded reconstruction noise by using $\ell_{\text{max}} = 10^5$ (top left) and $\ell_{\text{max}} = 10^6$ (top right). Bottom: The signal-to-noise ratio estimated by Eq. (5.88). For reference, we also show the curl mode signal and signal-to-noise ratio induced by PGWs with $r = 10^{-5}$ and which tensor-to-scalar ratio corresponds to the same amplitude of the second-order curl mode at $\ell = 2$

The above signal-to-noise ratio is derived by adopting the reconstruction noise spectrum from the quadratic estimator performed in Refs. [9, 10]. Reconstruction noise from the quadratic estimator is limited by the cosmic variance of the lensed CMB fluctuations. Ultimately, the iterative estimator proposed in Ref. [11] can reduce the reconstruction noise to zero. Even in that case, the fact that the curl mode from PGW with $r \lesssim 10^{-5}$ is concealed by that from the second-order vector mode does not change.

The signal-to-noise ratio of the second-order vector mode can reach higher than that of PGWs. PGWs do not induce the curl mode amplitude on smaller scales since PGWs decay on subhorizon scales. On the other hand, the second-order curl mode can remain large on smaller scales and at low redshift since the second-order vector mode is continuously sourced by the first-order scalar gravitational potential. The second-order vector mode grows on subhorizon scales. From this nature, the second-order vector mode may be easier to detect than PGWs on small scales.

There is another source of the curl mode, that is, the lens-lens coupling examined in Refs. [12–14]. The lens-lens coupling is sourced by the higher-order Born correction. However, this correction mainly contributes the curl mode on small scales such as $\ell \gg 10$. The curl mode on large scales is important to distinguish the PGWs and the second-order vector mode since the PGWs and the second-order vector mode affect the curl mode on large scales, that is, $\ell \lesssim 10$. When we consider the curl mode on all scales, the lens-lens coupling and the second-order vector mode should be taken into account.

To close this section, we describe a feature of the second-order vector mode. The second-order vector mode does not have the free parameter since its source, that is, the first-order scalar mode, is well determined by the current cosmological observations. Consequently, the prediction of the 21 cm lensing curl mode from the second-order vector mode is quite robust.

5.4 Conclusion

In this section, we studied the detectability of the second-order vector mode by using 21 cm radiation from the dark ages. 21 cm radiation during the dark ages is a powerful tool to explore small signals such as second-order signatures since 21 cm radiation anisotropy on small scales makes multipole moments available up to $\sim 10^6$. Furthermore, by multifrequency observations, we can use many redshift slices to decrease the lensing reconstruction noise. We focused on the weak lensing signal of the 21 cm radiation from the dark ages. As well as the CMB lensing, the 21 cm photons are deflected by foreground scalar, vector, and tensor perturbations. The deflection angle of the 21 cm photons can be decomposed into the scalar (gradient mode) and pseudoscalar (curl mode) potentials depending on its parity. The curl mode is a good tracer of the cosmological vector and tensor modes since the scalar mode induces only the gradient mode. It is known that the second-order tensor mode is the subdominant component in the large-scale structure signal such as weak lensing. On

5.4 Conclusion 127

the other hand, the second-order vector mode can have a comparable contribution on large-scale structure to primordial gravitational waves. Accordingly, the observation that can detect PGWs with small tensor-to-scalar ratio can be also used to detect the second-order vector mode with a high signal-to-noise ratio.

We discussed the detectability of the 21 cm lensing curl mode induced from the second-order vector mode for the first time. If the available multipole is limited to $\ell \leq 10^5$, the 21 cm lensing curl mode from the second-order vector mode cannot be detected. If we can extend the maximum multipole up to $\ell_{\rm max} \approx 10^6$, the signal-tonoise ratio reaches 73. We conclude that, in principle, we can explore the second-order vector mode by using 21 cm radiation from the dark ages. By comparing PGWs, it was also found that the PGWs with a tensor-to-scalar ratio $r \approx 10^{-5}$ become subdominant in the 21 cm lensing curl mode. In the previous study [1], they concluded that it is possible to detect the PGWs with $r \approx 10^{-9}$. However, when second-order effects are included in their analysis, a tensor-to-scalar ratio smaller than $r \leq 10^{-5}$ would be difficult to detect by the 21 cm lensing curl mode. We can generalize this discussion for any model, including the vector or tensor modes with model parameters. The second-order vector mode is generated from the first-order scalar mode that has been well determined by current observations. Therefore, the 21 cm curl mode from the second-order vector mode always exists. Even if 21 cm lensing is induced by other models, an amplitude smaller than the second-order vector mode is difficult to detect with 21 cm lensing.

Throughout this section, we assumed the ideal and challenging experiment for 21 cm signals. There are some forthcoming observations for 21 cm signals after the recombination epoch, e.g., from the Square Kilometer Array. Moreover, exploring 21 cm radiation must become an active topic in the near future. Before starting these observations, exploring the potentials of 21 cm radiation is important and this work gives one of the nontrivial solutions.

References

- L. Book, M. Kamionkowski, F. Schmidt, Lensing of 21-cm fluctuations by primordial gravitational waves. Phys. Rev. Lett. 108, 211301 (2012), arXiv:1112.0567
- S. Saga, D. Yamauchi, K. Ichiki, Weak lensing induced by second-order vector mode. Phys. Rev. D 92(6), 063533 (2015), arXiv:1505.02774
- 3. K.W. Masui, U.-L. Pen, Primordial gravity wave fossils and their use in testing inflation. Phys. Rev. Lett. **105**, 161302 (2010), arXiv:1006.4181
- K. Sigurdson, A. Cooray, Cosmic 21-cm delensing of microwave background polarization and the minimum detectable energy scale of inflation. Phys. Rev. Lett. 95, 211303 (2005), arXiv:astro-ph/0502549
- S. Furlanetto, S.P. Oh, F. Briggs, Cosmology at low frequencies: the 21 cm transition and the high-redshift Universe. Phys. Rept. 433, 181–301 (2006). arXiv:astro-ph/0608032
- A. Lewis, A. Challinor, The 21cm angular-power spectrum from the dark ages. Phys. Rev. D 76, 083005 (2007), arXiv:astro-ph/0702600
- L. Senatore, S. Tassev, M. Zaldarriaga, Cosmological perturbations at second order and recombination perturbed. JCAP 0908, 031 (2009), arXiv:0812.3652

- A. Lewis, A. Challinor, Weak gravitational lensing of the cmb. Phys. Rept. 429, 1–65 (2006), arXiv:astro-ph/0601594
- T. Namikawa, D. Yamauchi, A. Taruya, Full-sky lensing reconstruction of gradient and curl modes from CMB maps. JCAP 1201, 007 (2012), arXiv:1110.1718
- Planck Collaboration, P.A.R. Ade et al., Planck 2015 results. XV. Gravitational lensing, arXiv:1502.01591
- 11. C.M. Hirata, U. Seljak, Reconstruction of lensing from the cosmic microwave background polarization. Phys. Rev. D 68, 083002 (2003), arXiv:astro-ph/0306354
- 12. B. Jain, U. Seljak, S.D.M. White, Ray tracing simulations of weak lensing by large scale structure. Astrophys. J. **530**, 547 (2000), arXiv:astro-ph/9901191
- 13. D. Sarkar, P. Serra, A. Cooray, K. Ichiki, D. Baumann, Cosmic shear from scalar-induced gravitational waves. Phys. Rev. D 77, 103515 (2008), arXiv:0803.1490
- A. Cooray, W. Hu, Second order corrections to weak lensing by large scale structure. Astrophys. J. 574, 19 (2002), arXiv:astro-ph/0202411

Chapter 6 Summary of This Thesis

In this thesis, we studied the role of the second-order vector mode in the cosmological perturbation theory. The vector mode has been paid less attention so far since the vector mode has only decaying solution in the first-order perturbation theory. Contrary to the linear theory, according to the non-linear coupling of the first-order scalar modes, the vector mode inevitably appears in the second-order perturbation theory. Here, the first-order scalar mode is determined with a high precision by the current observations. Throughout this thesis, we discussed the observational effects of the second-order vector mode as follows.

First, we demonstrated the second-order perturbation theory in Chap. 2. Cosmological perturbation theory is based on the Einstein-Boltzmann system. We formulated the perturbed Einstein equation and Boltzmann equation worked in the Poisson gauge without any lack of their consistency up to the second order. In the standard cosmology after the neutrino decoupling, the fluids in the universe are assumed to consist of photons, neutrinos, dark matters, and baryons with the interaction between photons and baryons due to the Compton scattering. We derived the collision term in the Boltzmann equation up to the second order. Moreover, as an example, we showed the tight-coupling approximation of the second-order vector mode. Photons and baryons had strongly coupled through the Compton scattering in the early universe. In this limit, we can treat these fluids as a single fluid and expand the perturbation variables related to photons and baryons by using the tight-coupling parameter. We derived the solution in the tight-coupling approximation to implement in our Boltzmann code which makes us to rapidly solve the perturbed Einstein-Boltzmann system. In addition, we also discussed about configurations of the wavevector in Fourier space. Two Fourier modes couple, satisfying the triangle condition in the second-order theory. In Fourier space, we showed that there is some symmetry of the wavevector configuration.

Second, we applied the second-order vector mode to generation of magnetic fields in Chap. 3. There are many evidences that there exists cosmological magnetic fields on large scales. The origin of cosmological magnetic fields has not been figured

[©] Springer Nature Singapore Pte Ltd. 2018

¹²⁹

out yet although many generation mechanisms have been proposed. In our study, we tried to explain cosmological magnetic fields according to the vector mode in the second-order perturbation theory. Two previous studies showed the spectrum of second-order magnetic fields, their results are not consistent with each other. By using our original Boltzmann code, we revealed the reason why the discrepancy is appeared in the two previous studies. Moreover, we accurately determined the power spectrum of second-order magnetic fields. The amplitude of the second-order magnetic fields is about 10^{-23} Gauss at cosmological recombination ($z \approx 1100$). Although it seems that the amplitude of the resultant magnetic fields is sufficient for the seed of cosmological magnetic fields, we need to further understand about the dynamo mechanism, namely, the amplification mechanism on cosmological scales.

Third, we applied the second-order vector mode to the CMB lensing and cosmic shear in Chap. 4. Photons emitted from the CMB last scattering surface and galaxies are deflected by the foreground perturbations. The deflection angle induced by the vector mode includes an odd-parity mode which does not arise from the scalar mode. We discuss the detectability of the parity-odd modes, named the curl mode for the CMB lensing and the B-mode for the cosmic shear. Not only the second-order vector mode but also the second-order tensor mode and primordial gravitational waves induce the curl and B modes. We compared the angular power spectra induced from these modes and found that the second-order vector mode dominates on small scales in the CMB lensing measurements when we assume the tensor-to-scalar ratio $r \approx 0.1$. On the other hand, in the cosmic shear measurements, the second-order vector mode dominates on almost all scales. However, unfortunately, ongoing and forthcoming experiments cannot detect these parity-odd signals. In other words, the parity-odd mode is available for the consistency check of the weak lensing measurements as discussed in Ref. [1].

Fourth, we also applied the second-order vector mode to the 21 cm lensing in Chap. 5. After the recombination epoch, there are large amount of neutral hydrogen atoms which emit the 21 cm radiation due to the hyperfine structure of a neutral hydrogen atom. By using the 21 cm radiation, it is possible to reduce the amplitude of the noise spectrum since the 21 cm radiation can be stacked many redshift slices. Moreover, it is possible to use fluctuations on smaller scales compared with the CMB lensing since the 21 cm fluctuations do not have the diffusion mechanism such as a Silk dumping. We studied the detectability of the second-order vector mode by using the 21 cm radiation, i.e., the high-sensitivity experiments. In the 21 cm lensing, it is possible to detect the second-order vector mode with a high signal-to-noise ratio about S/N $\sim O(10)$. If we consider the effect of the second-order vector mode, it becomes difficult to detect the primordial gravitational waves with $r \lesssim 10^{-5}$ in the 21 cm lensing experiments.

Finally, in closing this thesis, we mention the future direction of the cosmological vector mode. As discussed in this thesis, the vector mode must appear in the early universe due to the nonlinear effects. The absence of the vector mode in cosmology is now old-fashioned ideas. For example, in the study of the large-scale structure, the standard perturbation theory is well discussed. The standard perturbation theory is based on the continuous and Euler equations in the non-relativistic limit. In this

case, the vector mode does not appear even in the higher-order perturbation theory if the initial vorticity is absent. However, it is possible to extrapolate the second-order vector mode to the standard perturbation theory, which is not trivial. The connection between the cosmological perturbation theory and the standard perturbation theory of the large-scale structure would be interesting. Thus, after accomplishment of the scalar mode cosmology, it will start the *vector mode cosmology* in the near future.

Reference

1. BICEP2, Keck Array Collaboration, P.A.R. Ade et al., BICEP2/Keck Array VIII: measurement of gravitational lensing from large-scale B-mode polarization, arXiv:1606.01968

Appendix A Riemannian Geometry

In this section, we summarize the formulae of Riemannian geometry which are used to derive the perturbed Einstein equation. Throughout this thesis, we work in the Poisson gauge and the following formulae are written in the Poisson gauge.

First of all, the line element in the Poisson gauge is written as

$$\mathrm{d}s^2 = a^2(\eta) \left[-e^{2\Psi} \mathrm{d}\eta^2 + 2\omega_i \mathrm{d}\eta \mathrm{d}x^i + \left(e^{-2\Phi} \delta_{ij} + h_{ij} \right) \mathrm{d}x^i \mathrm{d}x^j \right] \,. \tag{A.1}$$

According to this line element, the metric tensor can be expressed as

$$g_{00} = -a^2 e^{2\Psi} , (A.2)$$

$$g_{0i} = a^2 \omega_i , \qquad (A.3)$$

$$g_{ij} = a^2 \left(e^{-2\Phi} \delta_{ij} + h_{ij} \right) .$$
 (A.4)

The inverse matrix components are derived up to the second order as

$$g^{00} = \frac{1}{a^2} \left[-e^{-2\Psi} + \omega_k \omega^k \right] \,, \tag{A.5}$$

$$g^{0i} = \frac{1}{a^2} \left[e^{2(\Phi - \Psi)} \omega^i - h^i{}_j \omega^j \right] ,$$
 (A.6)

$$g^{ij} = a^{-2} \left[e^{2\Phi} \delta^{ij} - e^{4\Phi} h^{ij} + h^i{}_k h^{kj} \right]. \tag{A.7}$$

Moreover, the determinant of the metric tensor is calculated as

$$\sqrt{-g} = a^4 e^{\Psi - 3\Phi} \left[1 - \frac{1}{4} h_{ij} h^{ij} + \frac{1}{2} \omega_i \omega^i \right]. \tag{A.8}$$

Although we leave the first- and second-order terms of the scalar, vector, and tensor modes here, we will neglect the first-order vector and tensor modes following sections.

A.1 Connection Coefficient

Hereafter, we ignore the first-order vector and tensor modes. The definition of the connection coefficient is given by

$$\Gamma^{\alpha}{}_{\beta\gamma} = \frac{1}{2} g^{\alpha\mu} \left(g_{\mu\beta,\gamma} + g_{\mu\gamma,\beta} - g_{\beta\gamma,\mu} \right) . \tag{A.9}$$

The connection coefficient in the Poisson gauge can be concretely expressed as

$$\Gamma^0_{00} = \mathcal{H} + \dot{\Psi} \,, \tag{A.10}$$

$$\Gamma^{0}_{0i} = \Psi_{,i} + \mathcal{H}\omega_{i} , \qquad (A.11)$$

$$\Gamma^{i}_{00} = e^{2(\Phi + \Psi)} \Psi^{,i} + \dot{\omega}^{i} + \mathcal{H}\omega^{i} , \qquad (A.12)$$

$$\Gamma^{0}_{ij} = e^{-2(\Psi + \Phi)} \left(\mathcal{H} - \dot{\Phi} \right) \delta_{ij} - \frac{1}{2} \left(\omega_{i,j} + \omega_{j,i} \right) + \mathcal{H} h_{ij} + \frac{1}{2} \dot{h}_{ij} , \qquad (A.13)$$

$$\Gamma^{i}_{0j} = (\mathcal{H} - \dot{\Phi}) \, \delta^{i}_{j} + \frac{1}{2} \left(\omega^{i}_{,j} - \omega_{j}^{,i} \right) + \frac{1}{2} \dot{h}^{i}_{j} \,, \tag{A.14}$$

$$\Gamma^{i}{}_{jk} = -\Phi_{,k}\delta^{i}{}_{j} - \Phi_{,j}\delta^{i}{}_{k} + \Phi^{,i}\delta_{jk} - \mathcal{H}\omega^{i}\delta_{jk} + \frac{1}{2}\left(h^{i}{}_{j,k} + h^{i}{}_{k,j} - h_{jk}{}^{,i}\right). \tag{A.15}$$

A.2 Ricci Tensor

By using the connection coefficients, we can derive the Ricci tensor. The definition of the Ricci tensor is expressed by the contraction of the Riemann tensor as

$$R_{\mu\nu} = R^{\alpha}{}_{\mu\alpha\nu}$$

= $\Gamma^{\alpha}{}_{\mu\nu,\alpha} - \Gamma^{\alpha}{}_{\nu\alpha,\mu} + \Gamma^{\alpha}{}_{\sigma\alpha}\Gamma^{\sigma}{}_{\mu\nu} - \Gamma^{\alpha}{}_{\sigma\nu}\Gamma^{\sigma}{}_{\mu\alpha}$. (A.16)

Note that, the Ricci tensor is symmetrical under the permutation of subscripts, namely $R_{\mu\nu}=R_{\nu\mu}$. Consequently, the Ricci tensor in the Poisson gauge can be calculated as

$$R_{00} = -3\dot{\mathcal{H}} + 3\ddot{\Phi} + 3\mathcal{H} (\dot{\Psi} + \dot{\Phi}) + e^{2(\Psi + \Phi)} \Psi^{,i}_{,i} - 3\dot{\Phi}\dot{\Psi} - 3\dot{\Phi}^2 + (\Psi_{,i} - \Phi_{,i}) \Psi^{,i},$$
(A.17)

$$R_{0i} = 2(\dot{\Phi}_{,i} + \mathcal{H}\Psi_{,i}) - 2\dot{\Phi}\Psi_{,i} + 2\mathcal{H}^2\omega_i + \dot{\mathcal{H}}\omega_i - \frac{1}{2}\omega_i^{,a}_{,a}, \qquad (A.18)$$

$$R_{ij} = e^{-2(\Phi + \Psi)} \left(\dot{\mathcal{H}} + 2\mathcal{H}^2 \right) \delta_{ij}$$

$$- e^{-2(\Phi + \Psi)} \left[\ddot{\Phi} + 5\mathcal{H}\dot{\Phi} + \mathcal{H}\dot{\Psi} \right] \delta_{ij} + \left(\Phi_{,ij} - \Psi_{,ij} \right) + \Phi^{,a}_{,a} \delta_{ij}$$

$$+ \left[3\dot{\Phi}^2 + \dot{\Psi}\dot{\Phi} + \Phi^{,a} \left(\Psi_{,a} - \Phi_{,a} \right) \right] \delta_{ij} + \Phi_{,i} \Phi_{,j} - \Psi_{,i} \Psi_{,j} - \left(\Phi_{,i} \Psi_{,j} + \Phi_{,j} \Psi_{,i} \right)$$

$$+ \mathcal{H} \left[\dot{h}_{ij} + 2\mathcal{H}h_{ij} - \left(\omega_{i,j} + \omega_{j,i} \right) \right] + \frac{1}{2} \left[\ddot{h}_{ij} + 2\dot{\mathcal{H}}h_{ij} - \left(\dot{\omega}_{i,j} + \dot{\omega}_{j,i} \right) - h_{ij}^{,a}_{,a} \right] .$$
(A.19)

Furthermore, we can raise a index by the definition of the Ricci tensor, $R^\mu{}_\nu=g^{\mu\alpha}R_{\alpha\nu}$ as

$$\begin{split} a^{2}R^{0}{}_{0} &= e^{-2\Psi} \left[3\dot{\mathcal{H}} - 3\ddot{\Phi} - 3\mathcal{H} \left(\dot{\Psi} + \dot{\Phi} \right) \right] - e^{2\Phi}\Psi^{,i}{}_{,i} + 3\dot{\Phi}\dot{\Psi} + 3\dot{\Phi}^{2} - \left(\Psi_{,i} - \Phi_{,i} \right) \Psi^{,i} \;, \\ (A.20) \\ a^{2}R^{0}{}_{i} &= -2e^{-2\Psi} \left(\dot{\Phi}_{,i} + \mathcal{H}\Psi_{,i} \right) + 2\dot{\Phi}\Psi_{,i} + \frac{1}{2}\omega_{i}{}^{,a}{}_{,a} \;, \\ (A.21) \\ a^{2}R^{i}{}_{0} &= 2e^{2\Phi} \left(\dot{\Phi}^{,i} + \mathcal{H}\Psi^{,i} \right) - 2\dot{\Phi}\Psi^{,i} + 2\mathcal{H}^{2}\omega^{i} - 2\dot{\mathcal{H}}\omega^{i} - \frac{1}{2}\omega^{i,a}{}_{,a} \;, \\ a^{2}R^{i}{}_{j} &= e^{-2\Psi} \left(\dot{\mathcal{H}} + 2\mathcal{H}^{2} \right) \delta^{i}{}_{j} \\ &- e^{-2\Psi} \left[\ddot{\Phi} + 5\mathcal{H}\dot{\Phi} + \mathcal{H}\dot{\Psi} \right] \delta^{i}{}_{j} + e^{2\Phi} \left[\Phi^{,i}{}_{,j} - \Psi^{,i}{}_{,j} + \Phi^{,a}{}_{,a}\delta^{i}{}_{j} \right] \\ &+ \left[3\dot{\Phi}^{2} + \dot{\Psi}\dot{\Phi} + \Phi^{,a} \left(\Psi_{,a} - \Phi_{,a} \right) \right] \delta^{i}{}_{j} + \Phi^{,i}\Phi_{,j} - \Psi^{,i}\Psi_{,j} - \left(\Phi^{,i}\Psi_{,j} + \Phi_{,j}\Psi^{,i} \right) \\ &+ \mathcal{H} \left[\dot{h}^{i}{}_{j} - \left(\omega^{i}{}_{,j} + \omega_{j}{}^{,i} \right) \right] + \frac{1}{2} \left[\ddot{h}^{i}{}_{j} - \left(\dot{\omega}^{i}{}_{,j} + \dot{\omega}_{j}{}^{,i} \right) - h^{i}{}_{j}{}^{,a}{}_{,a} \right] \;. \end{split} \tag{A.23}$$

A.3 Ricci Scalar

The definition of the Ricci scalar is expressed by the contraction of the Ricci tensor as

$$R = R^{\mu}_{\ \nu} = g^{\mu\nu} R_{\mu\nu} \ . \tag{A.24}$$

Thus, the Ricci scalar in the Poisson gauge can be expressed as

$$a^{2}R = 6e^{-2\Psi} \left[\dot{\mathcal{H}} + \mathcal{H}^{2} \right] - 6e^{-2\Psi} \left[\ddot{\Phi} + \mathcal{H}\dot{\Psi} + 3\mathcal{H}\dot{\Phi} \right]$$

$$+ 2e^{2\Phi} \left[2\Phi^{,i}{}_{,i} - \Psi^{,i}{}_{,i} \right] + 12\dot{\Phi}^{2} + 6\dot{\Psi}\dot{\Phi} + 2\Phi^{,i}\Psi_{,i} - 2\Phi^{,i}\Phi_{,i} - 2\Psi^{,i}\Psi_{,i} .$$
(A.25)

A.4 Einstein Tensor

Finally, the Einstein tensor is defined by using the Ricci tensor and Ricci scalar as

$$G^{\mu}{}_{\nu} \equiv R^{\mu}{}_{\nu} - \frac{1}{2} \delta^{\mu}{}_{\nu} R . \tag{A.26}$$

We can calculate the Einstein tensor used in the Einstein equation (Eq. (2.27)) as

$$a^{2}G^{0}{}_{0} = e^{-2\Psi} \left[-3\mathcal{H}^{2} + 6\mathcal{H}\dot{\Phi} - 2e^{2(\Phi + \Psi)}\Phi^{,i}{}_{,i} - 3\dot{\Phi}^{2} + \Phi^{,i}\Phi_{,i} \right], \tag{A.27}$$

$$a^{2}G^{0}{}_{i} = -2e^{-2\Psi}\left(\dot{\Phi}_{,i} + \mathcal{H}\Psi_{,i}\right) + 2\dot{\Phi}\Psi_{,i} + \frac{1}{2}\omega_{i}^{,a}{}_{,a}, \tag{A.28}$$

$$a^{2}G^{i}{}_{0} = 2e^{2\Phi} \left(\dot{\Phi}^{,i} + \mathcal{H}\Psi^{,i}\right) - 2\dot{\Phi}\Psi^{,i} + 2\mathcal{H}^{2}\omega^{i} - 2\dot{\mathcal{H}}\omega^{i} - \frac{1}{2}\omega^{i,a}{}_{,a}, \tag{A.29}$$

$$\begin{split} a^{2}G^{i}{}_{j} &= e^{-2\Psi} \left(-2\dot{\mathcal{H}} - \mathcal{H}^{2} \right) \delta^{i}{}_{j} + 2e^{-2\Psi} \left[\ddot{\Phi} + \mathcal{H}\dot{\Psi} + 2\mathcal{H}\dot{\Phi} \right] \delta^{i}{}_{j} \\ &+ e^{2\Phi} \left[\Phi^{,i}{}_{,j} - \Psi^{,i}{}_{,j} - \Phi^{,a}{}_{,a} \delta^{i}{}_{j} + \Psi^{,a}{}_{,a} \delta^{i}{}_{j} \right] + \left[-3\dot{\Phi}^{2} - 2\dot{\Psi}\dot{\Phi} + \Psi^{,a} \Psi_{,a} \right] \delta^{i}{}_{j} \\ &+ \Phi^{,i} \Phi_{,j} - \Psi^{,i} \Psi_{,j} - \left(\Phi^{,i} \Psi_{,j} + \Phi_{,j} \Psi^{,i} \right) \\ &+ \mathcal{H} \left[\dot{h}^{i}{}_{j} - \left(\omega^{i}{}_{,j} + \omega_{j}{}^{,i} \right) \right] + \frac{1}{2} \left[\ddot{h}^{i}{}_{j} - \left(\dot{\omega}^{i}{}_{,j} + \dot{\omega}_{j}{}^{,i} \right) - h^{i}{}_{j}{}^{,a}{}_{,a} \right] \,. \end{split} \tag{A.30}$$